SMEARED FRACTURE ANALYSIS OF CONCRETE GRAVITY DAMS FOR STATIC AND SEISMIC LOADS

by

SUDIP SANKAR BHATTACHARJEE

Department of Civil Engineering and Applied Mechanics
McGill University, Montreal

February, 1993

A thesis submitted to the Faculty of Graduate Studies and Research
in partial fulfilment of the requirements for the degree of Doctor of Philosophy

ISBN 0-315-87800-2

Shortened version of the thesis title:

STATIC AND SEISMIC FRACTURE ANALYSES OF CONCRETE GRAVITY DAMS

by

SUDIP SANKAR BHATTACHARJEE

Department of Civil Engineering and Applied Mechanics
McGill University, Montreal

February, 1993

A thesis submitted to the Faculty of Graduate Studies and Research
in partial fulfilment of the requirements for the degree of Doctor of Philosophy

ABSTRACT

Smeared crack analysis models, based on nonlinear fracture mechanics concepts, have been developed to investigate the fracture behaviour of concrete gravity dams. The proposed constitutive models have been implemented in a finite element analysis computer program for nonlinear static and seismic analyses of plain concrete structures. Extensive verifications of the computational models have been carried out by studying the nonlinear static response of notched concrete beams, a model concrete dam, and a full scale concrete gravity dam: all experimentally or numerically investigated in the past. Seismic fracture and energy response of Koyna Dam, a classic example of seismic induced cracking in concrete dams, has also been studied. Finally, the seismic fracture behaviour of a typical concrete gravity dam has been investigated, considering severe ground motions and winter temperature effects as expected in Eastern Canada. Reduced frequency independent models of dynamic interactions in the dam-reservoir-foundation system have been considered in the nonlinear seismic analyses.

RÉSUMÉ

Des modèles de fissuration diffuse basés sur la mécanique nonlinéaire des fractures ont été développés pour l'étude des réponses statiques et sismiques des barrages-poids en béton. Les modèles constitutifs proposés ont été implantés dans un nouveau logiciel d'éléments finis pour les analyses statiques et sismiques nonlinéaires des structures de béton non-armé. Plusieurs vérifications des modèles proposés ont été faites par l'étude statique nonlinéaire de poutres, d'un modèle réduit de barrage, et d'un barrage de pleine grandeur, qui ont tous été testés expérimentalement ou analysés dans le passé. La fissuration sismique et la dissipation de l'énergie du barrage Koyna, un exemple classique de la fissuration sismique des barrages de béton, ont aussi été étudiées. Finalement, la fissuration sismique d'un barrage-poids typique, soumis au secousses du sol et aux conditions sévères des températures hivernales qui peuvent être anticipées au Québec, a été analysée. Une modélisation réduite et indépendante des fréquences a été considérée pour représenter les interactions dynamiques dans le système barrage-fondation-réservoir.

ACKNOWLEDGEMENTS

The author would like to express his sincere gratitude to Professor Pierre Léger for his profound interest in the research topic, and constant guidance during the course of this research. His tireless effort to provide with computing and relevant facilities, both at McGill University and at Ecole Polytechnique, Montreal, is gratefully acknowledged. Computing equipments available through a joint grant from NSERC, Hydro-Quebec, and Alcan, have been extensively used to produce a significant portion of the results presented in this thesis.

The deepest gratitude goes to the Canadian Commonwealth Scholarship and Fellowship Plan for an excellent fellowship that permitted the author to conduct this research. Thanks are also due to Professor B. Stafford Smith for his personal guidance during the author's early days in Canada. Limited financial supports available through teaching, research assistantship, and the Emil Nenninger Memorial Fellowship from the Department of Civil Engineering and Applied Mechanics are thankfully acknowledged. Final thanks are due to Mr. Aniruddha Bhattacharyya for his help in preparation of the thesis.

TABLE OF CONTENTS

LIST OF FIGURES

NOTATION

Following is a list of principal symbols used in the ma~uscript. All symbols are defined in the text when they appear.

MATHEMATICAL SYMBOLS:

{ }	:	Vector of the specified parameter.
[ ]	:	Matrix of the specified parameter.
$\{\ \}^T$, $[\ ]^T$	:	Transpose of the vector or matrix.

LATIN SYMBOLS:

a	:	Mass proportional damping factor.
a_0	:	Notch depth $=d_n$.
A	:	Thermal expansion coefficient.
b	:	Stiffness proportional damping factor.
[B]	:	Strain-displacement transformation matrix.
C_F^H	:	Foundation added damping in the horizontal direction.
C_F^V	:	Foundation added damping in the vertical direction.
CR	:	Computed response of the indirect displacement control analysis parameter.
C_R^H	:	Reservoir added damping in the horizontal direction.
[c]	:	Element damping matrix.
[c(t)]	:	Time dependent element damping matrix.
[C]	:	Damping matrix of the entire structural system.
$[C]_F$	:	Foundation added damping matrix.
$[C]_R$	:	Reservoir added damping matrix.
$[C(\bar{w})]$	:	Frequency dependent system damping matrix.
d	:	Structural dimension.
d_a	:	Maximum aggregate dimension.
d_c	:	Depth of crack penetration.
d_n	:	Notch depth $=a_0$.
du	:	Differential increment of the relative displacement.
du_g	:	Differential increment of the ground displacement.
du_t	:	Differential increment of the total displacement.
dV	:	Differential volume.
DMF_e	:	Dynamic magnification factor of the apparent tensile strength.
DMF_f	:	Dynamic magnification factor of the fracture energy.

$[D]$	:	Stress-strain relationship matrix in the undamaged state.
$[D]_{np}$	:	Total stress-strain relationship matrix in the local coordinate directions.
$[D]_s$	:	Total stress-strain relationship matrix in the global coordinate directions.
$[D]_s^{cr}$	:	Total crack stress-strain relationship matrix in the local directions.
$[D]_T$	:	Incremental stress-strain relationship matrix in the global coordinate directions.
$[D]_T^{cr}$	:	Incremental crack stress-strain relationship matrix in the local coordinate directions.
E	:	Young's modulus of concrete.
E^D	:	Energy dissipation due to damping in the structure.
E^F	:	Energy dissipated due to tensile cracking in the structure.
E^K	:	Absolute kinetic energy of the system.
E^P	:	Work done by pre-seismic applied forces.
E^Q	:	Absolute seismic input energy.
E^R	:	Work done by nonlinear restoring forces.
E^s,E_n^s	:	Damaged secant modulus during the tensile strain softening process.
E^t,E_n^t	:	Tangent softening modulus.
E^U	:	Recoverable strain energy in the system.
f,f_s	:	Applied load.
f_c'	:	Static compressive strength of concrete.
f_{norm}	:	Norm of residual forces in a nonlinear analysis.
$\{f\}$	:	Vector of total applied load.
$\{f(t)\}$	:	Time dependent applied load vector.
$\{f^T\}$	:	Equivalent load vector for the specified temperature condition.
g	:	Acceleration due to gravity.
g_i	:	Energy dissipation in each element due to tensile strain softening.
G_f	:	Static fracture energy of concrete.
G_f'	:	Dynamic fracture energy of concrete.
G	:	Shear modulus of the virgin material.
G^s, G_{np}^s	:	Softened shear modulus of a cracked element in the local coordinate directions.
h_c	:	Characteristic dimension of the crack band.
h_c^{max}	:	Maximum characteristic dimension that can be applied with a strain softening constitutive model.
i	:	load or time step no.
i_1,i_2	:	Element designations.
k	:	Iteration no. in a particular load or time step.
k_{max}	:	Maximum number of iterations allowed in a load or time step.
K_F^H	:	Foundation added stiffness in the horizontal direction.
K_F^V	:	Foundation added stiffness in the vertical direction.
K_i,K_I,K_{II},K_{III}	:	Stress intensity factors.
K_{Ic}	:	Static fracture toughness of concrete.

$[k]$	:	Element stiffness matrix.
$[k(t)]$	:	Time dependent element stiffness matrix.
$[k]_0$	:	Element stiffness matrix at the initial elastic state.
$[K]$	:	Stiffness matrix of the entire structural system.
$[K]_F$	:	Foundation added stiffness matrix.
$[K]_R$	:	Reservoir added stiffness matrix.
$[K(\bar{w})]$	:	Frequency dependent system stiffness matrix.
l_{ch}	:	Material characteristic dimension.
$M_R{}^H$	:	Reservoir added mass in the horizontal direction.
$[m]$	:	Element mass matrix.
$[M]$	:-	Mass matrix of the entire structural system.
$[M]_F$	:	Foundation added mass matrix.
$[M]_R$	:	Reservoir added mass matrix.
$[M(\bar{w})]$	:	Frequency dependent system mass matrix.
$[N]$	:	Crack strain transformation matrix.
P_0	:	Load resistance of a beam under three-point loading when the stress at the notch-tip is equal to the tensile strength σ_t.
P_u	:	Ultimate load resistance of a beam under three-point loading.
$\{p\}$	:	Dead load vector.
r_a	:	Restoring forces in the degrees-of-freedom under applied loading.
r_s	:	Restoring forces in the degrees-of-freedom under specified displacement.
$\{r\},\{r(u)\}$	:	Nonlinear restoring force vector of the system.
R_{norm}	:	Norm to indicate the change in applied loads in the indirect displacement control analysis.
t	:	Time.
t'	:	Instant of load application in the long term temperature stress analysis.
T	:	Current temperature.
TOL	:	Convergence tolerance in a nonlinear analysis.
TR	:	Target response of the indirect displacement control analysis parameter.
T_0	:	Stress-free reference temperature.
T_1,T_2,T_3,T_4,T_5	:	Periods of vibration of the structure.
$[T]$	:	Strain transformation matrix.
u	:	Relative displacement of the structure.
u_a	:	Displacements of the degrees-of-freedom under applied loads.
u_g	:	Ground displacement.
u_s	:	Specified displacement.
u_t	:	Total displacement of the structure.
$\dot{u}$	:	Relative velocity of the structure.
$\dot{u}_t$	:	Total velocity of the structure.
$\ddot{u}$	:	Relative acceleration of the structure.
$\ddot{u}_g$	:	Ground acceleration.
$\ddot{u}_t$	:	Total acceleration of the structure.

U_o	:	Area under the uniaxial stress-strain diagram up to the peak under static loading.
U_o'	:	Area under the uniaxial stress-strain diagram up to the peak under dynamic loading.
V	:	Volume of an element.
w_c	:	Width of the crack band.
$\bar{w}_1,\bar{w}_2,\bar{w}_3$	:	Frequencies of the input ground motion.

GREEK SYMBOLS:

α	:	Numerical dissipation parameter in the time integration procedure.
α_r	:	Reservoir bottom wave reflection coefficient.
β	:	Time integration parameter.
γ	:	Time integration parameter.
γ_{np}	:	Total shear strain in the local coordinate directions.
γ_{np}^{e}	:	Elastic shear strain in the local coordinate directions.
γ_{np}^{cr}	:	Crack shear strain in the local coordinate directions.
δ	:	Crack opening displacement.
δ_f	:	Final crack opening displacement of no tensile resistance.
Δ	:	Increment of quantities.
Δt	:	Incremental time step.
ΔV	:	Volume associated with individual Gauss point.
$\{\Delta f\}$	:	Incremental load vector or the unbalanced load vector.
$\{\Delta f_a^r\}$	:	Vector of unbalance between the applied loads and the restoring forces of the structure.
$\{\Delta\epsilon\}$	:	Incremental strain vector.
$\{\Delta\epsilon\}_{local}^{cr}$	:	Incremental crack strain vector in local coordinate directions.
$\{\Delta\sigma\}$	:	Incremental stress vector.
$\{\Delta\sigma\}_{local}^{cr}$	:	Incremental crack stress vector in local coordinate directions.
ϵ	:	Tensile strain.
ϵ_f	:	Final tensile strain of no-tensile resistance under static loads.
ϵ_f'	:	Final tensile strain of no-tensile resistance under dynamic loads.
ϵ_i	:	Strain corresponding to the apparent static strength of concrete.
ϵ_I	:	Residual elastic strain after relaxation of the temperature induced stresses.
ϵ_n	:	Strain in the crack normal direction.
ϵ_n^{e}	:	Elastic strain in the crack normal direction.
ϵ_n^{cr}	:	Normal strain corresponding to the crack opening displacement.
ϵ_{max}	:	Maximum tensile strain attained during the opening of a crack.
ϵ_p	:	Strain in the crack parallel direction.
ϵ_r	:	Residual tensile strain upon closing of a crack.
ϵ_t	:	Strain corresponding to the static tensile strength of concrete.
ϵ_T	:	Mechanical strain due to temperature changes.

ϵ_0, ϵ_0'	:	Biaxial strains of softening initiation in a finite element for static and dynamic loads respectively.
ϵ_1, ϵ_2	:	Principal strains.
$\{\epsilon\}$	:	Strain vector in the global coordinate directions.
$\{\epsilon\}_{gp}$	:	Global strain vector at a Gauss point.
$\{\epsilon\}_{global}^{cr}$	:	Crack strain vector in the global coordinate directions.
$\{\epsilon\}_{local}^{cr}$	:	Crack strain vector in the local coordinate directions.
$\{\epsilon_L\}$	:	Mechanical strains caused by applied loads.
$\{\epsilon_I\}$	:	Mechanical strains corresponding to volumetric deformations.
$\{\epsilon^T\}$	:	Strain vector corresponding to unrestrained temperature induced deformations.
$\{\epsilon_T\}$	:	Mechanical strain vector due to temperature changes.
η	:	Ratio between the damaged secant modulus and the initial isotropic elastic modulus.
λ	:	Ratio between the residual tensile strain upon closing of a crack and the maximum tensile strain attained.
θ	:	Orientation of the local axis system with respect to the global coordinate directions.
μ	:	Shear resistance factor.
μ_c	:	Critical shear resistance factor during the closing of cracks.
ν	:	Poisson's ratio.
σ	:	Tensile stress.
σ^{cr}	:	Maximum tensile stress resistance of the damaged material (corresponding to the tensile strain ϵ_{max}).
σ_i	:	Apparent tensile strength under static loading.
σ_i'	:	Apparent tensile strength under dynamic loading.
σ_{ij}	:	Near crack tip stresses.
σ_n, σ_n^{cr}	:	Stress in the crack normal direction.
σ_t	:	Tensile strength of concrete under static load.
σ_t'	:	Tensile strength of concrete under dynamic load.
σ_1, σ_2	:	Principal stresses.
σ_0, σ_0'	:	Biaxial stresses of softening initiation in a finite element for static and dynamic loads respectively.
$\{\sigma\}$	:	Stress vector in the global coordinate directions.
$\{\sigma\}_{gp}$	:	Global stress vector at a Gauss point.
$\{\sigma\}_{global}^{cr}$	:	Crack stress vector in the global coordinate directions.
$\{\sigma\}_{local}^{cr}$	:	Crack stress vector in the local coordinate directions.
τ_{np}^{cr}	:	Crack shear stress in the local coordinate system.
$\phi(t,t')$	:	Creep coefficient.
χ	:	Ageing coefficient.
ψ	:	Long term relaxation factor.

ACRONYMS:

AAR	:	Alkali-aggregate reactions.
BEM	:	Boundary element method.
CMOD	:	Crack mouth opening displacement.
CMSD	:	Crack mouth sliding displacement.
COD	:	Crack opening displacement.
CRCM	:	Coaxial rotating crack model.
$CTOD_c$	:	Critical crack tip opening displacement.
DCPM	:	Discrete crack propagation model.
DMF	:	Dynamic magnification factor.
DOF	:	Degree of freedom.
EDM	:	Elasto-brittle damping model.
FCM-VSRF	:	Fixed crack model with a variable shear resistance factor.
FEM	:	Finite element method.
FPZ	:	Fracture process zone.
ICL	:	Incremental crack length.
LDM	:	Linear damping model.
LEFM	:	Linear elastic fracture mechanics.
MCE	:	Maximum credible earthquake.
mNR	:	Modified Newton-Raphson method.
NLFM	:	Nonlinear fracture mechanics.
NR	:	Newton-Raphson method.
OBE	:	Operating basis earthquake.
PGA	:	Peak ground acceleration.
QDM	:	Quasi-linear damping model.
SCPM	:	Smeared crack propagation model.
SIF	:	Stress intensity factors.
SMS	:	Secant modulus stiffness.
SOM	:	Strength of material.
SRS	:	Size reduced strength.
TH	:	Time history.
TMS	:	Tangent modulus stiffness.

CHAPTER 1

INTRODUCTION

1.1 OVERVIEW

Safety of concrete dams is a world wide concern due to vested socio-economic interests involved with these infrastructures. The general concern has been raised particularly due to the aging and deterioration of numerous existing dams that were built during the early part and the middle of this century. Periodic assessment of the safety of existing dams is increasingly becoming a mandatory requirement on the part of utility companies responsible for maintenance and operation of the installations.

Concrete gravity dams constitute a significant proportion of existing dam structures in the world. A typical gravity dam section and the different environmental phenomena influencing the behaviour of the structure are illustrated in Fig. 1.1. The elaboration of a comprehensive safety evaluation procedure for these structures is a complex engineering problem due to intricate influences of several phenomena on the loading and the structural resistance. These are, for example, temperature effects, creep, shrinkage, mass swelling caused by hydration heat of cement and alkali-aggregate reaction, hydrostatic pressure, seismic excitations and the consequent dynamic interactions with the reservoir and the foundation, tensile fracture of mass concrete, and nonlinear deformations in the construction joints. Among the various internal and external factors, seismic safety of concrete dams has evoked the deepest concern among the industrial as well as the research communities. Practical experience about the structural resistance of concrete gravity dams, subjected to severe ground excitations, is very limited, and there is a lack of confidence regarding the safety of large concrete dams exposed to strong seismic environments (Hall [79]). Numerical simulations are very feasible, if not the only method, for comprehensive evaluation of the seismic safety of concrete dams.

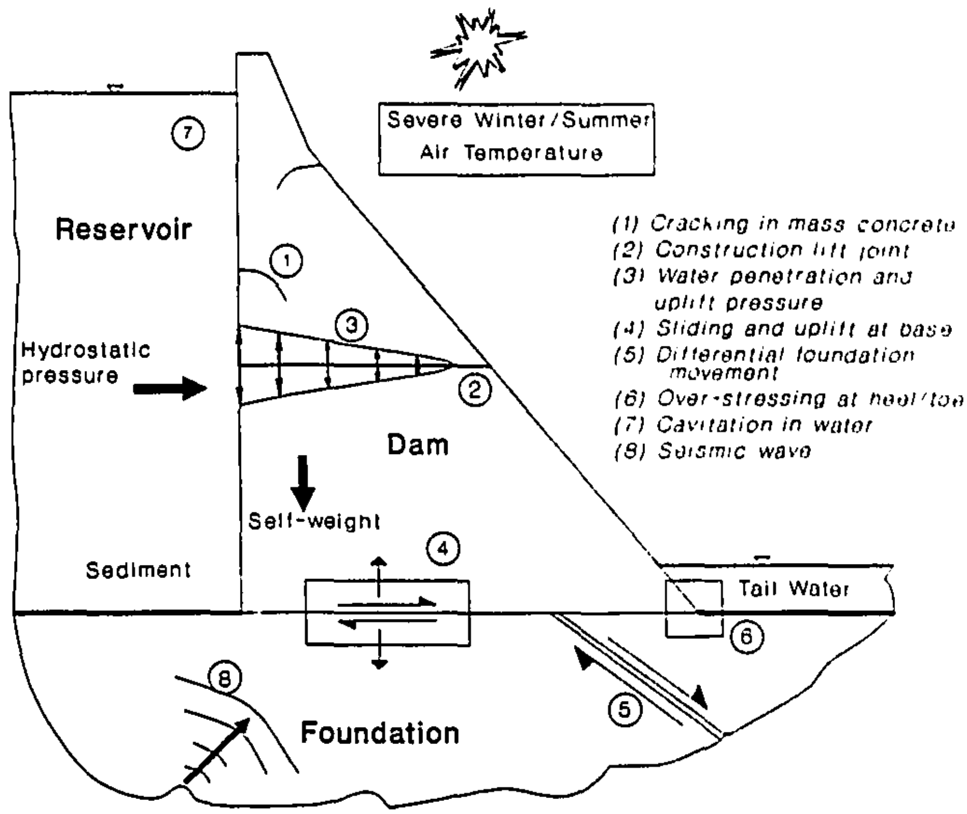

Figure 1.1 A typical gravity dam-reservoir-foundation system.

Mass concrete dams are likely to experience cracking due to the low tensile resistance of concrete. The safety assessment of concrete gravity dams inevitably relates to the cracking behaviour of concrete (Fig. 1.2). In general, most concrete dams present cracks. However, the surface micro-cracking does not endanger the structural safety of dams (Fanelli [59]). Cracks penetrating deep inside a dam (sometimes going through the thickness) constitute engineering concern, because, such cracks may considerably alter the structural resistance, and thereby endanger the safety of the installation. It is expected that under normal load actions from self-weight, hydrostatic pressure, and ambient temperature, concrete dams experience no cracking of structural significance. The accepted seismic design philosophy for concrete dams is to assume linear elastic response under moderate intensity earthquakes, often referred as the operating basis earthquake (OBE). During the most severe ground excitations, the maximum credible earthquake (MCE), potential crack formations can not be excluded from the design

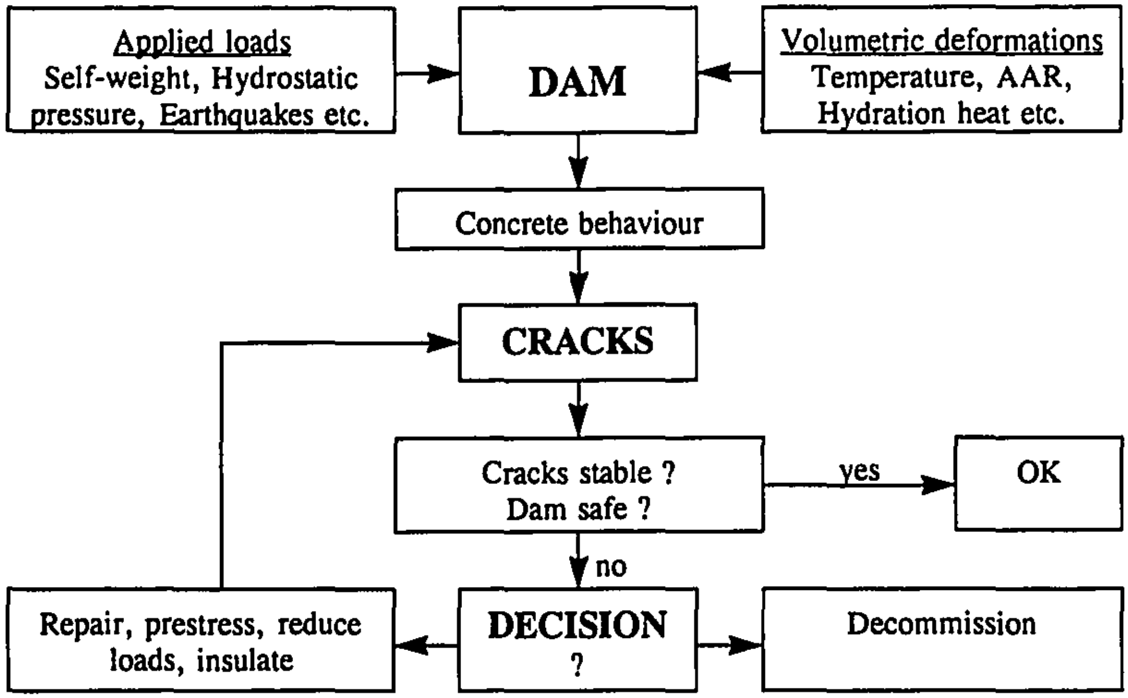

Figure 1.2 Safety evaluation of concrete dams (adapted from Lombardi [109a]).

considerations (Rescher [135]). A rational design approach is to expect moderate damage under the maximum credible earthquake without endangering the ability of a dam to retain the reservoir pressure (USBR [154]).

In the past design methodology for concrete dams, the earthquake effects have usually been taken into consideration by a seismic coefficient to define the additional static lateral load as a certain percentage of the self-weight of dams. Due to uncertainties regarding the tensile resistance of concrete, a 'no-tension' design criterion is satisfied assuming a linear stress distribution over the uncracked portion of presumed horizontal crack planes (Fig. 1.3(a)). However, the traditional 'no-tension' analysis of concrete dams with horizontal cracks may not guarantee a solution that would be on the safe side (Bažant [24], Gioia et al. [73]). The US Army Corps of Engineers has developed guidelines for evaluating the cracking hazard by linear dynamic analyses of gravity dam monoliths (Guthrie [77]). The procedure requires linear dynamic analyses of dam-foundation-reservoir systems with a variable critical damping ratio, depending on the intensity of

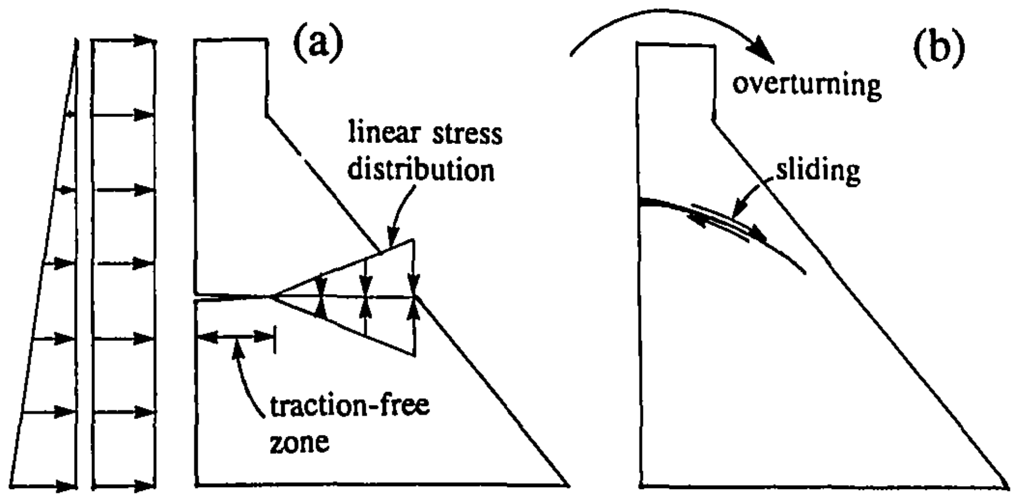

Figure 1.3 (a) No-tension analysis, and (b) a possible crack profile threatening the structural integrity.

tensile stresses in the dam. A significant feature of the proposed 'pseudo-nonlinear' transient seismic analysis procedure is the adjustment of damping ratio to represent the energy dissipation caused by nonlinear behaviour of the structure. The procedure, however, provides no specific recommendations about the orientation of expected crack planes, that is crucial in determining the sliding stability of a cracked dam. In fact, it is very difficult to make reasonable predictions about the crack profiles from linear analysis results, because, upon initiation of a crack, extensive stress redistribution will take place, resulting in a crack profile that may be different altogether from the zones of principal stress concentrations predicted by the linear analysis. A crack profile gradually dipping downward from the upstream face towards the downstream face (Fig. 1.3(b)), if emerges in reality, will make the structure vulnerable to sliding and overturning instability. Nonlinear analyses are required to predict a realistic crack profile for application in the post-earthquake stability analysis, and also to determine the safety of dams and the potential collapse mechanisms during the earthquake. Progressive damage under cyclic loading, and the energy dissipation characteristics of a dam undergoing nonlinear behaviour can be realistically addressed in such analyses. The International Commission on Large Dams (ICOLD [89]) recommends that full, nonlinear, dynamic analysis be carried out to assess the safety of important dams under extreme intensity earthquakes, that produce internal forces exceeding the elastic strength capacity of dams. Evaluation of the possible crack profiles and the corresponding structural resistance is of topmost necessity to ensure a safe operation of the structures. The engineering community involved with dam safety problems is actively seeking reliable and efficient constitutive models to investigate the cracking response of concrete dams.

1.2 DEFINITION OF THE RESEARCH PROBLEM

A progressive strategy to determine the safety of concrete gravity dams is outlined in Fig. 1.4. The key issue in a numerical simulation procedure is the constitutive model for concrete cracking. Extensive research has been performed over the last two decades

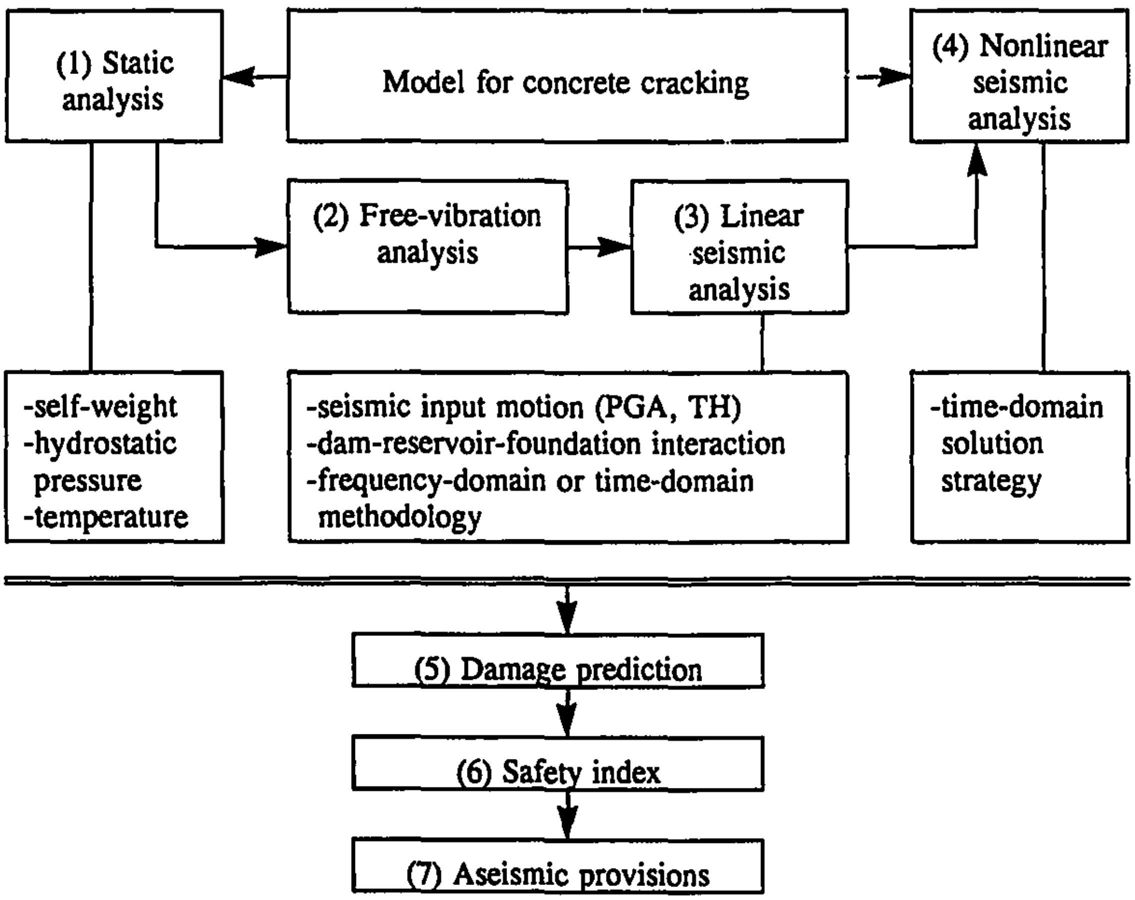

Figure 1.4 A progressive strategy for safety evaluation of concrete dams.

to comprehend the fracture behaviour of structural concrete having relatively small size aggregates. The concrete fracture theories and the relevant computational models have been primarily developed to predict the contribution of concrete fracture resistance on the ultimate strength of elementary structural members subjected to monotonic static loads. Fracture behaviour of concrete under oscillating dynamic loads, particularly for dam concrete, has not been adequately investigated in the past.

Concrete dams, generally not reinforced, are spatially configured to utilize the applied loads in normal operating conditions, such as the reservoir pressure in arch dams and the self-weight in gravity dams, to induce pre-compression inside the structure. Seismic excitations may result in removal of the pre-compression in certain parts of the structure. The fracture resistance of concrete plays a vital role at that state to determine the extent of cracking in the dam. The behaviour of mass concrete is considerably different from the structural concrete behaviour, due to the use of relatively large size aggregates and different construction methodology in dams. Constant exposure of dams to open atmospheric conditions, and the enormous size of these mass concrete structures also contribute to that difference in constitutive behaviour. Characterization of the behaviour of dam concrete is a formidable task due to the requirement of very large specimen sizes that make a realistic representation of the material embedded with large size aggregates. Few numerical investigations have been performed in the past using conventional static fracture models to predict the cracking behaviour of concrete dams subjected to non-seismic loading conditions (Ayari [5], Gioia et al. [73], Ingraffea [87], Linsbauer et al. [107,108]). Some of these models have also been applied with limited success to predict the seismic cracking behaviour of concrete gravity dams.

The extrapolation of fracture theories, derived on the basis of observed structural concrete behaviour, requires an adequate validation scheme to ensure a reliable prediction of the structural behaviour of dams (Fig. 1.5). Specific considerations are required in seismic fracture analyses, such as the strain rate effects, interaction with the generally used viscous damping model, and the closing and reopening of cracks. Finite

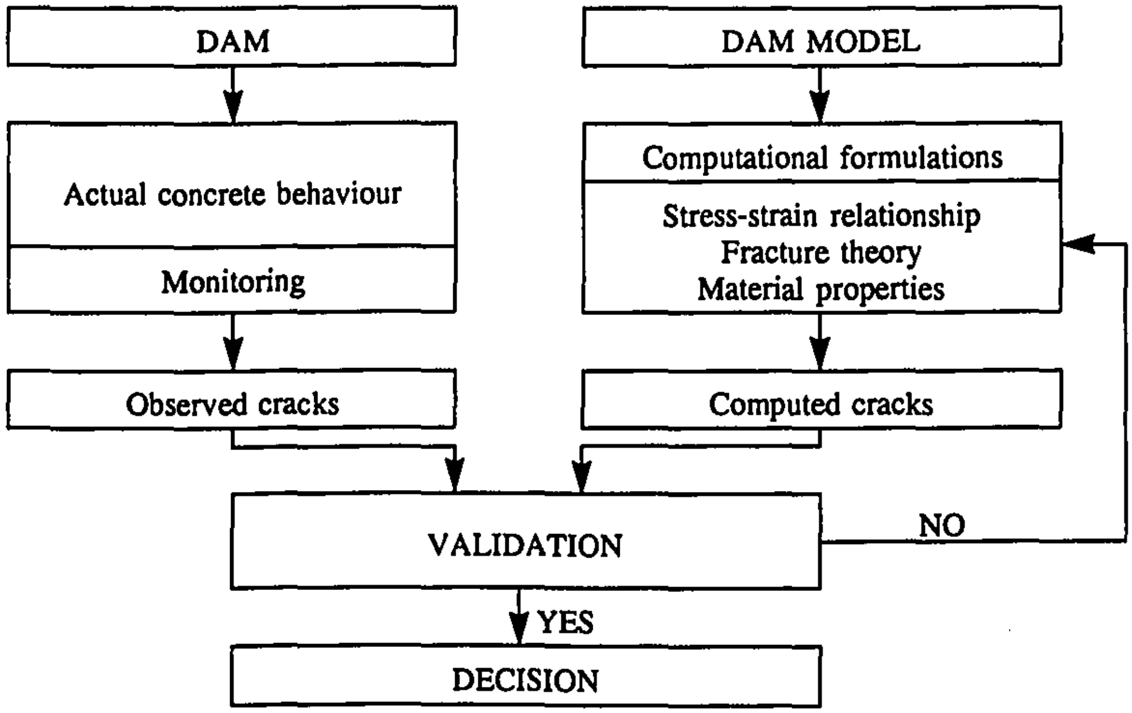

Figure 1.5 Validation of fracture theories and models (adapted from Lombardi [109a]).

element discretization of the giant structures, and mesh objectivity of the predicted response deserve special considerations. Seismic energy dissipation characteristics of concrete dams need to be investigated rigorously. Influences of severe environmental distress, such as the effects of seasonal temperature changes, should also be taken into consideration in the numerical models for concrete dams in Eastern Canada. Finally, guidelines for industrial application of the proposed constitutive models are strongly required.

1.3 OBJECTIVES OF THE RESEARCH

The following objectives have been considered in this research:

- to determine the state-of-the art of numerical models for fracture analysis of concrete gravity dams;

- to develop a nonlinear smeared fracture analysis model for investigating the cracking behaviour of mass concrete structures;
- to implement the constitutive models in a finite element analysis computer program for fracture analysis under static and seismic loading conditions;
- to develop a computational strategy for post-failure analysis of plain concrete structures subjected to static loading;
- to validate the proposed fracture analysis models by investigating the fracture response of concrete structures - experimentally and/or numerically studied by other researchers;
- to investigate the seismic fracture and energy response of concrete gravity dams;
- to investigate the influences of severe winter temperature condition on the seismic safety of concrete gravity dams located in Eastern Canada;
- to investigate the influences of dynamic interactions in the dam-reservoir-foundation system, on seismic fracture response of dams, and
- to provide recommendations for industrial application of the nonlinear fracture mechanics techniques in static and seismic analyses of concrete dams.

1.4 ORIGINAL CONTRIBUTIONS OF THE THESIS

To the best of the author's knowledge, the following items can be considered as original contributions of this thesis:

- A critical review of concrete constitutive models and their applications to seismic fracture analysis of gravity dams has been presented.
- Smeared crack analysis models have been developed based on the nonlinear fracture mechanics criteria, to apply in static and seismic fracture analyses of mass concrete structures.
- The strain softening of concrete due to micro-cracking, biaxial effects on the softening initiation criterion, shear deformations in the fracture process zone and the

subsequent rotation of crack directions, the dynamic magnification of fracture parameters, opening-closing-reopening of cracks, and the pre-seismic gravity and temperature load effects have been considered in the development of constitutive models.

- An incremental-iterative analysis technique has been developed to predict the ultimate resistance and the post-failure behaviour of plain concrete structures.
- Computational efficiencies of the tangent modulus approach and the damaged secant modulus approach, in finite element implementation of the strain softening constitutive models, have been investigated.
- An extensive validation procedure has been undertaken by predicting the static fracture response of plain concrete structures subjected to mode-I and mixed-mode loading conditions, and also by predicting the fracture response of a full scale gravity dam, all experimentally or numerically investigated in the past.
- A nonlinear fracture mechanics approach, in the framework of a smeared crack finite element analysis model, has been applied to predict the seismic fracture and energy response of concrete gravity dams. Influences of different viscous damping models on the seismic response of concrete dams have been studied.
- Severe winter temperature effects, and dynamic interactions with the reservoir and the foundation, have been considered in the fracture analysis of a standard section dam.

1.5 ORGANIZATION OF THE THESIS

Constitutive models and the finite element analysis program have been developed assuming that the structural behaviour can be represented with a plane stress finite element model. Figure 1.6 outlines the organization of the thesis.

Following the introduction of the thesis in this chapter, Chapter 2 presents a comprehensive review of the literature relevant to the main theme of the thesis. Spatial

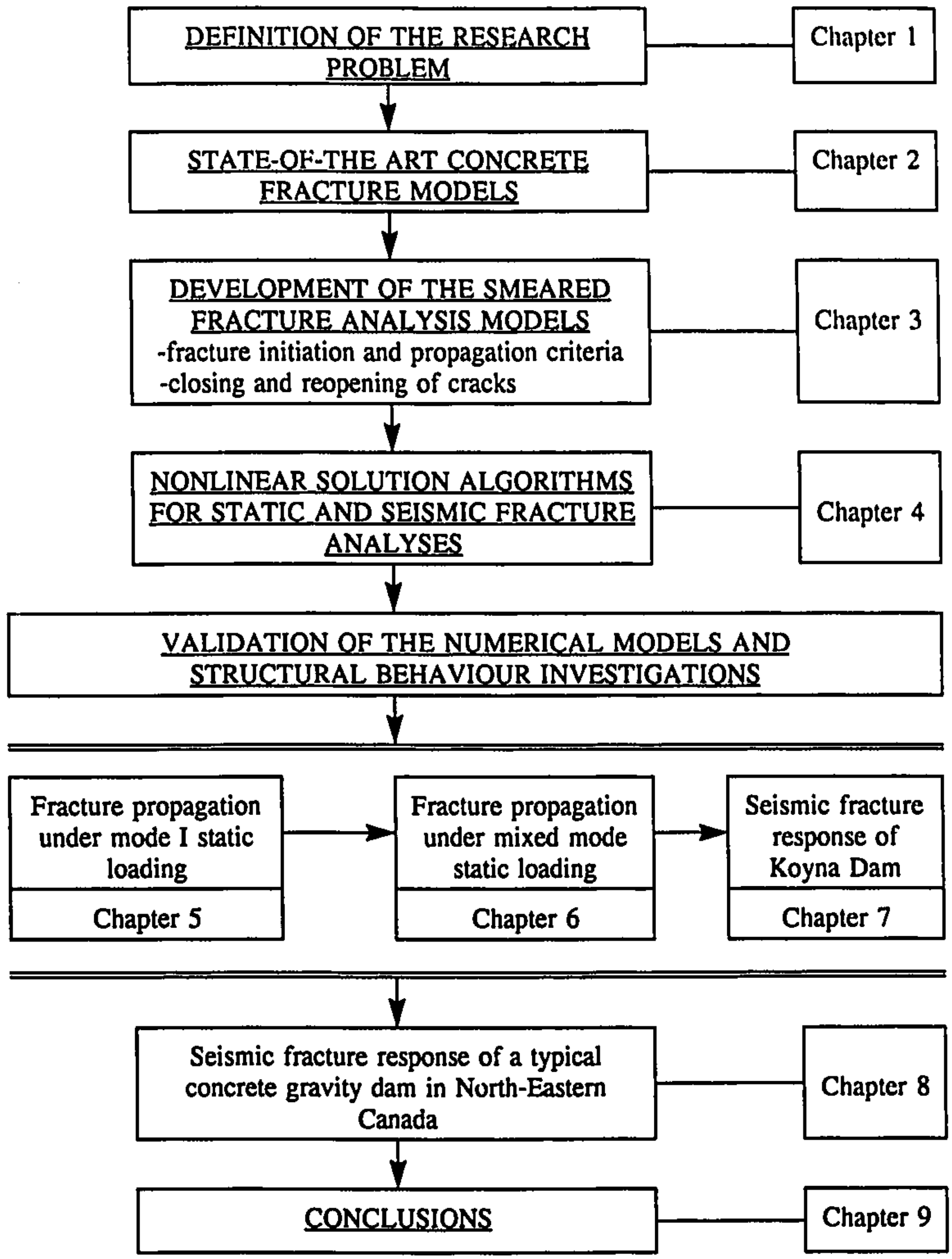

Figure 1.6 Organization of the thesis.

representation of cracks in a finite element model, various constitutive models that are generally applied in fracture analysis of concrete structures, and the material parameters required for the application of available constitutive models in dam fracture analyses are primarily reviewed in that chapter. A critical appraisal of the past investigations on seismic fracture response of concrete gravity dams is also presented.

Chapter 3 introduces the constitutive models developed for smeared fracture analysis of plain concrete structures. Different features of the proposed fracture analysis models, such as the softening initiation criterion, the strain softening of concrete and the fracture energy conservation, numerical simulation of the strain softening behaviour, shear deformations in the fracture process zone and the subsequent rotation of crack directions, and the opening-closing-reopening of cracks under oscillating loading conditions are outlined in this chapter.

Chapter 4 presents the nonlinear solution algorithms, adopted for the static fracture analysis under incremental force/displacement loadings, and for the time domain seismic fracture analysis of concrete dams. An indirect displacement control analysis technique is developed to predict the ultimate resistance and the post-failure behaviour of plain concrete structures subjected to static loads. The energy response of structures, the modelling of dynamic interactions in a dam-reservoir-foundation system, the viscous damping models for seismic fracture analyses of concrete gravity dams, the convergence indices of nonlinear solution algorithms, and the long term relaxation of temperature induced stresses are also discussed in this chapter.

Application of the computational models to predict the static fracture response of concrete members, subjected to mode I type loading conditions, is presented in Chapter 5. Computational efficiencies of the tangent modulus approach and the damaged secant modulus approach to model the strain softening behaviour of concrete, and the energy response of a simple beam subjected to the three-point loading are also investigated in this chapter.

Chapter 6 is devoted to predict the static fracture response of plain concrete structures subjected to mixed mode loading conditions. A notched beam subjected to shear loading, a model concrete gravity dam subjected to equivalent hydraulic loading conditions, and a full size concrete gravity dam subjected to the reservoir overflow are considered for investigations. The indirect displacement control analysis technique is applied to predict the post-failure behaviour of these plain concrete structures.

Application of the constitutive models to predict seismic fracture and energy responses of Koyna Dam, that experienced significant cracking due to an earthquake, is presented in Chapter 7. Sensitivity of the predicted response to analysis parameters and modelling assumptions is investigated in this chapter.

Chapter 8 presents a case study, investigating the seismic fracture response of a typical concrete gravity dam located in Eastern Canada. The severe winter temperature effects on seismic fracture response of the dam are specifically investigated in this chapter. The influences of reservoir and foundation interactions on seismic fracture response of the gravity dam are also studied.

Finally, the conclusions of this research program, and the recommendations for industrial application of the nonlinear fracture analysis model to predict the static and seismic responses of existing concrete dams are presented in Chapter 9. Recommendations for future research in this area are also listed in that chapter.

CHAPTER 2

SEISMIC FRACTURE ANALYSIS OF CONCRETE GRAVITY DAMS - STATE-OF-THE-ART

2.1 INTRODUCTION

A comprehensive model for seismic fracture analysis of concrete gravity dams comprises of three principal components, as outlined in Fig. 2.1: (i) a numerical scheme

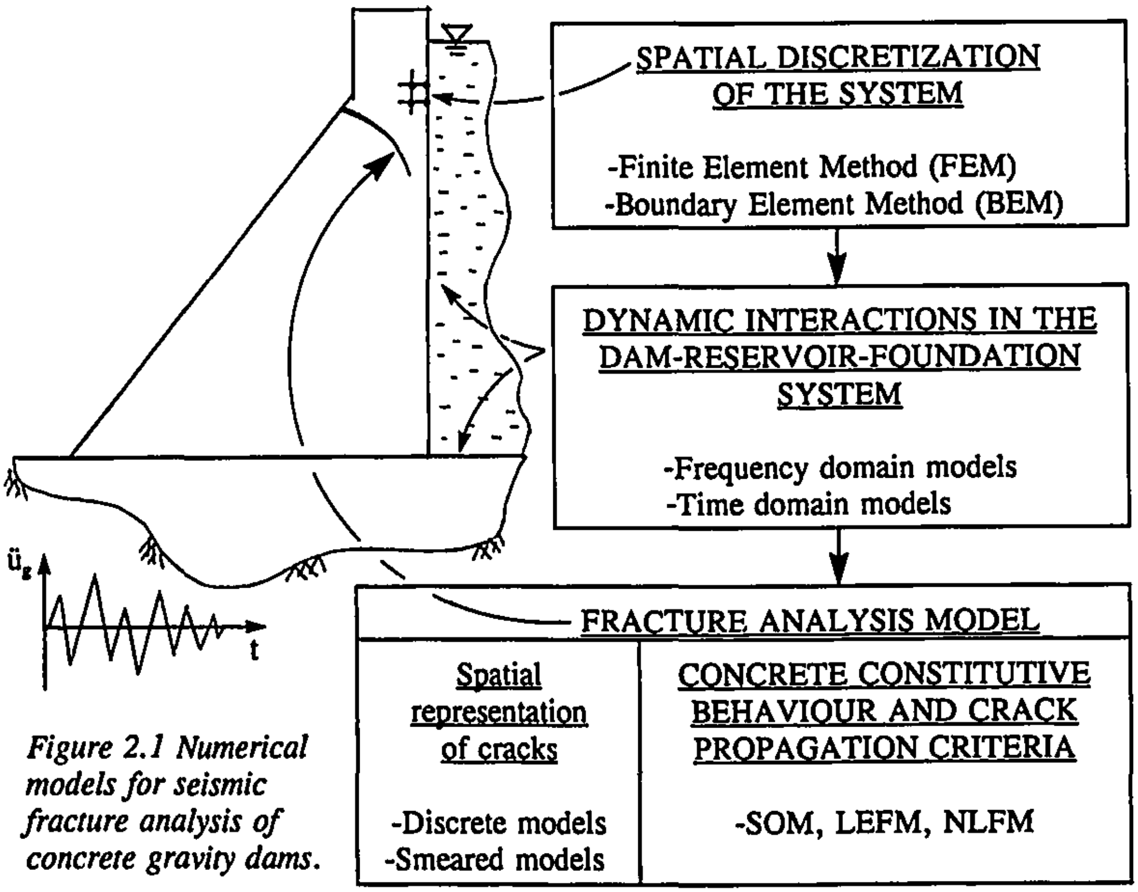

Figure 2.1 Numerical models for seismic fracture analysis of concrete gravity dams.

for spatial discretization of the system, (ii) a modelling procedure to take account of the dynamic interactions in the dam-reservoir-foundation system, and (iii) a fracture analysis model. The finite element method (FEM) has long been used for spatial discretization of concrete structures in both linear elastic and nonlinear analyses. Although fracture analysis using the boundary element method (BEM) has been presented in the literature (Pekau et al. [127,128]), extensive application of the method needs further compelling evidences regarding the reliability and computational efficiencies of the procedure. Discussions on fracture modelling procedures will be limited to finite element analysis techniques only.

The reservoir and foundation interaction effects have been rigorously considered in the past to study the linear elastic response of concrete dams subjected to a moderate intensity operating basis earthquake (OBE). A brief summary of various analytical models to take account of dynamic interactions in a dam-reservoir-foundation system is presented in section 2.2.

The fracture analysis model is by far the most important part of a nonlinear seismic response study of concrete dams. Several analytical methods have been proposed in the literature for two-dimensional finite element crack propagation analyses of concrete structures. Due to the lack of consistent results, and virtually impossible verifications because of the limited field experience in seismic cracking of concrete dams, the selection of a reliable constitutive model has become a complex task. Unlike the circumstances in an arch dam, where the nonlinear joint behaviour in the arch direction could be a decisive factor in determining the seismic stability of the structure (Niwa and Clough [117]), the structural response of gravity dams is mainly determined by gravitational forces. The concrete gravity dam monoliths, usually not keyed or lightly grouted, are expected to vibrate independently under severe ground excitations (Chopra [41]). Hence, two dimensional fracture propagation models seem appropriate for nonlinear seismic response analyses of concrete gravity dams. A state-of-the-art review on constitutive models for the two-dimensional finite element crack propagation analysis of concrete dams is presented in this chapter. Relative merits of various modelling procedures are critically examined. Special emphasis is put on the application of these models in seismic analyses of concrete dams, and the limitations of past investigations are examined. The phenomena of water penetration and uplift pressure on crack-open surfaces (Amadei et al. [1], Ayari [5]), the total/effective stress behaviour under pore water pressure (ICOLD [89]), and the hydrodynamic pressure gradient inside cracks (Tinawi and Guizani [150]), will not be discussed here. General aspects regarding the seismic analysis of concrete dams can be found in ICOLD[88,89], Jansen [92], NRC [114], and Priscu et al. [129].

2.2 DYNAMIC INTERACTIONS IN THE DAM-RESERVOIR-FOUNDATION SYSTEM

Dynamic interaction effects of the reservoir and the foundation are numerically modelled by adding mass, stiffness and damping terms to the corresponding dam system properties. Generally speaking, these added quantities are frequency-dependent. However, both frequency-dependent and independent approaches have been considered in the literature to model some or all of the interaction effects. Figure 2.2 summarizes the most common modelling procedures and solution techniques for a typical dam-reservoir-foundation system subjected to seismic excitations.

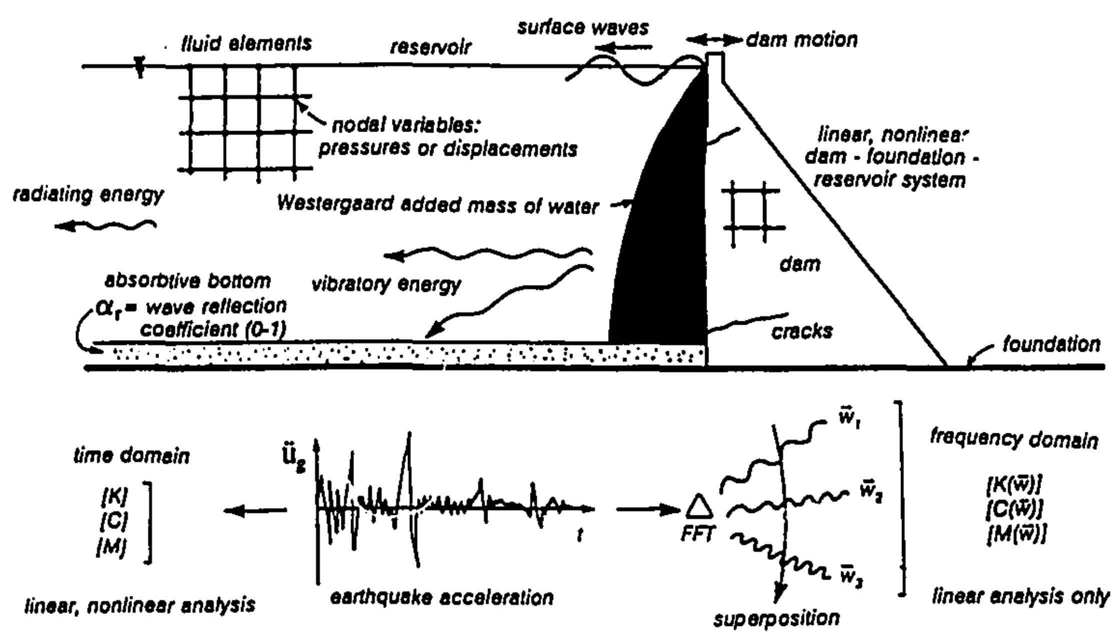

Figure 2.2 Dynamic interactions in a dam-reservoir-foundation system (Léger et al. [98])

One of the earliest attempts to model the reservoir interaction effects was due to Westergaard [159]. The hydrodynamic pressures were assumed to be generated by a parabolic body of incompressible water moving in unison with a rigid dam (Fig. 2.2). A deficiency of the traditional incompressible water approximation is that the hydrodynamic wave absorption effects of underlying reservoir bottom sediments cannot be taken into account (NRC [114]). Performance of the Westergaard added mass technique can be significantly enhanced by assigning damping properties on the upstream face of dams to simulate the energy dissipation in the reservoir (Léger and Bhattacharjee [103]).

Rigorous frequency-domain models of the reservoir and foundation interaction effects have been developed by A. K. Chopra and his co-workers (Chopra [41], Dasgupta and Chopra[46], Fenves and Chopra [65]). Dynamic interactions with the reservoir and the foundation have been observed to significantly influence the linear elastic seismic response of dams. The finite element analysis programs EAGD-84 (Fenves and Chopra[64]) and EACD-3D (Fok et al. [67]) are widely used in frequency domain analyses of two and three dimensional dam-reservoir-foundation models. El-Aidi and Hall [57,58] have conducted nonlinear seismic analyses of the Pine Flat Dam, taking into account some aspects of the reservoir and foundation interactions effects. The foundation has been modelled as a three-dimensional half-space with arbitrary dimensions. Frequency-independent foundation stiffness and damping coefficients have been derived by averaging the frequency-dependent properties. The reservoir has been modelled by using displacement based finite elements - the so called "mock" fluid elements (Cook et al. [42]). Energy radiations in the reservoir upstream direction and at the reservoir bottom are approximately modelled by applying non-reflecting boundary conditions. Time-domain models to represent the dam-reservoir-foundation interaction effects in finite element analyses are also available in Fenves and Vargas-Loli [66], Kuo [96], Léger et al. [99], and Wilson and Khalvati [160]. Boundary element methods are being increasingly used to model the reservoir and the foundation in seismic analyses of concrete dams (Feltrin et al. [62], Humar and Chandrashaker [86], Medina et al. [111]).

2.3 FINITE ELEMENT REPRESENTATION OF CRACKS

Two approaches have generally been followed for the spatial representation of tensile crack propagation in finite element analysis of concrete structures: the discrete crack model and the smeared crack model. Both models have been used over the decades because of the advantages and the inconveniences that they bring to the constitutive models in finite element crack propagation analysis of concrete structures.

2.3.1 Discrete crack propagation model (DCPM)

In the DCPM (Ngo and Scordelis [116]), cracks are represented as discrete gaps along the inter-element boundaries. The propagation of cracks is determined by strength or fracture mechanics based constitutive models. The progressive physical discontinuity in a structure is reflected instantaneously in the finite element model by modifying the mesh during the analysis (Fig. 2.3(a)). It is generally argued that the nonlinear response

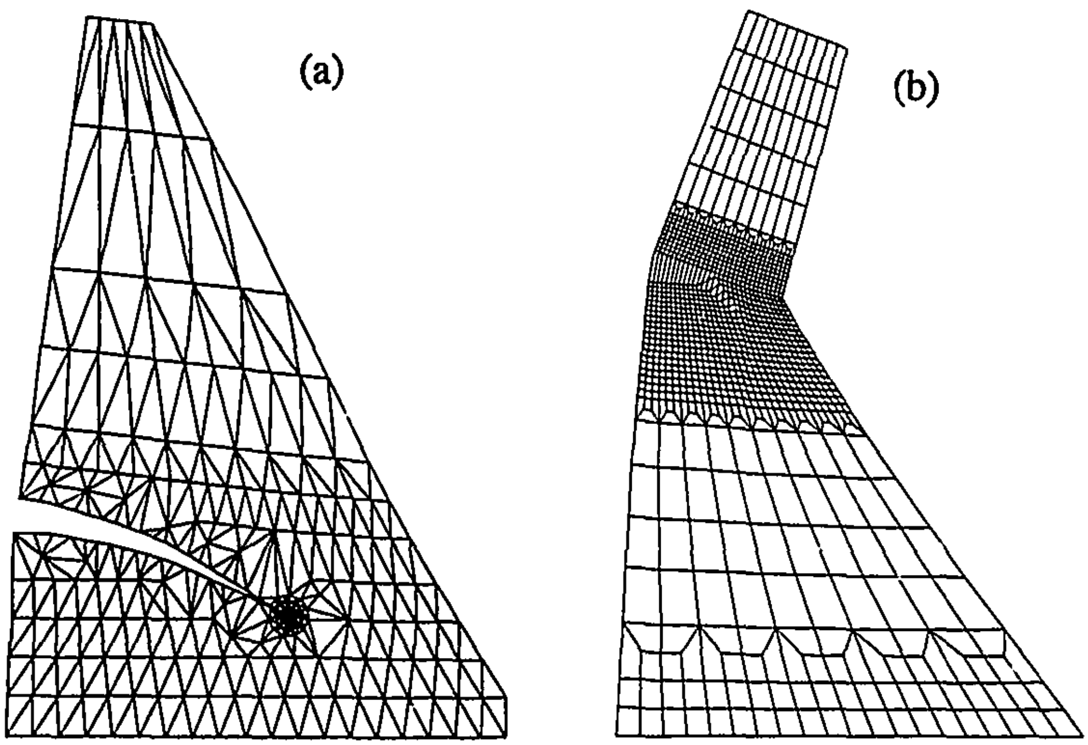

Figure 2.3 (a) Discrete crack analysis (adopted from Carpinteri et al. [35]), and (b) smeared crack analysis.

of concrete dams is dominated by a few discrete long cracks. From this consideration, the discrete crack model may be a sensible choice for dam fracture analysis. Specific advantages of the DCPM are the abilities to consider explicitly the water penetration and uplift pressure inside cracks, the aggregate interlock in a rough crack, and the direct estimation of crack-opening-displacement (COD) profile. The principal disadvantages in applying this model are the difficulty and high computational cost due to continuous change of the finite element topology during the analysis, and the non-objective effects of finite element meshes and crack length increments. A special case of discrete crack modelling is the application of interface elements to represent the *a priori* weak joints in the system, such as the dam-foundation interface and construction joints (Goodman et al. [74], Graves and Derucher [75], Hall and Dowling [78], Hohberg [85], Léger and Katsouli [97], O'Connor [119]).

2.3.2 Smeared crack propagation model (SCPM)

In the SCPM (Rashid [131]), fracture propagation is idealized as a blunt front smeared over a band of finite elements. After the initiation of fracture process, determined by a suitable constitutive model, the pre-crack material stress-strain relationship is replaced by an orthotropic relationship. The material reference axis system is aligned with the fracture direction in orthotropic formulations. The tension stiffness normal to a crack plane is either eliminated suddenly or a gradual stress release criterion is applied. Thus, only the constitutive relationship is updated with the propagation of cracks, and the finite element mesh is kept unchanged (Fig. 2.3(b)). The main advantage of this model lies in its simplicity and cost effectiveness, although the physical nature of crack representation is questionable. The tendency of smeared crack models to cause diffused crack patterns, and the directional bias caused by a slanted finite element mesh are still significant computational difficulties. However, the model is very effective in complex structural analyses, such as the seismic response study of concrete gravity dams, when the location and orientation of cracks may not be known *a priori*. Moreover, pre-existing diffused crack patterns in a structure can be efficiently represented by the smeared crack finite element model.

2.4 CONSTITUTIVE MODELS FOR CRACK PROPAGATION

A comprehensive constitutive model for fracture propagation analyses should describe the pre-fracture material stress-strain behaviour, the fracture initiation and propagation criteria, and the closing and reopening of cracks in a cyclic load analysis. The usual practice in concrete fracture analyses is to presume a linear elastic behaviour before the onset of tensile fracture process. The behaviour of concrete under high compressive loads is predominantly nonlinear. However, the maximum compressive stress in concrete gravity dams is expected to be low even under severe ground excitations. A reasonable assumption of linear elastic behaviour under compressive loading has been applied in almost all previous investigations related to dams.

The general practice in concrete fracture analyses is to assume the initiation of new cracks in a homogeneous structure, when the principal tensile stress reaches the tensile strength of concrete. The diversity in various fracture analysis models lies in the definition of fracture propagation criteria after a crack is introduced in the structure. Major developments in the realm of crack propagation analysis and their relative merits are discussed in the following sections.

2.4.1 Strength based criteria

The early investigations on cracking of concrete structures have mostly applied simple criteria based on the concepts of strength of material (SOM). A crack is assumed to propagate when the predicted stress or strain at the crack-tip exceeds a critical value representing the tensile strength of material. A sudden release of stress on the fracture plane is commonly assumed upon reaching the peak tensile strength. The gradual release of stress with increasing strain has also been used, mainly for the numerical stability of finite element crack propagation analyses (Lin and Scordelis [106]). The SOM criteria of crack propagation have been used in both discrete (Skrikerud and Bachmann [146]) and smeared (Bathe and Ramaswamy [8]) crack propagation finite element models. Comparison of the computed tensile stress with the material tensile strength is not rational in a cracked structure, because, spurious results may be obtained depending on the size of finite elements lying ahead of the propagating crack. The lack of finite element mesh objectivity of the SOM criterion has been demonstrated in Bažant and Cedolin [11].

2.4.2 Fracture mechanics criteria

Fracture mechanics is the theory to deal with propagation of cracks, and is based on the concept of energy dissipation in the structure undergoing fracture process. It has been recognized only recently that the tensile failure mechanism in concrete structures is different from the usual strength based concept, due to the progressive growth of fracture process (ACI [2]). Three elementary modes of failure are recognized in the fracture theory (Fig. 2.4). Modes I and II, the opening mode and the planar shear mode,

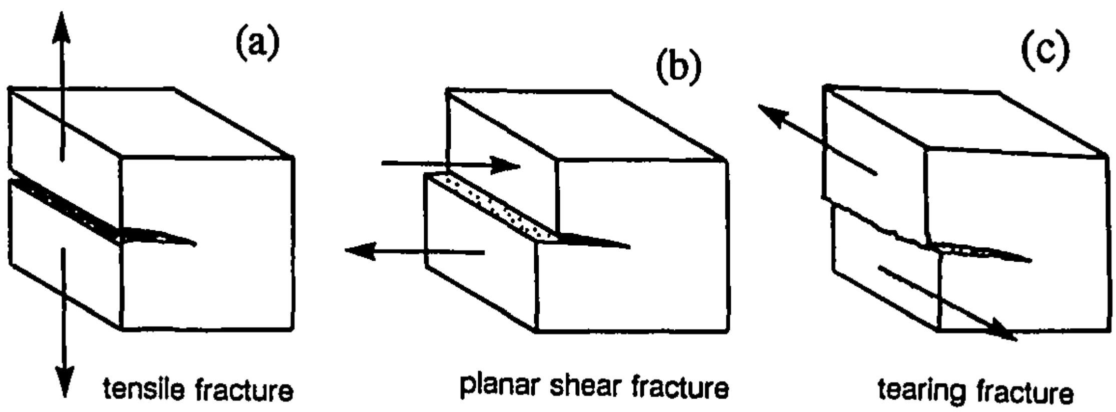

Figure 2.4 Modes of failure: (a) mode I, (b) mode II, and (c) mode III.

are usually considered in a two-dimensional fracture analysis. The third one, tearing mode (mode III), is considered in three-dimensional fracture propagation studies. Fracture mechanics crack propagation models can be broadly classified into two categories: the linear elastic fracture mechanics (LEFM) models, and the nonlinear fracture mechanics (NLFM) models.

According to LEFM, the fracture process occurs right at the crack-tip and the entire material volume remains elastic (Fig. 2.5(a)). The stress field around the tip of a sharp

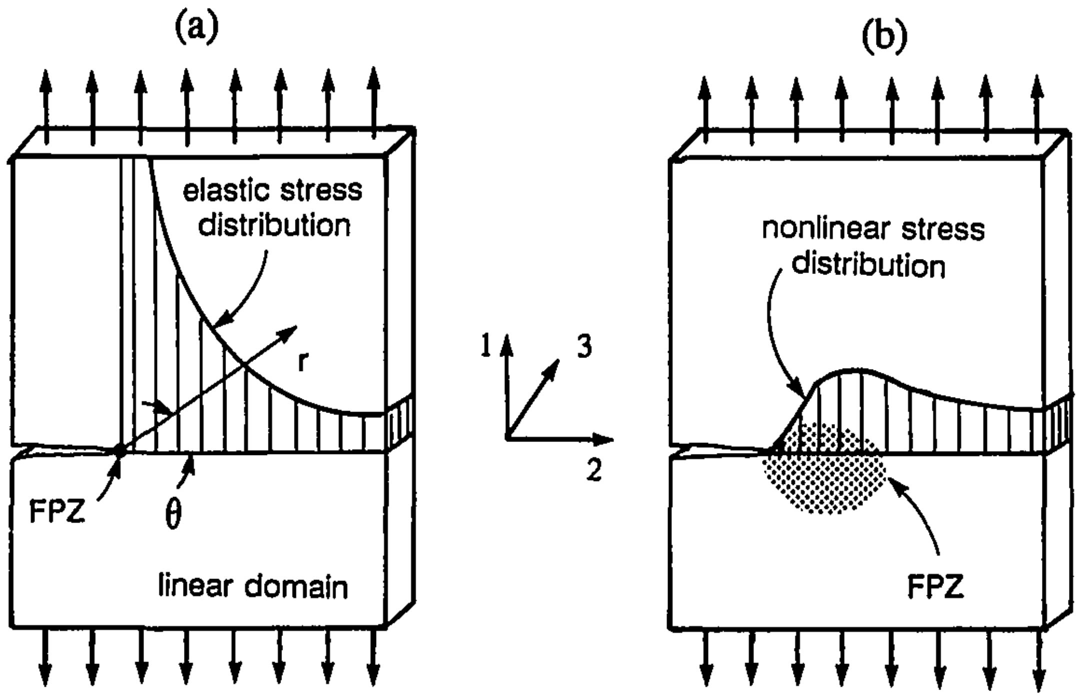

Figure 2.5 Fracture process zone (FPZ): (a) LEFM, and (b) NLFM.

crack is characterized by the stress intensity factors, K_i, determined from linear elastic solutions:

$$\begin{Bmatrix} K_I \\ K_{II} \\ K_{III} \end{Bmatrix} = \lim_{r \to 0, \theta \to 0} \sqrt{2\pi r} \begin{Bmatrix} \sigma_{11} \\ \sigma_{21} \\ \sigma_{13} \end{Bmatrix} \tag{2.1}$$

where σ_{ij} are the near crack tip stresses, r and θ are polar co-ordinates, and K_I, K_{II}, and K_{III} are the stress intensity factors (SIF) associated with three fundamental fracture modes. Once the SIF have been numerically (or analytically) computed, and the material fracture toughness, K_{Ic}, experimentally determined, a suitable functional relationship is applied as a criterion for propagation of existing cracks:

$$f\,(K_I, K_{II}, K_{III}, K_{Ic}) = 0 \tag{2.2}$$

Several functional forms of Eqn. (2.2) have been proposed in the literature. A review of various developments in the relevant field is available in Ayari[5]. In LEFM models, a sudden release of stress is assumed with the extension of cracks. Most investigators adopt the discrete crack propagation finite element model (DCPM) or an equivalent technique with the LEFM crack propagation criteria. Pekau et al. [127,128] have developed discrete crack analysis models to apply the LEFM criterion in boundary element models of concrete structures.

The question of whether or not the fracture process in concrete can take place at a localized point has been a subject of intense debate for quite long time. In reality, the fracture process zone (FPZ) must have a finite size (Fig. 2.5(b)). It is argued that the LEFM can be applied if the FPZ is much smaller than the dimension of the structure under consideration. Very large concrete structures, such as dams, are usually cited as the possible candidates for application of LEFM models. However, no rigorous experimental evidence has ever been put forward appraising the extent of FPZ in the dam concrete. The disregard of nonlinear behaviour in the FPZ is an assumption of unknown consequences in determining the local fracture behaviour of structures. It seems appropriate to consider the nonlinear behaviour in the FPZ, if the localization of crack profiles is a primary objective of the finite element analysis. In a gravity dam, a relatively stiff structure, crack opening displacements may be very small, which means that a long fracture process zone may exist (Dungar et al. [55]). Moreover, the size of FPZ may not be negligible in comparison to the dimension of concrete gravity dams around the neck region, which is the most critical location for seismic induced cracking. Hence the argument of a small fracture process zone in comparison to the thickness of the structure, usually cited to apply LEFM models, may not be true even for concrete gravity dams. The choice between LEFM and NLFM models may also be influenced by the strain rate under consideration. Under very slowly applied loads (Bažant et al. [25]), and also under impulsive loads (Du et al. [54], Yon et al. [162]), the concrete fracture behaviour seems to be adequately predicted by the LEFM models. In the intermediate range from short term static loading to seismic induced strain rates, the NLFM models considering the strain softening behaviour in the FPZ appear to be more appropriate.

The primary characteristic of nonlinear fracture mechanics (NLFM) theory is the recognition of strain softening behaviour of concrete in the FPZ. Two apparently different models have been proposed in the literature considering only mode I nonlinear fracture propagation in concrete. The most referenced work is due to Hillerborg et al.[82], where the existence of FPZ has been characterized as a fictitious crack lying ahead of the real crack tip (Fig. 2.6(a)). The behaviour of concrete in the FPZ is represented by a diminishing stress, σ, versus crack-opening-displacement (COD), δ, relationship; the tensile resistance is ceased at a critical COD value, δ_f (Fig. 2.6(a)). The area under a σ-δ curve represents the energy, G_f, dissipated during fracture process on a unit area:

$$G_f = \int_0^{\delta_f} \sigma(\delta)\,d\delta \tag{2.3}$$

G_f is a material property and often referred as the fracture energy or the specific fracture energy. The special feature of Hillerborg's fictitious crack model is the dissipation of energy over a discrete line crack. This basic nature of the model has made its extensive applications possible in discrete crack propagation analyses. In some recent studies, the key assumption of Hillerborg's model, that the tensile stress at the tip of a fictitious crack is equal to the tensile strength of concrete, has been modified using the concept of singular stress distribution at the fictitious crack tip (Yon et al. [162]). LEFM models, in the context of a discrete crack propagation analysis, have also been modified to take account of the effects of FPZ, using additional material parameters. The two-parameter model proposed by Jenq and Shah [93] is one those equivalent elastic crack models.

Bažant and Oh [15] have proposed that the energy dissipation in a heterogeneous material like concrete must involve a finite volume. The fracture process is assumed to propagate as a blunt front (Fig. 2.6(b)). The width of a blunt crack (or a band of micro-

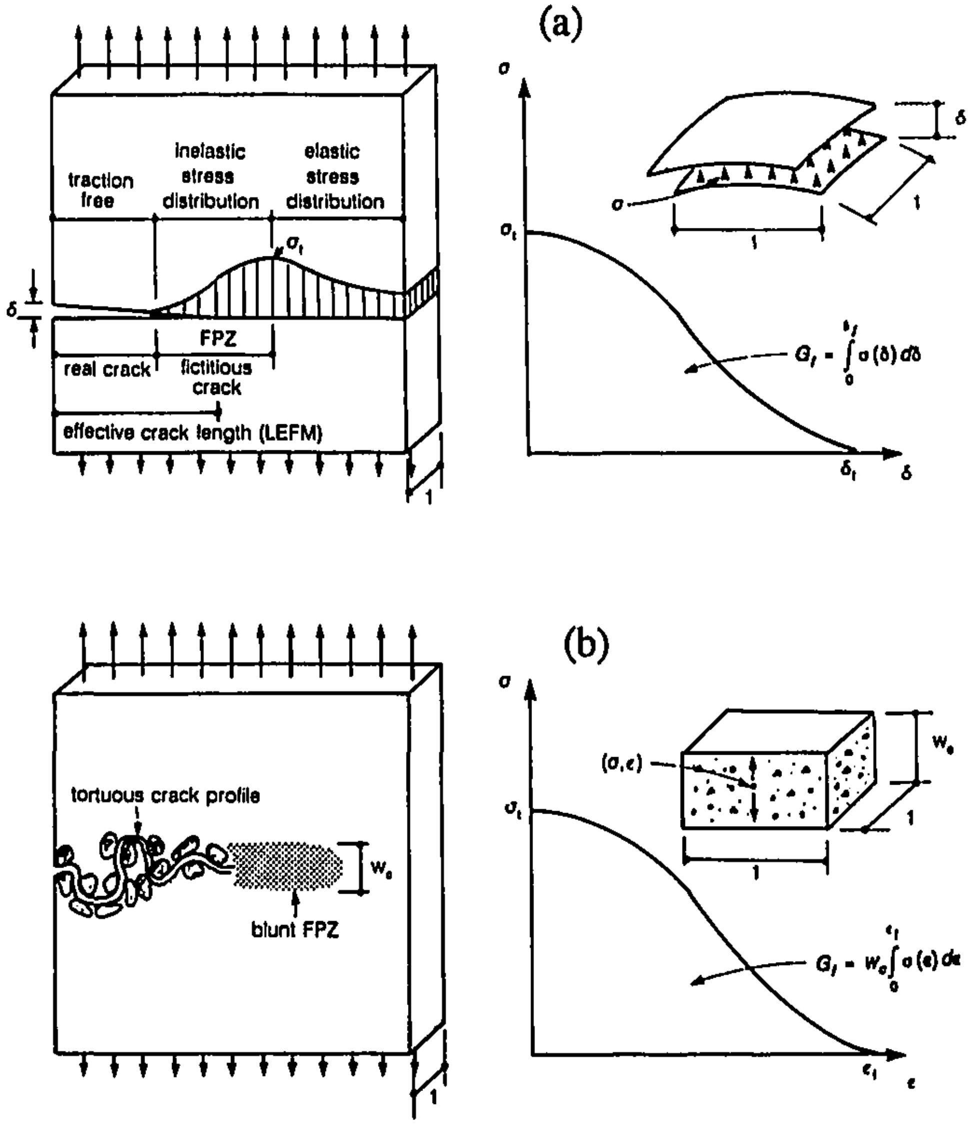

Figure 2.6 NLFM models: (a) fictitious crack model, and (b) crack band model.

cracks), w_c, represents the zone over which the distribution of micro-cracks can be assumed uniform. The strain softening behaviour of concrete in the FPZ is represented by a stress-strain relationship (Fig. 2.6(b)) and the fracture energy, G_f, is given by:

$$G_f = w_c \int_0^{\epsilon_f} \sigma(\epsilon)\,d\epsilon \qquad (2.4)$$

An inherent characteristic of the proposed crack band model is the smeared nature of crack distribution over a band width, w_c, which is usually assumed three to four times the maximum aggregate dimension. Smeared nature of the crack band model is a tempting feature for application in finite element analyses when the direction and the location of a crack propagation are not known *a priori*. Application of the crack band model in its original form to smeared fracture propagation analyses requires the size of finite elements be limited to three or four times the maximum aggregate dimension; a size often considered stringent for any practical finite element analysis of large concrete structures. Special finite element techniques have been proposed to ease this limit on the element size by smearing the fracture process effects over a zone of finite elements, and the average stress-strain relationship is adjusted to conserve the fracture energy (Dahlblom and Ottosen[45], de Borst and Nauta[47], Oliver[121]). Key issues pertinent to the finite element implementation of the fracture energy conservation principle are discussed in the following sections.

2.4.3 Conservation of fracture energy in smeared crack models

The development of cracks in concrete passes through stages, as outlined in Fig. 2.7(a). Generally a linear elastic relationship is assumed until the peak strength, σ_i, is reached, followed by a linear strain softening at the post-peak phase. The area under the average stress-strain curve of a finite element, undergoing the fracture process, is adjusted such that the dissipated fracture energy, G_f, for a unit area of crack extension, remains independent of the element characteristic dimension, h_c (Fig. 2.7(b)). Slope of the softening branch, E^t (Fig. 2.7(b)), is adjusted according to the following relationship to conserve the fracture energy:

$$E^t = \frac{\sigma_i^2 E}{\sigma_i^2 - 2EG_f/h_c} \tag{2.5}$$

If the peak strength, σ_i, the elastic modulus, E, and the fracture energy, G_f, are known for the material, the strain softening modulus for a particular element size, h_c, can be determined from Eqn. (2.5). For cracks parallel to the sides of a square shaped element, the characteristic dimension, h_c, can be taken equal to the element dimension across the crack plane (Fig. 2.7(b)).

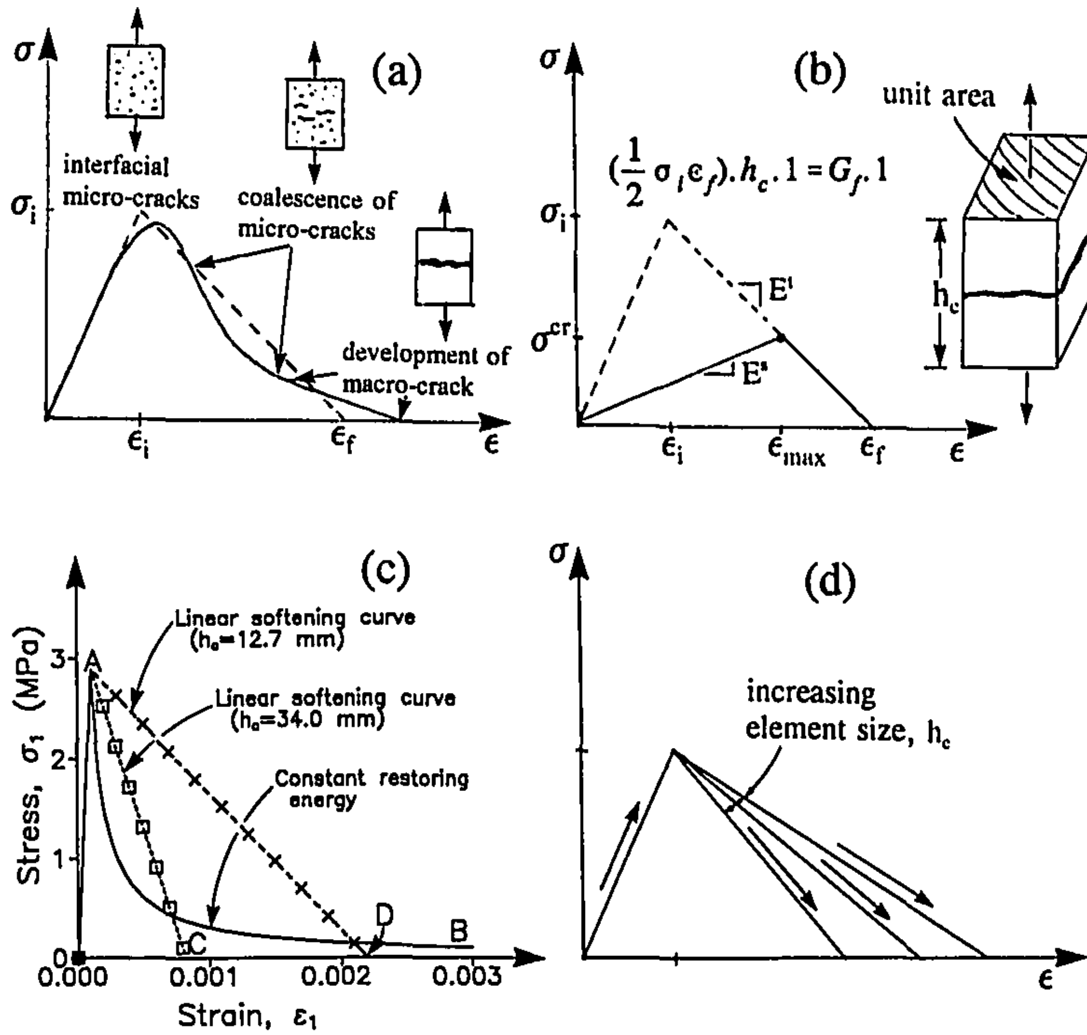

Figure 2.7 Strain softening constitutive models: (a) development of cracks (adapted from Nomura et al.[118]), (b) fracture energy conservation, (c) limitations of the linear softening model, and (d) adjustment of constitutive models depending on the element size.

In finite element analyses, the softening modulus defined by Eqn. (2.5) is generally applied to determine the degradation of material strength and stiffness (E') properties (Fig. 2.7(b)) (Bažant and Oh [15]). The restoring energy capacity of strain softening elements, however, does not follow that degradation pattern; it rather varies depending on the element size, that represents a zone of homogeneous material behaviour. The curve AB in Fig. 2.7(c) is the locus of points representing a constant recoverable tensile strain energy per unit volume:

$$\frac{1}{2}\sigma_1 e_1 = \frac{1}{2}\sigma_t e_t = constant \tag{2.6}$$

A softening relationship following the no-decay curve AB would imply that the material stiffness, E^t, is degraded with increasing strain, but the strain energy restoring capacity remains unchanged. Apparently, the curve AB in Fig. 2.7(c) represents the upper-bound of all softening models. To compare with the linear softening model, two structural concrete elements of characteristic dimensions 34.0 mm and 12.7 mm, subjected to a uniaxial loading condition, are considered. The material properties of peak strength σ_t=2.886 MPa, fracture energy G_f=40.29 N/m, elastic modulus E=27413 MPa, and the maximum aggregate size d_a=12.7 mm are taken as reasonable estimates of structural concrete properties (Bažant and Pfeiffer[20]). Using the above mentioned properties, line AC in Fig. 2.7(c) represents the linear softening relationship corresponding to the element characteristic dimension of 34.0 mm, which is slightly smaller than $3d_a$ - the optimum size of finite elements recommended by Bažant and Oh [15] for crack band analysis. Slope of the line AC, that approximately follows the curve AB in average sense, is equal to the empirical definition of the softening modulus:

$$E^t = \frac{-0.482E}{0.391+\sigma_t}\ ; \quad (data\ in\ MPa) \tag{2.7}$$

given by Bažant and Oh [15] to apply with the crack band model. When the element size is reduced to 12.7 mm, one-third of the recommended crack-band width, the linear softening line AD (Fig. 2.7(c)) proceeds wide apart from the no-decay curve before approaching to zero tensile resistance at a finite strain, that has been calibrated to conserve the fracture energy. This situation implies that the restoring energy capacity of the element does not begin to decline after reaching the peak strength even though the stiffness and the strength of the material start to degrade. The progress of softening along most part of the line AD will involve a positive external work done on the finite element, since the internal restoring energy increases with an increasing tensile strain. The local adjustment of constitutive formulations with a linear softening model, thus, violates the fundamental nature of unstable softening behaviour after reaching the peak strength. The precise shape of softening curves, therefore, exerts a significant influence on the predicted response (ACI [2]). A bi-linear softening curve is often applied to interpret the experimentally determined fracture energy values (Brühwiler [31], Nomura et al. [118]). The 'nonlocal' damage mechanics concept (Bažant and Lin [22]) is a possible remedy to the shortcomings of local smeared fracture models in the cases of extreme finite element mesh refinement. However, the application of 'nonlocal' model is impractical in large scale structural analysis, such as for dams, where the refinement of finite element meshes and the associated spatial averaging of local response quantities are generally limited by computational costs. A linear softening model, applied with element sizes not less than three to four times the maximum aggregate dimension, is a reasonable choice for fracture analyses of massive concrete gravity dams.

The softening modulus E^t, given by Eqn. (2.5), becomes steeper for an increasing value of h_c (Fig. 2.7(d)) up to a certain limit; afterwards an unrealistic snap-back appears in the tensile stress-strain relationship of concrete. In the limit case, the softening constitutive model degenerates to the traditional elasto-brittle failure criterion, dissipating the stored elastic strain energy instantly upon reaching the tensile strength of material. The maximum finite element size, h_c^{max}, that can be modelled with a linear strain-softening constitutive model is determined from Eqn. (2.5) as follows:

$$h_c^{\max} \leq \frac{2EG_f}{\sigma_i^2} \tag{2.8}$$

For typical dam concrete properties of E=30000 MPa, G_f=200 N/m, and σ_i=2 MPa, the limiting value is $h_c^{max} \leq 3$ m. This limit on maximum dimension, given by Eqn. (2.8), was considered stringent in the past, for large scale finite element analyses at a reasonable cost. To circumvent this limit on the size of finite elements, and at the same time respect the principle of conservation of energy, one proposition is to reduce the fracture initiation stress, σ_i, with the increasing finite element size, and assume an elasto-brittle failure criterion for element sizes greater than h_c^{max} (Fig. 2.8(a)). This is the so called Size Reduced Strength (SRS) criterion (Bažant and Cedolin [11,14], Bažant [16]). The size reduced strength criterion (or in other words the elastic fracture criterion) can be criticized for two reasons; (i) the size independent critical COD value, δ_f, of no

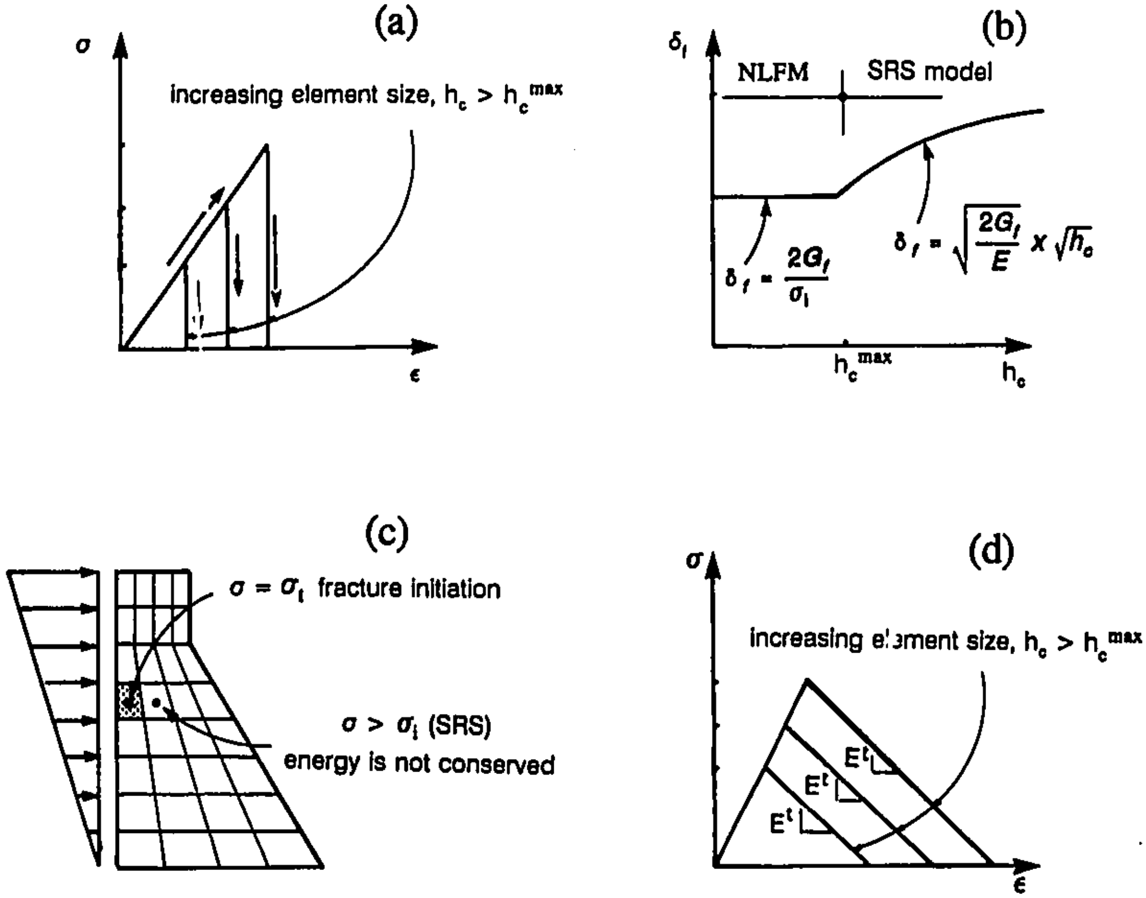

Figure 2. 8 Size adjustment of the constitutive relationship in smeared crack models.

tensile resistance, implied by the conservation of fracture energy in a nonlinear fracture model is violated (Fig. 2.8(b)), and (ii) when applied with a strength based crack initiation criterion, the principle of fracture energy conservation is likely to be violated in the interior elements as well as in the exterior element (Fig. 2.8(c)). A significant numerical side effect of the elasto-brittle SRS failure criterion is the generation of spurious shock waves in the finite element model (El-Aidi and Hall [57]). Constitutive models with a constant softening modulus, E^t, and a size reduced softening initiation stress (Fig. 2.8(d)) for conserving the fracture energy (Bažant [18]), appear to be based on weaker theoretical considerations and non-existent experimental justifications. Moreover, a size dependent reduction of the peak strength towards a zero value is neither realistic nor can be justified numerically (Tang et al. [149]). The limit on maximum size of finite elements, thus, appears to be a requirement to ensure the reliable application of nonlinear fracture mechanics criteria in a smeared crack propagation analysis.

The application of NLFM models in dynamic analyses requires the definition of unloading/ reloading behaviour during the fracture process. Very few studies have been reported in the literature on this aspect. Bažant and Gambarova [17] proposed a nonlinear stress-strain relationship for closing/reopening behaviour of partially open cracks, as depicted in Fig. 2.9(a). A simplified secant modulus formulation (Fig. 2.9(b)) was

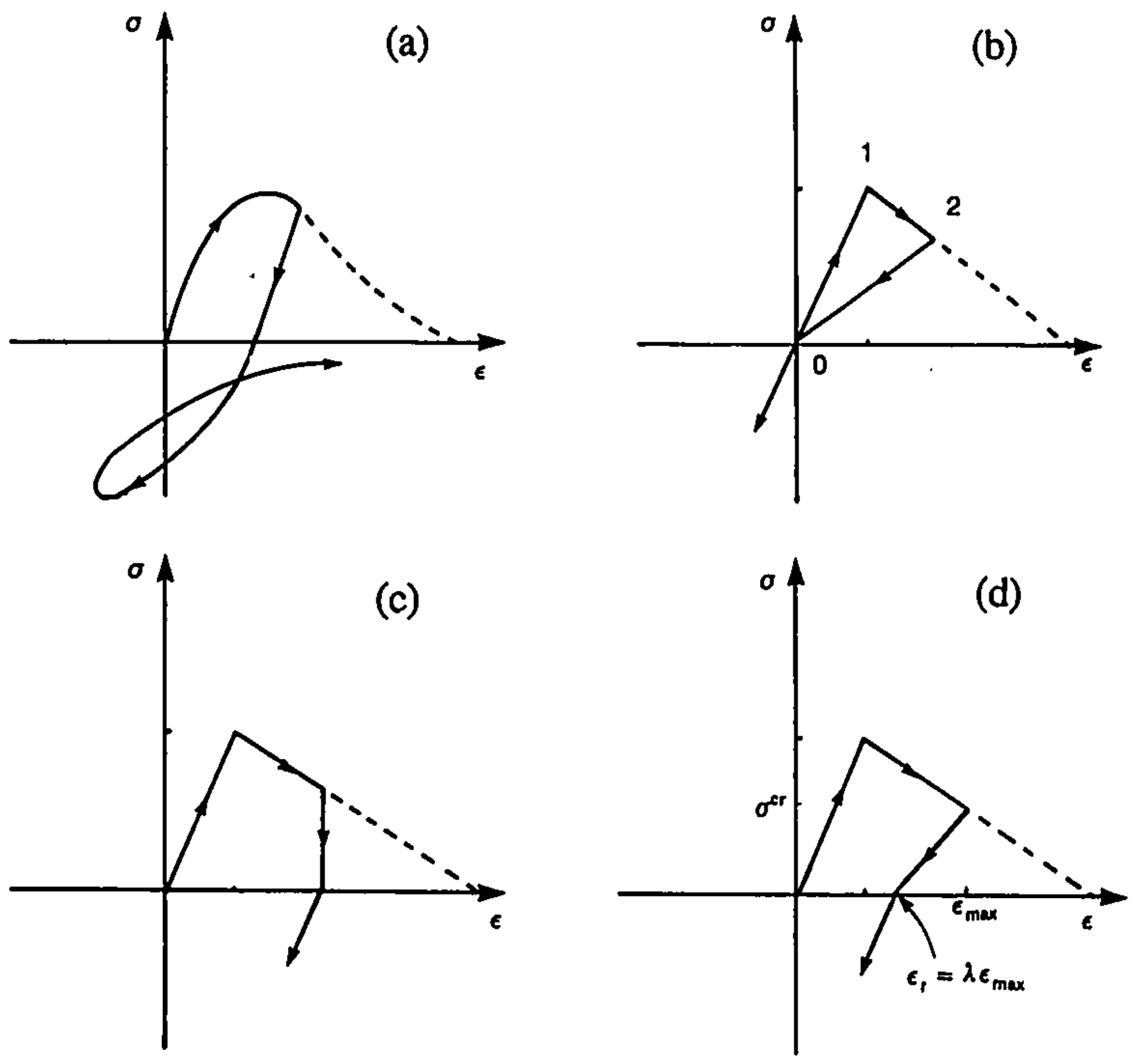

Figure 2.9 Closing and reopening of partially formed cracks.

adopted by de Borst and Nauta [47] to represent the closing of partially open cracks. Gambarova and Valente [70] assumed a sudden stress release when the closing of partially open cracks was detected at any instant of the fracture process (Fig. 2.9(c)). Dahlblom and Ottosen [45] proposed the following relationship for closing/reopening behaviour of partially fractured concrete:

$$\epsilon = [\lambda + (1-\lambda)\frac{\sigma}{\sigma^{cr}}]\epsilon_{max} \qquad 0\leq\lambda\leq1 \tag{2.9}$$

where λ is the ratio between the residual strain upon closing of cracks and the maximum strain of open cracks (Fig. 2.9(d)). It appears that the techniques applied by de Borst and Nauta [47], and Gambarova and Valente [70], are subsets of this generalized model with $\lambda=0$ and 1 respectively. The physical behaviour of concrete during closing and reopening of partially formed cracks is yet to be investigated rigorously.

2.4.4 Shear resistance of fractured concrete

After the initiation of fracture process on a plane perpendicular to the direction of principal tensile stress, it is not unlikely that shear deformations will occur on the partially formed fracture planes, resulting in a rotation of the principal stress directions. Bažant and Oh [15] ignored the shear deformation on fracture planes, and the material stiffness matrix was derived considering only the normal strain components. This formulation is not compatible with the linear elastic isotropic stiffness matrix of the initial state. The shear deformation in FPZ was latter considered in the so called 'crack band microplane model' (Bažant and Gambarova [17]). Gambarova and Valente [70] retained the initial shear modulus unchanged until the complete fracture had taken place, and applied an aggregate interlock model at the post-softening state. The concept of simple shear 'retention' factor (Suidan and Schnobrich [147]) was adopted by de Borst and Nauta[47], and Gajer and Dux [69], to derive the shear stiffness of crack bands. The simplified approach of applying a constant shear resistance factor ignores the dependence of crack shear stiffness on the crack-opening-displacement (COD), and causes significant stress locking in smeared crack analyses (El-Aidi [56], Rots [139]). Definitions for variable shear resistance factor were also proposed for partial alleviation of the stress locking problem (Dahlblom and Ottosen [45]).

The 'fixed' smeared crack models, where the fracture plane is fixed perpendicular to the major principal stress direction at the instant of softening initiation, generally cause a significant stress locking due to the zigzag propagation of crack bands in a finite element model. In reality, cracks of one direction at a local point may close and lock in shear while cracks of another direction may form (Bažant and Lin [22]). In some computational models, the orthotropic material reference axis system is rotated when the principal stress direction deviates by a certain amount from the direction that initiates the crack (Cope et al. [43], Gupta and Akbar [76]). In a strain softening constitutive model, the rotating principal stresses (σ_1, σ_2) and principal strains (ϵ_1, ϵ_2) can be maintained coaxial by using an implicit definition for the softened shear modulus, G^s (Bažant [13]):

$$G^s = \frac{\sigma_1 - \sigma_2}{2(\varepsilon_1 - \varepsilon_2)} \tag{2.10}$$

A special numerical technique to represent non-orthogonal multiple crack formations was developed by de Borst and Nauta [47]. However, the non-orthogonal crack model occasionally results in an ill-conditioned element stiffness matrix under closely aligned cracks (Gajer and Dux [69]). The effect of non-orthogonal multiple cracks on the fracture energy dissipation is also an unknown phenomenon. Rots and de Borst [138] proposed a shear-softening constitutive model based on the concept of mode II fracture energy dissipation, which seems to be controversial in concrete fracture analyses. The spurious stress locking of continuum mechanics models can also be relieved by using the isotropic damage mechanics models, that are more appropriate to model the volumetric degradation of concrete properties, such as mass swelling in dams (Cervera et al. [36,37]).

2.4.5 Post-softening behaviour of concrete

The post-softening deformation of concrete is essentially a discontinuous phenomenon. Several analytical models have been proposed to represent the aggregate interlock behaviour of cracked concrete (Bažant and Gambarova [12], Chen and Schnobrich[39], Reinhardt and Walraven [132], Riggs and Powell [136], Skrikerud and Bachmann [146], Walraven[158]). A comparative study on different rough crack models is available in Feenstra et al. [60,61]. Feltrin et al. [62,63] applied the aggregate interlock model at the post-softening phase of the Hillerborg's fictitious crack model, in seismic fracture analyses of concrete gravity dams. Application of an aggregate interlock model in standard smeared crack analyses, where continuous shape functions are used to derive the finite element stiffness matrices, may cause an unpredictable behaviour of the computational model. Substitution of the standard finite elements with specially derived joint elements, or application of the discontinuous shape functions (Droz [53], Ortiz et al. [122]) may be considered to represent the post-softening behaviour of concrete. A recent experimental investigation on dam concrete, reported by Brühwiler and Wittmann [32], has shown that the crack does not travel around the aggregates; it goes straight through them. The roughness on resulting fracture planes, thus, will be mild providing low shear resistance.

A very special post-fracture problem, associated with dynamic analyses, is the modelling of contact-impact phenomenon occurring upon closing/reopening of cracks. Special numerical techniques to simulate the impact behaviour in discrete crack models have been proposed in the literature (Ayari and Saouma [7], Pekau et al. [127]). El-Aidi and Hall [57] have presented a discussion on numerical difficulties arising from high velocity closing/ reopening of cracks in smeared crack analyses. The viscous damping in finite elements, and the energy dissipative numerical integration schemes generally ensure adequate stability of smeared cracks analyses under closing/reopening conditions (as will be demonstrated in chapter 7 of this thesis).

2.5 MATERIAL PARAMETERS FOR FRACTURE PROPAGATION ANALYSIS

The present development of numerical analysis models is relatively ahead of the current knowledge of material behaviour, especially under transient conditions. Material parameter data determined from reliable experimental studies is limited in the literature of dam concrete. Recent experimental investigations, such as the one by Brühwiler (Brühwiler [31], Brühwiler and Wittmann [32]), are revealing significant differences in the mechanical properties of structural concrete and mass concrete. Ideally, the selection of material properties for safety analyses of concrete dams should be dealt with on a case-to-case basis, because, the material properties may vary widely from dam to dam. However, a review of literature is presented here to establish a reasonable limit of parametric values.

Poisson's ratio, ν, and elastic modulus, E, are applied to represent the elastic behaviour of concrete in all analyses, irrespective of the constitutive model selected for propagation of cracks. Jansen [91] has suggested the Poisson's ratio between 0.17 to 0.28 for one year old dam concrete. A value of 0.20 has been applied almost universally in the past studies. Brühwiler [31] has observed the reduction of Poisson's ratio with an increasing compressive strain rate applied to concrete cylinders. However, the influences of rate sensitive ν may be insignificant in comparison to the influences of other material parameters. The static elastic modulus for one year old dam concrete is suggested by Jansen [91] in the range of 28000-48000 MPa. A 25% magnification of the static modulus is often assumed in approximate dynamic analyses of concrete dams (CEA [34], NRC [114]). The Young's modulus of concrete is generally considered less sensitive to strain rate than the tensile strength, or even not affected at all (Reinhardt [133]). Simple or few cycles of compression pre-loading may also cause a complete elimination of the strain rate sensitivity of Young's modulus (Brühwiler and Wittmann [32]).

The following sections briefly review the material parameters generally used in three major crack propagation criteria: strength of material, linear elastic fracture mechanics, and nonlinear fracture mechanics. Special material parameters used in the equivalent elastic crack models, such as the critical crack tip opening displacement ($CTOD_c$), are not considered in the discussions.

2.5.1 Strength-of-material parameters

The governing material parameter in SOM based fracture propagation models is either the critical stress or the critical strain, that are usually determined from direct tension or split cylinder tests. From a rigorous study with some 12000 published test results, Raphael [130] has proposed the following relationship between tensile and compressive strengths of concrete under static loading:

$$\sigma_t = 0.324 f_c'^{\,2/3} \quad MPa \tag{2.11}$$

where f'_c and σ_t are static compression and tensile strengths of concrete in MPa. The tensile strength of concrete increases significantly with the increasing rate of applied loading. In the limited dynamic tests performed on mass concrete, the dynamic load rate effect is observed to be higher than that in usual structural concrete. Raphael [130] has proposed a dynamic magnification factor of 1.5 to amplify the tensile strength of concrete in dynamic analyses. Brühwiler and Wittmann [32] have observed a dynamic magnification of up to 80% in the investigated strain rates between 10^{-5} to 10^{-2} per sec, and this magnification decreases significantly due to the compression pre-loading on tested specimens.

A confusion, however, exists about the interpretation of tensile stresses computed from finite element analyses. Since the pre-peak stress-strain relationship is assumed to be linear elastic in most analyses, some investigators have suggested to compare the predicted tensile stresses with the apparent strength of material (Fig. 2.10(a)). Experimental evidences seem to support an apparent static tensile strength about 30% higher than the value given by Eqn. (2.11) (Raphael [130]). However, a similar magnitude of increase in the dynamic tensile strength (Raphael [130]) is not justified due to the reduced near-peak nonlinearity of stress-strain relations under dynamic loads (Fig. 2.10(b)) (Bhattacharjee and Léger [26]).

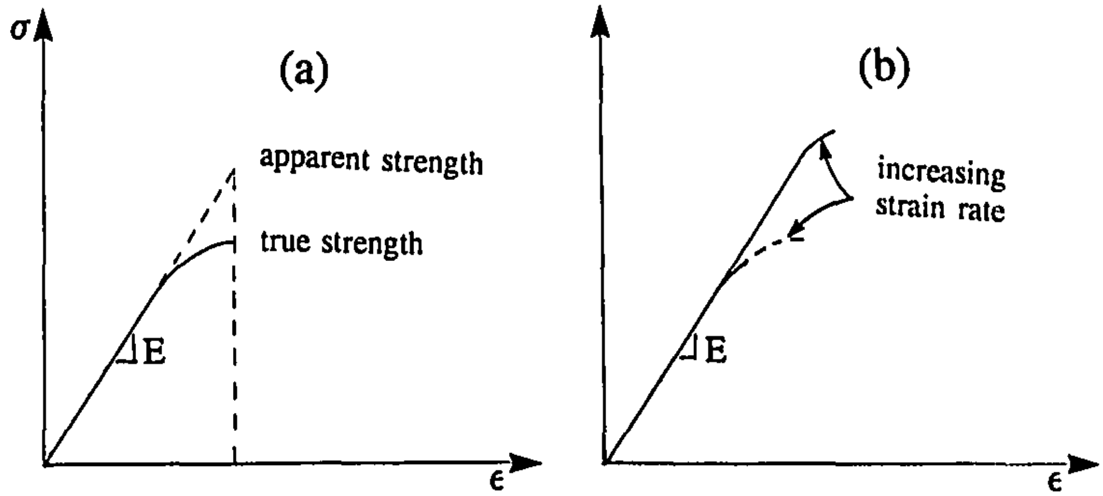

Figure 2.10 (a) Apparent tensile strength, and (b) the dynamic load effects.

2.5.2 Linear elastic fracture mechanics parameters

The principal parameter applied in LEFM crack propagation models is the fracture toughness, K_{Ic}, of concrete. A handful of experimentally determined K_{Ic} values of dam concrete is available in the literature. Saouma et al. [141] have found a K_{Ic} value of 1.1 MPa$\sqrt{m}$. Linsbauer [109] has reported K_{Ic} values in the range of 2.0 to 3.5 MPa$\sqrt{m}$. The following guideline has been proposed by Saouma et al. [142] to select K_{Ic}; zero value as a first approximation, should the response be unacceptable, a value of K_{Ic}=1.0 MPa$\sqrt{m}$ is used, and if this value still results in unacceptable crack lengths, laboratory experiments may be performed on recovered core specimens. Due to multiaxial confining stresses in the field condition, in situ values of the fracture toughness may be three times the unconfined laboratory test values (Saouma et al. [141,144]). The fracture toughness can also be estimated from the following well known relationship (Irwin [90]):

$$K_{Ic} = \sqrt{G_f . E} \tag{2.12}$$

where E is the elastic modulus, and G_f the fracture energy. The strain rate sensitivity of K_{Ic} for mass concrete is not well addressed in the literature. In a seismic analysis of Koyna Dam, Ayari and Saouma [6] have assumed an arbitrary dynamic magnification factor of 60, which seems too high for concrete. Brühwiler[31] has predicted the rate sensitivity of K_{Ic} to be lower than that of concrete tensile strength.

2.5.3 Nonlinear fracture mechanics parameters

The fracture energy, G_f, is applied in conjunction with the elastic modulus, E, the peak tensile strength, σ_i, and a desired shape of the strain softening curve to define the entire constitutive behaviour of concrete in a nonlinear fracture mechanics model. The peak strength, σ_i, beyond which the strain softening process occurs, is usually assumed equal to the tensile strength, σ_t. The fracture energy, G_f, is generally determined from three-point loading tests (Bažant and Pfieffer[20]) or from wedge splitting tests (Brühwiler and Wittmann[32]). Empirical relationships have been proposed to determine the fracture energy value from standard material parameters (Bažant and Oh[15], Oh and Kim[120]). Those relationships have been derived using the experimentally determined results, obtained with small size aggregates that are normally used in structural concrete.

Limited results have been reported from experimental investigations on concrete collected from dam construction sites (Brühwiler[31], Brühwiler and Wittmann[32]). The G_f value under a static loading condition has been determined to be in the range of 175 to 310 N/m, which is two to three times larger than that of structural concrete. Fracture energy values of the specimens subjected to compressive pre-loading have been found considerably low. The G_f parameter determined under simulated seismic loading rates has shown substantial strain rate sensitivity, and a maximum 80% dynamic magnification over the pseudo-static value has been observed. Brühwiler and Wittmann[32] have attributed the rate sensitivity of G_f mainly to the rate sensitivity of tensile strength, σ_t. Influences of specimen size and aggregate dimensions on the fracture energy parameter, G_f, have been discussed in Dungar et al.[55] and Saouma et al.[143]. Bažant and Prat[23] have investigated the influences of working temperature on the fracture energy value. Laboratory tests performed by Brühwiler and Saouma[33] have shown significant reductions of the fracture properties of concrete with an increased water pressure inside the crack. Biaxial and triaxial loads may have moderate effects on fracture energy dissipation characteristics of the mass concrete (Kreuzer et al.[95]).

2.6 PAST INVESTIGATIONS ON SEISMIC FRACTURE OF CONCRETE GRAVITY DAMS

Several attempts have been made in recent years to investigate the fracture response of concrete dams. The simulation of crack profiles in concrete dams, under static and environmental load effects, has attracted considerable attention of several investigators (Ayari [5], Cervera et al. [36,37], Gioia et al. [73], Ingraffea [87], Linsbauer et al. [107,108]). Unlike the static response, the nonlinear seismic response of concrete gravity dams is a little understood phenomenon due to the limitations in previous studies. Hall [79] has presented a comprehensive review on dynamic response of concrete dams, based on field, experimental and corroborative numerical observations. Past earthquake experiences do not appear to provide a reasonable confidence about the seismic safety of large concrete dams with a full reservoir. Additional reviews of numerical and experimental investigations on nonlinear seismic response of concrete gravity dams have been presented by El-Aidi [56] and Donlon [51]. A bibliography on performance of dams during earthquakes is available in USCOLD [153]. Significant contributions made in the realm of nonlinear seismic behaviour of concrete gravity dams are reviewed in the following.

The linear seismic response study of Koyna Dam in India and the Pine Flat Dam in USA, performed by Chopra and Chakrabarti [40], is worth mentioning because that was one of the early finite element investigations predicting possible seismic cracking in concrete gravity dams. Both dams were analysed for the 1967 Koyna earthquake without considering reservoir and foundation interaction effects. Linear elastic analyses showed high tensile stress concentrations, with a maximum value of 6.9 MPa, at the elevation of change in the downstream slope of the unusually shaped Koyna Dam (Fig. 2.11(a)). The corresponding tensile stress value in the standard section of Pine Flat Dam was 5.5 MPa. These high tensile stress concentrations, that were attributed to the high frequency

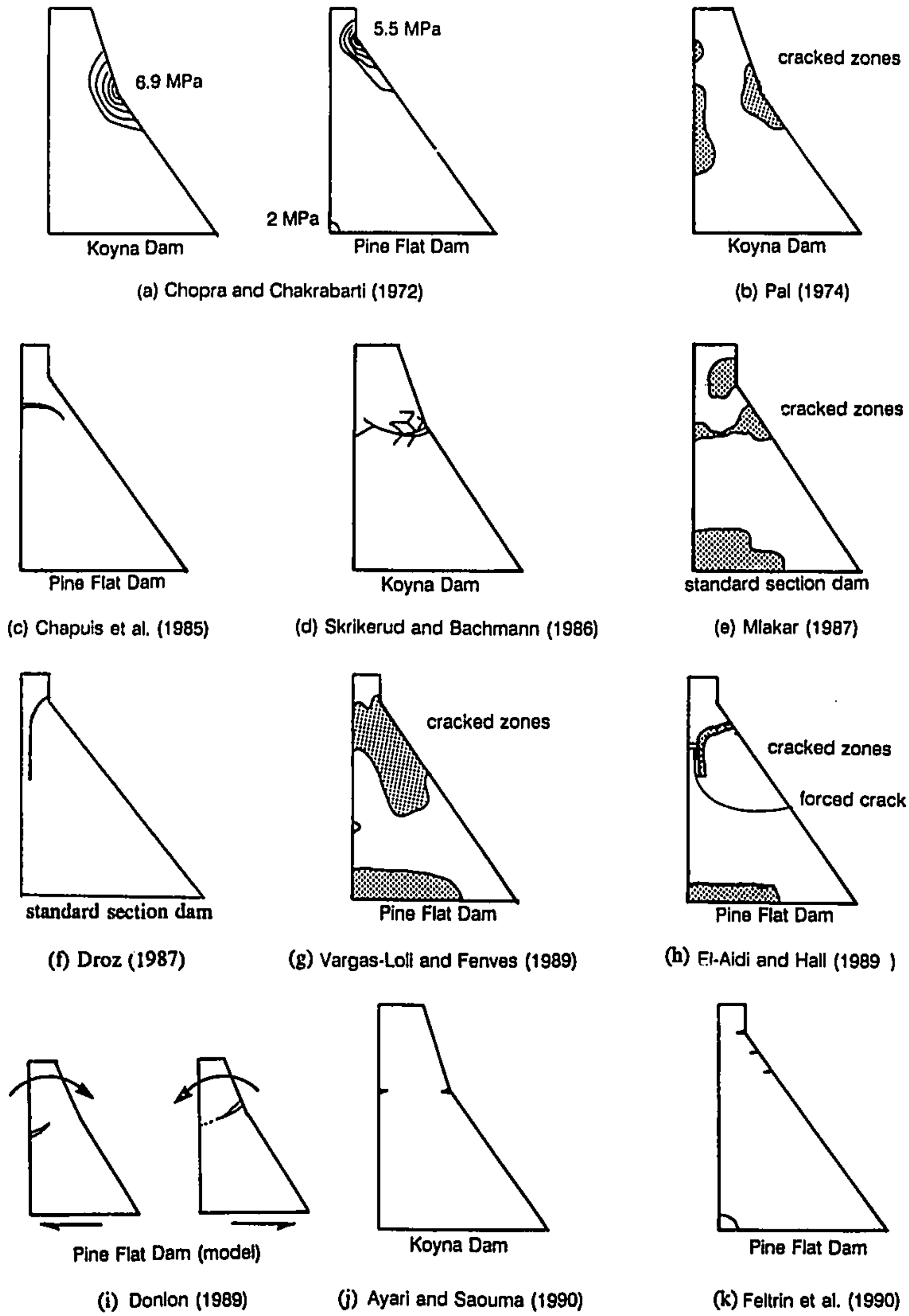

Figure 2.11 Past investigations on seismic cracking of concrete gravity dams.

content of the particular earthquake and the heavy crest mass inevitably present in most gravity dams, indicated seismic vulnerability of the structures under strong ground excitations.

The first rigorous nonlinear finite element analysis of a concrete gravity dam was performed by Pal [124,125]. The highest monolith of Koyna Dam was analysed assuming a rigid base and no reservoir interactions. A nonlinear stress-strain relationship including approximate strain rate effects was applied in the analyses. The propagation of cracks was determined by a smeared crack model with the strength of material failure criterion. The predicted crack profiles penetrated only little inside the dam and spread in the vertical direction (Fig. 2.11(b)). The crack pattern was found to be very sensitive to the selected material strength parameter and the degree of refinement of finite element meshes - a standard problem with the strength based failure criterion.

Chapuis et al. [38] applied a hybrid smeared-discrete crack model in seismic crack analysis of the Pine Flat Dam, subjected to an artificial accelerogram in the horizontal direction with a peak ground acceleration (PGA) equal to 0.1 g. The hydrodynamic forces on the rigid base dam, calculated from linear elastic analyses of a coarse finite element model of the dam-reservoir system, were applied on a finer mesh of the dam in nonlinear seismic analyses. A smeared representation of the crack profile was applied in the seismic analysis, followed a LEFM based localized discrete crack propagation analysis for the surrounding region of the crack tip subjected to the same displacement field. A crack in the top region of the dam propagated horizontally from the upstream face for a brief instance, and then gradually dipped downward (Fig. 2.11(c)). The inadequate mesh refinement reportedly influenced the computation.

A rigorous discrete crack propagation finite element analysis of the Koyna Dam, with no reservoir and foundation interactions, and subjected to an artificially generated ground motion, was performed by Skrikerud and Bachmann [146]. The tensile strength criterion was used for initiation and propagation of cracks. Discrete cracks were represented along the inter-element boundaries by splitting the finite elements and often moving the existing nodes to accommodate the crack extension. Special 'crack elements', capable of representing the aggregate interlock mechanism, were introduced along the inter-element cracks. The number of cracks predicted in the analysis increased considerably, when the tensile strength was reduced from 3 MPa to 2 MPa. The crack pattern was not influenced by the aggregate interlock model; but the pattern changed substantially with the refinement of finite element mesh. A remarkable crack branching was visible in the presented results (Fig. 2.11(d)). The assumption of discrete crack propagation with increments equal to the lengths of finite element boundaries, and the use of a strength based criterion apparently resulted in the mesh dependent response.

Mlakar [112] studied the seismic response of three concrete gravity dams of different heights, subjected to 1966 Parkfield earthquake. A smeared crack model based on the critical tensile stress failure criterion was employed. Reservoir interaction effects were taken into consideration through an added mass technique. The study demonstrated an important aspect of the occurrence of tensile cracks depending on the height of dam. Cracks appeared at the base of a short dam, and in the top region of the tallest dam. As expected for standard smeared crack models applied with strength based criterion, the crack zones spanned over several elements in the vertical direction (Fig. 2.11(e)).

Droz [53] investigated the seismic fracture response of a concrete gravity dam using the LEFM crack propagation criterion. Crack profiles were spatially represented using a special finite element formulation based on discontinuous shape functions: an approach conceptually equivalent to the discrete crack model. The analysis predicted localized crack profiles propagating deep inside the dam (Fig. 2.11(f)).

A numerical investigation on seismic response of the 122 m high Pine Flat Dam (USA) was performed by Vargas-Loli and Fenves [155]. A full reservoir model including energy dissipation mechanisms was adopted in the analysis; foundation interaction effects were not considered. The 1952 Taft and the 1971 Pacoima ground motions were scaled in magnitude to induce cracking in the structure. A smeared crack model was adopted in the finite element analysis scheme. The elasto-brittle tensile failure criterion was employed assigning the lowest strength of 3.66 MPa to the largest element, and proportionately increased strengths to smaller elements, resulting in a maximum value of 5.03 MPa. This selection criterion of tensile strength implied the conservation of fracture energy at a level about 30 times higher than the value assumed appropriate for the material. The computed crack pattern was diffused over a significant portion of the dam height (Fig. 2.11(g)). Reservoir interaction effects were observed to considerably influence the response of the dam. Computations in several analyses ceased, and that were presumed as signs of imminent failure of the structure. Numerical instabilities may be attributed to the sudden release of very high internal strain energy, stored in the elements that were assigned arbitrary high tensile strengths. The results should be interpreted with caution due to the limitations of the applied constitutive model.

El-Aidi and Hall [57,58] investigated seismic response of the Pine Flat Dam, subjected to 1940 El Centro earthquake, that was scaled in amplitude by a factor of 1.5. Dam-reservoir-foundation interaction effects, including the cavitation in water, were considered. The smeared crack propagation ahead of a crack tip or at a known location of stress singularity, was governed by the elasto-brittle size reduced strength model (similar to that in Fig. 2.8(a)). Initially the dam was analysed for *a priori* known location and orientation of weak planes. Substantial sliding of the order of 1.04 m was predicted with a pre-determined crack plane sloping downward from the upstream face towards the downstream face. A homogeneous dam was then analysed with no prior defects in the structure. The crack profile determined from an automated analysis was reported to be unrealistic (El-Aidi and Hall [57]). The analyst's choice was therefore incorporated in the solution procedure to guide the smeared crack profile in a desired direction (Fig. 2.11(h)). The coarse finite element mesh reportedly influenced the propagation of cracks. Nevertheless, the study provided a significant insight into the various aspects of applying the smeared crack propagation finite element models in seismic analysis of large concrete dams.

Donlon (Donlon[51], Donlon and Hall[52]) performed shaking table tests on three small scale models of the top profile of Pine Flat Dam, fulfilling the strength, stiffness and density requirements of the laws of similitude. Interesting observations were made using a high speed photography, regarding the mechanism of crack propagation from one side of the dam to the other. Cracks propagated into the interior in one swing, and extended to the opposite face probably from the old tip during the other swing (Fig. 2.11(i)). Fulfilment of the crack propagation criterion at the old crack tip, rather than the fulfilment of a new crack initiation criterion on the opposite face, possibly resulted in an all through crack plane. The fractured models showed significant stability even under very strong excitations. However, pertinent limitations of the shaking table test, such as the unscaled fracture parameters and the inadequate representation of reservoir and foundation interaction effects, should be taken into consideration to interpret the results.

In a preliminary study performed by Ayari and Saouma[6], a linear elastic fracture mechanics criterion was applied with the discrete crack propagation finite element model, in a seismic analysis of Koyna Dam, without considering reservoir and foundation interaction effects. Cracks initiated on both faces of the dam, at the elevation of a sharp change in the downstream slope, where a significant stress concentration is expected (Fig. 2.11(j)). However, the crack trajectories propagating from two sides did not appear to merge, which might be the consequence of a very high dynamic magnification of the fracture toughness value assumed in the analysis.

Feltrin et al.[62] studied the seismic response of Pine Flat Dam using a boundary element technique to represent the reservoir interaction effects; the foundation condition was assumed rigid. Hillerborg's fictitious crack model was applied to determine the propagation of discrete cracks. Finite element mesh of the dam was updated with the extension of cracks, and aggregate interlock elements were introduced along the inter-element discrete cracks: a technique similar to that adopted by Skrikerud and Bachmann[146]. The dam with an empty reservoir did not experience any cracking when subjected to the horizontal component of 1952 Taft ground motion (PGA=0.18g). A crack appeared at the heel of the dam followed by few more in the top region when the reservoir interaction effects were included (Fig. 2.11(k)). Use of the discrete crack model with a nonlinear fracture mechanics criterion predicted localized crack profiles in the dam. In a latter study (Feltrin et al. [63]), the aggregate interlock mechanism was observed to cause branching of the primary crack profiles.

Simulating a crack trajectory by nonlinear analyses was the highlight of most previous investigations. Reviewing the past investigations, it is apparent that tall gravity dam monoliths would experience seismic cracking in the heel and in the top region at about the elevation of the downstream slope change. However, the expected crack profile and the extent of cracking are not reliably known from the previous studies. Moreover, with all the nonlinear analyses performed so far, the question about the safety of concrete dams during strong ground excitations is still unresolved. In one past investigation (Léger and Katsouli [97]), efforts were made to define specific criteria for the seismic safety of concrete gravity dams, that were allowed to uplift and slide along the dam-foundation interface. Most of the past investigations, except the ones by El-Aidi and Hall [58] and Hall et al. [80], considered uniform structures with no pre-existing defects. The initial stresses and strains, induced by changes in the environmental factors, have not been considered in the previous nonlinear seismic response studies. Effects of seasonal temperature changes and mass swelling, on the normal behaviour of concrete dams, have been extensively reported in the literature (Cervera et al. [36,37], Mamet et al. [110], Tahmazian et al. [148]). However, a methodology to consider the initial stress-strain effects in nonlinear seismic response analyses of concrete dams is yet to be developed.

2.7 CONCLUSIONS

Presently, nonlinear solution methods can be applied with parametric analyses for *a posteriori* determination of the causes of cracking in concrete dams. The *a priori* determination of the nonlinear seismic response of concrete dams is, however, a difficult task due to the lack of general confidence in nonlinear analyses. The predicted response is often very sensitive to the modelling parameters and assumptions. State-of-the-art numerical techniques are still unable to provide reasonable predictions about the safety of concrete dams during earthquakes. However, a rational choice of computational models may help to identify the potential path of crack extensions during severe ground excitations. The predicted crack profile can be considered favourable or unfavourable depending on its orientation. A crack profile sloping upward from the upstream side towards the downstream face of a gravity dam is usually considered favourable in the presence of reservoir pressure. A crack profile with the reverse slope may be unfavourable from safety considerations of the top profile. After a realistic prediction of crack profiles from nonlinear analyses, sliding and overturning stabilities of the top profile can be determined from separate analyses (Saini and Krishna [140]).

Crack propagation analyses performed with the conventional tensile strength based criterion have been found unreliable in general. Nonlinear fracture mechanics criteria, applied with a smeared crack propagation technique, appear to be promising for predicting the crack profiles at a reasonable cost. An energy based safety criterion can also be developed within the framework of a nonlinear fracture mechanics analysis procedure. The presently available computer programs, implementing the conventional strength based smeared crack analysis models, can be adapted for the nonlinear fracture mechanics constitutive models. The limit on maximum element sizes should not be a major drawback of nonlinear smeared fracture models. The refinement of finite element meshes can be localized along the path of expected crack extensions from few trial analyses. The initial analysis may start with a relatively coarse finite element mesh, followed by an adaptive approach to refine the mesh in required zones. The material parameters in a nonlinear analysis should be selected with caution. Data obtained from laboratory tests may not be always representative of the actual field behaviour of concrete dams.

CHAPTER 3

CONSTITUTIVE MODELS FOR FRACTURE ANALYSIS OF CONCRETE GRAVITY DAMS

3.1 INTRODUCTION

Development of a constitutive model for crack propagation analyses is strongly influenced by the numerical technique adopted for spatial discretization of cracks. Continuum mechanics approaches to represent the tensile crack propagation are very efficient for applications in complex structural analyses when the location and the orientation of crack profiles are not known *a priori*. Extensive behavioural studies of concrete dams, under a wide range of modelling assumptions, can be performed using the cost effective local smeared fracture models. A discrete crack analysis may be performed for *a posteriori* validation of the smeared crack analysis results.

Smeared crack analyses, using the traditional tensile strength based crack propagation criteria (Rashid [131]), have long been criticised for mesh dependent response predictions (Bažant and Cedolin [11]). The strain softening crack band constitutive model, derived on the basis of fracture energy conservation principle (Bažant and Oh [15]), was a significant achievement in finite element analysis of concrete fracture problems. However, the direction of fracture propagation was not rigorously addressed in the crack band model. Crack constitutive models, fixing the local crack band at the initial inclination, generally result in a severe stress locking due to the zigzag propagation of crack profiles in a continuous finite element mesh. The constitutive framework proposed by de Borst and Nauta [47] allows non-orthogonal multiple crack formations to alleviate the stress locking in smeared crack analyses. In this approach, element stiffness matrices are derived using an incremental stress-strain relationship with the negative softening modulus, that may occasionally result in an ill-conditioned stiffness matrix. Moreover, the angular spacing of non-orthogonal cracks requires to be limited by a hypothetical minimum admissible value for numerical stability reasons (Gajer and Dux [69]).

Application of the rotating crack concept (Cope et al.[43], Gupta and Akbar[76]) may also alleviate the stress locking in smeared crack analyses (Rots [139]). The directional sensitivity of a crack band propagation in slanted finite element meshes may be eliminated using a 'nonlocal' constitutive model (Bažant and Lin [22]). However, application of the 'nonlocal' model in dam fracture analyses is limited, because of the requirement of an extremely fine mesh, and high computational costs related to the spatial averaging of local response quantities. The definition of constitutive parameters to obtain a mesh objective response, the interaction between two or more damaged zones, and the unloading/ reloading under damaged conditions need to be addressed more rigorously in the nonlocal formulation. The localized smeared fracture models are very promising for application in the analysis of complex structural systems, because of the significantly less computational cost and the simplified definition of material constitutive behaviour. The extension of local fracture models to transient and three-dimensional analyses is also relatively simpler.

Most of the existing smeared crack models have been primarily developed for fracture analysis of small scale structures, subjected to monotonic static loading conditions. A general constitutive framework, applicable to both static and seismic fracture analyses of mass concrete structures, has been lacking in the literature. The purpose of this chapter is to develop smeared crack propagation models for static and seismic fracture analyses of concrete gravity dams. Different features of the constitutive models will be considered for investigations in the subsequent chapters.

Nonlinear behaviour in the fracture process zone (FPZ), which is significantly large for dam concrete, has been considered in the smeared crack propagation models. Figure 3.1 represents the general framework of a strain softening constitutive model applicable to concrete fracture analyses. Following features of the proposed constitutive model are discussed in the subsequent sections: (i) the pre-softening material behaviour, (ii) the criterion for softening initiation, (iii) the fracture energy conservation, (iv) the numerical simulation of strain softening behaviour, (v) shear deformations in the fractured elements, (vi) the closing and reopening of cracks, and (vii) the finite element implementation of constitutive models. The strain rate sensitivity of concrete behaviour under seismic loading conditions is also discussed. A linear elastic relationship is assumed between compressive stresses and strains. The tensile stresses and strains are referred as positive quantities in the presentation.

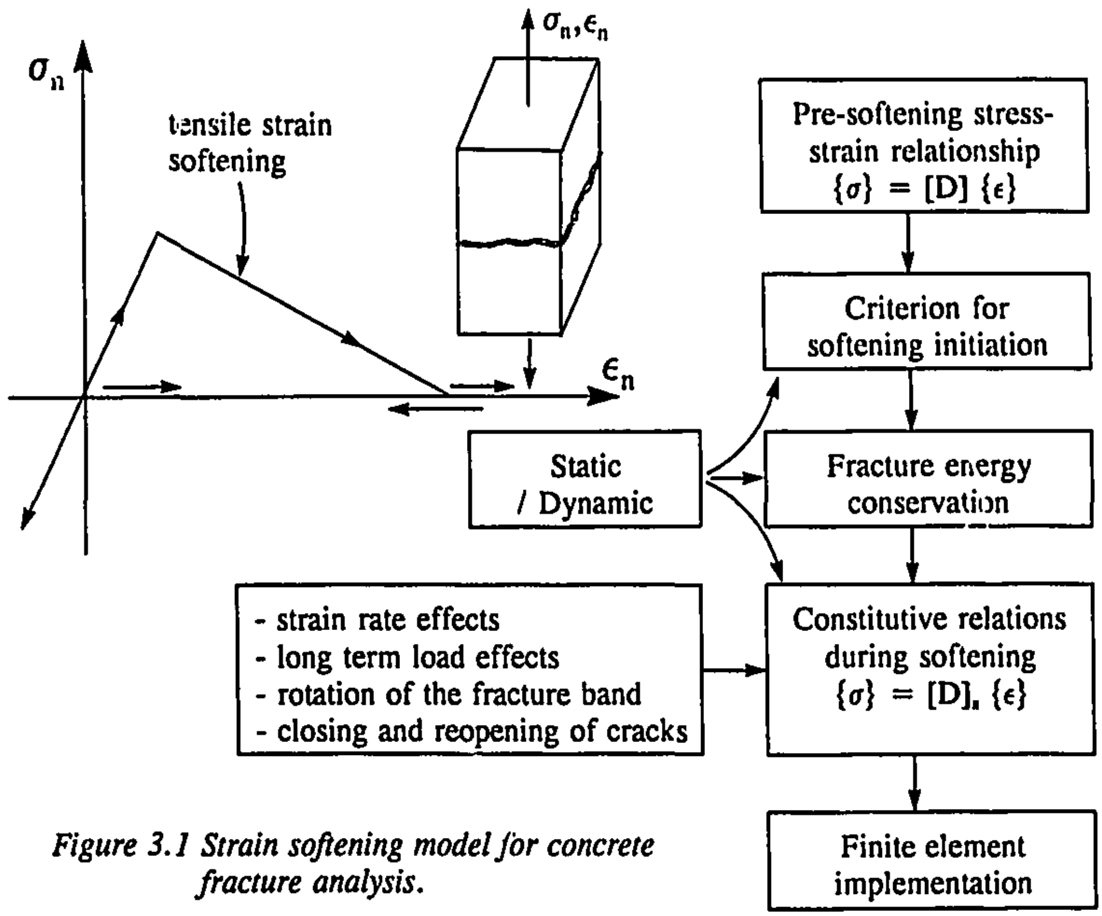

Figure 3.1 Strain softening model for concrete fracture analysis.

3.2 PRE-SOFTENING STRESS-STRAIN BEHAVIOUR OF CONCRETE

In the finite element analysis, the mechanical stresses and strains at a material point are algebraically related as,

$$\{\sigma\} = [D]\{e\} \tag{3.1}$$

where [D] is the constitutive relationship matrix, $\{\sigma\}$ the vector of stress components σ_x, σ_y etc., and $\{\epsilon\}$ the corresponding strain vector. Assuming a linear elastic isotropic behaviour, the matrix [D] for a plane stress finite element model is given by:

$$[D] = \frac{E}{1-\nu^2}\begin{pmatrix} 1 & \nu & 0 \\ \nu & 1 & 0 \\ 0 & 0 & \frac{1-\nu}{2} \end{pmatrix} \tag{3.2}$$

where E is the Young's modulus, and ν the Poisson's ratio. Definition of the Young's modulus is somewhat ambiguous, because, creep effects exist even for an extremely short duration of loading. The strain which corresponds to a service range stress (usually less than 40% of the ultimate strength), applied over a duration between 0.001 to 1 day, is considered as the 'elastic' strain (Bažant[21]), and the ratio between the applied stress and the measured 'elastic' strain is taken as the Young's modulus. Short-term laboratory tests with recovered dam concrete specimens can be performed to determine the value of E. Constitutive behaviour of concrete under static and seismic loadings are discussed in the following sections.

3.2.1 Non-seismic loads/ deformations

Under statically applied loads, the Young's modulus, E, determines the complete elastic resistance of the material. The mechanical strains under non-seismic loads are decomposed into two components:

$$\begin{aligned}\{\sigma\} &= [D]\{\epsilon\} \\ &= [D](\{\epsilon_L\} + \{\epsilon_I\})\end{aligned} \tag{3.3}$$

where $\{\epsilon_L\}$ is the mechanical strain due to applied loads, and $\{\epsilon_I\}$ is the mechanical strain due to external and internal restraints to the volumetric deformations caused by temperature change, swelling etc. The short term elastic modulus, E, will be used to determine the strain $\{\epsilon_L\}$ and the corresponding stress response under the applied loads of self weight, hydrostatic pressure etc. The long term creep effects under 'constant' applied loads will not be considered in the present constitutive modelling procedure. However, an approximate procedure to take account of the long term relaxation effects under imposed volumetric deformations, such as due to temperature changes, will be discussed in section 4.6.

3.2.2 Seismic load effects

The finite element resistance to applied dynamic loads (Fig. 3.2(a)) is expressed as:

$$[m]\{\ddot{u}\} + [c]\{\dot{u}\} + \{r(u)\} = \{f(t)\} \tag{3.4}$$

where the first two components represent the inertia and the viscous resistance of the material, and the third component represents the elastic resistance. The elastic

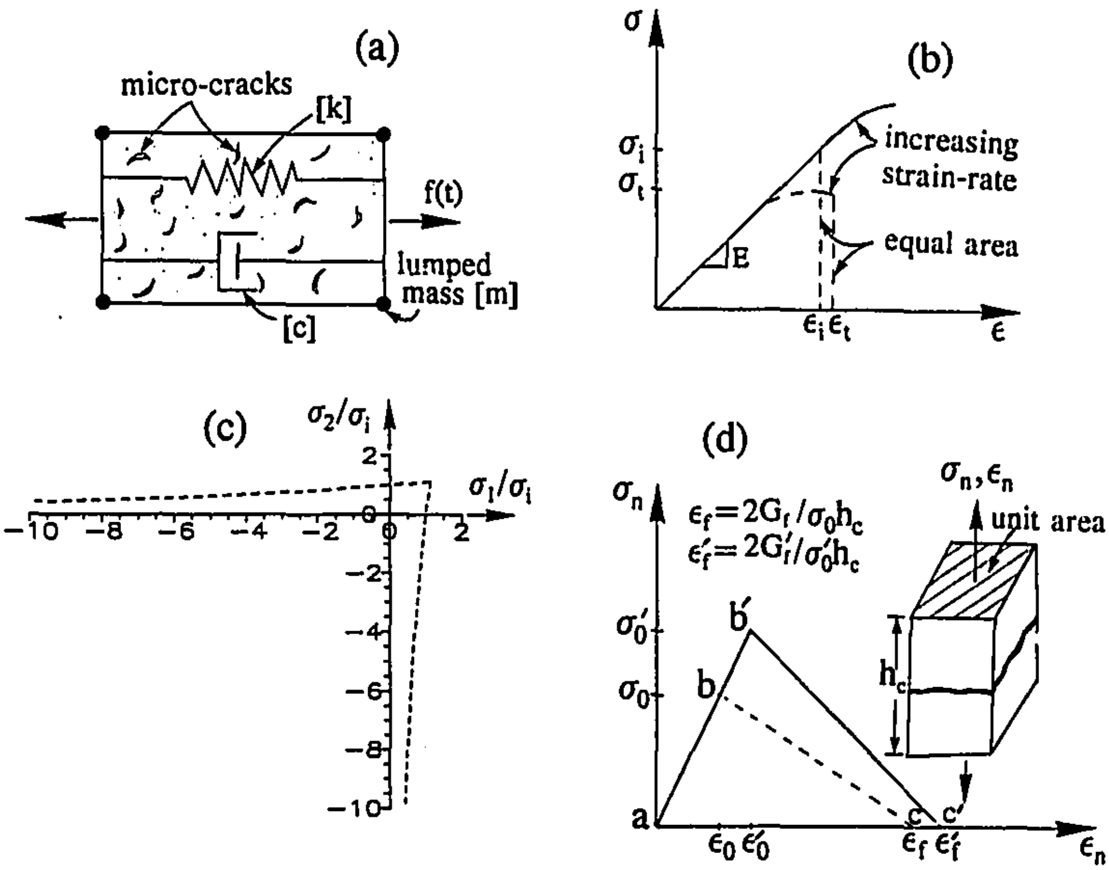

Figure 3.2 Nonlinear smeared fracture model.

component is determined using the standard stress-strain relationship (Eqn. 3.1), which in turn is influenced by the Young's modulus of concrete. Any arbitrary dynamic amplification of the Young's modulus is unwarranted in a rigorous finite element analysis with explicit considerations for the inertia and the viscous resistance components. Moreover, review of the published experimental results (Brooks and Samaraie[30], Brühwiler[31], Reinhardt[133]) does not justify a strong dynamic magnification of the elastic modulus of concrete. Selection of a strain rate independent elastic modulus, and calibration of the viscous damping resistance of the material using the assumed elastic properties of the structure, appear to be consistent for nonlinear seismic analyses of concrete dams.

3.3 THE CRITERION FOR INITIATION OF STRAIN SOFTENING

The stress-strain relationship of concrete becomes considerably nonlinear near the peak strength (Fig. 3.2(b)). In the post-peak strain softening phase, coalescence of the micro-cracks causes a gradual reduction of the stress resistance. The area under the uniaxial stress-strain curve up to the peak, defined in Eqn. (3.5), is taken as the index for softening initiation:

$$U_0 = \int_0^{\epsilon_i} \sigma \, d\epsilon = \frac{\sigma_i \epsilon_i}{2} = \frac{E\epsilon_i^2}{2} = \frac{\sigma_i^2}{2E} \tag{3.5}$$

where σ_i is the apparent tensile strength, calibrated such that a linear elastic uniaxial stress-strain relationship up to σ_i will preserve the value U_0 (Fig. 3.2(b)). Assuming $E \approx 10000\sigma_t$, the tensile stress-strain relationship specified in the CEB code (Hilsdorf and Brameshuber[83]) provides an apparent tensile strength approximately 40% higher than the true static strength σ_t. However, an apparent tensile strength, not exceeding the true strength of concrete by an amount of 30%, seems to be a reasonable assumption (Raphael[130]). In finite element analyses, the softening under a static load is assumed to initiate when the tensile strain energy density, $\frac{1}{2}\sigma_1\epsilon_1$ (σ_1 and ϵ_1 are the major principal stress and the major principal strain, respectively), becomes equal to the material parameter, U_0:

$$\frac{1}{2}\sigma_1\epsilon_1 = U_o = \frac{\sigma_i^2}{2E} ; \qquad (\sigma_1 > 0) \tag{3.6}$$

Taking square roots of both sides, the biaxial effect in the proposed strain softening initiation criterion (Eqn. 3.6) is represented as,

$$\frac{\sigma_1}{\sigma_t} = \sqrt{\frac{\sigma_1}{E\epsilon_1}} \tag{3.7}$$

Figure 3.2(c) schematically represents a biaxial failure envelope as defined by Eqn. (3.7). The principal stress and strain, σ_1 and ϵ_1, at the instant of softening initiation under statically applied loads, are designated by σ_0 and ϵ_0 respectively (Fig. 3.2(d)).

Under dynamic loads, the pre-peak nonlinear behaviour decreases with increasing values of both σ_t and ϵ_t (Fig. 3.2(b)) (Brooks and Samaraie [30]). The dynamic amplification of the material parameter U_0 can be considered through a constant magnification factor, DMF_e, as follows:

$$U_0' = \frac{\sigma_t'^2}{2E} = (DMF_e)^2 U_0 \tag{3.8}$$

where the primed quantities correspond to the dynamic constitutive parameters. All three components of the material resistance under applied dynamic loads, as expressed in Eqn. (3.4) and in Fig. 3.2(a), should be considered to determine the applied stress on the element at a particular instant. However, in the present modelling procedure, only the elastic component of stresses in an element, determined using the usual stress-strain relationship (Eqn. 3.1), will be compared with the assumed material resistance. The DMF_e in Eqn (3.8), therefore, does not embody the increased material resistance due to viscous and inertia effects; only the effects due to a change in the cracking mechanism under dynamic loads are represented. The micro-cracks under rapidly applied loads may be forced through relatively stronger aggregate particles rather than around the aggregates, thereby causing an increased tensile resistance of the macroscopic structure (Reinhardt [133]). Compression pre-loadings, on the other hand, may reduce the strain rate sensitivity of tensile strength (Brühwiler and Wittmann [32]). A 10-20% dynamic magnification of the apparent tensile strength may be assumed in seismic analyses of concrete dams. The presence of free water in concrete may not have significant influences for the seismic induced strain rates (Rossi [137]). Under dynamic loading, the material parameter U_0 in expression (3.6) is replaced by the corresponding dynamic value, U'_0. At the instance of softening initiation under a dynamically applied load, the principal stress, σ_1, and the principal strain, ϵ_1, are respectively designated by σ_0' and ϵ_0', as shown in Fig. 3.2(d).

3.4 FRACTURE ENERGY CONSERVATION

The tensile resistance of concrete is assumed to decrease linearly from the pre-softening undamaged state to the fully damaged state of zero tensile resistance (Fig. 3.2(d)). Slope of the softening curve is adjusted such that the energy dissipation due to a unit area of crack plane propagation is conserved. The static fracture energy, G_f, is magnified by a dynamic magnification factor, DMF_f, to represent the increased fracture energy dissipation under dynamic loads:

$$G_f' = DMF_f \, G_f \tag{3.9}$$

The dynamic magnification of fracture energy can be mainly attributed to that of tensile strength (Brühwiler and Wittmann [32], Reinhardt and Weerheijm [134]). DMF_f can therefore be assumed equal to DMF_t. In finite element analyses, the final strains of no tensile resistance for static and dynamic loadings are respectively defined as (Fig. 3.2(d)),

$$\epsilon_f = \frac{2G_f}{\sigma_0 h_c} \; ; \qquad \epsilon_f' = \frac{2G_f'}{\sigma_0' h_c} \tag{3.10}$$

where h_c is the characteristic dimension defined in section 3.8. The dynamic magnification of constitutive parameters is schematically demonstrated in Fig. 3.2(d). A pre-seismic state in the linear elastic range (line ab in Fig. 3.2(d)) will proceed through line ab′ in dynamic analyses until the dynamic softening initiation criterion is satisfied. Upon satisfaction of this criterion, the dynamic softening model (line b′c′ in the figure) determines the element behaviour. If an element has been softening in the pre-seismic state, the static softening model (line bc in the figure) governs the element behaviour until the complete fracture takes place.

3.5 CONSTITUTIVE RELATIONSHIPS DURING SOFTENING

After the initiation of softening process, a smeared band of micro-cracks is assumed to appear in the direction perpendicular to the principal tensile strain. The material reference axis system, referred as the local axis system, is aligned with the principal strain directions (directions n-p in Fig. 3.3(a)). Two approaches have been considered

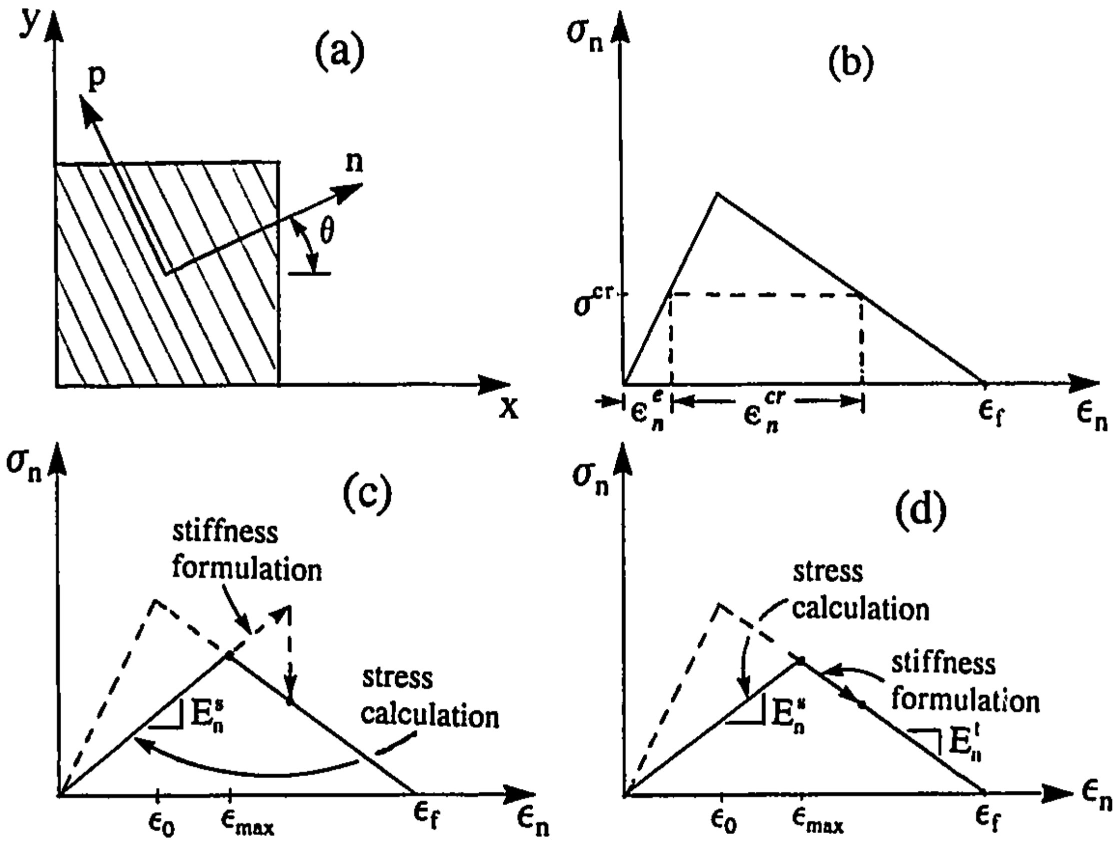

Figure 3.3 (a) The local axis system, (b) the decomposition of strain, (c) the SMS model, and (d) the TMS model.

for numerical simulation of the softening phenomenon: (i) the secant modulus stiffness (SMS) based on the concept of stiffness degradation, where the constitutive relationship is defined in terms of total stresses and strains, and (ii) the tangent modulus stiffness (TMS), where element stiffness matrices are derived using an incremental stress-strain relationship. Features of the two softening models are discussed in the following sections. Discussions on the shear deformation in strain softening material is deferred until the section 3.6. Only the static constitutive parameters, ϵ_0 and ϵ_f, are shown in Fig.

3.3 for the brevity of presentations. However, the principles discussed in the following sections are applicable to dynamic analyses as well.

3.5.1 The total stress-strain relationship

The total strain in softened concrete can be decomposed into the elastic concrete strain and the crack strain as follows,

$$\begin{aligned} \epsilon_n &= \epsilon_n^e + \epsilon_n^{cr} \\ \gamma_{np} &= \gamma_{np}^e + \gamma_{np}^{cr} \end{aligned} \tag{3.11}$$

where ϵ_n and γ_{np} are respectively normal and shear strains, the subscripts 'n' and 'p' refer to the crack normal and parallel directions, and the superscripts '*e*' and '*cr*' stand for elastic and crack components respectively. The decomposition of normal strain is pictorially represented in Fig. 3.3(b). The local crack strains, $\{\epsilon_n^{cr}, \gamma_{np}^{cr}\}^T$, can be transformed to the global coordinate directions using the following relationship:

$$\begin{Bmatrix} \epsilon_x \\ \epsilon_y \\ \gamma_{xy} \end{Bmatrix}^{cr} = \begin{pmatrix} \cos^2\theta & -\cos\theta\sin\theta \\ \sin^2\theta & \cos\theta\sin\theta \\ 2\cos\theta\sin\theta & \cos^2\theta - \sin^2\theta \end{pmatrix} \begin{Bmatrix} \epsilon_n^{cr} \\ \gamma_{np}^{cr} \end{Bmatrix} ; \qquad \{\epsilon\}_{global}^{cr} = [N]\{\epsilon\}_{local}^{cr} \tag{3.12}$$

where θ is the angle between the global x-axis and the normal to the fracture plane (Fig. 3.3(a)). Considering that uncoupled normal and shear deformations occur on the crack plane, the crack stress-strain relationship in the local coordinate directions can be defined as,

$$\begin{Bmatrix} \sigma_n^{cr} \\ \tau_{np}^{cr} \end{Bmatrix} = \begin{pmatrix} \dfrac{EE_n^s}{E-E_n^s} & 0 \\ 0 & \dfrac{\mu}{1-\mu}G \end{pmatrix} \begin{Bmatrix} \epsilon_n^{cr} \\ \gamma_{np}^{cr} \end{Bmatrix} ; \qquad \{\sigma\}_{local}^{cr} = [D]_s^{cr}\{\epsilon\}_{local}^{cr} \tag{3.13}$$

where E is the elastic modulus, E_n^s the damaged Young's (secant) modulus in the crack normal direction (Fig. 3.3(c)), and μ is the ratio between the softened shear modulus, G_{np}^s, and the pre-softening shear modulus, G (discussed later in section 3.6). After algebraic manipulations, the total stress-strain relationship matrix in the global coordinate system, $[D]_s$, is obtained as (de Borst and Nauta[47]):

$$[D]_S = [D] - [D][N]([D]_S^{cr}+[N]^T[D][N])^{-1}[N]^T[D] \tag{3.14}$$

where [D] is the elastic constitutive relationship matrix defined in Eqn. (3.2).

The constitutive matrix of Eqn. (3.14) is equivalent to the conventional formulation,

$$[D]_s = [T]^T[D]_{np}[T] \tag{3.15}$$

where [T] is the strain transformation matrix defined as:

$$[T] = \begin{bmatrix} \cos^2\theta & \sin^2\theta & \cos\theta\sin\theta \\ \sin^2\theta & \cos^2\theta & -\cos\theta\sin\theta \\ -2\cos\theta\sin\theta & 2\cos\theta\sin\theta & \cos^2\theta-\sin^2\theta \end{bmatrix} \tag{3.16}$$

and $[D]_{np}$ is the local stress-strain relation matrix defined from the degradation concept:

$$[D]_{np} = \frac{E}{1-\eta\nu^2}\begin{pmatrix} \eta & \eta\nu & 0 \\ \eta\nu & 1 & 0 \\ 0 & 0 & \mu\dfrac{1-\eta\nu^2}{2(1+\nu)} \end{pmatrix} ; \quad \eta = \frac{E_n^s}{E} \tag{3.17}$$

where η $(0 \leq \eta \leq 1)$ is the ratio between the softened Young's modulus, E_n^s (Fig. 3.3(c)), in the direction normal to the fracture plane, and the initial isotropic elastic modulus, E. The total stress-strain relationship matrix, defined by Eqn. (3.17), is similar to the formulation presented by Bažant and Oh [15], except that they did not include the shear deformation, and the consequent rotation of fracture bands in the constitutive formulation. The present formulation, with the degraded shear modulus term (defined in section 3.6), maintains a backward compatibility with the pre-softening elastic formulation when $\eta=1$ and $\mu=1$. The total stress-strain relationship matrix, $[D]_s$, defined using a degraded elastic modulus, E_n^s, is hereafter referred as the secant modulus stiffness (SMS) of the material. During a monotonic increase of the tensile strain, ϵ_n, in the crack normal direction, the secant modulus in the corresponding direction, E_n^s, gradually decreases until finally reaching a zero value after complete fracture, $\epsilon_n > \epsilon_f$ or ϵ_f' (Fig. 3.3(c)). The constitutive relationship matrix, $[D]_s$, is updated as the modulus, E_n^s, decreases. The direction of softening, θ, may also change during the softening process. During unloading and reloading, when the strain, ϵ_n, is less than the previously attained maximum value, ϵ_{max} (Fig. 3.3(c)), the secant modulus, E_n^s, remains unchanged; the parameter μ, however, changes during that process.

3.5.2 The incremental stress-strain relationship

The incremental stress-strain relationship during the progress of softening can be defined using the tangent softening modulus, E_n^t (Fig. 3.3(d)). Assuming uncoupled normal and shear deformations, the incremental crack strains, $\{\Delta\epsilon\}_{local}^{cr}$, and stresses, $\{\Delta\sigma\}_{local}^{cr}$, in the local axis system, are related by (de Borst and Nauta[47]):

$$[D]_T^{cr} = \begin{pmatrix} \dfrac{EE_n^t}{E-E_n^t} & 0 \\ 0 & \dfrac{\mu}{1-\mu}G \end{pmatrix} \tag{3.18}$$

The tangent formulation, $[D]_T^{cr}$, of Eqn. (3.18) can be substituted for $[D]_s^{cr}$ in Eqn. (3.14) to obtain the tangent constitutive matrix, $[D]_T$, representing the incremental stress-strain relationship in global coordinate directions. The constitutive matrix, $[D]_T$, is hereafter referred as the tangent modulus stiffness (TMS). During the monotonic softening of elements, ϵ_n exceeding ϵ_{max} at successive steps, the tangent softening modulus, E_n^t, in the linear softening model remains unchanged until complete fracture takes place. The constitutive matrix, $[D]_T$, remains unchanged as the softening progresses from ϵ_o to ϵ_f (Fig. 3.3(d)), provided the direction of fracture remains unchanged and the parameter μ is assumed constant. At completely fractured state, $\epsilon_n > \epsilon_f$, the tangent modulus E_n^t becomes zero, and requires updating of the TMS matrix. In the case of unloading before complete fracture, $\epsilon_n < \epsilon_{max}$, the secant unloading modulus, E_n^s, (Fig. 3.3(d)), is used instead of E_n^t in Eqn. (3.18). The tangent constitutive matrix, $[D]_T$, during unloading, virtually becomes identical to the constitutive matrix, $[D]_s$, that relates the total stresses to the total strains.

3.5.3 Constitutive models for softening stress-strain behaviour

Two numerical models, depending on the use of constitutive formulations to derive the element stiffness matrix, are considered for finite element analyses:

SMS model: The total stress-strain relationship matrix, $[D]_s$, is used to determine the stiffness matrices of softened elements (Fig. 3.3(c)). The stresses in element integration points are computed from total strains using the most recent secant modulus constitutive matrix, $[D]_s$.

TMS model: The tangent constitutive matrix, $[D]_T$, is used to determine the stiffness matrices of softened elements. The stress response at individual integration point is, however, not computed from incremental strains. Instead, the stresses at integration points are computed from the total strains using the constitutive relationship matrix, $[D]_s$, derived to represent the average resistance of an element (discussed in section 3.8). A distinct feature of the presented TMS model is the adoption of a hybrid approach of computing the element stiffness matrix from the tangent constitutive model, and determining the stress response at integration points from the total strains (Fig. 3.3(d)).

3.6 SHEAR DEFORMATIONS IN FRACTURED ELEMENTS

The isotropic behaviour of a finite element is terminated after satisfaction of the softening initiation criterion. The orthotropic material reference axis system is aligned with the principal strain directions at the instance of softening initiation. In subsequent load steps, shear deformations in the crack band may cause rotation of the principal stress directions, thereby requiring re-alignment of the material reference axis system. The principal stresses and strains can be maintained coaxial in a rotating reference axis system by using an implicit definition of the softened shear modulus term, G_{np}^*, given in Eqn. (2.10). Using the stress-strain relations in Eqn. (3.17) and the definition of the softened shear modulus in Eqn. (2.10), the shear resistance factor μ is defined as:

$$\mu = \frac{1+\nu}{1-\eta\nu^2}\left(\frac{\eta\epsilon_n-\epsilon_p}{\epsilon_n-\epsilon_p}-\eta\nu\right), \qquad (0\le\mu\le 1) \tag{3.19}$$

Here ϵ_n and ϵ_p are the normal strain components in the directions normal and parallel to the fracture plane, respectively. With the progression of softening, the shear resistance factor, μ, decreases and may finally reach a zero value. The constitutive matrices are updated as the parameter, μ, changes its value. The following options have been considered with respect to the orientation of crack bands in finite element analyses.

Coaxial rotating crack model (CRCM): The local axis system n-p is always kept aligned with the directions of principal strains , ϵ_1 and ϵ_2. In this model, the strains ϵ_n and ϵ_p are respectively ϵ_1 and ϵ_2 at the newly oriented material reference state.

Fixed crack model with a variable shear resistance factor (FCM-VSRF): In this model, the local reference axis system is first aligned with the principal strain directions at the instant of softening initiation, and kept non-rotational for the rest of analysis. In the fixed crack model, the shear resistance factor, μ (Eqn. 3.19), is derived using the strain components ϵ_n and ϵ_p corresponding to the fixed local axis directions (which are not necessarily coaxial with the principal stress directions). The variable shear resistance factor, defined in Eqn. (3.19), takes account of deformations in both lateral and normal directions of the fracture plane.

The fixed crack model can also be applied in the usual form with a constant shear resistance factor, μ. Application of this procedure in finite element analyses will be discussed in Chapter 5.

3.7 CLOSING AND REOPENING OF CRACKS

Under reversible loading conditions, the tensile strain, ϵ_n, in an element may alternately increase and decrease. With the reduction of ϵ_n, the shear resistance factor, μ, increases gradually. The softened Young's modulus in the direction n, E_n^s (which may have reached a zero value), is substituted by the undamaged initial value, E, if the parameter μ is greater than a threshold value μ_c. Parametric analyses have shown that the seismic fracture response of concrete gravity dams is not affected by the value of

μ_c varying between 0.90-0.9999. A relatively flexible tolerance, μ_c=0.95, can be used to minimize spurious stiffness changes during the closing of cracks. When $\epsilon_n>0$ in subsequent load steps, the value of μ is computed using the damaged value of η, attained in the previous tension cycles, to determine the reopening of cracks. If μ becomes less than μ_c, the element behaviour is determined by either the reloading or the re-opening path, depending on the final state attained in previous tension cycles. The appropriate value of damaged secant modulus, E_n^*, is reused in the constitutive formulations at that state. Figure 3.4 summarizes the criteria for closing and reopening of cracks, as implemented in the finite element analysis procedure.

A novel feature of the proposed crack closing/reopening criterion is the residual strain upon closing of cracks. Substituting the parameter μ_c for μ in Eqn. (3.19), and rearranging the terms, the crack normal strain at the instance of closure is given by:

$$\epsilon_n = \frac{(1-\eta)\nu+(1-\eta\nu^2)(1-\mu_c)}{(\mu_c-\eta)+\eta\nu^2(1-\mu_c)}.(-\epsilon_p) \tag{3.20}$$

The crack closure strain, often observed in experimental investigations, and also considered empirically in the past numerical models (Fig. 2.9), is implicitly defined in the proposed numerical model. For $\mu_c \approx 1$, the residual strain upon closing of a crack is obtained from Eqn. (3.20) as ϵ_n=-$\nu\epsilon_p$. With this relation, the tensile stress in a crack normal direction evidently becomes zero at the instance of crack closure. In a special case, when $\epsilon_p \approx 0$, the normal strain at crack closure approaches to a zero value, as depicted in Fig. 3.4.

3.8 FINITE ELEMENT IMPLEMENTATION OF THE CONSTITUTIVE MODELS

Four node isoparametric elements are considered for finite element implementation of the constitutive models. The 2 by 2 Gauss integration rule is used to compute the element stiffness matrices in order to prevent the occurrence of spurious zero energy modes to the maximum possible extent (de Borst and Rots [50], Molenkamp et al. [113]).

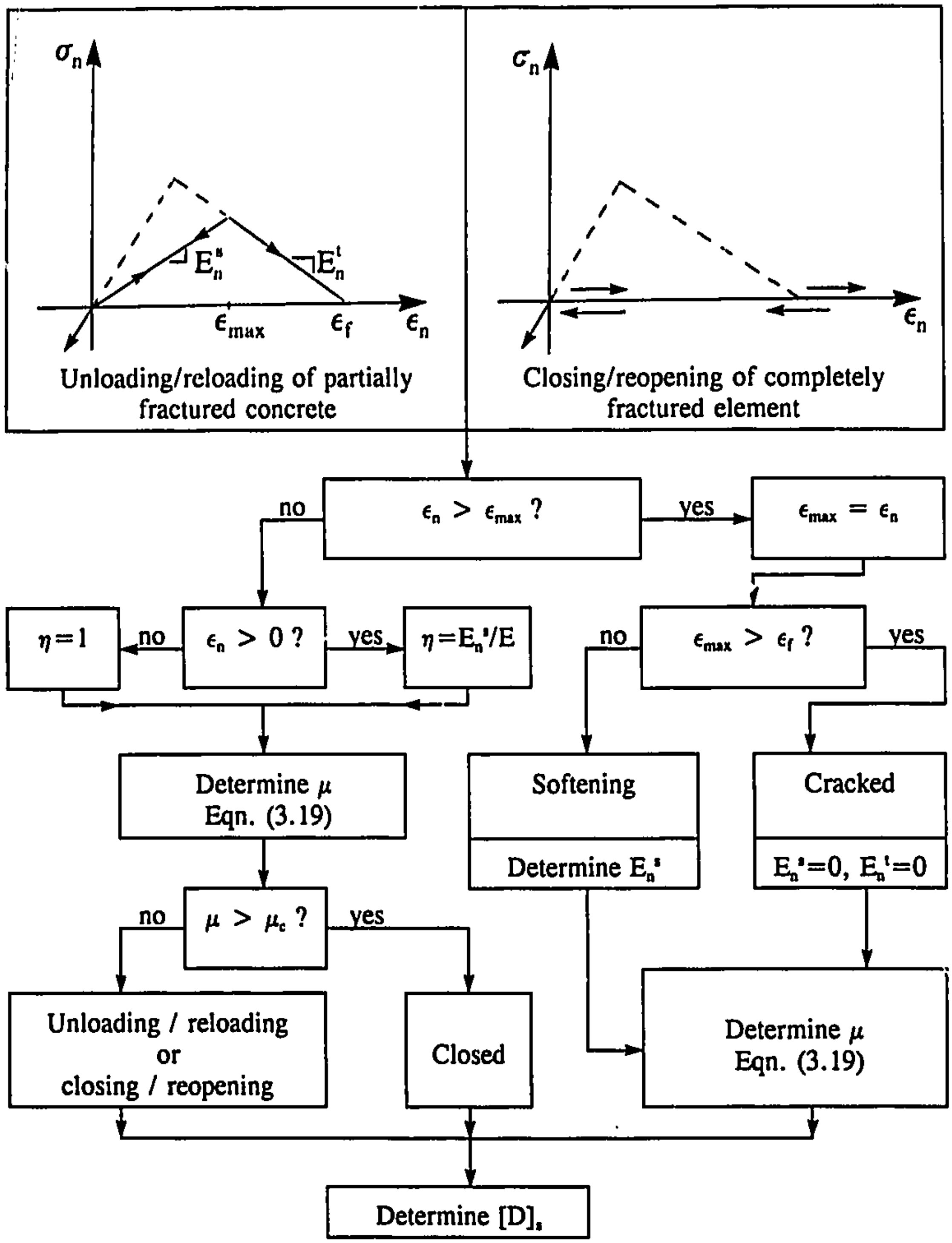

Figure 3.4 The state determination of fractured elements.

During analyses, total strains are computed at each integration point, and the average of Gauss point strains is taken as representative of the behaviour of the element as a whole (Hinton and Campbell [84]). The principal strains computed from average strain response of the element, and the characteristic dimension, h_c (defined below), are used to determine the constitutive model parameters. The total stress-strain relationship matrix, $[D]_s$, in the post-elastic state, thus represents the average resistance of the element. The stresses at individual Gauss points are computed from the respective total strains using the most recent $[D]_s$ matrix. Smearing of the fracture energy dissipation over the entire element area, and determination of the constitutive parameters based on the average element response, help to suppress spurious deformation modes that may arise at individual Gauss points during the curvilinear crack propagation in finite element models. The element stiffness matrix is updated using either the TMS or the SMS model as described in section 3.5.3. Figure 3.5 demonstrates the finite element implementation of constitutive models.

The characteristic dimension, h_c, represents the width of a crack band, over which the fracture energy is dissipated in a finite element model. In elementary fracture problems with a known location and direction of fracture propagation, the finite element meshes can be oriented to bound the crack band by parallel sides of the elements (Fig. 3.6(a)). The definition of characteristic dimension in that situation is obviously defined by the element dimension across the direction of crack band propagation. In the case of an oblique crack propagation in a relatively irregular finite element mesh (Fig. 3.6(b)), h_c will be approximately defined as the square root of an element area; a more rigorous definition of the characteristic dimension is available in Oliver [121]. Finite element meshes will be adequately refined in the expected zones of a fracture band propagation to conserve the fracture energy without violating the maximum admissible element dimension, defined in Eqn. (2.8).

In conventional smeared crack analysis models, the energy dissipation over two or more adjacent integration points in parallel (Fig. 3.6(c)) leads to a mesh sensitive response

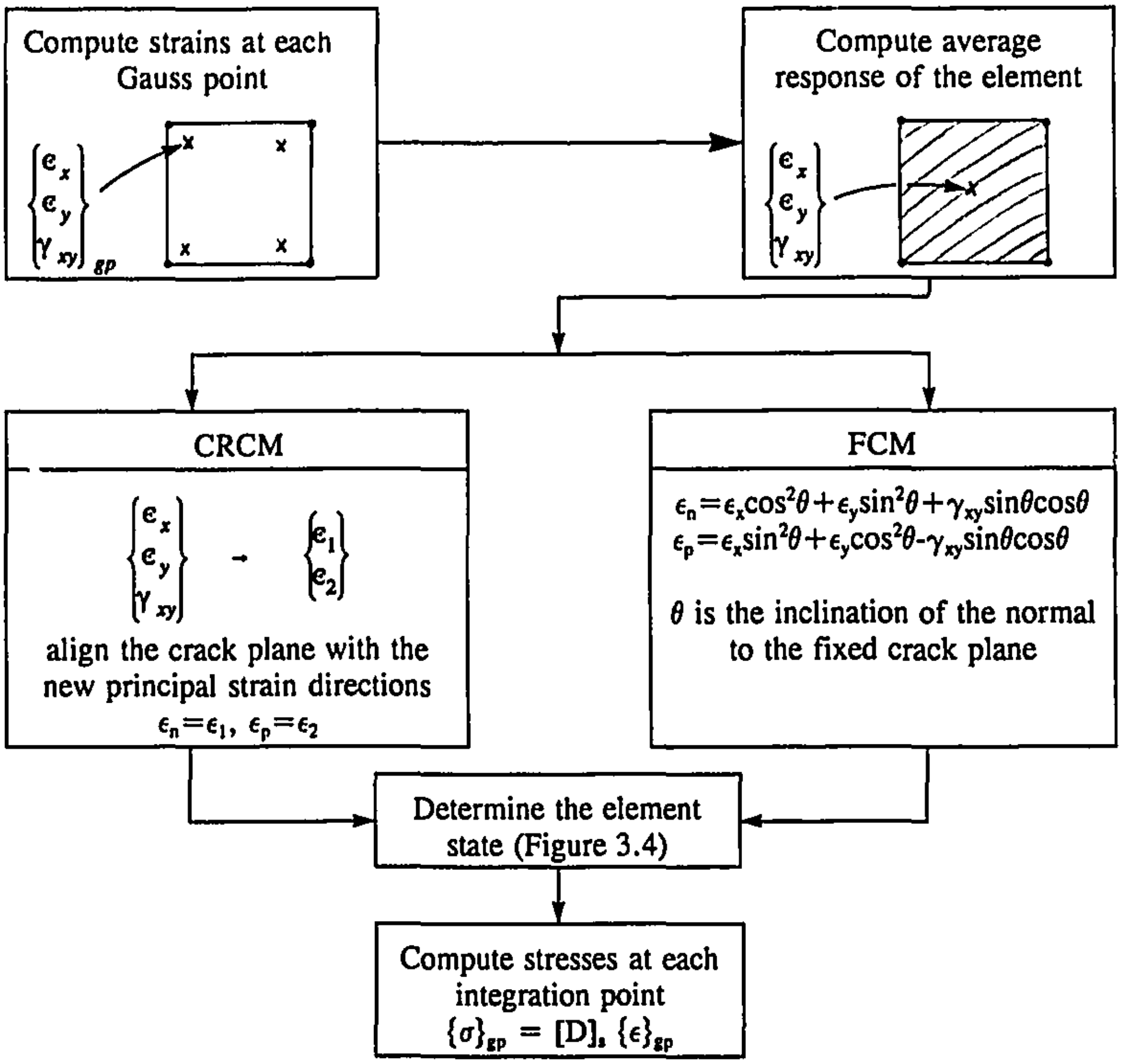

Figure 3.5 Computation of the element response.

prediction, because, in reality the fracture energy is dissipated locally owing to the propagation of a discrete sharp crack. In the crack-band model, which Bažant and Oh[15] proposed as a smeared equivalence of the Hillerborg's fictitious crack model[82], the energy dissipation was assumed to take place over a one element wide band. The crack band model was initially based on the premise of a constant strain condition prevailing in a finite element; thus effectively excluding the application of higher order elements in the analysis. In the incremental constitutive formulation of de-Borst and Nauta[47], the response quantities are computed at each integration point of finite elements; the size adjustment of constitutive relations and the resultant fracture energy dissipation need to

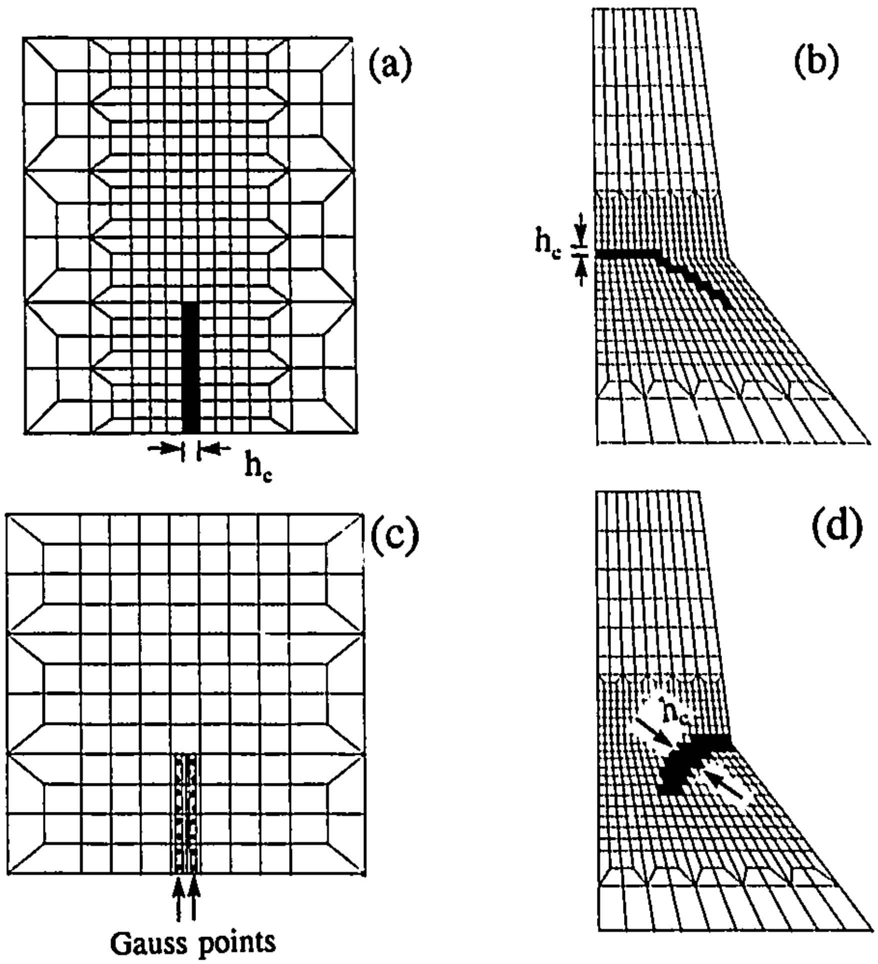

Figure 3.6 Definition of the characteristic dimension, h_c.

be determined on the basis of local response quantities. Artificial measures, such as attributing fractions of the fracture energy to the parallel integration points within a quadrilateral finite element (Dahlblom and Ottosen[45]), are sometimes undertaken to achieve a mesh objective response. In the present finite element implementation of constitute models, the artificial splitting of fracture energy to individual Gauss points is avoided by determining the constitutive parameters based on the average response of each element. The fracture energy is thereby dissipated over an entire element area. The energy dissipation in a finite element analysis with size adjusted constitutive relations still may not be objective, if the blunt fracture front is subdivided into more than one element (Fig. 3.6(d)). An approximate value of h_c (Fig. 3.6(d)) may be used to reduce the amount of fracture energy dissipation in individual elements on the crack band.

The size adjustment of softening response for individual elements may cause a spurious localization of cracks in seismic analyses of concrete dams, when the size of elements in successive layers varies widely (Fig. 3.7). Stress wave propagation in a

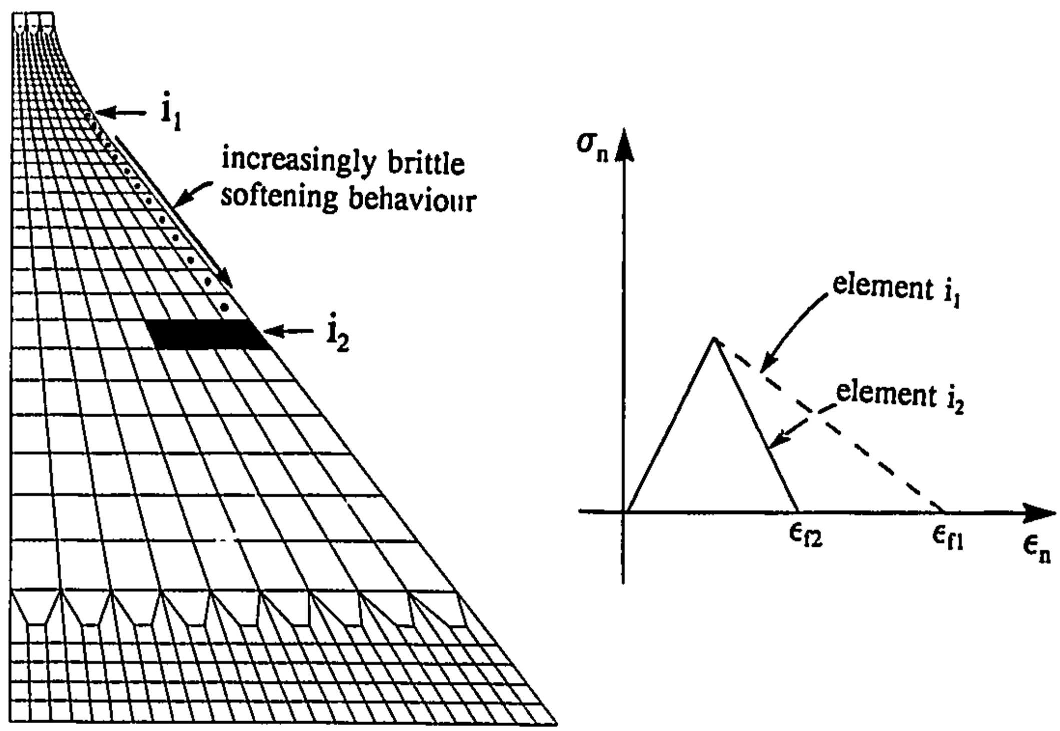

Figure 3.7 The spurious localization of cracks caused by the wide variation of element size in successive layers.

dynamic analysis may cause all elements between i_1 and i_2 in Fig. 3.7 to soften in a particular interval of time. In the absence of any physical discontinuity to cause a crack localization, the element with faster post-peak stiffness degradation (the biggest element) will induce a spurious crack in the finite element model. To avoid such spurious localization of cracks in seismic fracture analyses, the zone of a structure having homogeneous material properties should be subdivided into a nearly uniform grid. In the case of a nonuniform finite element mesh, an approximate average value of h_c can be applied to represent a uniform material softening behaviour over the particular zone.

3.9 SUMMARY

The key features of proposed smeared crack propagation models are summarized in Fig. 3.8. The following properties have been considered in the development of numerical models: (i) the strain softening of concrete due to micro-cracking, (ii) the biaxial effect on the softening initiation stress, (iii) the conservation of fracture energy, (iv) the softening of shear resistance with a progressive evolution of micro-crack damage in finite elements, (v) the dynamic magnification of concrete fracture parameters, and (vi) the closing and reopening of cracks under cyclic loading conditions. The localized strain softening behaviour of concrete has been modelled by two approaches: (a) the stiffness degrading model (SMS) based on a total stress-strain relationship, and (b) the tangent softening model (TMS) based on an incremental stress-strain relationship. Either a coaxial rotating constitutive formulation (CRCM) or a fixed crack model with the variable shear resistance factor (FCM-VSRF) can be applied in crack propagation analyses of concrete structures. The residual strain upon closing of a crack has been implicitly defined using a novel crack closing/reopening criterion.

In the proposed numerical models, the continuum mechanics formulations are retained during the post-softening deformations of finite elements. Although perfect rigid body opening and sliding modes of deformation are not reproduced in this approach, the adoption of a shear softening relationship efficiently alleviates the stress-locking in smeared crack analyses. The finite element solution strategies, developed for nonlinear static and seismic analyses of plain concrete structures, will be presented in the next chapter. Computational efficiencies of the SMS and the TMS models will be examined in chapter 5. Chapter 6 will investigate the relative performances of the CRCM and the FCM-VSRF. Efficiency of the shear softening relationship in alleviating the spurious stress locking response of smeared crack models will be particularly studied in that chapter. Seismic fracture analyses of concrete gravity dams will be performed in chapters 7 and 8. The sensitivity of predicted responses to mesh refinement and different modelling assumptions will also be examined during the course of analyses.

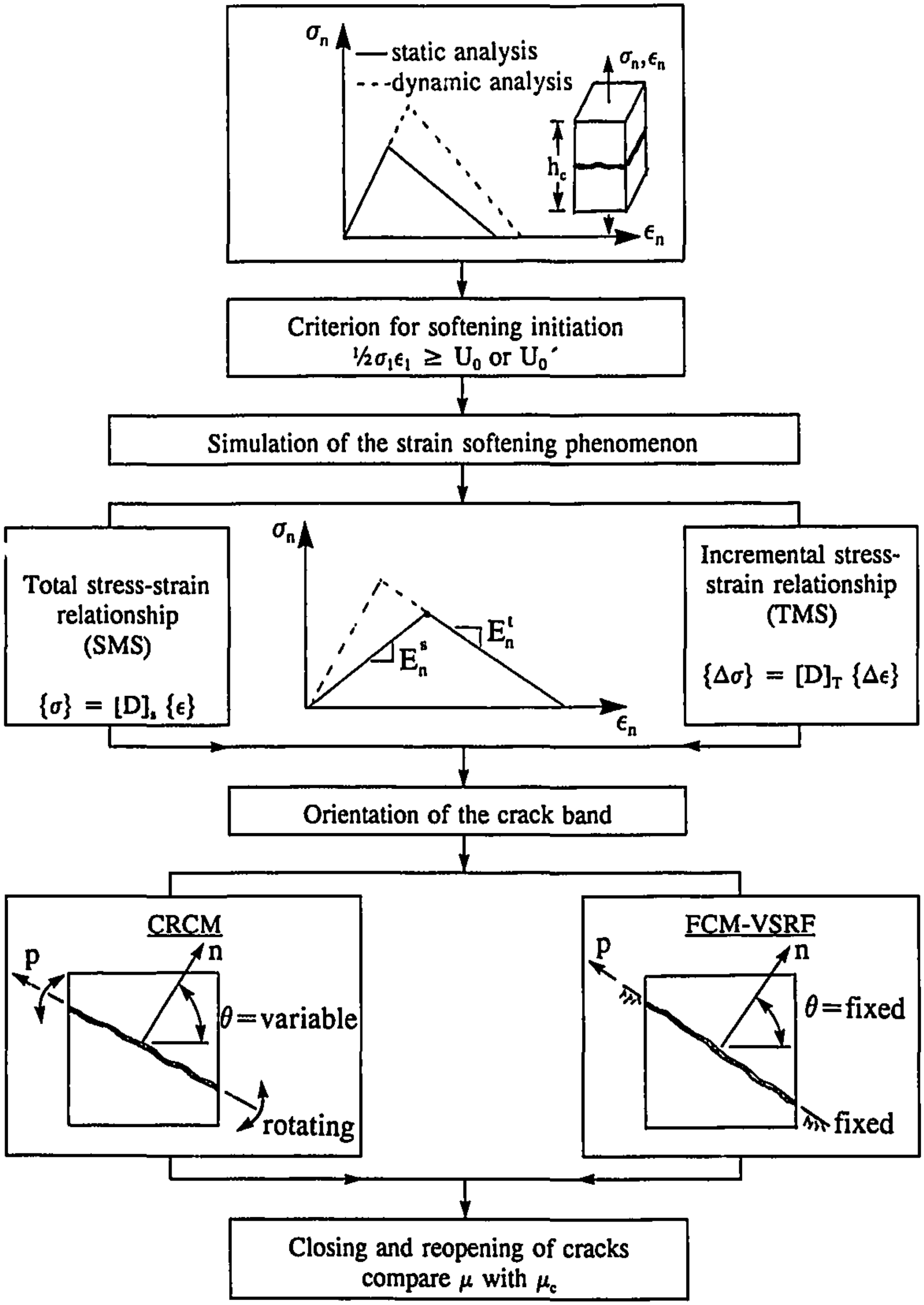

Figure 3.8 Significant features of the smeared crack analysis model.

CHAPTER 4

FINITE ELEMENT ANALYSIS OF SMEARED FRACTURE PROPAGATION IN CONCRETE STRUCTURES

4.1 INTRODUCTION

A nonlinear finite element analysis computer program has been developed to predict the FRACture and DAMage (FRAC_DAM) response of plain concrete structures subjected to seismic, static, and temperature loading conditions. The finite element solution initially starts with the elastic stiffness matrix of uncracked elements. Among all candidate elements that want to initiate softening at a particular iteration, an element with the highest tensile strain energy density, $\frac{1}{2}\sigma_1\epsilon_1$, is allowed to soften first. The fracture propagation in a structure is achieved by allowing one new element to soften per iteration; several iterations may be performed in a particular load step. Figure 4.1 summarizes the crack propagation algorithm, as performed in a particular iteration of the nonlinear static and seismic response analyses.

Smeared crack analysis of concrete structures can be performed with either of the following structural stiffness matrix formulation strategies:

Newton-Raphson (NR) technique: The structural stiffness matrix is updated at each iteration until convergence is achieved at a particular load step. Several updating of the stiffness matrix may be required within a load step.

Modified Newton-Raphson (mNR) technique: The structural stiffness matrix is updated only at the beginning of each load step, and constant stiffness iterations are performed within the step to reduce the unbalance between applied loads and restoring forces of the structure.

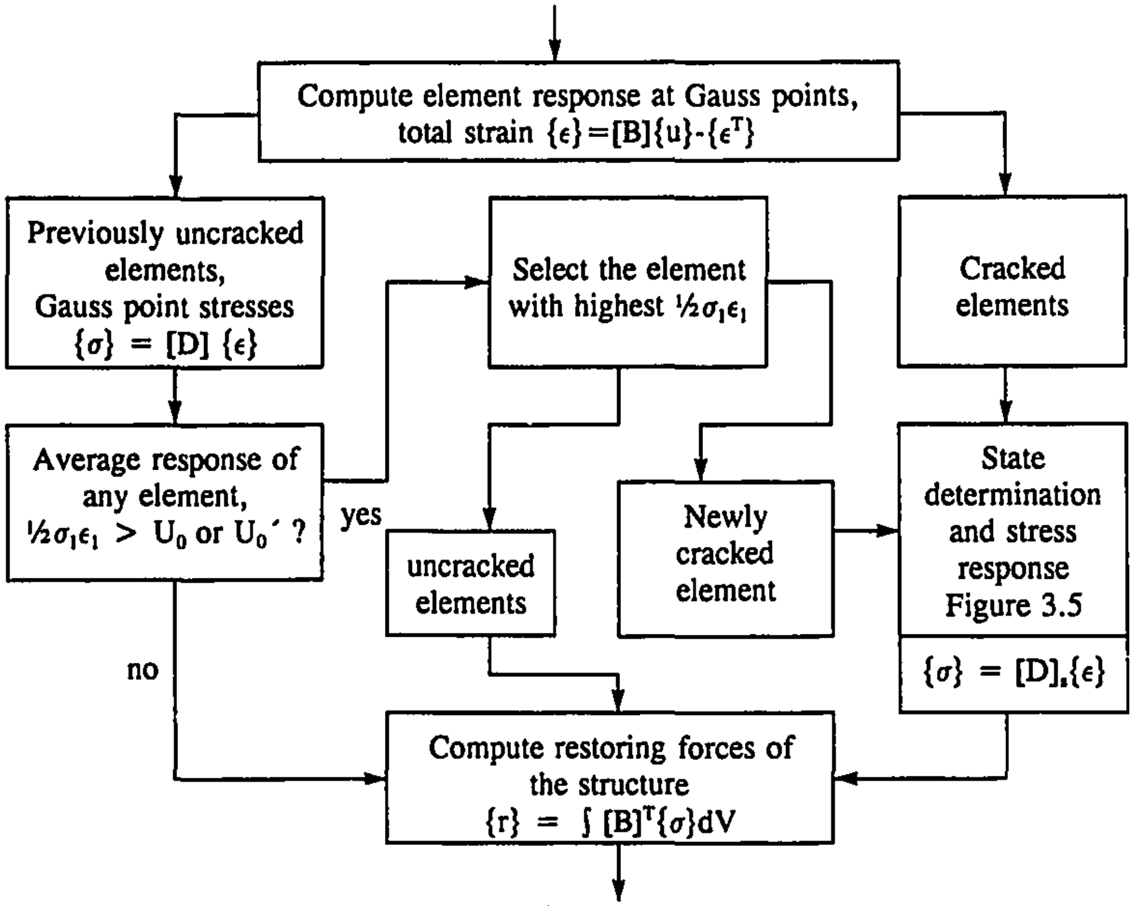

Figure 4.1 Element response computation in a smeared crack analysis.

Crack propagation analysis of a structure, subjected to incremental applications of the specified static or seismic loads, may be preceded by a single step nonlinear static analysis for existing gravity loads (self-weight, hydrostatic pressure etc.) and temperature condition. Figure 4.2 summarizes the key steps involved in that analysis step. The long term effects on the temperature induced stresses will be discussed in section 4.6.

In an incremental static analysis, the nonlinear pre-peak response of a structure can be predicted by solving the standard finite element equilibrium equations:

$$[K]\,\{\Delta u\} = \{\Delta f\} \tag{4.1}$$

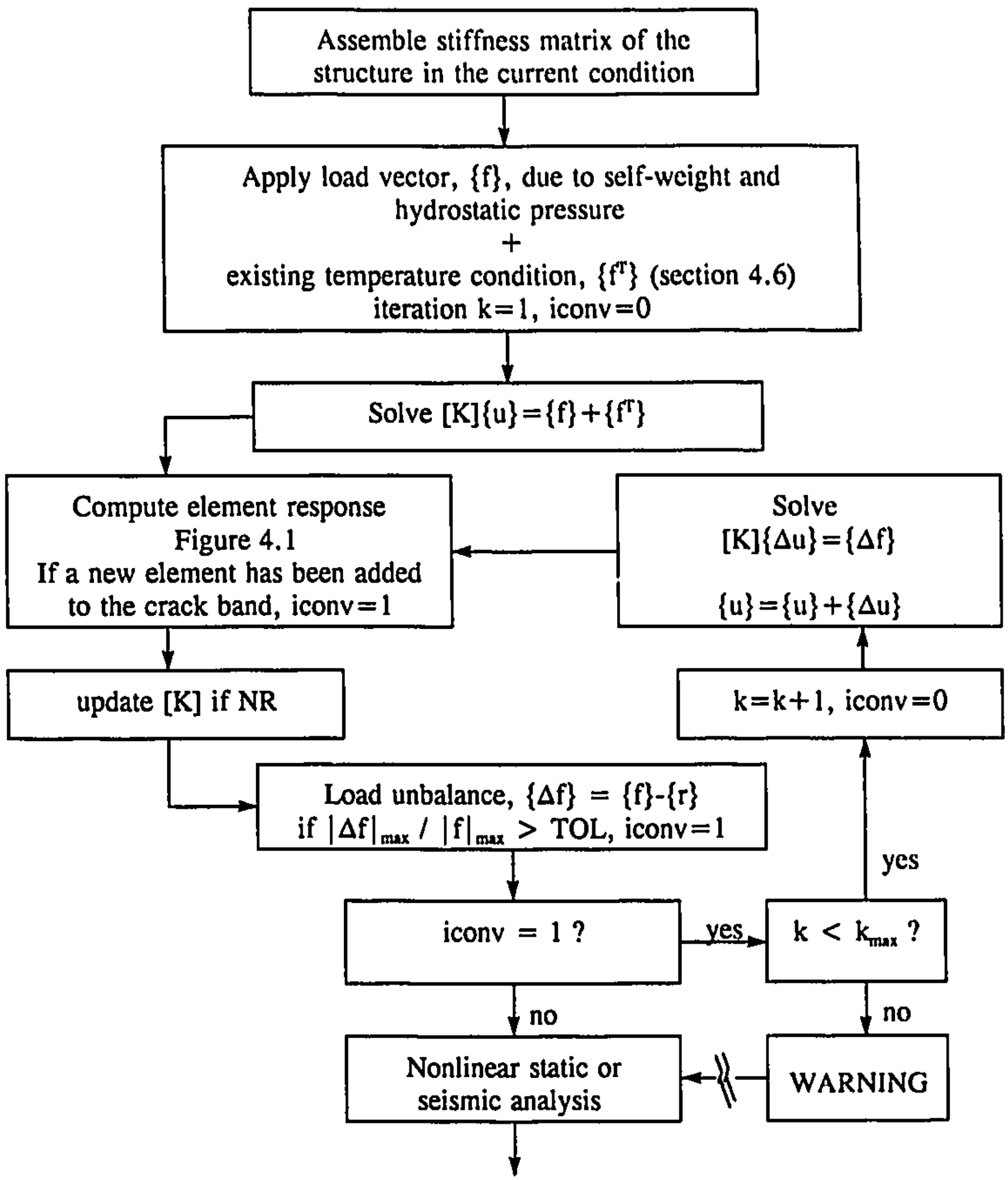

Figure 4.2 Nonlinear analysis for gravity and temperature loads.

where [K] is the stiffness matrix, and $\{\Delta f\}$ and $\{\Delta u\}$ are the vectors of applied incremental loads and unknown incremental displacements. This standard analysis procedure can not be applied to determine the post-peak softening response of structures. Two analysis methods: (i) the applied displacement control (section 4.2), and (ii) an incremental-iterative method with the indirect displacement control (section 4.3), will be considered to predict the nonlinear static response of concrete structures. Various features of the nonlinear seismic analysis procedure, such as the time domain solution of dynamic equilibrium equations, modelling of the material damping effects, and the dynamic interactions in dam-reservoir-foundation systems will be discussed in section 4.4. The computation of energy dissipation due to tensile fracture in the structure will be described in section 4.5. Figure 4.3 presents a general framework of the computational model developed for fracture analyses of concrete structures subjected to static or seismic loading conditions.

4.2 NONLINEAR STATIC ANALYSIS UNDER SPECIFIED DISPLACEMENT

The ultimate resistance and the post-failure behaviour of simple concrete structures can be predicted by specifying the displacements at one or more control points (Fig. 4.4). The structural degrees-of-freedom (DOF) can be separated into two groups:
(i) DOF with specified displacement conditions:

$$\{u_s\}_i = \{u_s\}_{i-1} + \{\Delta u_s\} \tag{4.2}$$

(ii) DOF under applied loading conditions:

$$\{f_a\}_i = \{f_a\}_{i-1} + \{\Delta f_a\} \tag{4.3}$$

where the subscript 's' refers to the DOF subjected to specified deformation conditions, and 'a' to other DOF that may be subjected to applied loads. The structural equilibrium equations under incremental displacements and loads can be expressed as:

$$\begin{pmatrix} K_a & K_{as} \\ K_{sa} & K_s \end{pmatrix}_i \begin{Bmatrix} \Delta u_a \\ \Delta u_s \end{Bmatrix}_i = \begin{Bmatrix} \Delta f_a \\ \Delta r_s \end{Bmatrix}_i \tag{4.4}$$

where $\{\Delta r_s\}$ is the increment of unknown reaction forces at the displacement specified DOF, and $\{\Delta u_a\}$ is the unknown displacement increments at other DOF. Partitioning the system equilibrium equations, the displacement increments at unknown DOF can be obtained solving the following reduced system of equations (4.5):

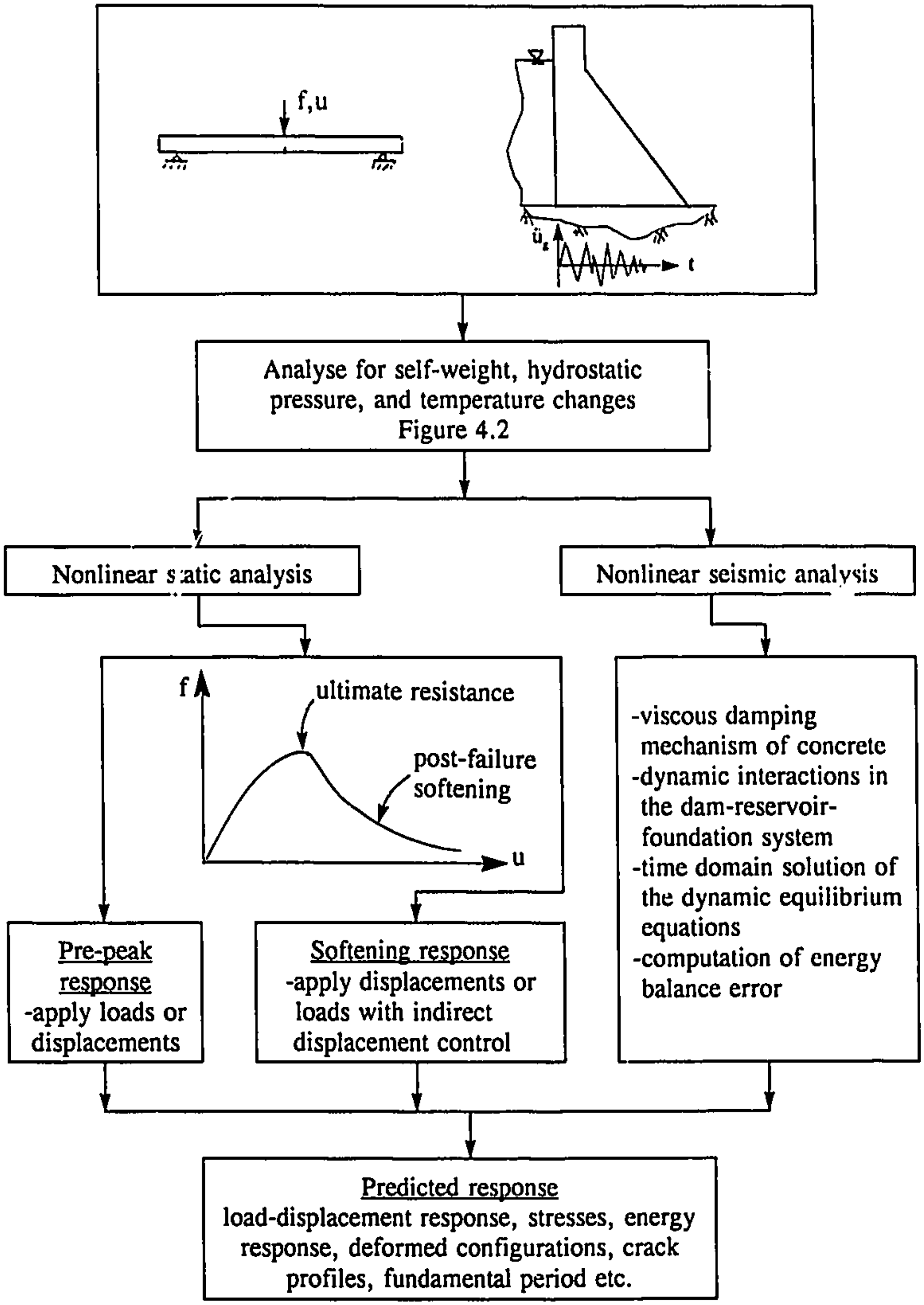

Figure 4.3 Computation models to predict nonlinear static and seismic responses of concrete structures.

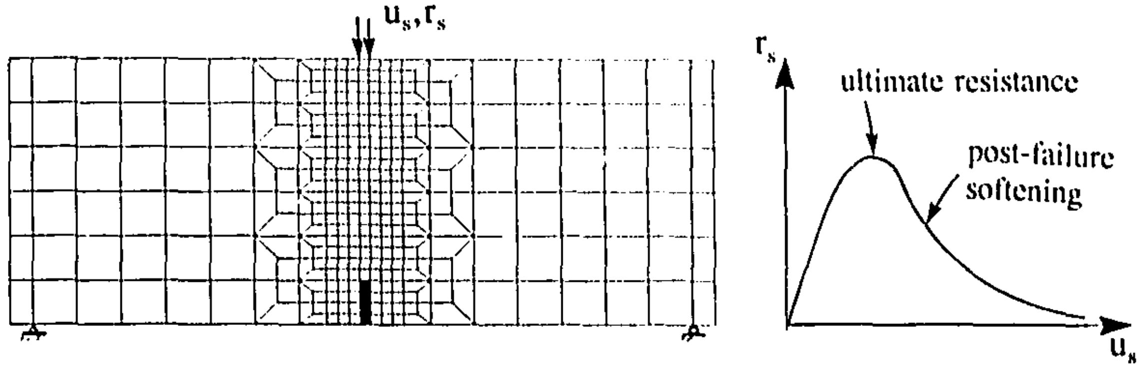

Figure 4.4 Failure behaviour of a beam under three-point loading.

$$[K_a]_i \{\Delta u_a\}_i = \{\Delta f_a\} - [K_{as}]_i \{\Delta u_s\} = \{\Delta f_a^r\}_i^k \tag{4.5}$$

The logical diagram for smeared fracture analysis of concrete structures, subjected to incremental displacement loading, is shown in Fig. 4.5.

Unbalance between the applied loads, $\{f_a\}$, and the restoring forces at corresponding DOF, $\{r_a\}$, is computed after each iteration:

$$\{\Delta f_a^r\}_i^k = \{f_a\}_i - \{r_a\}_i^k \tag{4.6}$$

The residual norm is defined as:

$$f_{norm} = \frac{\max|\Delta f_a^r|_i^k}{\max|\ r\ |_i^k} \tag{4.7}$$

where $max\ |\ \Delta f_a^r\ |\ _i^k$ is the maximum force unbalance at DOF not subjected to specified displacements, and $max\ |\ r\ |\ _i^k$ is the maximum of restoring forces among all DOF. A relatively fine convergence tolerance (TOL=0.001) is assumed in the finite element analyses discussed in Chapter 5. The maximum number of iterations (k_{max}) required to satisfy this convergence criterion varies depending on the stiffness formulation model (TMS or SMS) and the iteration procedure (NR or mNR) adopted in the analysis. The computational efficiencies of different numerical schemes are investigated in Chapter 5.

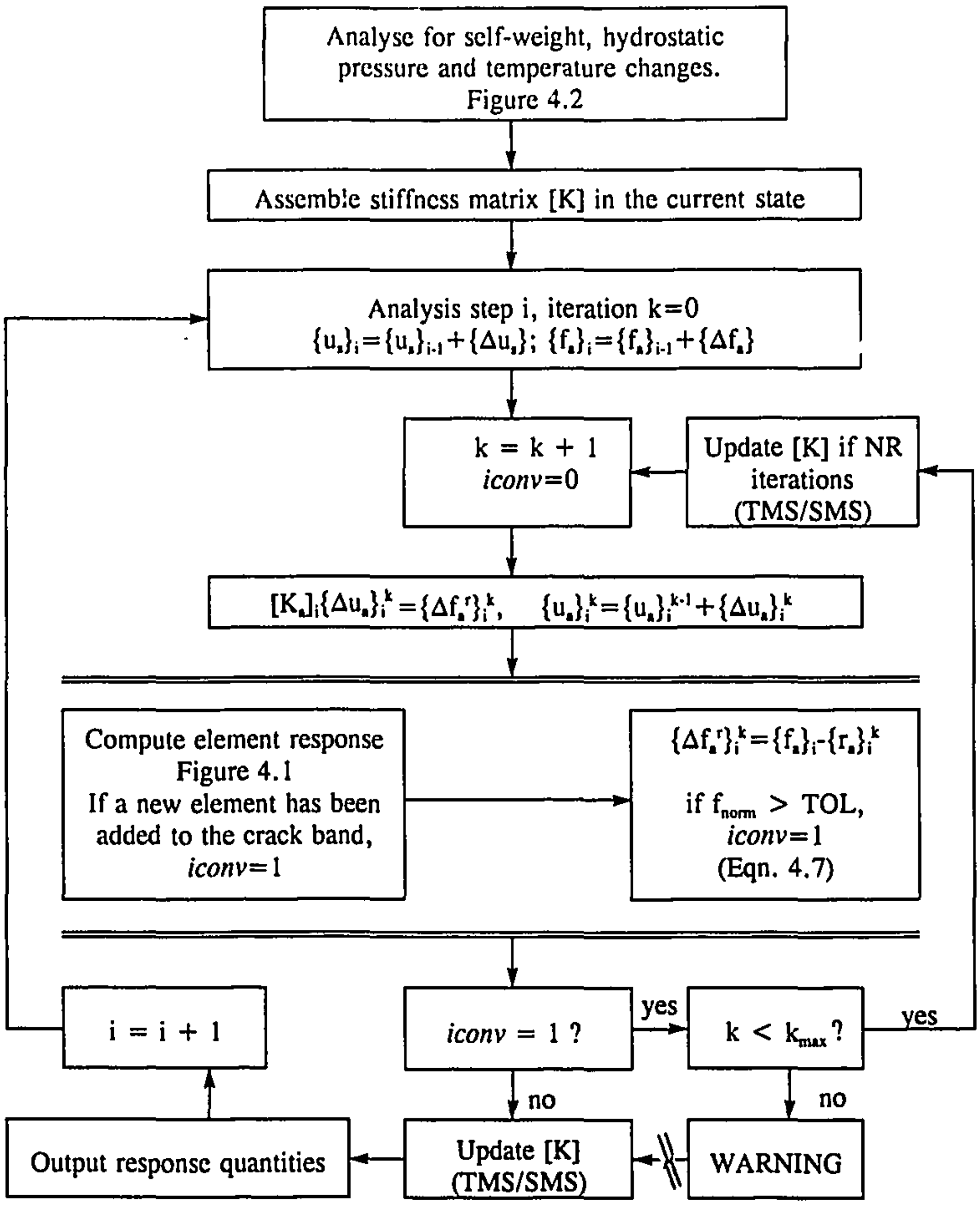

Figure 4.5 Fracture analysis under incremental displacement control.

4.3 NONLINEAR STATIC ANALYSIS UNDER AN INDIRECT DISPLACEMENT CONTROL

The direct displacement control analysis technique can be efficiently applied when displacements at the control points experience a monotonic increase. In special cases, (Fig. 4.6(a)), the load-displacement response at control points may show a snap-back behaviour (Fig. 4.6(b)). Moreover, when a structure is subjected to load applications at several points (Fig. 4.6(c)), the algebraic relation between the displacements at different application points may not be known before hand. Special response quantities, such as the crack mouth opening displacement (CMOD), crack mouth sliding displacement (CMSD), incremental crack length (ICL), or the displacement at a selected point, that exhibit a monotonic increase during load applications (Fig. 4.6(d)), are often considered as the control parameters in experimental investigations of notched concrete members. The selected control parameter is measured during the course of investigation, and used as a feed-back signal to adjust the loads applied to the structure.

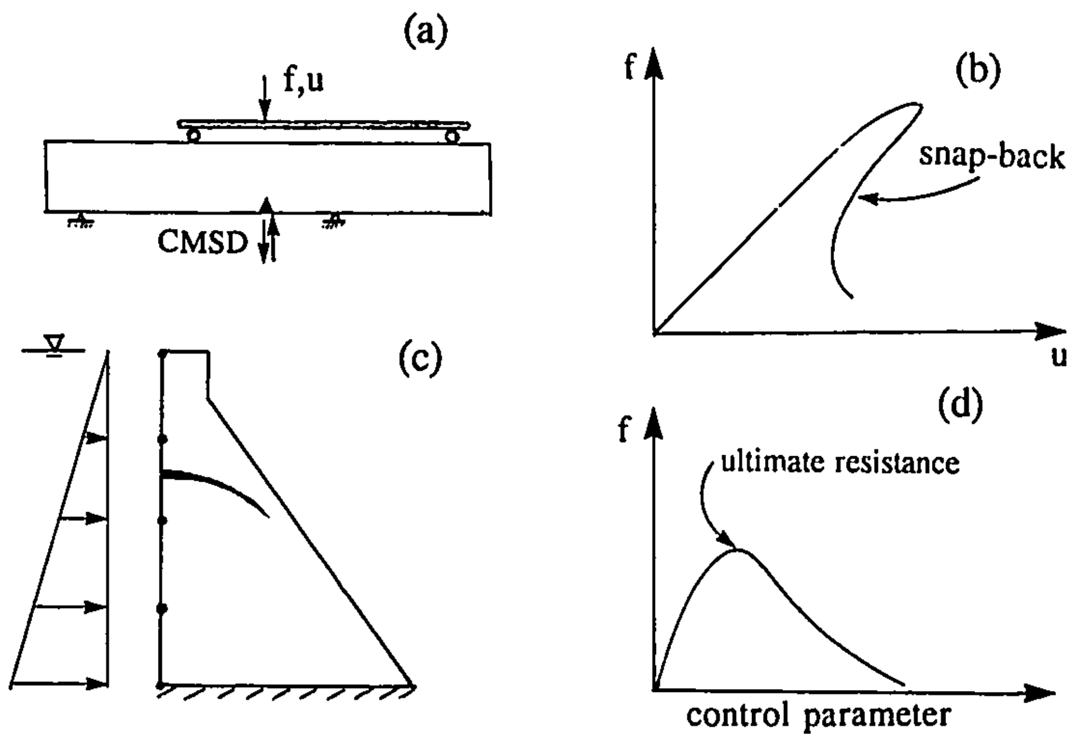

Figure 4.6 Post failure behaviour of concrete structures.

Special numerical techniques have been proposed in the literature to predict post-bifurcation and post-failure responses of strain softening solids. Carpinteri et al.[35] have applied the ICL control method in discrete crack analysis of a model dam. A similar technique with the dynamic relaxation solver (Underwood[152]) has also been considered by Bittencourt et al. [29]. The standard 'arc length' method (Crisfield[44]) may fail to converge in the fracture analysis of concrete structures, due to the highly localized nature of failure or bifurcation modes (de Borst[49]). Consequently, a modified strategy has been proposed using only a few dominant DOF in the constraint equation that determines the load increment during iterations (de Borst[49]). A similar technique is applied in the following incremental-iterative analysis procedure, developed in this research, to predict the post-failure behaviour of plain concrete structures.

In the failure analysis of concrete structures, two DOF, DOF_m and DOF_n, are selected such that the relative displacement between them shows a monotonic increase during the course of analysis. The computed relative displacement is taken as the control parameter to adjust the applied loads on the structure during iterations. The fundamental assumption in the proposed load adjustment procedure is that the applied load vector, {f}, is directly proportional to the controlling response parameter. The target response (TR) of the controlling relative displacement parameter is increased in discrete steps:

$$TR_i = TR_{i-1} + \Delta TR \tag{4.8}$$

and the structural equilibrium equations are solved at the beginning of each step for the following differential load, $\{\Delta f\}_i$:

$$\begin{aligned} \{\Delta f\}_i &= \left(\frac{\Delta TR}{TR_i}\right)\{f\}_{i-1} \\ \{f\}_i &= \{f\}_{i-1} + \{\Delta f\}_i \end{aligned} \tag{4.9}$$

The difference between the target response, TR, and the computed response, CR, is determined at each iteration:

$$CR_i^k = u(DOF_m) - u(DOF_n)$$
$$R_{norm} = \left|\frac{TR_i - CR_i^k}{CR_i^k}\right| \tag{4.10}$$

where k is the iteration number. If R_{norm} is greater than a specified tolerance, the total applied loads on the structure are adjusted during the iteration:

$$\{f\}_i^k = \frac{TR_i}{CR_i^k}\{f\}_i^{k-1} \tag{4.11}$$

Several iterations may be performed at each step to minimize the unbalance between the applied loads, {f}, and the restoring forces {r}:

$$\{\Delta f\}_i^k = \{f\}_i^k - \{r\}_i^k \tag{4.12}$$

The residual norm is defined as:

$$f_{norm} = \frac{\max|\Delta f|_i^k}{\max|\ r\ |_i^k} \tag{4.13}$$

where $max\ |\ \Delta f\ |_i^k$ is the maximum unbalance force among all DOF, and $max\ |\ r\ |_i^k$ is the maximum of restoring forces. Figure 4.7 summarizes the key steps involved in this analysis procedure, that will be applied in Chapter 6 to predict the fracture response of plain concrete structures. The convergence tolerance (TOL) has been assumed to be 0.001 in the analyses. The Newton-Raphson iteration technique with the SMS stiffness formulation method has been adopted in the analyses, presented in Chapter 6.

4.4 NONLINEAR TIME DOMAIN ANALYSIS OF CONCRETE GRAVITY DAMS

The dynamic equilibrium equations of a concrete gravity dam under seismic excitations, including the pre-seismic applied forces, are expressed as,

$$[M]\{\ddot{u}\} + [C]\{\dot{u}\} + \{r\} = -[M]\{\ddot{u}_g\} + \{p\} = \{f\} \tag{4.14}$$

where [M] is the mass matrix, [C] the damping matrix, {r} the vector of restoring forces, {p} the vector of pre-seismic applied loads, $\{\ddot{u}\}$, $\{\dot{u}\}$, and {u} are acceleration,

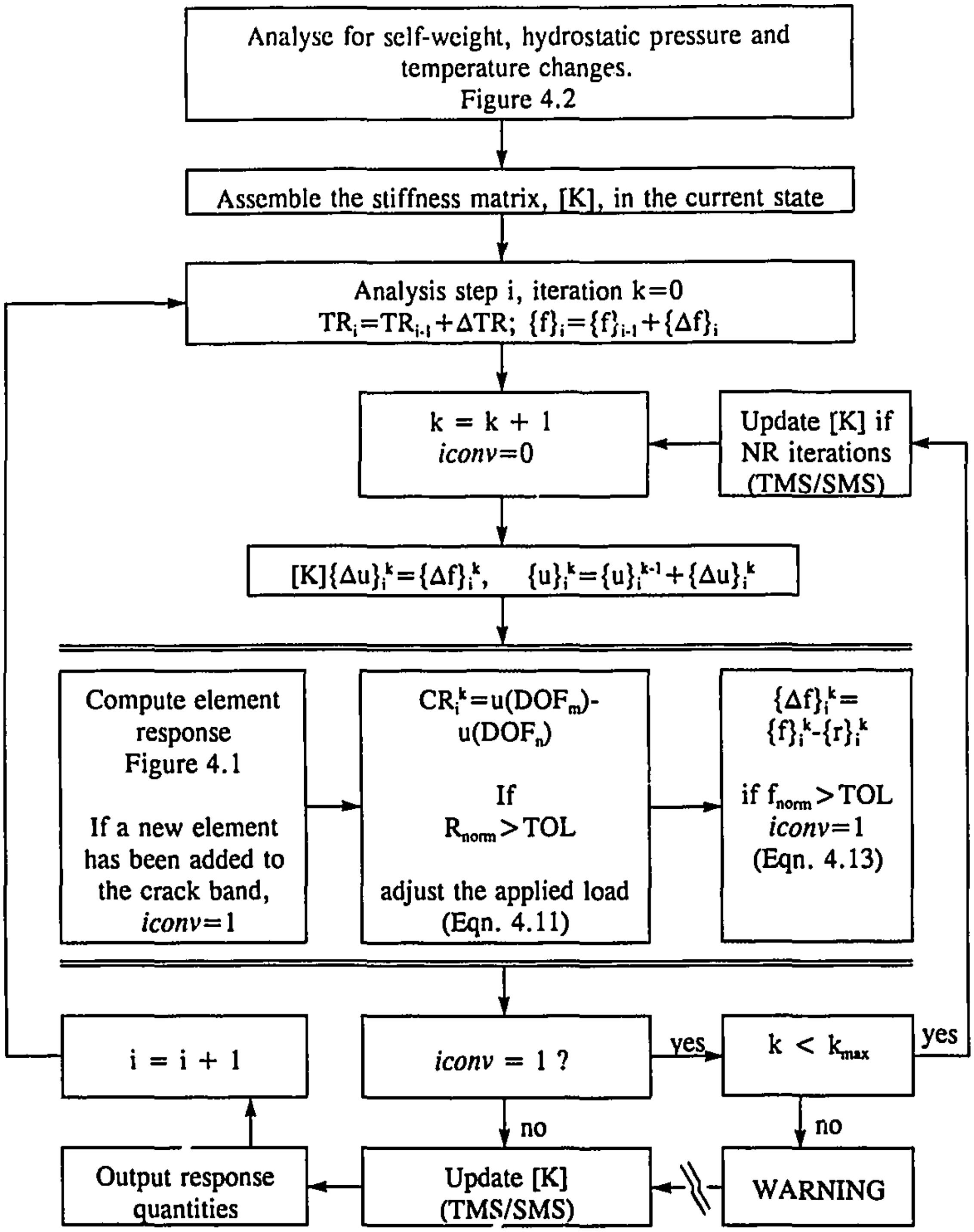

Figure 4.7 Fracture analysis under indirect displacement control.

velocity, and displacement vectors respectively, and $\{\ddot{u}_g\}$ is the vector due to uniform free-field accelerations in horizontal and vertical directions. Self-weight and hydrostatic pressure loads generally contribute to the vector {p}. The row-sum lumped formulation (Zienkiewicz and Taylor [163]) has been used to develop the mass matrix, [M], of the dam finite element model. The reservoir added mass may also contribute to the system mass matrix, [M], when dynamic interactions with the reservoir are taken into consideration. The restoring force vector, {r}, can be computed from the contributions of each finite element integration point using the standard assembly procedure. The damping matrix, [C], includes the viscous effects of the material as well as the added damping terms representing energy dissipations due to reservoir and foundation interaction effects. Modelling of the material damping effects, dynamic interactions in the dam-reservoir foundation system, numerical integration of the dynamic equilibrium equations, and computation of the energy balance error in nonlinear seismic analyses are discussed in the following sections.

4.4.1 Viscous damping of concrete in gravity dams

Phenomenological modelling of the material damping mechanisms is very uncertain due to the lack of experimental results on the behaviour of mass concrete under seismic loading conditions. Small amplitude forced vibration tests are often conducted to determine the amount of damping on the vibration modes of concrete dams. The equivalent linear viscous damping matrix in the dynamic equilibrium equations (4.14) is usually expressed as:

$$[C] = a[M] + b[K] \tag{4.15}$$

where [M] and [K] are respectively mass and elastic stiffness matrices of the structure, and 'a' and 'b' are the proportionality factors, calibrated to provide the desired amount of damping, usually 3 to 7 percent, in two selected vibration modes of the dam. Non-viscous energy dissipation mechanisms in a concrete gravity dam system, such as (i) the added damping effects due to dynamic interactions with the reservoir and the foundation, and (ii) the structural damping due to frictional losses at the interfaces will also contribute to the damping matrix, [C], calibrated on the basis of over all modal response of an existing dam. Moreover, the calibration of material viscous effects, based on the modal response of concrete dams, is yet to be justified through experimental investigations, and by rigorous finite element analyses using phenomenological models of the material strain rate effects (Bićanić and Zienkiewicz [28]).

The stiffness proportional damping term is considered in the present investigations as an approximate representation of the material viscous properties. The proportionality factor, b, is calibrated to provide a specified amount of damping in the initial fundamental mode of dams. The mass proportional term is excluded to avoid undesirable restraining effects on the fracture response of finite elements (El-Aidi and Hall [57]). However, the stiffness proportional damping matrix, represented by the term [c] in Fig 3.2(a), may contribute to a significant part of the element resistance under dynamically applied loads. If this damping term is retained constant in the smeared crack analysis of concrete dams, significant tensile forces may be carried across the cracked elements, providing misleading prediction about the severity of cracking in the structure (as will be shown in Chapter 7). The following finite element damping models are considered to determine their influences on the seismic fracture response of concrete gravity dams. The structural damping matrix, [C], is assembled from the contributions of all finite elements and added damping terms (if considered in the analysis).

Linear damping model (LDM): The element damping matrix, [c] (Eqn. 3.4), is defined as follows:

$$[c] = b[k]_0 \tag{4.16}$$

where $[k]_0$ is the initial elastic stiffness matrix of the element. The damping matrix, [c], defined in Eqn (4.16), is retained constant throughout the analysis.

Quasi-linear damping model (QDM): The material damping matrix is assumed proportional to the instantaneous stiffness of the element:

$$[c(t)] = b[k(t)] \tag{4.17}$$

where [k(t)] is the nonlinear stiffness matrix of the element. The element stiffness is degraded with progressive evolution of micro-crack damage. To avoid artificial restraints on the crack opening in damaged elements, the viscous resistance of the softening material is also assumed to decrease proportionally. The element regains pre-softening damping properties after closing of the crack. Damping resistance of the bulk of the material, behaving linearly outside the localized tensile cracking zones, will remain largely unaffected in the quasi-linear model.

Elasto-brittle damping model (EDM): The damping resistance of an element is assumed to be completely lost ([c]=[0]) instantly after initiation of the tensile softening process, and maintained at that condition for the rest of analysis. Only the linear elastically behaving finite elements contribute to the structural damping matrix [C].

4.4.2 Dynamic interactions in a dam-reservoir-foundation system

The dynamic interactions in dam-reservoir-foundation systems can be represented by adding mass, damping, and stiffness terms to the system property matrices in Eqn. (4.14). Figure 4.8(a) shows the added properties to be considered in the seismic analysis of concrete gravity dams. In the time domain seismic analysis, the reservoir interaction

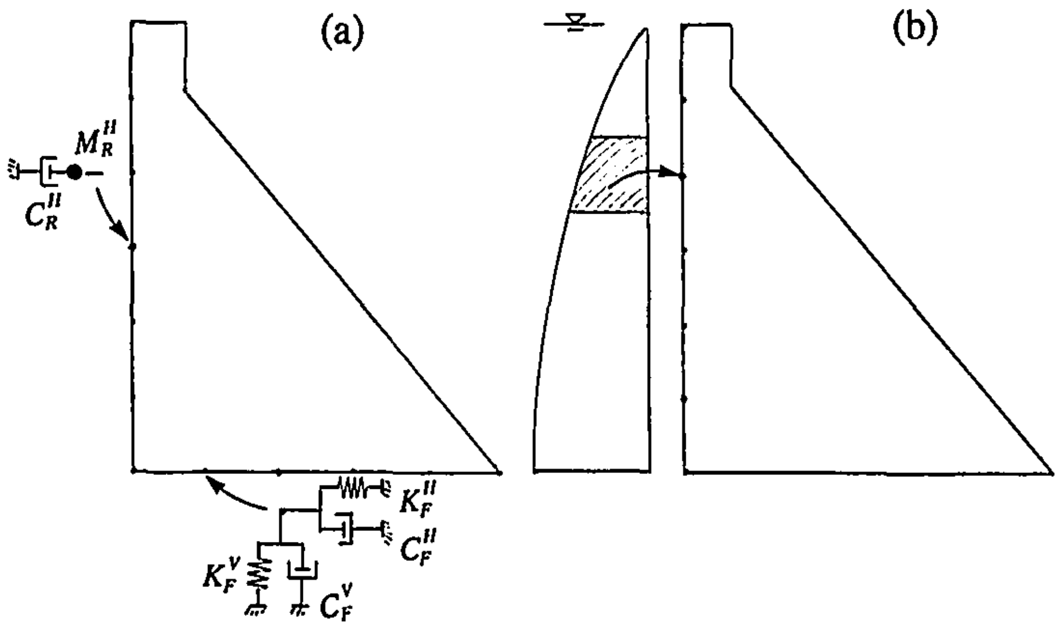

Figure 4.8 (a) Dynamic interaction effects of the reservoir and the foundation, and (b) the Westergaard[159] added mass.

effects are often represented by a parabolic body of water mass (Fig. 4.8(b)), forced to move in unison with the dam (Westergaard [159]). The foundation added stiffness and damping terms can be determined using the analytical expressions available in Wolf [161]. Rigorous modelling procedures to take account of reservoir and foundation interaction effects in the time domain seismic analysis of concrete gravity dams will be discussed in Chapter 8.

4.4.3 Numerical integration of the dynamic equilibrium equations

Due to cracking in concrete dams, the restoring force vector, {r}, the stiffness matrix, [K], and the damping matrix, [C], may vary with time. The dynamic equilibrium equations (4.14) are solved in time-domain at discrete steps, Δt. Using the α integration method (Hilber et al. [81]), equations (4.14) can be recast in the following incremental form for a particular iteration, k, at a time step, i,

$$\begin{aligned}\frac{1}{\beta\Delta t^2}[M+\gamma\Delta t C+(1+\alpha)\beta\Delta t^2 K]_i^{k-1}\{\Delta u\}_i^k = \{f\}_i &+ \frac{1}{\beta\Delta t^2}[M]\{u_{i-1}+\Delta t\dot{u}_{i-1}+(\frac{1}{2}-\beta)\Delta t^2 \\ &+[C]_i^{k-1}\{\frac{\gamma}{\beta\Delta t}(u_{i-1}+\Delta t\dot{u}_{i-1}+(\frac{1}{2}-\beta)\Delta t^2\ddot{u}_{i-1})-(\dot{u}_{i-1}+(1-\gamma)\Delta t\ddot{u}_{i-} \\ &+\alpha\{r\}_{i-1} \\ &-\frac{1}{\beta\Delta t^2}[M+\gamma\Delta t C]_i^{k-1}\{u\}_i^{k-1}-(1+\alpha)\{r\}_i^{k-1}\end{aligned} \tag{4.18}$$

The parameters α ($-\frac{1}{3} \leq \alpha \leq 0$), $\beta=(1-\alpha)^2/4$, and $\gamma=(\frac{1}{2}-\alpha)$ determine the characteristics of the numerical integration procedure. This integration scheme degenerates to the Newmark average acceleration method (Newmark [115]) when $\alpha=0$. The numerical dissipation parameter, α, has been applied only on the elastic resistance part of the finite element equilibrium equations. However, that can be extended to include inertia and damping components as well. The nonlinear time domain solution scheme adopted for seismic fracture analysis of concrete gravity dams is outlined in Fig. 4.9. The Newton-Raphson iteration technique, with the SMS stiffness formulation method, will be applied in all seismic analyses to minimize the unbalance between dynamic force components. The convergence norm used during iterations, f_{norm}, is defined in Eqn. (4.19):

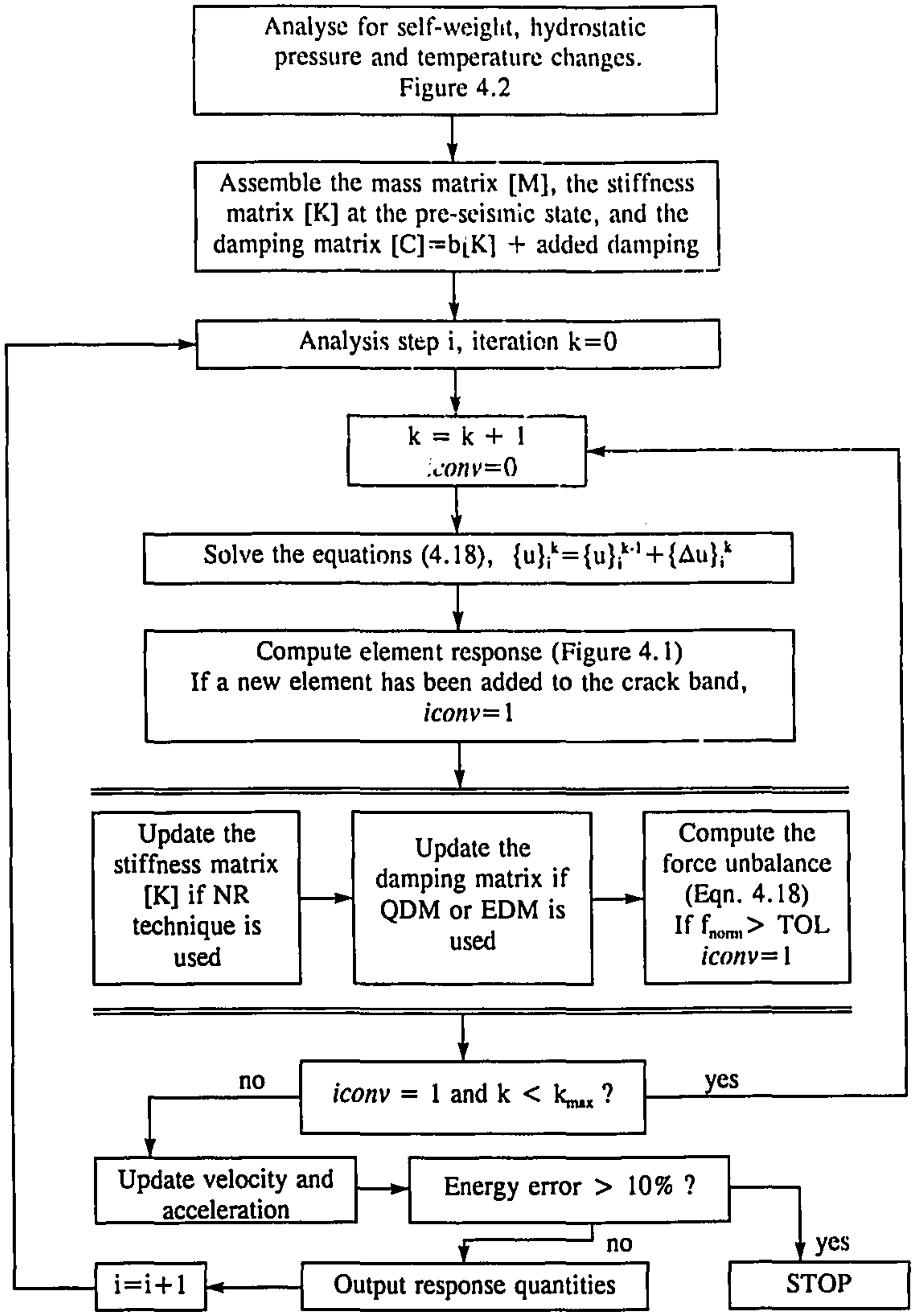

Figure 4.9 Seismic fracture analysis of concrete gravity dams.

$$f_{norm} = \frac{\max|\Delta f|_i^k}{\max|f|_i} \tag{4.19}$$

where $max|\Delta f|^k_i$ is the absolute maximum of unbalance forces on the right hand side of equations (4.18) after the iteration k, and $max|f|_i$ is the absolute maximum of forces applied at the time step i. The solution advances to the next time step when f_{norm} is less than a specified tolerance, TOL (assumed between 10^{-10} and 10^{-3}), or the number of iterations in a time step exceeds a pre-assigned value, k_{max} (assumed 10 for a small time step of 0.002 sec in Chapter 7). Any unbalance at the local level is taken account of, by enforcing the dynamic equilibrium condition during the computation of velocity and acceleration vectors:

$$\begin{aligned} \{\dot{u}\}_i &= \{\dot{u}\}_{i-1} + (1-\gamma)\Delta t\{\ddot{u}\}_{i-1} + \frac{\gamma}{\beta\Delta t}\{u_i - u_{i-1} - \Delta t\dot{u}_{i-1} - (\frac{1}{2}-\beta)\Delta t^2\ddot{u}_{i-1}\} \\ \{\ddot{u}\}_i &= [M]^{-1}(\{f\}_i + \alpha\{r\}_{i-1} - [C]_i\{\dot{u}\}_i - (1+\alpha)\{r\}_i) \end{aligned} \tag{4.20}$$

The additional convergence check of nonlinear dynamic solutions, based on the energy balance error at each time step, is discussed in the following section.

4.4.4 Seismic energy balance in the dam

The energy calculations under seismic loading conditions are performed using the absolute energy terms (Uang and Bertero [151]). The dynamic equilibrium equations (4.14) can be rearranged as follows,

$$[M]\{\ddot{u}_t\} + [C]\{\dot{u}\} + \{r\} = \{p\} \tag{4.21}$$

where the vector $\{\ddot{u}_t\}$ represents the absolute acceleration, which is the sum of the relative acceleration, $\{\ddot{u}\}$, and the ground acceleration, $\{\ddot{u}_g\}$. The dynamic equilibrium of energy components can be obtained by integrating equations (4.21) with respect to the relative displacement, u:

$$\int\{\ddot{u}_t\}^T[M]\{du\} + \int\{\dot{u}\}^T[C]\{du\} + \int\{r\}^T\{du\} = \int\{p\}^T\{du\} \tag{4.22}$$

Replacing $\{du\}$ with $\{du_t - du_g\}$, where u_t and u_g are the total displacement and the ground displacement respectively, the first term in equation (4.22) can be rearranged as follows:

$$\int \{\ddot{u}_t\}^T[M]\{du\} = \int \{\ddot{u}_t\}^T[M]\{du_t\} - \int \{\ddot{u}_t\}^T[M]\{du_g\}$$
$$= \frac{1}{2}\{\dot{u}_t\}^T[M]\{\dot{u}_t\} - \int \{\ddot{u}_t\}^T[M]\{du_g\} \tag{4.23}$$

Substituting the above expression in equation (4.22),

$$\frac{1}{2}\{\dot{u}_t\}^T[M]\{\dot{u}_t\} + \int \{\dot{u}\}^T[C]\{du\} + \int \{r\}^T\{du\} = \int \{\ddot{u}_t\}^T[M]\{du_g\} + \int \{p\}^T\{du\} \tag{4.24}$$

The first term in equation (4.24) represents the absolute kinetic energy, E^K, which can be evaluated in a time step using the absolute velocity vector, $\{\dot{u}_t\}$, of that instance. The trapezoidal integration rule is applied to evaluate the other integral terms that successively represent the following energy components:

Energy dissipation due to damping mechanisms (E^D):

$$E_i^D = E_{i-1}^D + \frac{1}{2}\{\{\dot{u}\}_i^T[C]_i + \{\dot{u}\}_{i-1}^T[C]_{i-1}\}\{u_i - u_{i-1}\} \tag{4.25}$$

Internal work done by nonlinear restoring forces (E^R):

$$E_i^R = E_{i-1}^R + \frac{1}{2}\{r_i + r_{i-1}\}^T\{u_i - u_{i-1}\} \tag{4.26}$$

Absolute seismic input energy (E^Q):

$$E_i^Q = E_{i-1}^Q + \frac{1}{2}\{\ddot{u}_{t,i} + \ddot{u}_{t,i-1}\}^T[M]\{u_{g,i} - u_{g,i-1}\} \tag{4.27}$$

Work done by pre-seismic applied loads (E^P):

$$E_i^P = E_{i-1}^P + \{p\}^T\{u_i - u_{i-1}\} \tag{4.28}$$

The energy balance error is computed as a percentage of the absolute seismic input energy:

$$Error = \frac{(E^Q + E^P) - (E^K + E^D + E^R)}{E^Q} x\,100\,\% \tag{4.29}$$

A seismic analysis is abandoned when the energy balance error exceeds 10%, a moderate value also assumed by Ayari and Saouma[6]. The energy convergence criterion was also used by Mlakar[112] in smeared crack analysis of concrete gravity dams.

4.5 COMPUTATION OF ENERGY DISSIPATION IN THE STRUCTURE DUE TO TENSILE FRACTURE

Equation (4.26), that computes the internal work done by nonlinear restoring forces, can be applied in both static and seismic fracture analyses of concrete structures. The internal work done, E^R, contributes to two energy components: (i) the stored elastic energy in the system, E^U, and (ii) the energy dissipation due to tensile fracture, E^F. E^U in any load step can be computed by summing the contributions of all finite element integration points:

$$E_i^U = \sum \frac{1}{2}\{\sigma\}^T\{\epsilon\}\Delta V \tag{4.30}$$

where ΔV is the volume associated with individual integration point. The fracture energy dissipation in the entire structure, E^F, can be determined from:

$$E_i^F = E_i^R - (E_i^U - E_0^U) \tag{4.31}$$

where E_0^U is the initial elastic strain energy in a system due to the application of self-weight, hydrostatic pressure, and temperature changes.

The energy dissipation due to tensile fracture can also be approximated by summing the dissipated energy in all softening elements. Assuming that a directly proportional relationship exists between tensile stresses and strains in the crack normal direction, the amount of dissipated energy in an element, that has attained the average maximum tensile strain value, ϵ_{max} ($\epsilon_{max} \leq \epsilon_f$ or ϵ_f') (Figs. 3.3(c,d)), is given by:

$$g_i = \frac{1}{2}E\epsilon_0(1-\eta)V\epsilon_{max} \quad ; \qquad \eta = \frac{E_n^s}{E} \tag{4.32}$$

where V is the volume of the element. The final strain of no tensile resistance, ϵ_f (or ϵ_f'), is substituted for ϵ_{max} in Eqn. (4.32) for completely cracked elements. The total dissipated energy in the structure, E^F, is the sum of dissipations, g_i, in all softening elements. Computation of energy dissipation by this approach is approximate since the Poisson's effect has not been considered in Eqn. (4.32). The element characteristic dimension, over which the fracture energy dissipation occurs, is also defined approximately. Comparison of the results obtained by the two proposed approaches will be presented in Chapter 5.

4.6 LONG TERM EFFECTS IN TEMPERATURE STRESS ANALYSIS

During an internal temperature change from a reference state of T_0 to the current state T, the unrestrained thermal strain, ϵ^T, in a two-dimensional case is given by:

$$\{\epsilon^T\} = \begin{Bmatrix} \epsilon_x^T \\ \epsilon_y^T \\ \gamma_{xy}^T \end{Bmatrix} = \begin{Bmatrix} A(T-T_0) \\ A(T-T_0) \\ 0 \end{Bmatrix} \tag{4.33}$$

where A is the coefficient of thermal expansion, that is assumed independent of the temperature within the range of seasonal variations in the vicinity of dams. The unrestrained strain due to temperature changes, $\{\epsilon^T\}$, can be modelled as a pseudo-load, $\{f^T\}$, applied on the structure:

$$\{f^T\} = \int [B]^T [D] \ \{\epsilon^T\} \ dV \tag{4.34}$$

where [B] is the strain-displacement transformation matrix, and [D] the constitutive relation matrix (Eqn. 3.2), derived using the short term Young's modulus of concrete. The displacement, {u}, corresponding to this pseudo-load can be obtained by solving the following system of equations:

$$[K]\{u\} = \{f^T\} \tag{4.35}$$

where [K] is the structural stiffness matrix. Assuming that the entire mechanism develops instantly at a time t, the elastic strain, ϵ_T, caused by external and internal restraints to the temperature induced volumetric changes can be obtained as:

$$\{\epsilon_T\} = [B] \ \{u\} - \{\epsilon^T\} \tag{4.36}$$

The seasonal temperature change in concrete dams, induced by climatic variations, develops over a relatively long period of time, causing a part of the predicted elastic strain, $\{\epsilon_T\}$, to be offset by creep effects. The resultant behaviour in a uniaxial case can be idealized as a gradual development of internally induced residual elastic strain, ϵ_I, over the time period (t-t′) (Fig. 4.10(a)). Assuming that the Young's modulus, E,

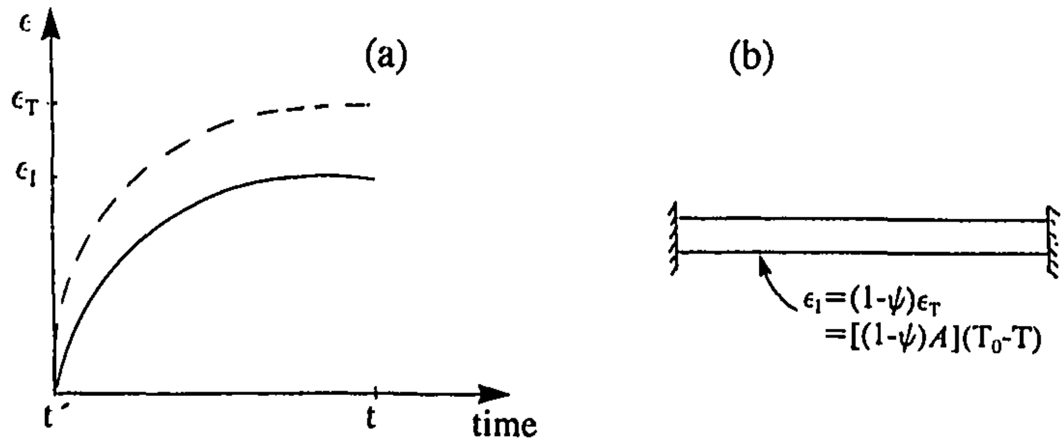

Figure 4.10 Long term effects on the temperature induced stresses.

remains constant over this time period, the relaxation process can be expressed as:

$$
\begin{aligned}
\epsilon_I &= \frac{\epsilon_T}{1+\chi\phi(t,t')} \\
&= [1 - \frac{\chi\phi(t,t')}{1+\chi\phi(t,t')}]\ \epsilon_T \\
&= (1 - \psi)\epsilon_T\ ; \qquad\qquad \psi = \frac{\chi\phi(t,t')}{1+\chi\phi(t,t')}
\end{aligned}
\tag{4.37}
$$

where χ is the ageing coefficient (Bažant [10]) that accounts for creep under gradually applied stress, and $\phi(t,t')$ is the usual creep coefficient. The parameters χ and $\phi(t,t')$ can be determined from data available in the literature (Ghali and Favre [72]). The relaxation factor, ψ, in Eqn. (4.37), can have a value between 0.0 to 1.0; the upper bound represents the situation where the induced elastic strain has been completely offset by creep effects, and the lower bound represents the situation where no such effects exist. In the linear elastic range, the relaxation process in a uniaxial case can be predicted by using a modified value of the thermal expansion coefficient A (Fig. 4.10(b)). This approximate procedure will be adopted in the analysis of concrete dams (Fig. 4.2). No further relaxation is applied to the elastic strain predicted from finite element analyses (Fig. 4.1). However, a rigorous finite element investigation would require a coupled temperature-creep stress analysis with different creep effects for tensile and compressive strains in finite elements. Use of a code specified effective modulus in two or three dimensional finite element models of concrete dams is a gross simplification of the actual constitutive behaviour (Bažant [21]). Viscoelastic material models may be considered to study the fracture response of concrete under long term load effects (Bažant and Chern [19], de Borst [48]).

4.7 SUMMARY

Nonlinear static and seismic analysis algorithms for the smeared fracture analysis of concrete structures have been developed in this chapter. Static fracture responses of plane concrete structures, subjected to mode I loads, will be investigated in Chapter 5, using the direct displacement control analysis technique. The indirect displacement control analysis technique, developed in section 4.3, will be applied in Chapter 6 to study the static failure behaviours of a notched shear beam, a model concrete dam, and a full scale concrete gravity dam. All these structures have been experimentally or numerically investigated in the past. Predicted responses will be compared with the results published in the literature. Seismic fracture response of Koyna Dam, that experienced severe cracking during a seismic event, will be investigated in Chapter 7 to validate the application of numerical models in nonlinear seismic analyses. Energy response of the dam, and the influences of different modelling parameters and assumptions on the predicted fracture response, will also be studied. Finally, the numerical models will be applied to predict the seismic fracture response of a standard section concrete gravity dam in Chapter 8. Seasonal temperature effects, and energy dissipations due to dynamic interactions with the reservoir and the foundation, will be considered in that chapter. Recommendations for industrial applications of the numerical models, to determine the fracture responses of existing concrete gravity dams, will be provided in Chapter 9.

CHAPTER 5

STATIC FRACTURE RESPONSE OF PLAIN CONCRETE STRUCTURES SUBJECTED TO MODE I LOADING

5.1 INTRODUCTION

Fracture responses of a simple tensile specimen and a beam under three-point loading (Fig. 5.1) are mode I type, because no shear deformations occur in the fracture process zone. Directions of the fracture band propagation are also known *a priori*. Finite

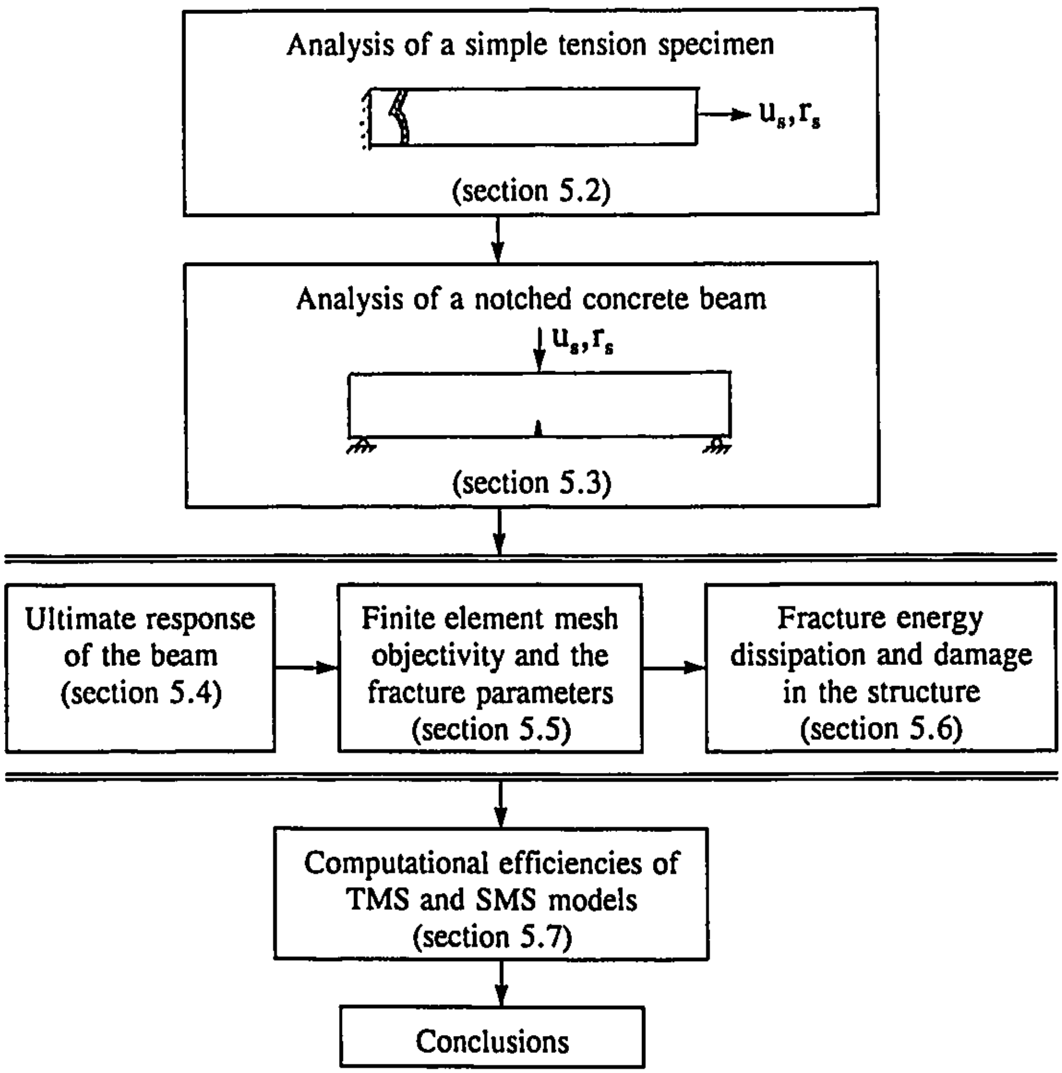

Figure 5.1 Fracture responses of concrete structures subjected to mode I static loading.

element meshes can be oriented such that the crack band is bounded by two parallel sides of square elements (Fig. 3.6(a)). The fixed smeared crack model with a constant shear resistance factor, μ, can be applied to predict the predominantly mode I fracture response of simple concrete structures. Elementary fracture specimens, such as a wedge splitting specimen (Brühwiler [31]) or a notched beam under three-point loading (Bažant and Pfieffer [20]), are extensively used in experimental investigations to determine the concrete fracture energy (Shah and Carpinteri [145]). Numerical simulations of the tested fracture specimens are conducted to calibrate the fracture energy of concrete, using known values of the elastic modulus and the tensile strength, and a specified shape of the tensile strain softening curve. The main objectives of this chapter are to validate the finite element crack propagation analysis models, elaborated in chapters 3 and 4, by investigating the mode I fracture response of concrete structures subjected to static loads, and to demonstrate the importance of fracture energy conservation principle in obtaining a mesh objective response from smeared crack analyses.

A simple tension specimen, and a simply supported notched concrete beam under three-point loading are considered for numerical investigations (Fig. 5.1). The elementary tension specimen, similar to that investigated by Oliver [121], is considered for a preliminary validation of the finite element computational models. The notched concrete beam under three-point loading is identical to that experimentally and numerically investigated by Bažant and Pfieffer [20]. Parametric analyses are performed with the notched beam, to determine the influences of material parameters and constitutive modelling assumptions on the finite element analysis results. Finite element mesh objectivity and energy dissipation characteristics of the structural components are also investigated in this chapter. Figure 5.1 outlines the organization of this chapter.

The softening response of concrete structures has been independently investigated in the past using two computational techniques: (i) the stiffness degrading model based on a total stress-strain relationship (Bažant and Oh [15]), and (ii) the tangent softening model based on an incremental stress-strain relationship (de Borst and Nauta [47]).

However, the relative advantages and inconveniences of using the two different simulation techniques of the concrete strain softening behaviour have not been investigated in the past. Section 5.7 in this chapter is particularly devoted to investigate the numerical efforts required by the two element stiffness formulation models: TMS and SMS models, that have been presented in Chapter 3. The displacement control analysis program, discussed in section 4.2, is applied to predict softening responses of the tension specimen and the beam under three point loading; physical snap-back behaviour is not expected for any of the structures considered here. The loading condition is assumed to be such that the material properties are defined with strain-rate independent parameters.

5.2 ANALYSIS OF THE SIMPLE TENSION SPECIMEN

A simple tension specimen under the constant stress state is considered first to validate the computer implementation of numerical models. Finite element model of the unit thickness structure, similar to that investigated by Oliver [121], is shown in Fig. 5.2(a). The strain softening response of a similar simple tension specimen was also considered by de Borst [49] to investigate the post-bifurcation stability of local smeared crack analysis models. However, the present investigation is limited to predicting the overall force-displacement and energy response of the specimen. The material properties are arbitrarily selected as, E=20000 MPa, ν=0.0, σ_i=2 MPa, and G_f=40 N/m. A non-zero shear resistance factor, μ, is required to ensure stability of the solution in this particular uniaxial case. However, the response is independent of the value assumed. The softening is limited only in the elements adjacent to the rigid boundary by artificial initiation of softening in those elements. The force displacement response and the energy dissipation in the structure are shown in Figs. 5.2(b) and 5.2(c). Due to a pure uniaxial stress field, the two approaches of computing the dissipated fracture energy: one from the difference between the external work done and the recoverable internal strain energy (Eqn. 4.31), and the other directly from the element stress-strain responses (Eqn. 4.32),

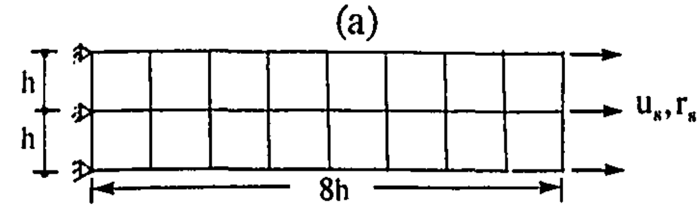

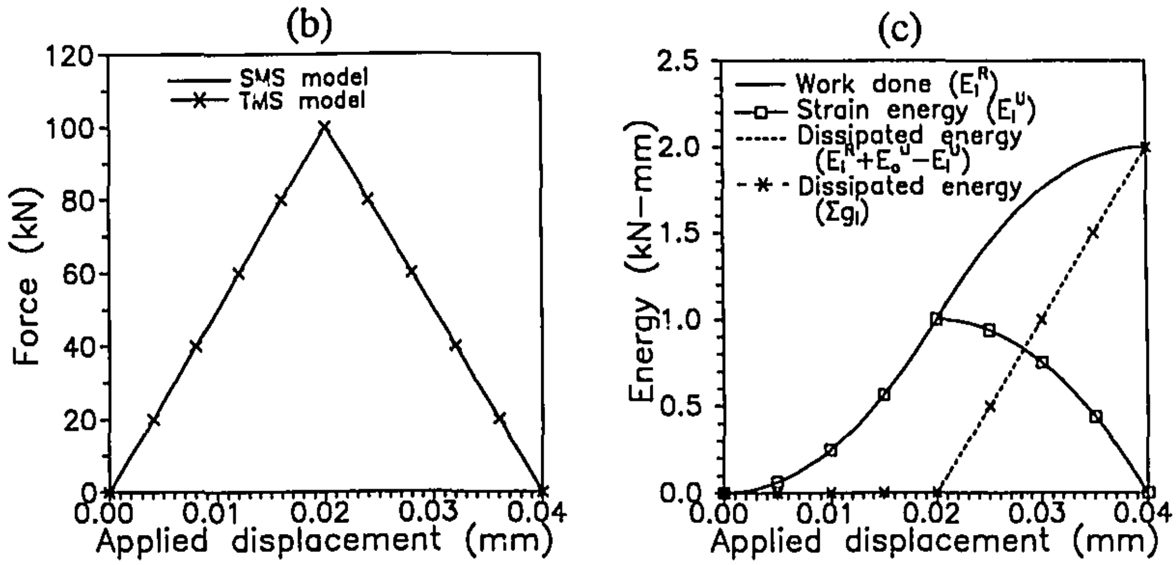

Figure 5.2 Analysis of a simple tension specimen: (a) the finite element model, (b) the force-displacement response, and (c) the energy response.

have provided identical results. Force-displacement and energy responses, obtained by the SMS and the TMS models, virtually overlap with the theoretical solution in this particular case. However, a significant difference exists in computational times of the two numerical models, which will be discussed in the following example.

5.3 NOTCHED BEAM UNDER THREE-POINT LOADING

One of the several concrete beams tested by Bažant and Pfeiffer[20], 0.3048 m deep, 38.1 mm thick, and made with a maximum aggregate size of 12.7 mm, is considered here for parametric studies (Fig. 5.3(a)). The only material parameter determined from

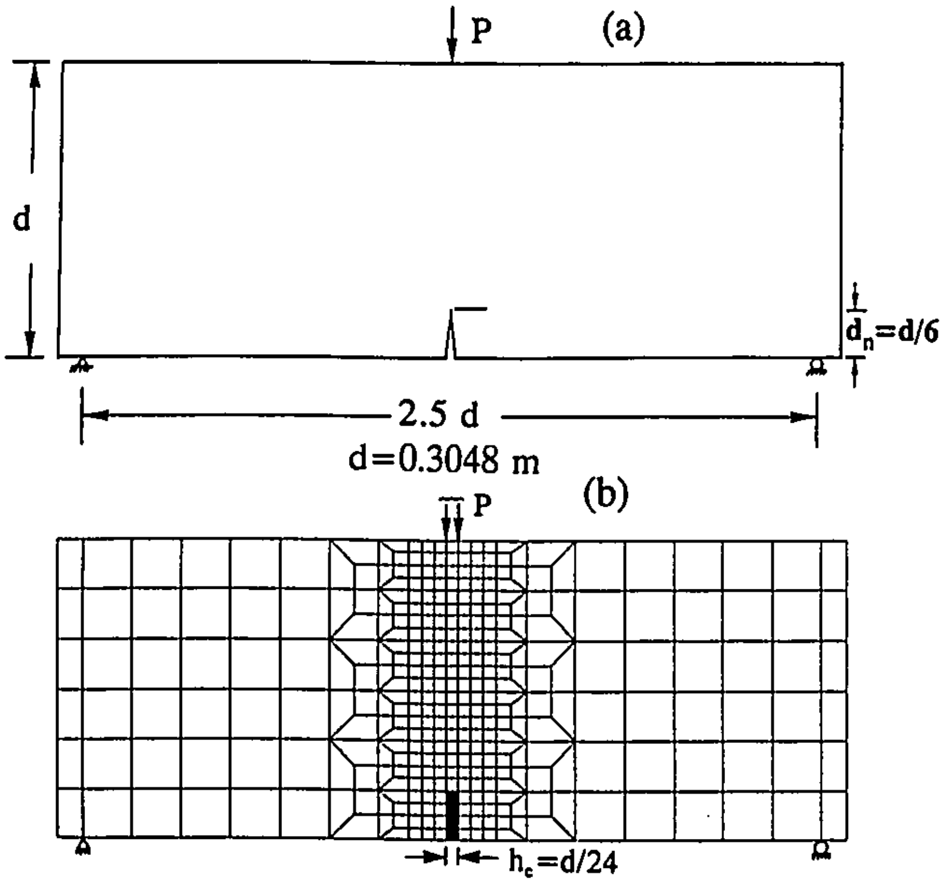

Figure 5.3 The notched beam under three-point loading.

laboratory tests was the compressive strength of concrete, f'_c=33.5 MPa (4865 psi). For numerical investigations, the following material properties are assumed after Bažant and Pfeiffer[20]:

$$E = 57000\sqrt{f_c'}\ psi \qquad \sigma_t = 6\sqrt{f_c'}\ psi$$
$$= 27413 MPa \qquad = 2.886\ MPa \tag{5.1}$$
$$G_f = 40.29\ N/m \qquad \nu = 0.18$$

The fracture energy value was calibrated by Bažant and Pfeiffer[20] to provide a close prediction of the peak load resistance, as observed in the laboratory test. A typical finite element model having 24 subdivisions along the depth of the beam, d, with a characteristic dimension, h_c=d/24, is shown in Fig. 5.3(b). The notch at the centre-bottom is modelled by assigning a null stiffness and strength to the finite elements, shown shaded in the figure. Displacement control analyses have been performed by applying a displacement increment, $\Delta u_x=1.0\times10^{-6}$ m, at the two surface nodes adjacent to the centre line of the beam (Fig. 5.3(b)). The constitutive parameter σ_i (section 3.3) has been assumed equal to σ_t in all analyses, except the case discussed in section 5.5.

5.4 ULTIMATE RESPONSE OF THE BEAM

The ultimate load resistance determined in the laboratory experiment was $P_u=7.784$ kN, which was the average response of three same size specimens tested. Applying the elastic bending theory, the load at the centre of the beam that causes the crack-tip stress equal to σ_t (Fig. 5.4(a)) is, $P_0=6.206$ kN, giving a P_u/P_0 ratio of 1.254 for the experimental response. Three analyses of the finite element model (Fig. 5.3(b)) have been performed: one for the TMS model applied with the Newton-Raphson iteration technique, and two analyses for the SMS model applied in conjunction with the Newton-

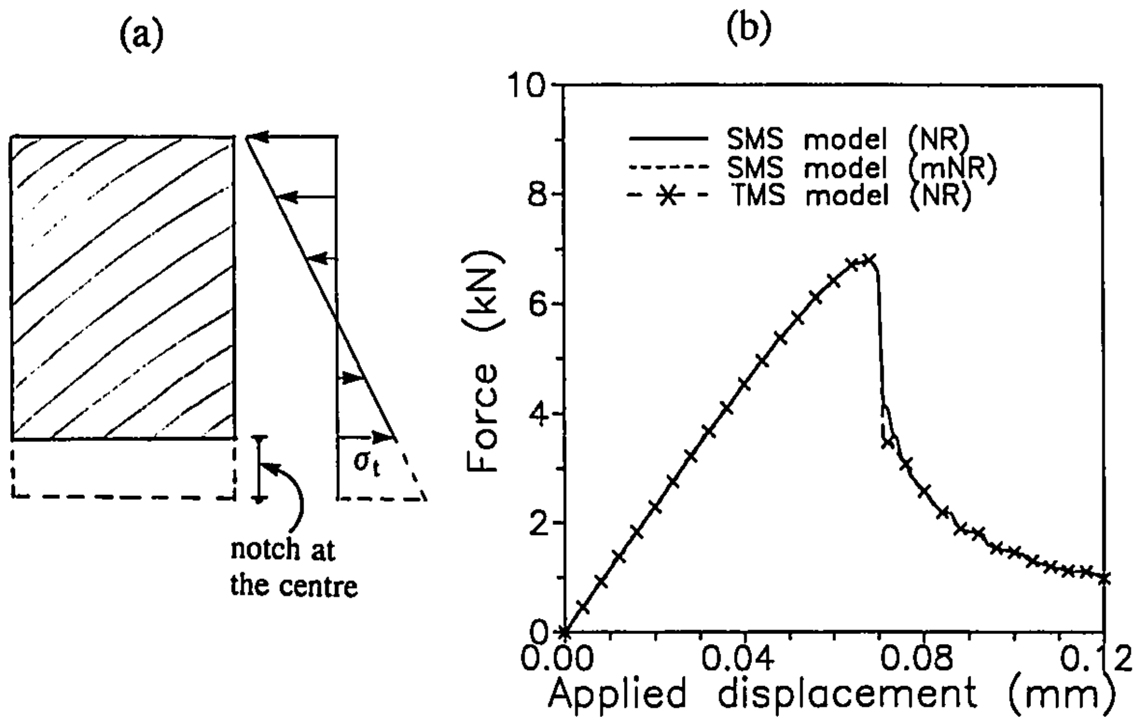

Figure 5.4 (a) Linear elastic stress distribution on the cross-section at mid-span, and (b) force-displacement response of the beam.

Raphson and the modified Newton-Raphson methods. The force-deformation responses of these analyses are presented in Fig. 5.4(b). Two analyses with the SMS model provided identical responses. The TMS model also provides a response that is almost identical to the SMS model predictions. Applying the elastic bending theory, the total load on the beam to cause the tensile stress at the crack tip equal to σ_t, under the loading configuration of Fig. 5.3(b), is determined to be P_0=6.31 kN. The ultimate resistance obtained from numerical analyses is 6.8 kN, giving a P_u/P_0 ratio of 1.08, which is about 16% less than the experimental result. The response predicted from numerical analyses is, however, approximate due to uncertainties related to the material properties that are not known precisely. The sensitivity of predicted peak response, to the assumed material parameter values and the finite element model used in the analyses, is discussed in the following section. In a laboratory test situation, the beam response is also influenced by the self-weight which has not been included in the present analyses.

5.5 FINITE ELEMENT MESH OBJECTIVITY AND THE FRACTURE PARAMETERS

The most important verification of any softening model, to apply in finite element fracture propagation analyses, is the mesh objectivity. Three finite element models with different characteristic dimensions of the crack band, h_c=d/6, d/12, and d/24, have been considered to study the softening response of the beam in Fig. 5.3(a) (d=0.3048 m). The energy conserving SMS model has been applied to determine the peak response of all three finite element models, using the material properties assumed earlier. A series of analyses has also been performed using the conventional elasto-brittle strength-of-material (SOM) concept of fracture analysis, where no post-peak tensile resistance is assumed to exist. Using the elastic bending theory, loads causing the crack-tip tensile stress equal to σ_t, are determined as P_0=6.65 kN, 6.42 kN, and 6.31 kN, respectively for h_c=d/6, d/12, and d/24 models. The value of P_0 varies with the value of h_c since the spacing, over which the loading is applied (Fig. 5.5), varies in three finite element

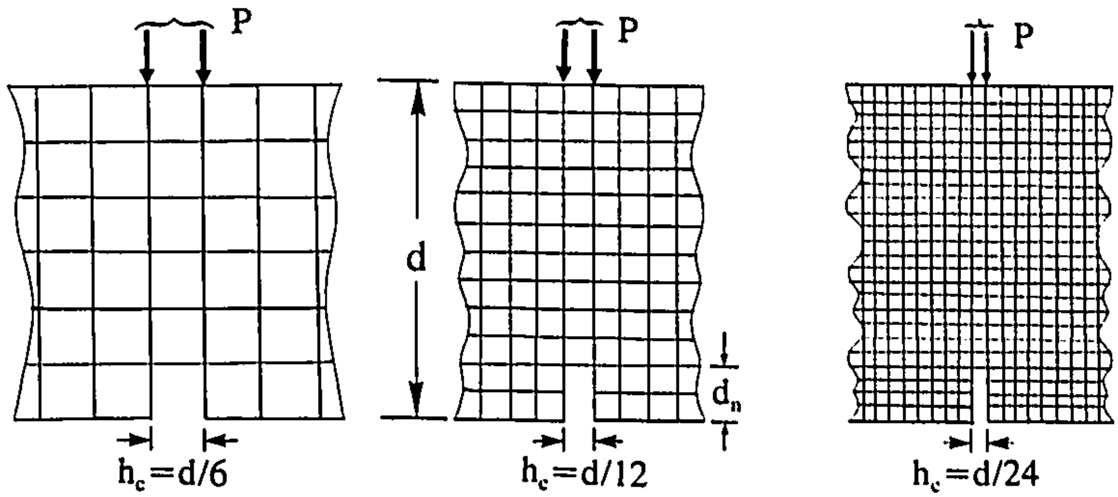

Figure 5.5 Different finite element meshes of the notched concrete beam.

models. The ratio of peak load resistance, P_u, determined from finite element analyses, to P_0 is plotted against the d/h_c ratio in Fig. 5.6(a), for all analyses. The inadequacy of SOM criterion becomes evident as the fineness of the finite element model, d/h_c, increases. On the other hand, the P_u/P_0 ratio obtained with the energy conserving model is almost independent of the finite element mesh refinement. The structural response, thus, appears to be independent of the width of crack bands in the mode I static fracture analysis. The difference between finite element analysis results and experimental findings, does not appear to depend on the refinement of finite element meshes.

The transition parameter between the pre-peak linear elastic state and the post-peak softening state is not uniquely defined in the literature. The finite element model of 24 subdivisions (h_c=d/24), has been reanalysed with an increased value of σ_i (=1.3 σ_t). The predicted force-deformation response is compared with the previous analysis results, obtained with $\sigma_i=\sigma_t$, in Fig. 5.6(b). The peak structural resistance is moderately sensitive to the softening initiation parameter. A 30% increase in σ_i value causes about a 10.3% increase of the peak structural resistance, although the same amount of fracture energy, G_f=40.29 N/m, is conserved in two cases. The sensitivity would be much higher if the responses of un-notched beams are compared. In a subsequent analysis, the

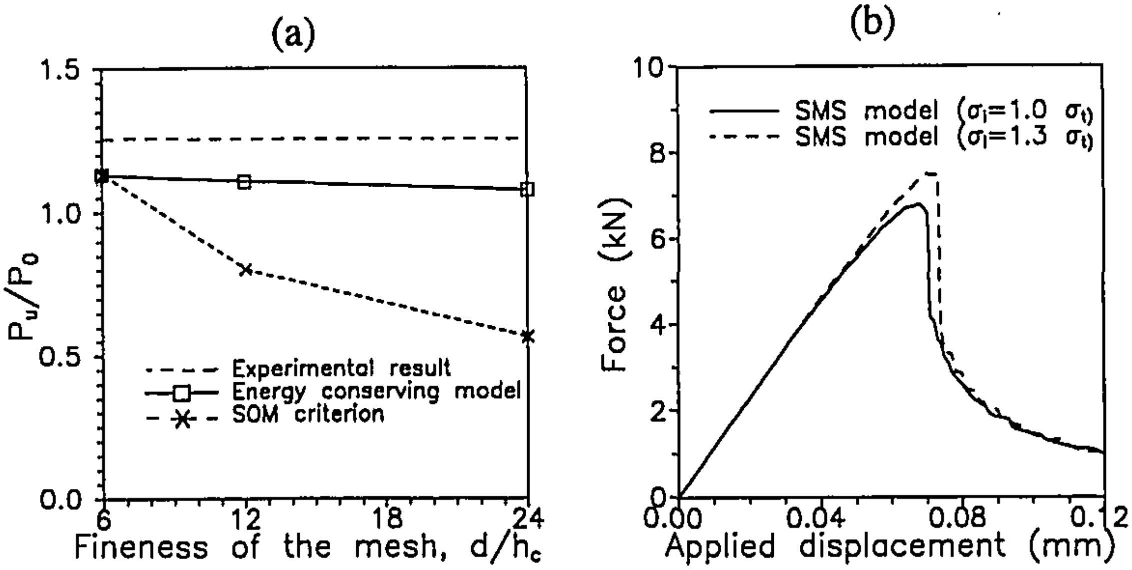

Figure 5.6 Sensitivity of the structural resistance to (a) the finite element mesh refinement, and (b) the constitutive parameter σ_i.

peak response has been observed to increase by 7.4% if the fracture energy G_f is increased by 30%, while the softening initiation parameter is assumed constant at $\sigma_i = \sigma_t$. Difference between the numerically predicted response and the experimental observation may have been caused by uncertainties related to these fracture parameters. The shear resistance parameter, μ, has not been a critical factor in relation to the peak response of the particular beam under consideration. This behaviour can be attributed to the fact of a dominant mode I fracture propagation under the applied loading configuration.

5.6 ENERGY DISSIPATION AND DAMAGE IN THE BEAM

Energy response of the beam, obtained during a SMS analysis with the NR iteration technique (discussed in section 5.4), is shown Fig. 5.7(a). Separate presentations for the other two analyses, using the TMS model and the SMS model with a mNR technique, are unwarranted since almost identical responses were obtained from three analyses. The internal recoverable strain energy in Fig. 5.7(a) reaches the peak value almost

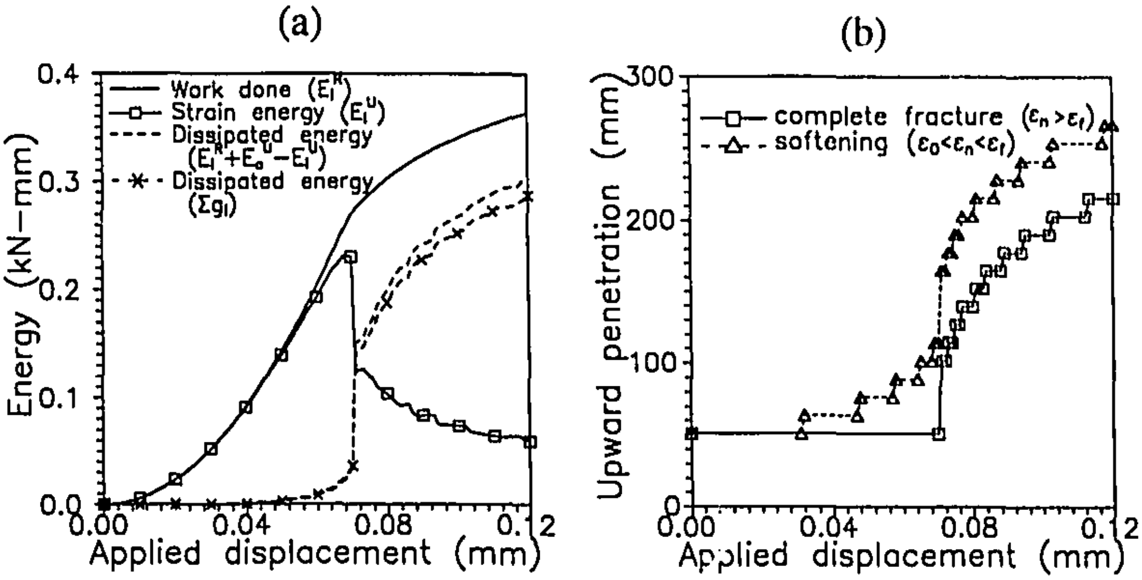

Figure 5.7 (a) Energy response of the beam, and (b) the propagation of softening and crack tips.

simultaneously with the ultimate load resistance, and then drops sharply showing a nearly brittle behaviour. The total energy dissipation due to local tensile softening in finite elements is insignificant, compared to the total internal strain energy (about 12%), before the structure reaches the peak resistance level. The energy dissipation capacity, and thereby the sustained damage by the beam, are very limited before the collapse occurs under the applied loading condition. Upon reaching the peak response, the stored elastic energy is released instantly, causing a sudden increase of energy dissipation through tensile fracture. The two approaches of computing the energy dissipation (Eqns. 4.31 and 4.32) provide close predictions before the beam passes through the peak load level. The difference between two approaches emerges during the post-peak response of the structure. The difference also tends to increase with coarser finite element meshes and with a reduction of the notch depth.

The upward propagation of softening front ($\epsilon_0<\epsilon_n<\epsilon_f$) with an increasing imposed displacement is represented in Fig. 5.7(b). The propagation of crack-tip, where the crack normal strain, ϵ_n, has exceeded ϵ_f, is also plotted against the imposed displacement. In general, the softening-tip appears to lie approximately 50 mm ahead of the crack-tip. This dimension is about one-fifth of the material characteristic dimension, $l_{ch}=2EG_f/\sigma_t^2$ (Hillerborg et al. [82]). The crack-tip as well as the softening-tip extends suddenly by about one-sixth of the beam depth when the structure passes through the maximum resistance level. Then the load resistance reduces drastically, as the crack-tip penetrates about one-third the total depth of the structure. The behaviour of the structure, however, depends also on the initial notch depth. Figure 5.8(a) shows the influence of the notch depth, d_n, on the propagation of cracks as the applied displacement is increased. For a small notch depth, the crack starts to propagate at a

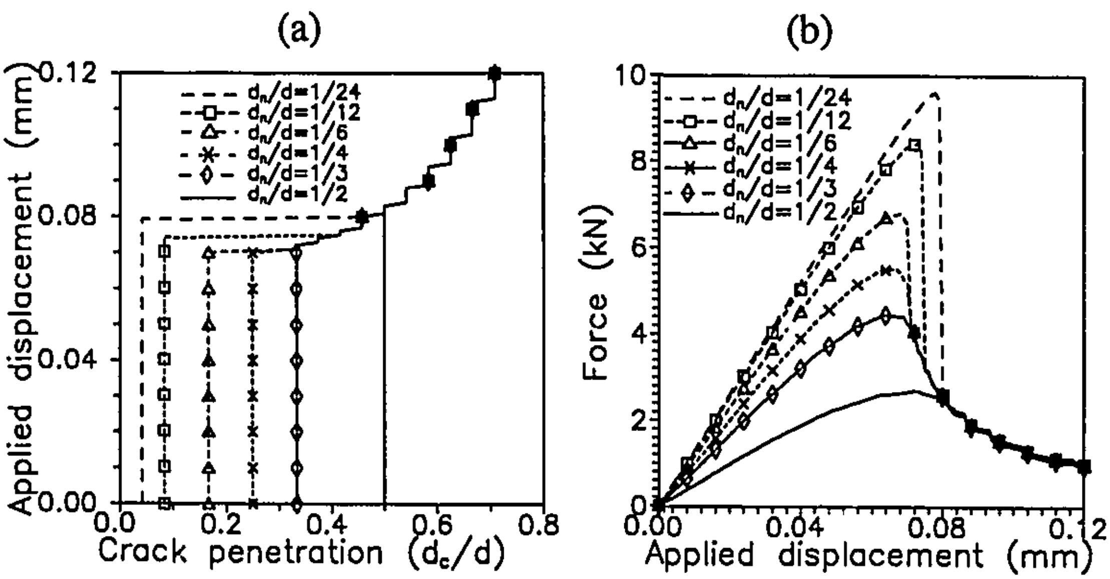

Figure 5.8 Influences of the notch depth on (a) the crack propagation, and (b) the force-displacement response.

relatively high applied displacement, and penetrates instantly to a substantial depth. The displacement, at which a crack starts to propagate, reduces to a minimum value when the notch depth is in the range of 1/4 to 1/3 of the beam depth. The crack propagation is gradual for a notch depth greater than 1/3 of the beam depth. Force-displacement responses of the beam, obtained with different notch depths, are shown in Fig. 5.8(b). The brittle failure mechanism for relatively smaller notch depths is evident in this presentation. When the notch depth is relatively high, $d_n/d \geq 1/3$, the elastic energy stored in the structure at the pre-peak state is reduced. Consequently, the energy flux to the fracture front is also reduced, thus eliminating any sudden growth of crack in the structure. The total amount of dissipated energy, before the structure approaches the ultimate resistance level, varies from 4% to 30% of the stored elastic energy, as the notch depth increases from 1/24 to 1/2 of the beam depth. A catastrophic failure scenario is, thus, expected for an undamaged or lightly damaged structure. The notch sensitivity of force-displacement responses of the concrete beam, predicted here, is analogous to the behaviour reported by Karihaloo and Nallathambi [94].

5.7 COMPUTATIONAL EFFICIENCIES OF THE TMS AND THE SMS MODELS

The computer execution times of three analyses, discussed in section 5.4, are plotted against the applied displacements in Fig. 5.9(a). The SMS model, applied with the Newton-Raphson iteration technique, takes the maximum time for solution, because of the repeated changes in secant modulus stiffness of the softening elements. The computer execution time required by the SMS model is reduced substantially when applied with the modified Newton-Raphson method, since the stiffness matrix of the structure is updated once in each displacement step. The computer execution time required by the TMS model is significantly less than that required by SMS model analyses. Use of the tangent stiffness formulation during strain softening, and at the same time computing stresses from the total strains using a secant stress-strain relationship, appear to be an efficient solution strategy.

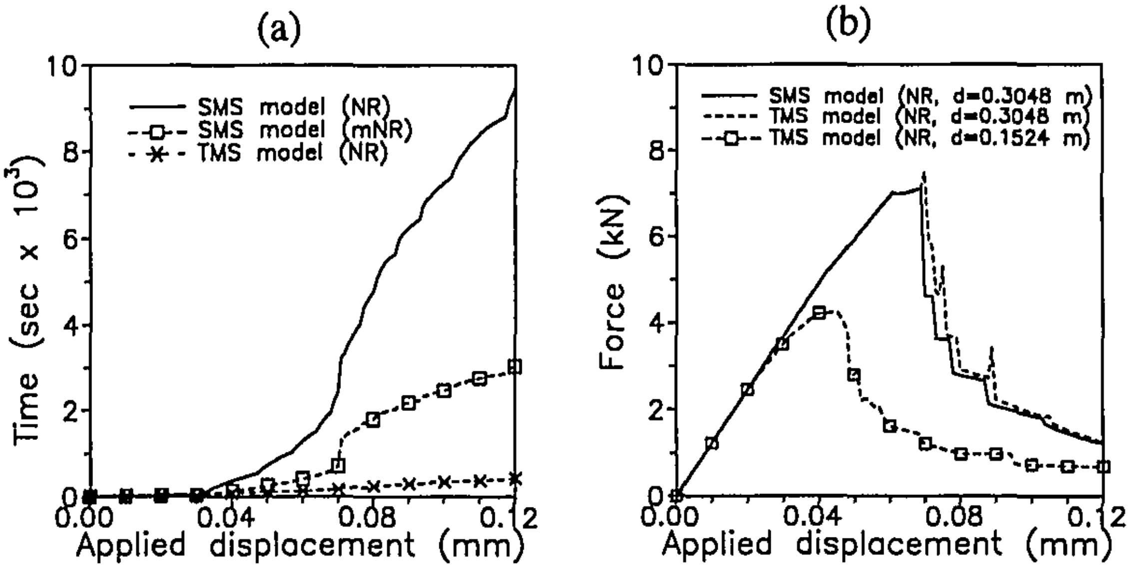

Figure 5.9 (a) The computer execution times of SMS and TMS analyses, and (b) computational instability of the TMS model.

However, the TMS model may not always provide a stable response in finite element analyses. The use of a negative softening modulus in the element stiffness formulation may cause ill conditioning of the structural stiffness matrix. One such situation has been encountered when the TMS model is applied with the Newton-Raphson method to analyse the beam of Fig. 5.3(a) with a relatively coarser finite element model having 12 subdivisions along the depth (h_c=d/12, d=0.3048 m). SMS and TMS models provide identical force-displacement responses up to the peak (Fig. 5.9(b), d=0.3048m). In the post-peak phase, the analysis with TMS model fails to satisfy the convergence criterion even after 100 iterations within a displacement step. The spikes in the force-displacement curve of TMS analysis correspond to the un-converged solution states. With the increased size of finite elements, the linear softening curve becomes steeper, meaning a higher negative modulus, E_n^1, applied to formulate the incremental stress-strain relation of Eqn. (3.18). To further investigate the influences of mesh coarseness on the stability of TMS model, one analysis has been performed by scaling the geometric dimensions of the beam to half, but still modelling with 12 elements along the depth of the beam ($h_c=d/12$, $d=0.1524$ m). The softening modulus of finite elements in this reduced model corresponds to the same value, obtained for the elements in the full size model of $d=0.3048$ m and $h_c=d/24$. A stable force-deformation response is predicted without any convergence problem (Fig. 5.9(b)). The peak response of the reduced size beam is predicted to be 4.25 kN, which is about 8% less than the laboratory test value of 4.64 kN (Bažant and Pfeiffer[20]). In subsequent analyses of the full size finite element model ($d=0.3048$m, $h_c=d/24$), the TMS model has been observed to become unstable for an initial notch depth, d_n, less than 1/6 of the beam depth. The application of modified Newton-Raphson technique has been observed to eliminate the unstable behaviour of the TMS model. The instability can also be suppressed by using a high value of the shear resistance factor, $\mu \approx 1.0$. The value of $\mu=1.0$ corresponds to the situation of permitting only mode I (opening mode) deformations in the crack band. However, computational efficiencies of the TMS model, observed during the fine mesh analysis (Fig. 5.9(a)), may diminish in the analysis of a structure subjected to mixed mode loading; since a shear softening model, possibly with a rotating crack formulation, needs to be considered.

5.8 CONCLUSIONS

Computational efficiencies of two numerical models, developed to simulate the localized softening behaviour of concrete, have been investigated. The stiffness degrading model (SMS), that uses a total stress-strain relationship to derive element stiffness matrices, appears to provide a stable response even with a relatively coarse finite element model of structures. The model is computationally intensive since the secant stiffness properties change with the progression of element softening. However, the gradual change in element stiffness properties makes the solution algorithm very stable, which is of great importance in nonlinear response studies. The stiffness degrading model can also be adapted without a significant increase in computational efforts to take account of the nonlinear stress-strain curves at both pre-peak and post-peak states. The variable shear resistance factor, either in a fixed crack analysis or in the framework of a rotating crack model, can also be accommodated without a significant increase in the computational cost.

In the alternative tangent modulus stiffness model (TMS), element stiffness matrices are determined based on an incremental stress-strain relationship, but the stresses at Gauss integration points have been computed from the total strains using a total stress-strain relationship derived for the entire element. The proposed approach ensures the correct fracture energy dissipation in strain softening elements. With the linear softening model and a constant shear resistance factor, the tangent model appears to be computationally efficient, and numerically stable, provided that an adequately refined finite element mesh is used. However, the computational efficiency of this model is expected to diminish when applied with a variable shear resistance model, which is required in most practical fracture problems. Moreover, a solution becomes non-convergent when the model is applied with relatively large size elements.

The traditional tensile strength based failure analysis has been found to be extremely sensitive to the refinement of finite element meshes. The energy conserving nonlinear smeared fracture model has provided a finite element mesh objective response of the concrete beam. The size of finite elements, representing the width of smeared crack bands, may not be limited to any minimum value in the mode I static fracture analysis of notched beams, subjected to a three-point loading configuration. The structural response has been moderately influenced by the constitutive model parameters of softening initiation and fracture energy dissipation; but not by the width of crack bands. Hence, the proposed finite element crack propagation analysis model can be applied to calibrate the fracture energy value of concrete, by a numerical simulation of the experimentally determined ultimate resistance of notched concrete beams under three-point loading.

CHAPTER 6

STATIC FRACTURE RESPONSE OF PLAIN CONCRETE STRUCTURES SUBJECTED TO MIXED MODE LOADING

6.1 INTRODUCTION

Cracking in concrete dams is inevitable due to the low tensile resistance of concrete. Evaluation of possible crack profiles, and the corresponding structural resistance, are of topmost necessity to ensure safe operation of these structures. The discrete crack propagation model, with linear elastic fracture mechanics (LEFM) crack propagation criterion, has been applied in the past to investigate the static fracture response of concrete gravity dams (Ayari [5], Gioia et al. [73], Ingraffea [87], Linsbauer et al. [107,108]). The application of traditional LEFM criterion in concrete fracture analysis has always been questionable, because of the development of significantly large fracture process zone (FPZ) in concrete. This is even more true for usual dam concrete that has substantially large material characteristic length (Brühwiler and Wittmann [32]). Standard LEFM fracture analysis, that results in a pair of traction free surfaces instantly upon fulfilling the propagation criterion, appears to have limited resemblance with the fracture process behaviour of concrete. Carpinteri et al. [35] applied the Hillerborg's cohesive crack model (Hillerborg et al. [82]) to investigate the fracture response of a model concrete gravity dam subjected to equivalent hydrostatic pressures. The use of discrete crack model in fracture analysis of huge concrete gravity dams remains limited, because of tremendous computational costs. Although nonlinear smeared fracture models have been applied to study the behaviour of elementary beams under flexural or shear loading, application of these models in fracture analysis of concrete dams has not been completely explored yet.

Depending on the type of loading and the elevation of cracking zones, the fracture in concrete gravity dams is expected to develop under a combination of flexure and shear type forces. The nonlinear response of notched concrete beams subjected to mode I loading conditions (for example, beams under three-point loading), can be predicted using the fixed smeared crack models, without considering shear deformations in the constitutive formulations (Bažant and Pfieffer[20]), or with a constant shear resistance factor (as demonstrated in Chapter 5). However, in most practical fracture problems, shear deformations may ensue a rotation of crack bands in the finite elements. Crack constitutive models fixing the local crack band at the initial inclination, result in a severe stress locking due to the zigzag propagation of crack profiles in a continuous finite element mesh. The stress locking phenomenon has been observed to cause spurious diffusions of cracking and overly stiff responses of investigated structures. The rotating crack concept, introduced by Cope et al.[43], and Gupta and Akbar[76], can be applied to consider mixed mode deformations in the fracture process zone. Rots[139] used a non-orthogonal multiple crack formation model (de Borst and Nauta[47]) to simulate the mixed mode deformations in the FPZ. A new crack was allowed to form as the principal stress direction deviated by an infinitesimal amount from the existing crack normal direction. The model appeared to provide a better prediction of the post-failure snap-back behaviour of a single-notched shear beam, in comparison to that obtained using the fixed crack model with a constant shear resistance factor.

The purpose of this chapter is to investigate the applications of localized strain-softening constitutive models, namely (i) the coaxial rotating crack model (CRCM) (section 3.6), and (ii) the fixed crack model with a variable shear resistance factor (FCM-VSRF) (section 3.6), in studying the two-dimensional cracking behaviour of concrete structures subjected to mixed mode static loading conditions. The SMS formulation is applied to simulate the strain softening behaviour of finite elements. The smeared crack models are applied first to investigate the response of a single notched shear beam, tested by Arrea and Ingraffea[3], and also analysed by other investigators (de Borst[49], Gerstle and Xie[71], Rots and de Borst[138], Rots[139]). The single notched beam under shear loading is supposedly a 'classic' example of physical snap-back behaviour at the structural level (de Borst[49]). Investigation of this problem is, therefore, intended to validate the indirect displacement control analysis technique, developed in section 4.3. The proposed analysis technique is applied subsequently to determine the ultimate resistance and the post-failure behaviour of a model dam, tested and analysed by Carpinteri et al. [35]. Final analyses are performed for a full scale concrete gravity dam subjected to reservoir overpressure. Analysis of the full scale dam is similar to that preformed by Gioia et al. [73]. Sensitivities of the predicted fracture response of the full scale dam to geometric configurations and finite element analysis parameters, such as mesh refinement, notch depth, and fracture energy value, are discussed in section 6.4. Application of the standard incremental load control analysis technique to determine the ultimate resistance of the full scale dam is presented in section 6.4.6. Figure 6.1 represents the organization of this chapter.

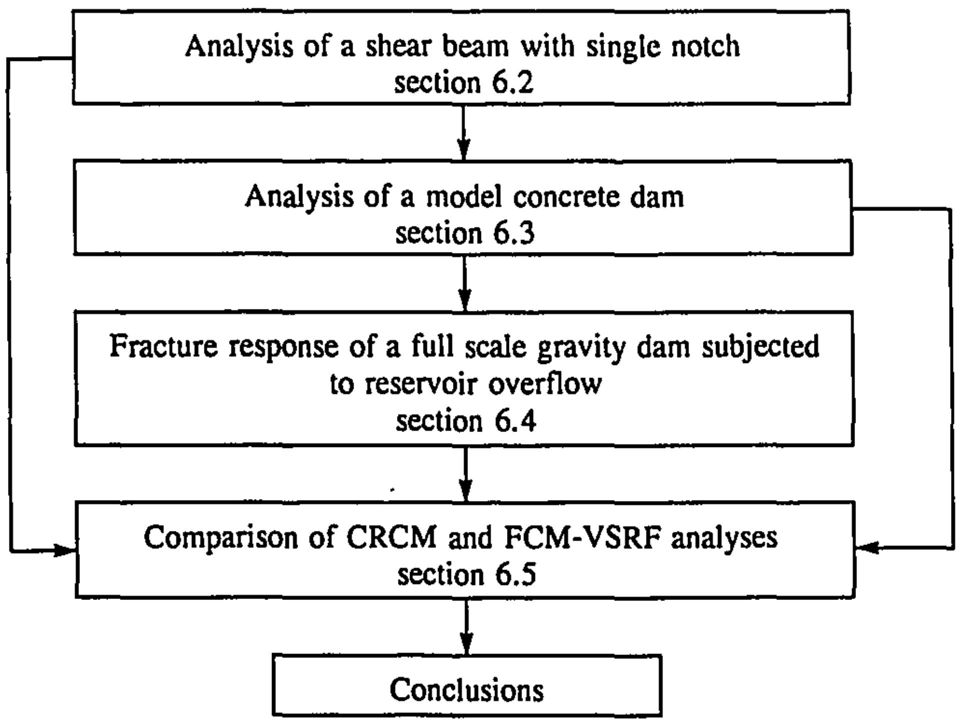

Figure 6.1 Fracture analyses of concrete structures subjected to mixed mode loading.

Structural resistances and crack profiles obtained from the present analyses are compared with the results published in the literature. The completely cracked condition of a finite element is indicated by shading the entire element area in finite element meshes. The incomplete fracture condition is indicated by a dot at the element centre. Elements that never softened will be kept unmarked in the illustrations. The loading conditions are assumed to be such that the material properties are defined with strain-rate independent parameters.

6.2 ANALYSIS OF A SHEAR BEAM WITH SINGLE NOTCH

The unreinforced single notched shear beam, experimentally investigated by Arrea and Ingraffea[3], is considered first to validate the finite element implementation of the constitutive models. The plane-stress finite element model of the 156 mm thick shear beam is shown in Fig. 6.2. In the laboratory test, a load was applied at point C of the

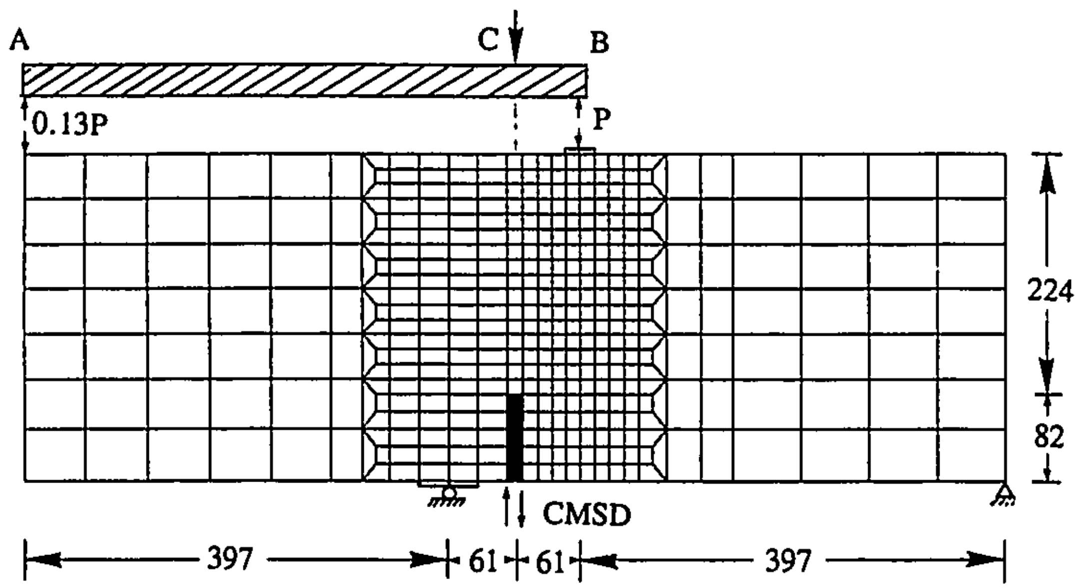

Figure 6.2 Single notched shear beam (dimensions in mm).

highly stiff steel beam ACB. The notch at the bottom of the concrete beam, and the load application point C, were on the line of asymmetry. The crack mouth sliding displacement (CMSD) was used as a feed-back signal to control the applied load in the experimental study. In the present numerical investigation, loads are applied directly on the concrete beam at points corresponding to A and B, according to the proportion shown in Fig. 6.2. The CMSD is used as the indirect displacement control analysis parameter to capture the snap-back response of the beam, as was predicted by other investigators (de Borst[49], Rots and de Borst[138], Rots[139]). The constitutive parameters are taken as, E=24800 MPa, ν=0.18, σ_t=2.8 MPa, and G_f=100 N/m (Rots[139]).

The applied force P versus the vertical displacement at point C, obtained with two constitutive models: (i) the CRCM, and (ii) the FCM-VSRF, together with the response obtained by Rots[139], are shown in Fig. 6.3(a). The displacements at points A and B of the concrete beam have been interpolated to obtain the vertical displacement at point C, assuming that the steel beam ACB used in the experiment was infinitely stiff. The snap-

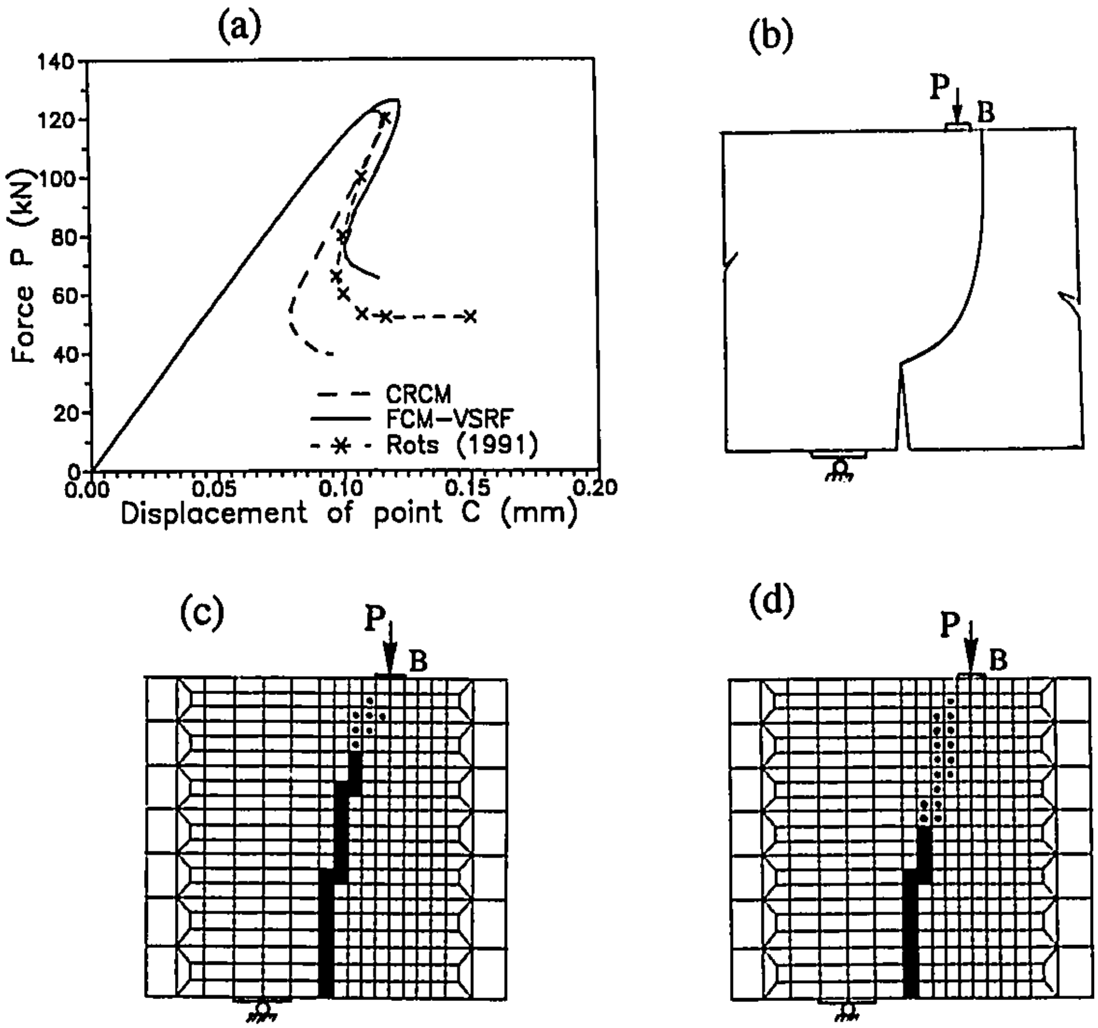

Figure 6.3 Response of the shear beam: (a) snap-back in the force-displacement response, (b) approximate experimental crack profile, (c) crack profile predicted by the CRCM, and (d) crack profile predicted by the FCM-VSRF.

back response of the structure, as evident in Fig. 6.3(a), has been well reproduced by the proposed indirect displacement control analysis procedure. However, the predicted snap-back behaviour can not be compared with the experimental results since the displacement at point C has not been reported in the referred literature. The predicted peak responses are, however, within the range of experimental results. The peak response obtained using the CRCM is in excellent agreement with the results obtained by Rots [139] who used a non-orthogonal crack formation model (de Borst and Nauta [47]) to simulate the effects of crack band rotation in the strain softening elements. Rots [139], however, obtained a relatively higher post-failure residual strength. The use of quadrilateral elements, instead of triangular elements as used by Rots [139], and the determination of constitutive parameters based on the average response of an element, have provided a softer response in the present study. The FCM-VSRF provides a relatively higher peak resistance, and also a higher post-peak response. However, the proposed variable shear resistance factor formulation provides a significantly better response than that obtained by using non-zero constant shear resistance factors (Rots [139]).

The crack profile observed in the laboratory test is approximately represented in Fig. 6.3(b). Rots [139] performed a discrete crack analysis of the beam using interface elements along the *a priori* known crack trajectory. The peak structural resistance was predicted to be in the range obtained by the CRCM analysis, and the applied force, P, approached an almost zero value at the end of analysis. Neither of the smeared crack models, used in the present study, has predicted a structural resistance approaching to a zero value at the end of analysis. This discrepancy in the post-peak response may be attributed to the incorrect crack profiles predicted by the smeared crack propagation models (Figs. 6.3(c) and 6.3(d)). The smeared crack profiles start to propagate with a steep vertical slope, and eventually get restrained by highly compressed elements underneath the applied load at point B. Close observation of the analyses have revealed that, although the elements in neighbourhood of the notch-tip start to soften initially at slanted angles, the vertical mesh lines in the course of analyses result in a vertical orientation of crack planes in those elements. In a subsequent analysis (not presented here) with the smeared band of fracture forced to follow approximately the profile shown in Fig. 6.3(b), the peak resistance of the structure has been predicted to be very high. Analyst's interference with the direction of a fracture band propagation in smeared crack analyses is possibly undesirable due to the misleading prediction of structural resistances.

6.3 ANALYSIS OF A MODEL CONCRETE DAM

Carpinteri et al. [35] tested two 1:40 scaled models of a gravity dam subjected to equivalent hydraulic loads. Material properties of the model dam were reported to be E=35700 MPa, ν=0.1, σ_t=3.6 MPa ($\sigma_i=\sigma_t$ assumed), and G_f=184 N/m. Density of the material is assumed to be 2400 kg/m^3. Following an unsuccessful experimental attempt to simulate the prototype self-weight effects, the repaired first model, that failed prematurely along the foundation interface, and the second model, were tested without any adjustment for the self-weight condition. In the present study, only the second model is analysed, and the predicted responses are compared with the reported experimental and discrete crack analysis results of Carpinteri et al. [35]. The plane stress finite element model of the 30 cm thick dam model, and the applied loads are shown in Fig. 6.4. The crack mouth opening displacement (CMOD) is applied as the control parameter in nonlinear analyses performed using the CRCM and the FCM-VSRF. The applied hydraulic load versus the CMOD responses are presented in Fig. 6.5(a). Both smeared crack models provide very close predictions of the ultimate resistance of the structure (within 4% of the experimental result). The CMOD responses predicted by smeared crack models are relatively high. The discrete crack analysis prediction of CMOD, obtained by Carpinteri et al. [35], is approximately in between the experimental result and the smeared crack analysis results obtained here. Refinement of the finite element mesh did not influence the CMOD response in smeared crack analyses. The geometric configuration adopted in the finite element model of the structure, might have contributed to the apparent discrepancy in the CMOD response.

The continuity of displacement field, inherent in smeared fracture analyses, enabled to predict long stretches of the post-failure response, as observed in Fig. 6.5(a). The FCM-VSRF analysis provided a relatively stiffer post-peak response in this case as well. Crack profiles obtained from two smeared crack analyses are compared with the reported experimental and discrete crack analysis results in Fig. 6.5(b). The horizontal mesh lines seem to cause a horizontal propagation of the crack profile in the CRCM analysis. On the other hand, the FCM-VSRF provides a considerably better performance in predicting the crack profile of this particular case. The stress locking developed due to a fixed crack direction in the finite elements probably gives rise to high internal forces, that are able to overcome the restraining effects of mesh lines, and drive the crack profile downward. As the crack front propagates forward in the CRCM analysis, the crack bands in elements behind the fracture front orient themselves parallel to the general direction of the crack profile. With a decreasing applied force in the post-peak phase, there is an increasingly less restraint to the forward propagation of a horizontal crack. In the absence of any mechanism to retard the propagation of cracks, the post-peak resistance of the structure diminishes with an increasing CMOD response. An interesting observation can be made from Fig. 6.5 (b), regarding the discrete crack profile predicted by Carpinteri et al.[35].

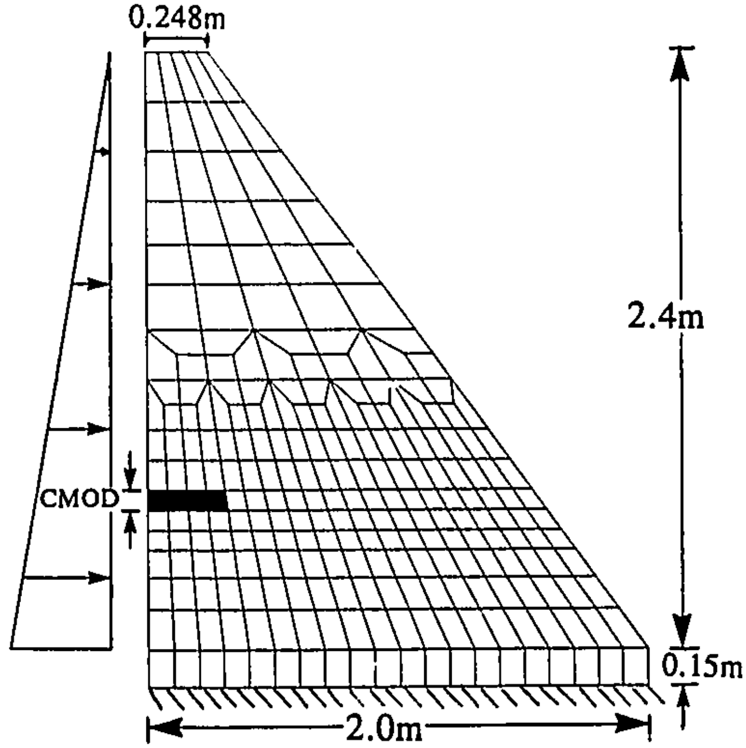

Figure 6.4 Finite element model of the notched dam and the applied loads.

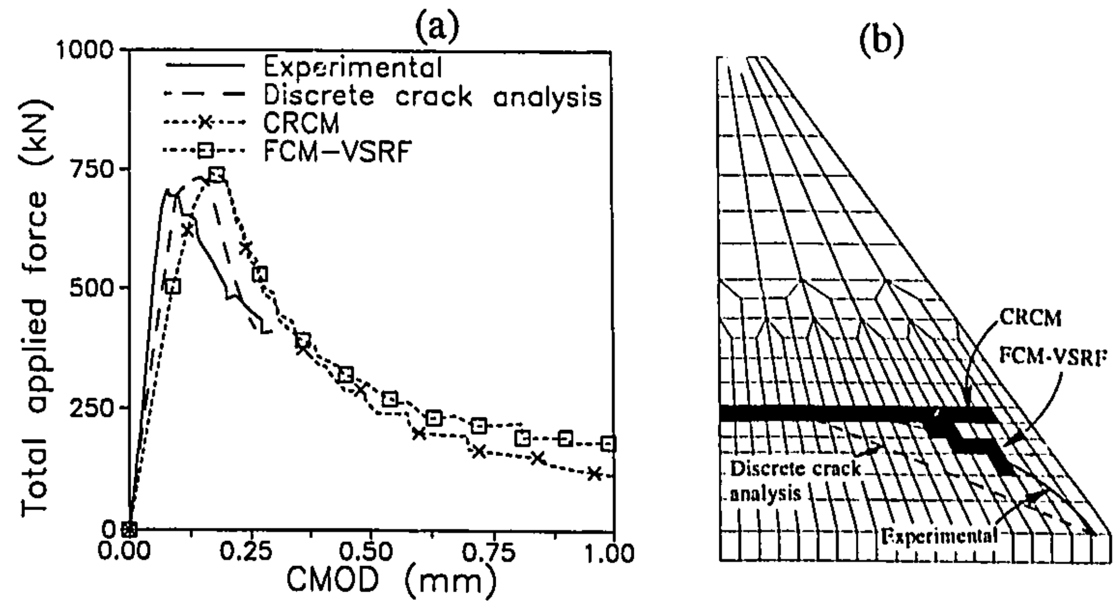

Figure 6.5 Response of the model dam: (a) the total applied load versus the CMOD, and (b) crack profiles in the structure.

The profile tips downward right from the beginning, and propagates at a nearly constant slope showing a significant deviation from the experimentally observed crack profile. The discrete crack propagation technique does not appear to be significantly better than the smeared crack analysis models in predicting the crack profile of the particular problem under investigation. However, the behaviour of crack propagation models, as observed in the model dam analysis, can not be extrapolated directly to prototype dam analysis, since the self-weight of the model was not scaled to simulate the situation of a full size dam. Analyses of a full scale concrete gravity dam are presented in the following section.

6.4 FRACTURE ANALYSIS OF A FULL SCALE CONCRETE GRAVITY DAM SUBJECTED TO RESERVOIR OVERPRESSURE

The Koyna Dam, analysed by several investigators over the last decades, is considered to study the behaviour of smeared fracture models. Plane stress finite element models of the dam and the applied loads are shown in Fig. 6.6. The geometric configuration of finite element models is similar to that reported in the literature (Chopra and Chakrabarti [40]), except for the upstream face slope which has been assumed straight vertical in the present models. The dimension, d, at the elevation of change in

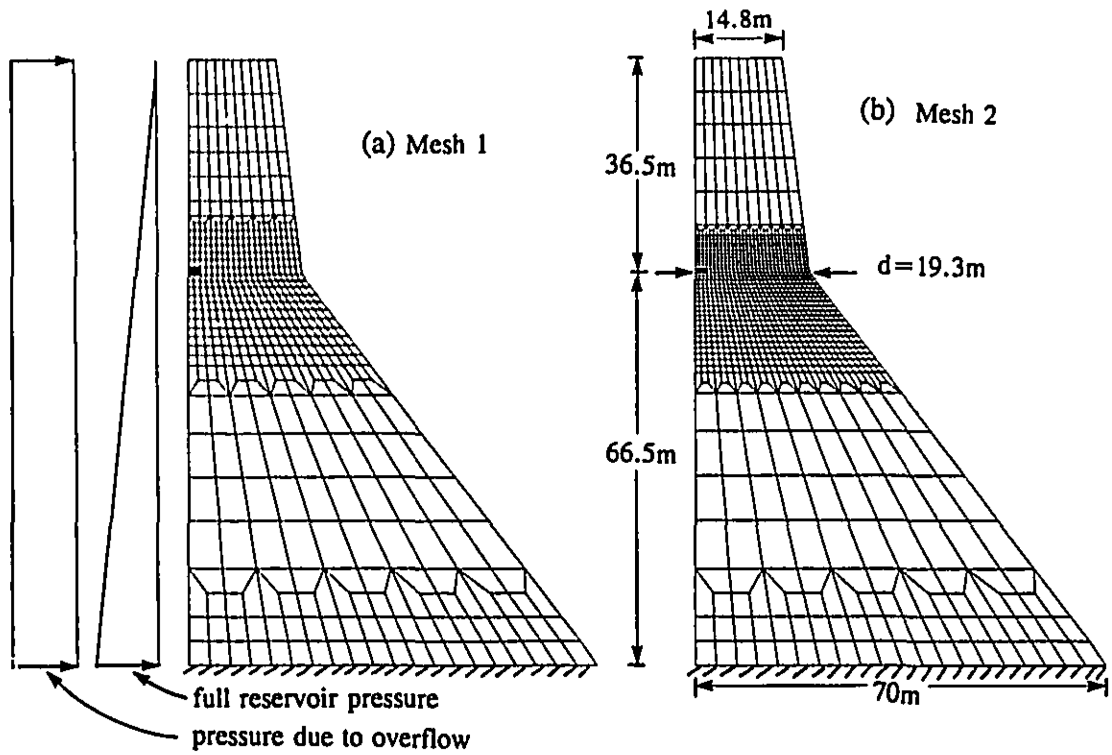

Figure 6.6 Finite element models of Koyna Dam subjected to reservoir overflow.

the slope of the downstream face, is varied in subsequent analyses to determine its influences on the structural resistance. The following material properties are assumed in the analyses: E=25000 MPa, ν=0.20, σ_i=1.0 MPa, and mass density=2450 kg/m^3. Two fracture energy values, G_f=100 N/m and 200 N/m, are considered for parametric investigations. Analyses are performed with the self-weight and the full reservoir pressure load, prior to the incremental application of the hydrostatic pressure that corresponds to a reservoir overflow condition. The horizontal displacement at the top upstream point of the dam is considered as the indirect displacement control parameter in these analyses. Nonlinear response of the structure is investigated for the single crack propagating from a pre-assigned imperfection, located on the upstream side at the elevation of downstream slope change. Cracking at that location was reported to be most critical to the ultimate structural resistance (Gioia et al. [73]). Water penetration and uplift pressure inside the cracks are not considered in the analyses presented here. Results obtained from the present analyses are compared with those reported by Gioia et al. [73].

6.4.1 Structural resistance to the reservoir overflow

Resistance of the dam to the reservoir overflow versus the horizontal displacement at the top of the dam is presented in Fig. 6.7(a). The solid curve in the figure represents the structural resistance predicted with the finite element model in Fig 6.6(a) ($d=19.3$ m). The analysis has been performed with the CRCM assuming $G_f=100$ N/m. Figure 6.7(a) also reproduces two curves from Gioia et al. [73] who performed a plasticity based analysis assuming a peak tensile strength equal to 1.0 MPa, and another analysis using the LEFM criterion with a material fracture toughness value of $K_{Ic}=1.0$ MPa$\sqrt{m}$. The initial displacement at the top of the dam corresponds to a loading combination of self-weight and full reservoir pressure with no overflow. Structural resistance predicted by the nonlinear smeared fracture model appears to lay slightly below the response corresponding to the LEFM analysis. However, the predicted response is very sensitive to the dimension, d. A preliminary analysis with an increased value of $d=22$ m (Fig. 6.7(b)) predicted a significantly higher structural resistance, as represented by the dotted curve in Fig. 6.7(a). The exact dimension adopted by Gioia et al. [73] is not precisely known. However, the plasticity based analysis appears to provide the most unrealistic structural resistance.

The depth of an initial imperfection, placed on the upstream side at the elevation of downstream slope change, has been varied between $a_0=0.05$ d to 0.20 d, to investigate its influences on the structural resistance (Fig. 6.7(c)). Resistance of the structure with a relatively smaller initial imperfection ($a_0=0.05$ d) increases initially, and then drops suddenly for a short instance. The structural resistance again starts to increase, and ultimately stabilizes at a level higher than the initial hump in the resistance curve. The

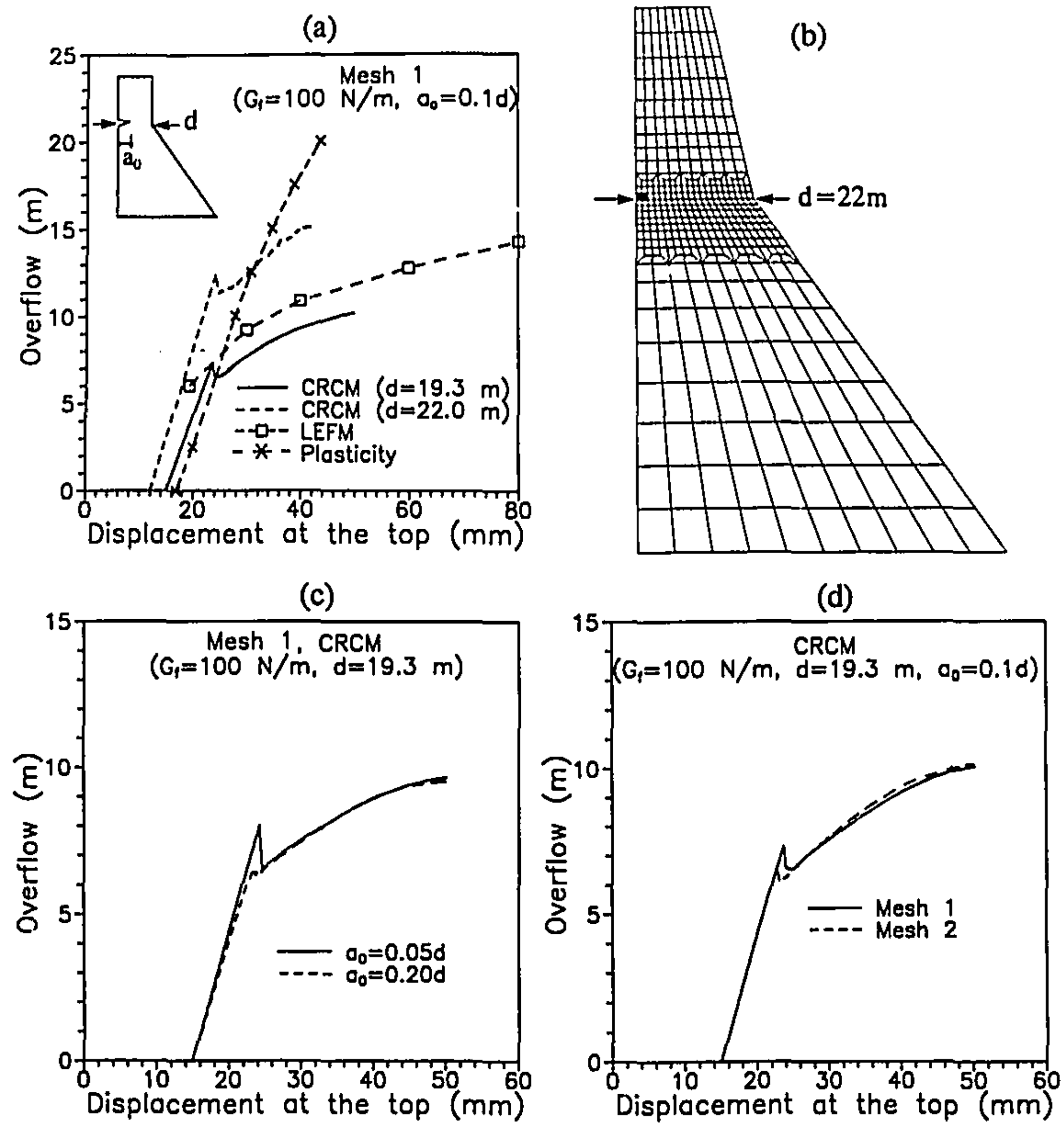

Figure 6.7 (a) Structural resistance to reservoir overflow, (b) a change in the geometric configuration, (c) influences of the notch depth, and (d) influences of the mesh refinement (Mesh 1 and Mesh 2 in Fig. 6.6).

initial peak resistance, which corresponds to the instance of a brief unstable crack propagation, is dependent on the initial notch depth. However, the ultimate structural response is not sensitive to the depth of initial imperfection in this particular case. The sensitivity of predicted response to the finite element mesh refinement is shown in Fig. 6.7(d). The initial peak structural resistance, prior to the brief unstable crack growth, is slightly reduced due to the mesh refinement. Nevertheless, a mesh independent ultimate resistance has been predicted for the dam subjected to a reservoir overflow.

6.4.2 Predicted crack profiles and the dissipated fracture energy

The crack profiles obtained in CRCM analyses of the finite element mesh 1 (Fig. 6.6(a)), are identical for different initial notch depths; consequently the profile of only one case (a_0=0.1 d) is shown in Fig. 6.8(a). After a stretch of horizontal propagation, the crack profile gradually curves downward due to the increasing compressive stresses on the downstream side. The crack profile predicted in the case of relatively finer mesh is presented in Fig. 6.8 (b). The predicted crack profiles appear to be independent of the refinement of finite element models. The dissipated fracture energies in two finite element models are also approximately similar (Fig. 6.8 (c)). An amplified deformed configuration of the dam, corresponding to the cracking response in Fig. 6.8(b), and the discrete crack response reported by Gioia et al. [73], are shown in Fig. 6.8(d). The CRCM appears to provide a crack response very similar to that obtained from the discrete crack analysis. The external forces due to self-weight and hydrostatic pressure are strong enough to overcome the spurious influences of mesh lines on the predicted fracture response of a full scale dam. Curvature of the crack profile, however, depends on the elevation of initial imperfection, due to the variation of self-weight and hydrostatic pressure intensities with the height.

6.4.3 Influences of the fracture energy value

The finite element mesh 1 (Fig. 6.6(a)), with an initial notch depth of a_0=0.10 d, has been analysed with two values of G_f, 100 and 200 N/m, to study the sensitivity of the predicted response to this constitutive parameter. Structural resistances obtained with the CRCM are presented in Fig. 6.9(a). The initial peak resistance corresponding to the brief unstable growth of the crack has been increased due to an increase in G_f value. The ultimate responses are, however, very similar for two cases. The stabilizing effects

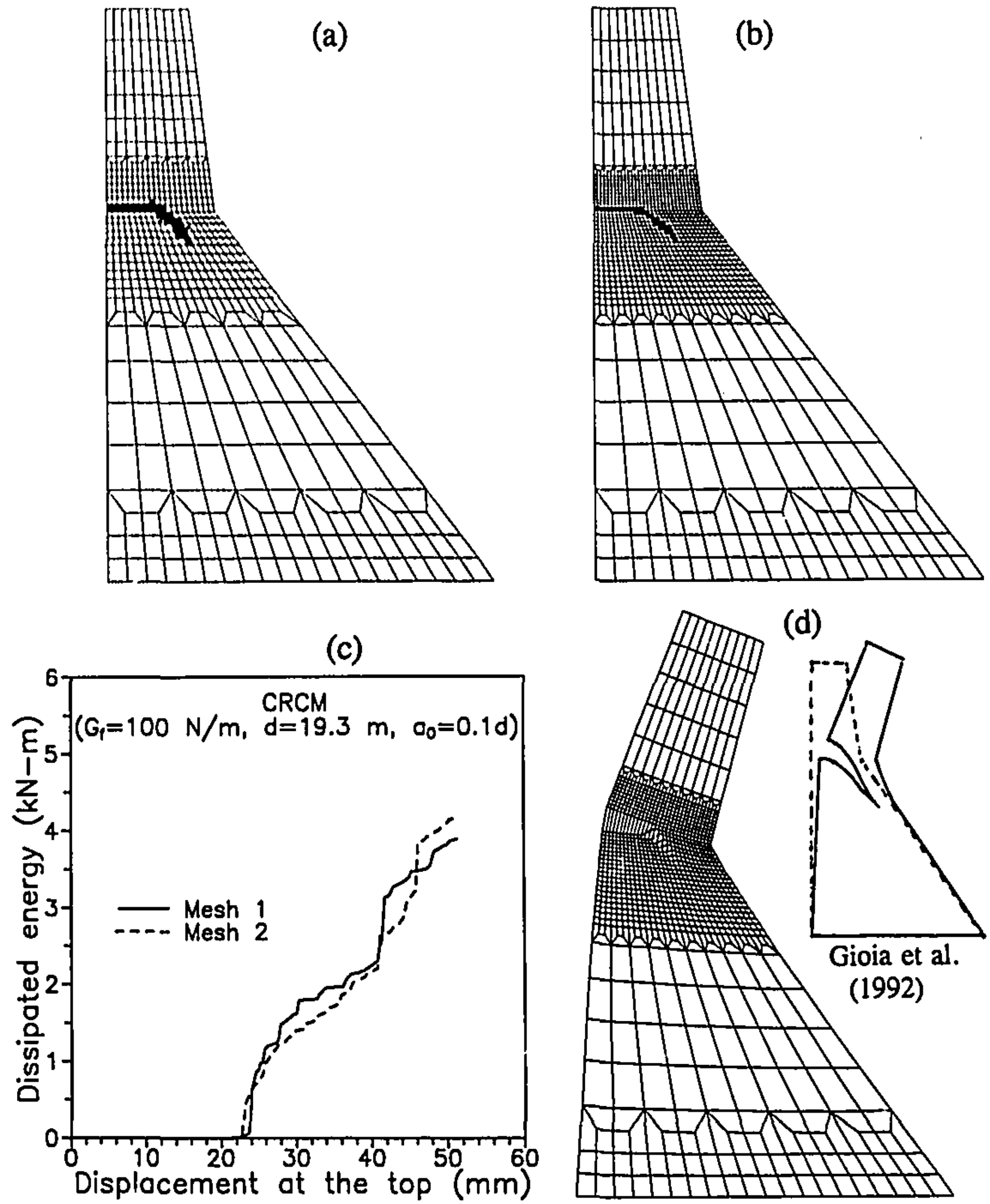

Figure 6.8 (a,b) Crack profiles corresponding to the instance of horizontal displacement at the top = 45mm, (c) dissipated fracture energy, and (d) the deformed configuration corresponding to the state in (b).

of self-weight and hydrostatic pressure are so dominant that the fracture energy value, that determines the evolution of damage at the local finite element level, does not induce

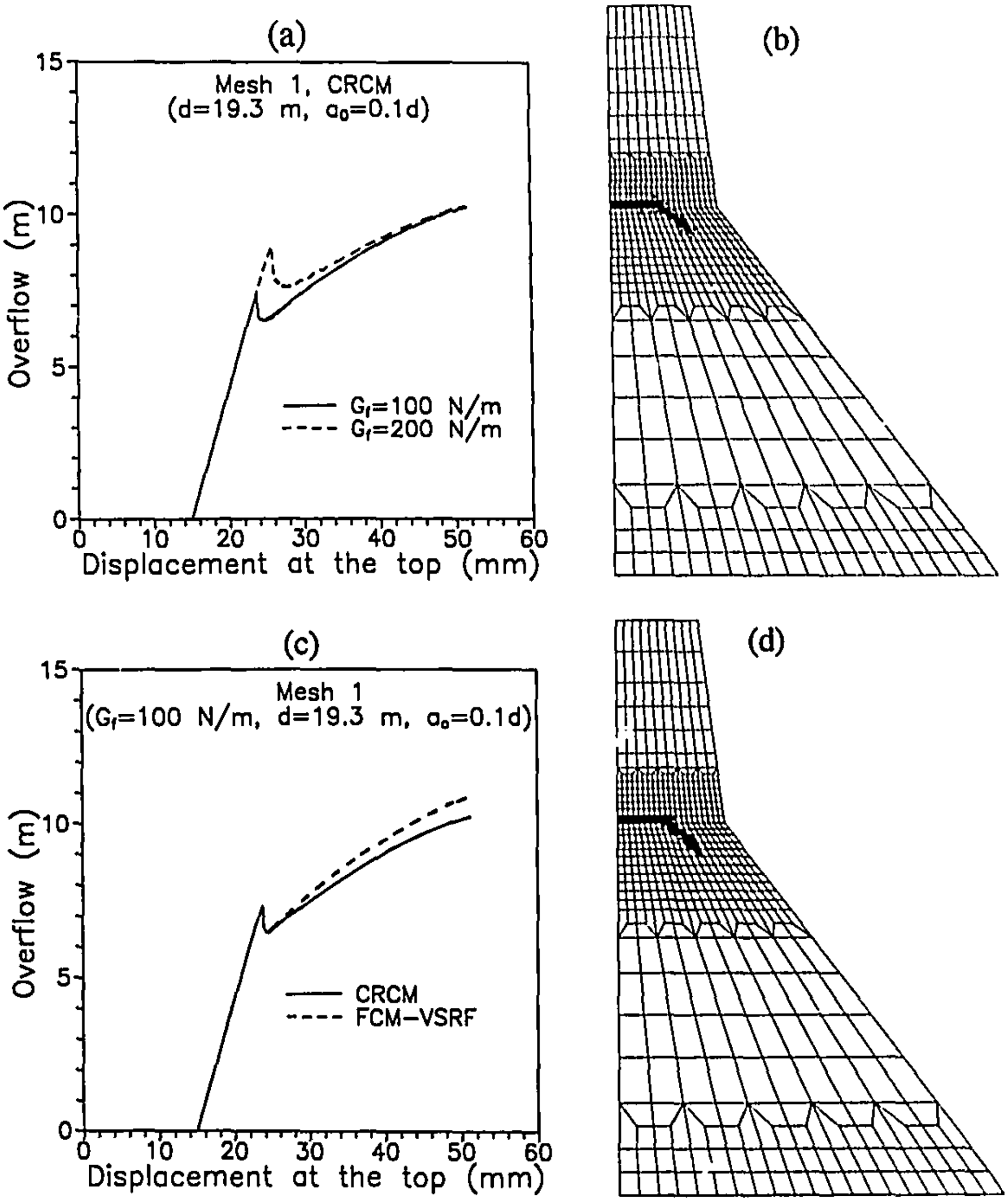

Figure 6.9 (a) Sensitivity of the structural resistance to the fracture energy value, (b) the crack profile for G_f=200 N/m (displacement at the top = 45mm), (c,d) responses predicted by the FCM-VSRF.

a significant change in the structural resistance after the initial peak. The crack profile obtained from the analysis with G_f=200 N/m (Fig. 6.9(b)) is very similar to that in Fig.

6.8(a), which was obtained with G_f=100 N/m. The structural redistribution of internal resistances to self-weight and hydrostatic pressure loads, thus, appears to have relatively greater influence on the ultimate resistance than that of the local material resistance to fracture propagation (the value of G_f).

6.4.4 Responses predicted by the FCM-VSRF

The finite element mesh 1 (Fig. 6.6(a)), with an initial notch depth of a_0=0.10 d, has been analysed with the FCM-VSRF, assuming G_f=100 N/m. The structural resistance predicted from an indirect displacement control analysis is compared with the corresponding result obtained with the CRCM, in Fig. 6.9(c). The FCM-VSRF analysis predicts a relatively higher ultimate resistance of the structure. The crack profile obtained in the FCM-VSRF analysis (Fig. 6.9(d)) is not significantly different from that obtained in the CRCM analysis (Fig. 6.8(a)).

6.4.5 Ultimate resistance of the dam

The resistance of a notched dam, observed in the analyses presented in Figs. 6.7 to 6.9, generally increases with increasing reservoir overflow. A nonlinear analysis can, therefore, be performed by applying the equivalent hydrostatic pressure loading in discrete steps without any indirect displacement control. Moreover, the incremental load analysis is more efficient to determine the ultimate resistance, since the indirect displacement control parameter (horizontal displacement at top of the dam) increases at a fast rate as the structure approaches towards the ultimate resistance. Figure 6.10(a) compares the response predicted by the incremental load analysis with that obtained earlier using the indirect displacement control technique. Responses predicted by the two analysis techniques are almost identical, except during the instance of a brief unstable crack growth, when the displacement in the load control analysis increases suddenly from 23.7 mm to 29.7 mm. However, the crack propagation is stabilized thereafter, and the structural resistance increases gradually; a behaviour also observed during the indirect displacement control analyses of the system.

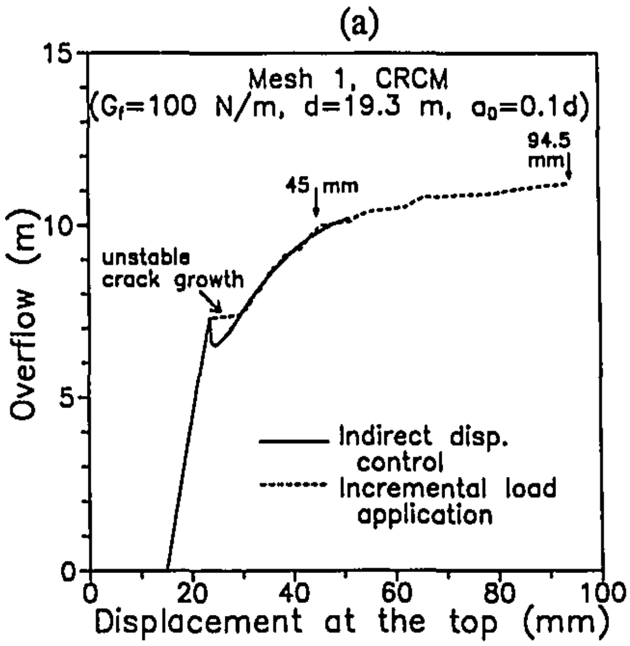

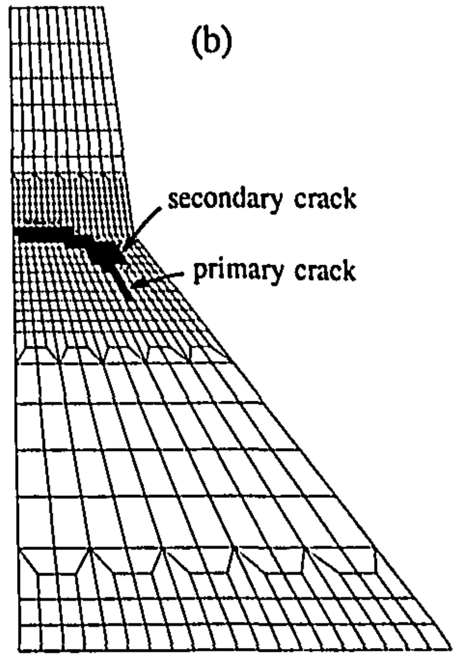

Figure 6.10 Incremental load analysis of the dam: (a) the ultimate resistance, and (b) the crack profile at the instance of horizontal displacement at the top = 94.5 mm.

The incremental load control analysis has indicated an approximately 5% force unbalance (Eqn. 4.13) after 100 iterations, at the load level equivalent to a reservoir overflow of 11.2 m, and the horizontal displacement at the top of the dam has increased to 94.5 mm (Fig. 6.10(a)). Figure 6.10(b) shows the crack profile at that instance of analysis. Apparently, the finite element model has been unable to contain the profile within a narrow band at the ultimate state. Nevertheless, failure of the structure appears to be caused by a secondary crack band, emanating from the primary crack profile. The maximum compressive stress near the neck region of the dam has reached only about 10 MPa, which is not high enough to cause the crushing failure of concrete. Continuation of the analysis a few steps beyond the first unconverged solution state (overflow=11.2 m) has predicted a rapid increase of the displacement (more than 300 mm) at the top of the dam, which probably indicates the overturning instability of the top part.

6.5 COMPARATIVE EVALUATION OF THE CRCM AND THE FCM-VSRF

Analyses of the shear beam and the model dam reveal that the peak structural resistance can be reasonably predicted using the CRCM. The FCM-VSRF provides a stiffer response in general, due to the significant stress locking in finite element models. In the shear beam problem, spurious mechanisms, arising due to the inaccurate prediction of crack profiles, result in considerable post-peak structural resistances for both smeared crack models. The CRCM prediction of a crack trajectory in the model dam appears to be influenced by the finite element mesh lines. In the FCM-VSRF analysis of the model dam, an increasing stress locking mechanism develops with the advancement of a fracture band, which together with the restraining effects of self-weight and applied forces propels a curvilinear crack band extension. The stress locking of fixed crack analysis models is a mesh dependent phenomenon (Droz [53]). The refinement of finite element mesh, however, has not been observed to influence the crack profiles predicted by the CRCM.

The discrete crack propagation analysis of the model dam, performed by Carpinteri et al. [35], provides a rather interesting observation regarding the performance of the incremental crack length control analysis, that was applied with the Hillerborg's fictitious crack model. In the cohesive discrete crack model, orientation of the incremental crack profile segment is fixed instantly upon reaching the tensile strength limit in a tip element. Any subsequent rotation of the crack segment is expected to involve a stiff scenario with elastic deformations of the material on two sides of the fictitious crack. In a heterogeneous material like concrete, with aggregates of different sizes embedded in the cement paste, the strain softening degradation of material properties occurs over a finite band area (Bažant and Oh [15]). The final crack trajectory is expected to emerge during the progress and reorientation of softening in that band. This behaviour of concrete in the FPZ can be effectively simulated in the context of a continuum mechanics formulation.

Cracking response of the full scale concrete gravity dam, subjected to a reservoir overflow, appears to be significantly different from that of the model dam, which has been investigated without any self-weight simulation. After a brief unstable penetration of the crack, the full scale dam shows a remarkable redistribution of the internal resistance, that stabilizes the crack propagation, and thereby increases the load resistance capacity of the structure. The ultimate resistance of the structure considerably exceeds the initial peak load corresponding to a brief unstable crack penetration. Finite element analysis parameters, such as the mesh refinement and the fracture energy value, and the depth of initial imperfections in the structure, do not induce significant changes in the ultimate structural resistance. The localized deformations due to tensile cracking of the dam, as predicted by the smeared crack analysis models, are similar to those observed in the discrete crack analysis by Gioia et al.[73]. Two smeared crack analysis models, the CRCM and the FCM-VSRF, have predicted similar curvilinear crack trajectories in the dam. Spurious influences of the finite element mesh lines seem to be relatively insignificant in the analysis of massive concrete structures, where the redistribution of internal resistances exerts the most dominant influence on the ultimate structural response.

6.6 CONCLUSIONS

In the shear beam analysis, the FCM-VSRF appears to provide a substantially higher post-peak resistance. A similar trend is observed in the model dam analysis as well. In light of those observations, the FCM-VSRF appears to be less reliable than the CRCM in predicting the post-peak structural resistance. Although the discrepancy between two models is not substantial in the Koyna dam analysis, the FCM-VSRF may not yield an acceptable post-peak structural response under different loading conditions and failure scenarios. The CRCM has performed consistently better than the FCM-VSRF in all three cases investigated here. Effectiveness of the CRCM, in alleviating the stress locking disturbances of smeared crack analyses, also needs to be verified for many other failure scenarios expected for concrete dams. Behaviour of this model in predicting the seismic fracture response of concrete gravity dams, one of the most hazardous scenario of dam safety investigation, will be examined in the following chapters.

The indirect displacement control analysis technique, developed in section 4.3, has provided favourable post failure responses of the shear beam and the model dam. However, application of the standard incremental load control analysis technique may be more efficient to predict the ultimate resistance of a full scale dam. The considerable redistribution of internal resistances in the full scale dam results in a stable crack growth with an increasing structural resistance against the reservoir overflow. The gradually dipping crack profile, from the upstream face towards the downstream face, may result in a sliding or overturning instability of the top part. However, more rigorous analyses should be performed considering the water penetration and uplift pressure inside cracks, to obtain quantitative information about the ultimate structural resistance of concrete gravity dams.

CHAPTER 7

SEISMIC FRACTURE AND ENERGY RESPONSE OF KOYNA DAM

7.1 INTRODUCTION

Cracking of concrete is an important factor to consider in the seismic safety evaluation of gravity dams. Severe cracking during the maximum credible earthquake (MCE) may adversely affect the safety of dams. Review of the most recent numerical investigations, presented in Chapter 2, reveals a trend of developing computationally expensive discrete crack analysis models to predict the seismic cracking behaviour of concrete gravity dams. The smeared crack analysis technique is generally criticised for predicting diffused crack patterns. The diffusion of micro-cracking due to a stress wave propagation is not unrealistic (Freund [68]). However, an evident localization of the damage zone with the progression of analysis was lacking in the early investigations. The relatively localized smeared crack profile predicted by El-Aidi and Hall [58], was largely dictated by the analyst's choice. Improved performances of the continuum mechanics models, and particularly of the CRCM, have been demonstrated in Chapter 6, for monotonic static load cases.

The practical experience about structural resistance of concrete gravity dams, subjected to severe ground excitations, is very limited. A 'classic' example on seismic cracking of concrete gravity dams is related to Koyna Dam in India. The dam was designed to satisfy the traditional 'no-tension' criterion with a seismic load coefficient of 0.05, applied uniformly over the height. The 1967 Koyna earthquake, Richter scale magnitude 6.5, induced significant cracking damages on either the upstream or the downstream face, or on both faces of the taller non-overflow monoliths of the dam (Chopra and Chakrabarti [40]). Apparently, the cracks penetrated all the way from the downstream face to the upstream face at the elevation where slope of the downstream face changes abruptly (Fig. 7.1(a)) (Hall [79], Saini and Krishna [140]). Shaking table tests

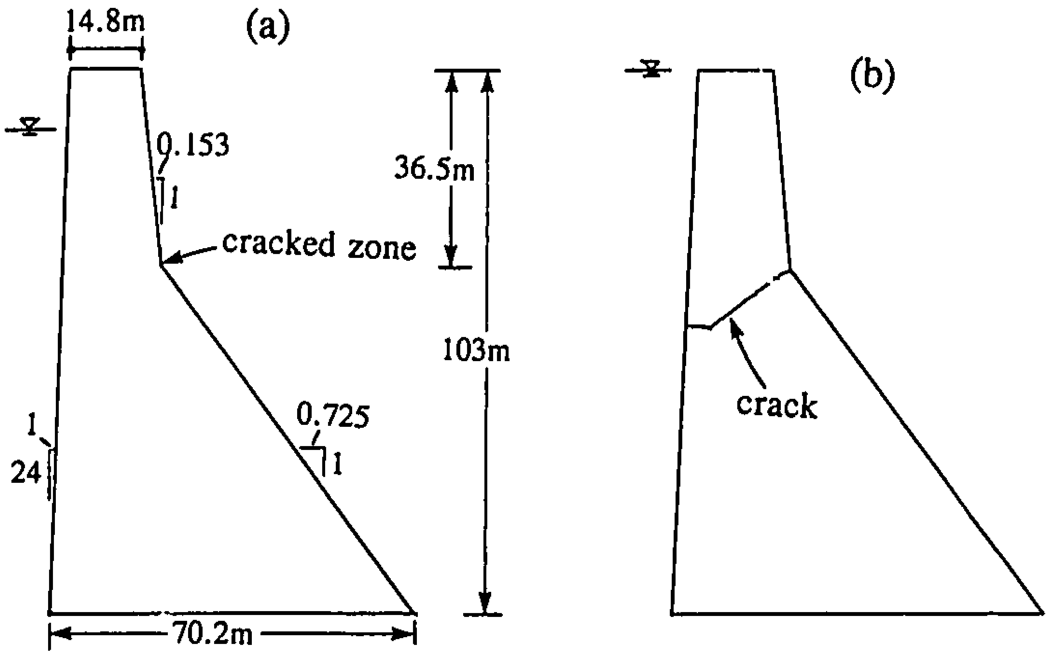

Figure 7.1 (a) The tallest non-overflow monolith of Koyna Dam, (b) the experimentally observed fracture response of a 1:150 scaled model (adopted from Hall[79]).

on Koyna Dam models, performed at the University California, Berkeley and by the US Army Corps of Engineers (Hall[79]), evidenced an all through cracking at the elevation of downstream slope change (Fig. 7.1(b)). Numerical investigations on the seismic response of Koyna Dam, performed by Ayari and Saouma[6], Chopra and Chakrabarti[40], Pal[125], and Skrikerud and Bachmann[146], have been reviewed in Chapter 2. Apparently, no past numerical investigation has satisfactorily explained the mechanism of developing an all through crack profile in the dam.

The objective of this chapter is to investigate the seismic fracture response of Koyna Dam by using the CRCM presented in Chapter 3. The nonlinear time domain solution algorithm, detailed in Fig. 4.9, is applied with the SMS formulation (section 3.5.3) to simulate the strain softening behaviour of finite elements. Seismic fracture and energy responses of the tallest non-overflow monolith of Koyna Dam are discussed. Influences of different modelling assumptions and material parameters, on seismic cracking response of the concrete dam are also investigated.

7.2 SYSTEM ANALYSED

A finite element model of the tallest non-overflow monolith of Koyna Dam is shown in Fig. 7.2(a). The upstream face of the dam has been assumed straight vertical, which

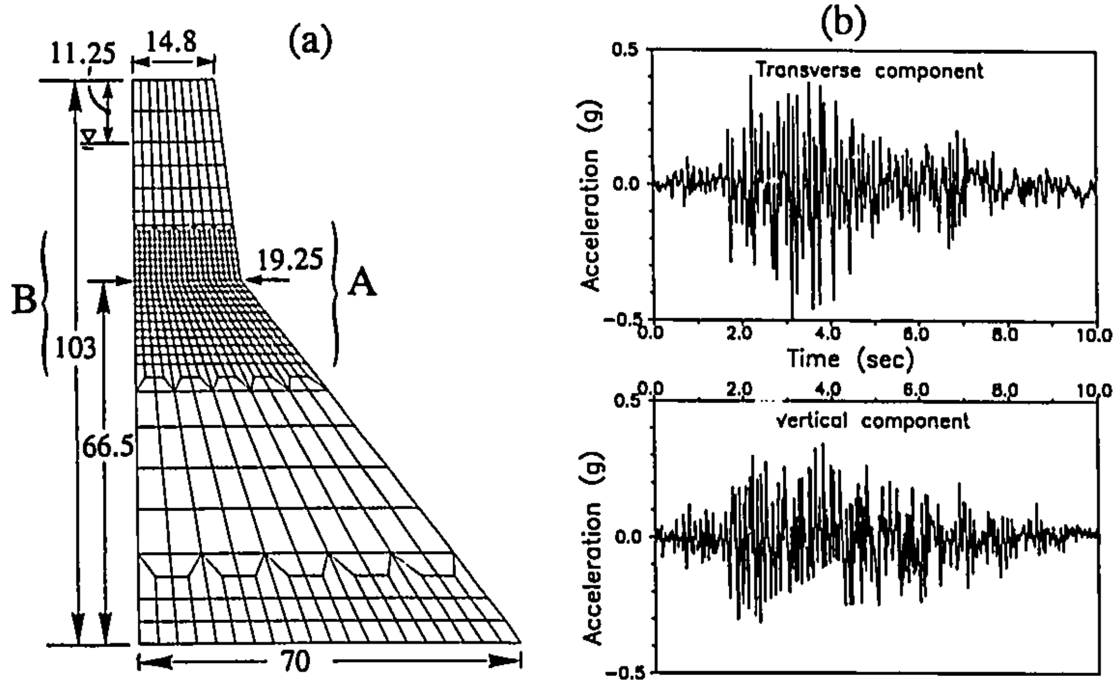

Figure 7.2 (a) A finite element model of Koyna Dam (dimensions in m), and (b) the Koyna accelerograms.

is a slight deviation from the actual configuration (Chopra and Chakrabarti [40]). A plane stress finite element idealization has been adopted since the dam monoliths were not grouted, and possibly vibrated independently during the ground excitation (Chopra and Chakrabarti [40], Hall [79]). The dam has been subjected to self-weight and hydrostatic pressure loads to determine the pre-seismic state. No cracking has been predicted at that state in the analyses presented here. Seismic analyses have been performed with transverse and vertical components of the Koyna accelerogram (Fig. 7.2(b)), that was recorded during the seismic event by a strong motion accelerograph located in a rigid gallery (Chopra and Chakrabarti [40]). Numerical integrations have been performed with a small time step of 0.002 sec, to have very few new elements initiate softening in a time step.

The elastic material properties, E=31027 MPa, ν=0.20, and mass density=2643 kg/m^3, and the first four fundamental periods of the finite element model, T_1=0.330 sec, T_2=0.125 sec, T_3=0.092 sec, and T_4=0.063 sec are consistent with those reported in the literature (Ayari and Saouma [6], Chopra and Chakrabarti [40]). The constitutive parameter, σ_i, has been assumed 1.5 MPa, which is consistent with the static fracture toughness value, K_{Ic}=1.5 MPa$\sqrt{m}$, assumed by Ayari and Saouma [6]. The fracture energy, G_f, has been assumed 150 N/m, that is typical for concrete normally used in dams (Brühwiler and Wittmann [32]). The dynamic magnification parameters have been assumed as DMF_ϵ= DMF_f=1.20 in all analyses.

Time domain solutions with different values of the algorithmic damping parameter, α, varying between -0.20 to -0.05, generally predicted identical responses of the structure. Seismic fracture and energy responses of the dam, predicted by the QDM (quasi-linear damping model) (section 4.4.1), and assuming α=-0.1, are presented in sections 7.3 and 7.4. The amount of damping in the initial fundamental mode response of the dam has been assumed 5% in all analyses except a case with 3% damping, briefly mentioned in section 7.5.2. Influences of different viscous damping models and mesh refinement on seismic fracture response of the dam are discussed in section 7.5. Considering the principal objective to investigate the performance of the proposed fracture analysis model, dynamic interactions in the dam-foundation-reservoir system have not been modelled rigorously in this chapter. The foundation condition has been assumed rigid in all analyses. Dynamic interactions with the reservoir, modelled in the simplest form using the Westergaard [159] added mass technique, have been considered in the final analysis presented in section 7.6.

Cracking in zones A and B (Fig. 7.2(a)) are mainly discussed, since that region of the dam reportedly experienced significant damage due to the earthquake. Finite elements at the completely cracked and open condition are indicated by shading the respective areas on the finite element mesh. Closed and incomplete fracture conditions are represented by dots in the element centres. Elements that never softened are unmarked in the presentations. Amplified deformed configurations of the structure are also presented in the illustrations.

7.3 SEISMIC FRACTURE RESPONSE OF THE DAM

The time history of horizontal displacement at the top of the dam, shown in Fig. 7.3(a) (α=-0.10), is used here as a reference to describe the evolution of cracking in zones A and B of the dam. During the upstream movement of dam (3.946 sec, Fig. 7.3(a)), the elements in zone A soften, and finally a localized band of cracked elements emerges in that zone (Fig. 7.3(b)). The average crack propagation velocity of the first horizontal stretch has been computed to be about 200 m/s, which is a typical value for crack propagation in concrete (Reinhardt and Weerheijm[134]). The finite element fracture analysis model, applied with the QDM, appears to provide a reasonable estimate of the crack propagation velocity in concrete dams. The crack on downstream side closes when the top of the dam swings towards the downstream direction (4.144 sec, Fig. 7.3(a)). The elements in zone B begin softening at that instance; however, no localization takes place on the upstream side. When the top swings towards the upstream direction again (4.338 sec, Fig. 7.3(a)), the downstream crack re-opens and propagates deep inside the dam (Fig. 7.3(c)). During the next reversal of dam's movement (4.542 sec, Fig. 7.3(a)), the elements in zone B soften further with the eventual localization of a crack band, that meets the downstream crack profile in the dam interior (Fig. 7.3(d)). The upstream crack profile, approximately 4.67 m in length, has evolved within a single time step between 4.490 sec and 4.492 sec. The evolution of an all through crack profile, predicted with the smeared crack model, is consistent with the response observed in the shaking table tests (Fig. 7.1(b)).

Time histories of the major principal stress in elements i_1 and i_2, as identified in Fig. 7.3(d), are shown in Fig. 7.4(a). Evidently, the rotating constitutive formulation has been very effective to eliminate an artificial tensile stress build up in the fully cracked

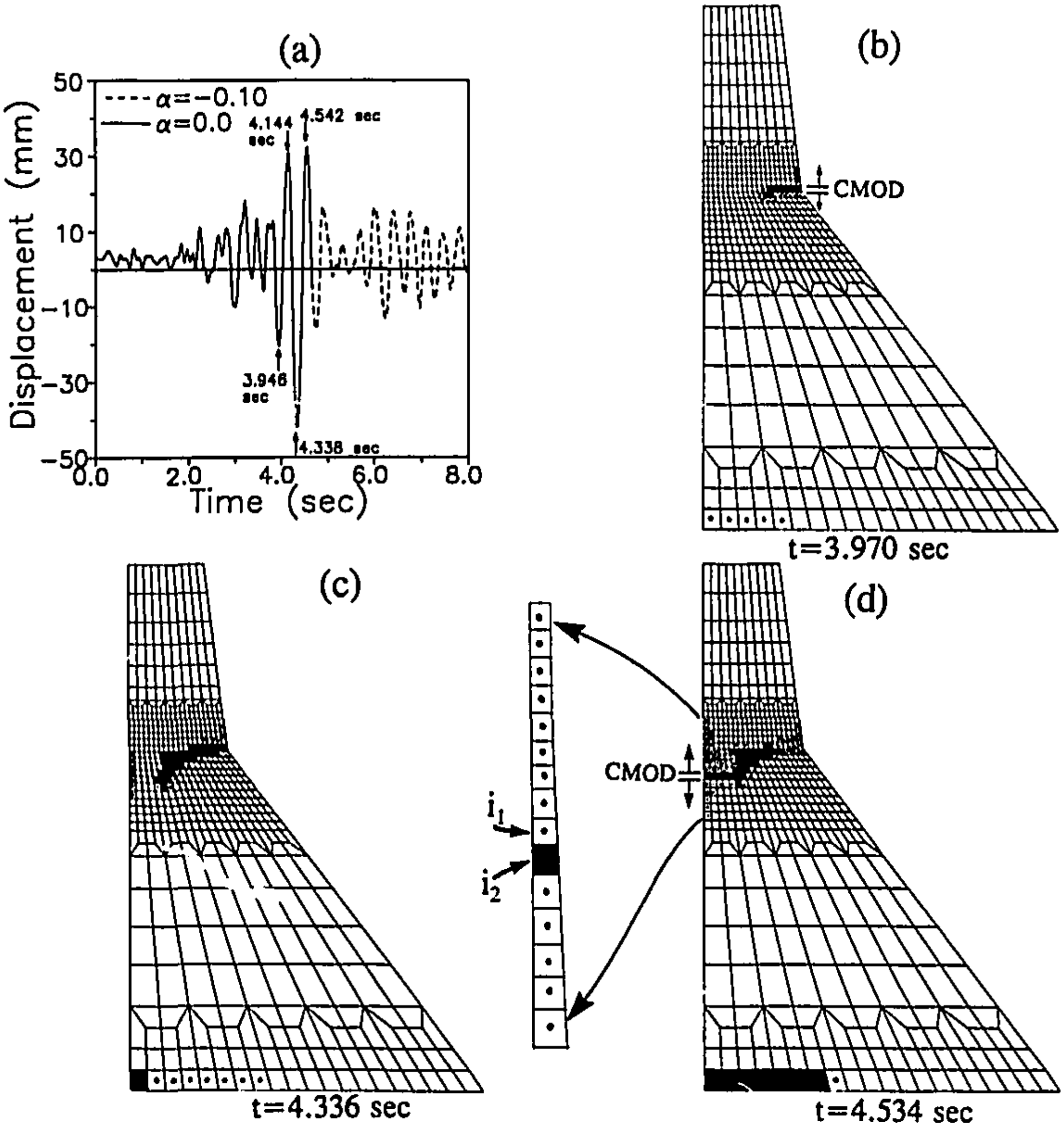

Figure 7.3 (a) Time histories of horizontal displacement at the top of the dam, and (b,c,d) seismic fracture response of the structure.

element i_2. The gradual degradation of viscous damping resistance in the cracked element also effectively eliminates the tensile stresses in the adjacent element i_1. The maximum compressive stress in the vicinity of the closed crack mouth remains low (8 MPa). A similar behaviour has also been observed for the cracking in zone A. The time histories of crack-mouth-opening-displacement (CMOD), computed as the relative

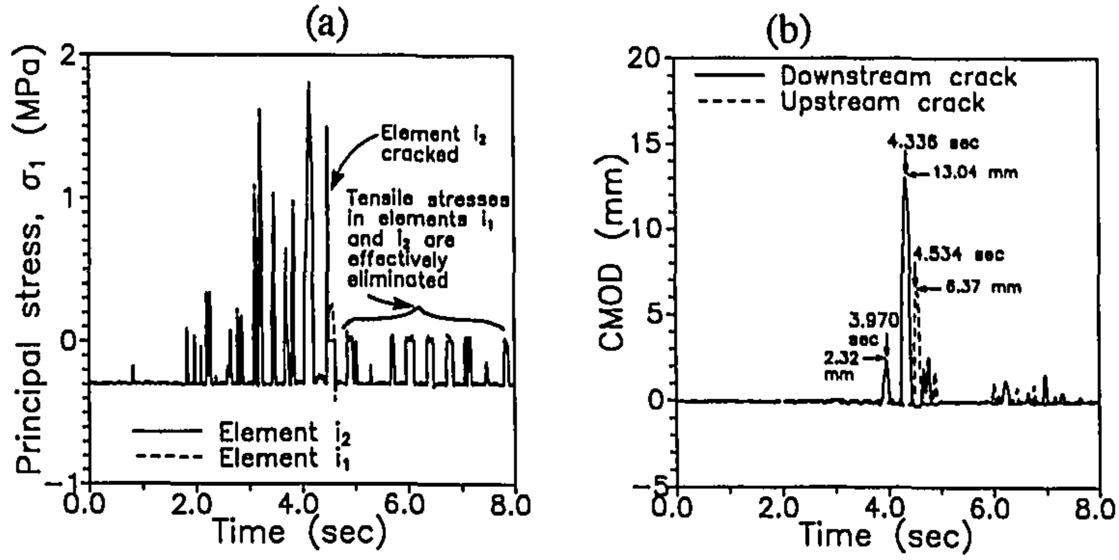

Figure 7.4 Time histories of (a) the major principal stress, σ_1, and (b) the crack-mouth-opening displacement (CMOD).

vertical opening between two surface nodes at the crack mouths, are shown in Fig. 7.4(b). The alternate opening and closing of two crack mouths on two faces of the dam indicates a stable response of the separated top part. The peak CMOD on the upstream face is about 6.4 mm, and remains open for a considerable amount of time, that may permit water penetration in the crack during the seismic event. Deformed shapes of the dam at three instances of significant openings of the two crack mouths, as shown in Fig. 7.4(b), are represented in Fig. 7.5. The smeared crack propagation model, together with the degrading damping model (QDM), appears to reproduce the localized deformations very well. The finite element analysis performed for 8 sec duration of the seismic excitations has not predicted any dynamic instability of the separated top part of the dam. This behaviour is consistent with that experienced in the actual structure as well as in the subsequent model tests. Nevertheless, the present analysis is not claimed to have corroborated the observed behaviour perfectly, since reservoir and foundation interaction effects, generally considered important to determine the dynamic response of concrete gravity dams, have not been considered in the present analysis. The material parameters have also been defined approximately in the analysis. Sensitivity of the predicted response to modelling parameters and assumptions is discussed in section 7.5

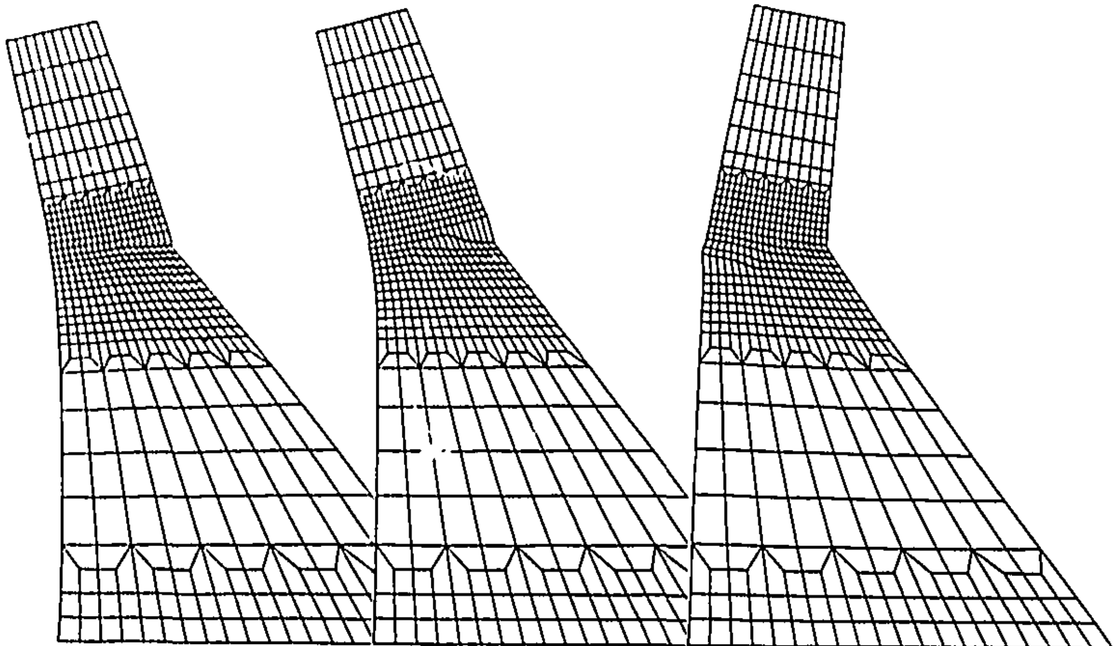

Figure 7.5 Deformed configurations of the dam.

7.4 SEISMIC ENERGY RESPONSE AND CHANGES IN FUNDAMENTAL PERIOD OF THE DAM

The seismic input energy, E^Q, the kinetic energy, E^K, and the dissipated damping energy, E^D, obtained from the analysis discussed in section 7.3, are presented in Fig. 7.6(a). The viscous damping mechanism dissipates most of the seismic energy imparted to the dam. The internal strain energy, E^U, and the dissipated fracture energy, E^F (Eqn. 4.31), obtained from the same analysis are presented in Figs. 7.6(b) and 7.6(c) respectively. The non-zero value of E^U (84 kN-m) at the beginning of time history (Fig. 7.6(b)) corresponds to the pre-seismic internal strain energy due to self-weight and hydrostatic pressure loads. The dissipated fracture energy, E^F, does not appear to have a significant influence on the total strain energy in the structure. Evidently, the total energy dissipation due to tensile fracture is insignificant compared to the magnitude of other energy components. This observation, however, does not undermine the

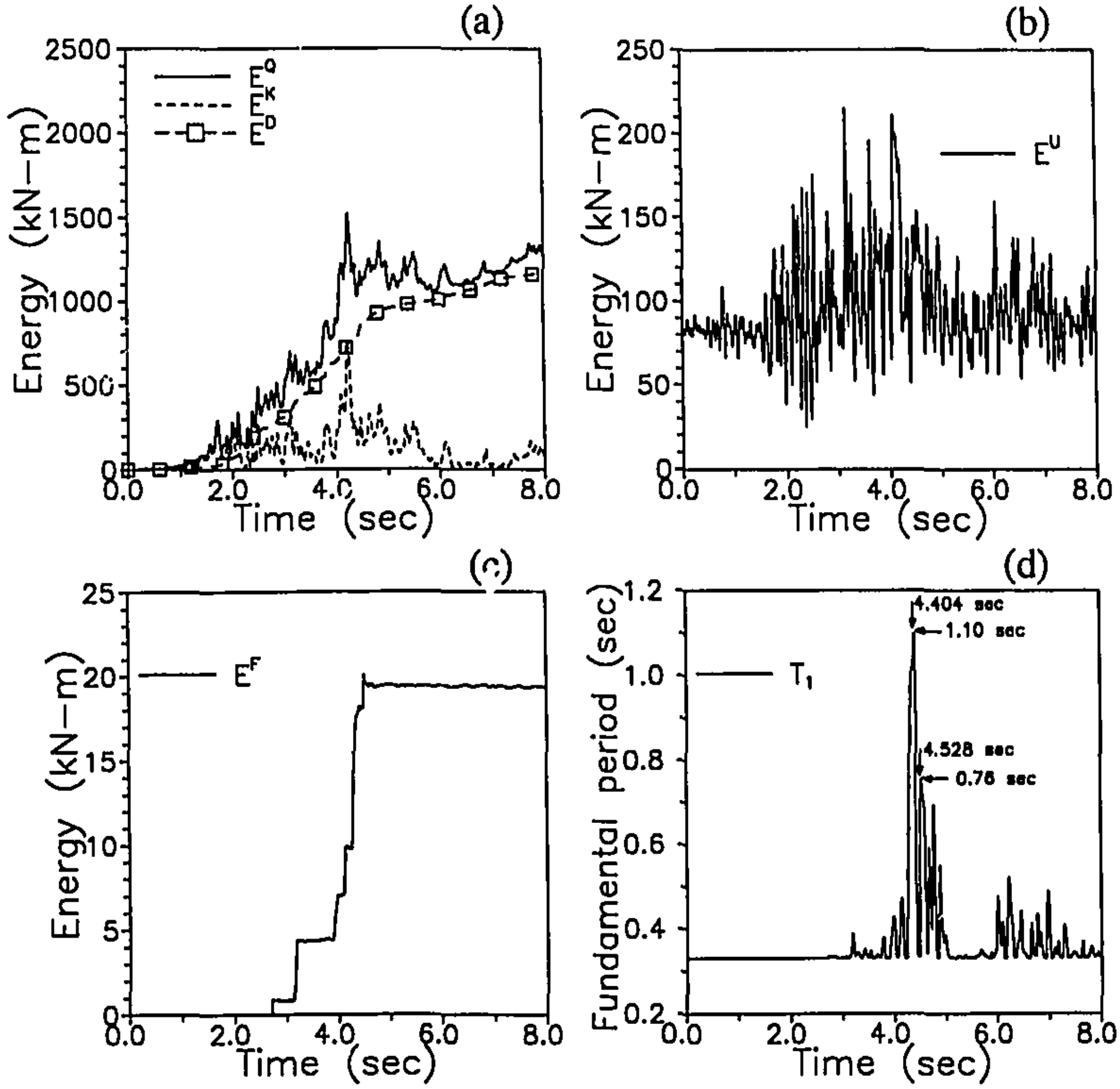

Figure 7.6 (a,b,c) Energy response of the dam, and (d) changes in the fundamental period of dam.

importance of the fracture energy parameter, G_F, that determines the evolution of micro-crack damage in finite elements

Recalling that the fracture energy dissipation due to a unit crack length extension has been assumed to be 180 N/m in the seismic analysis, the total dissipated fracture energy, 19.2 kN-m in Fig. 7.6(c), should correspond to an approximate crack length of 106 m. The crack length at the heel of the dam is about 28 m, and this leaves a length of the top crack about 78 m, which is more than twice the actual length traversed by the crack band. The slanted finite element mesh has caused the crack band to diffuse over more than one element, particularly during severe deformations of the cracked elements, when the dam swings towards the upstream direction at 4.336 sec (Figs. 7.3(c) and 7.5). The diffusion of micro-cracking, caused by the viscous damping model, has also contributed to the excessive fracture energy dissipation in the finite element analysis. Influences of different viscous damping models on seismic fracture response of the dam are discussed in section 7.5.

The time history evolution of the fundamental period of the dam is shown in Fig. 7.6(d). The maximum amplification of fundamental period occurs at 4.404 sec, following the event of a peak CMOD response of the downstream crack (4.336 sec, Fig. 7.4(b)). The second highest amplification occurs at 4.528 sec, immediately preceding the peak CMOD response of the upstream crack (4.534 sec, Fig. 7.4(b)). For the crack profile sloping upward from the upstream face, the downstream crack opening appears to be more damaging to the structural integrity. A positive value of the fundamental period has been obtained at the end of each time step using the subspace iteration technique (Oughourlian and Powell [123]). This observation indicates the stability of the finite element analysis, and possibly of the structure as well. The energy balance error, that is presented in Fig. 7.7(a) with other parametric results, has remained much below 1% at the end of the analysis.

7.5 SENSITIVITY OF THE PREDICTED RESPONSE TO MODELLING PARAMETERS AND ASSUMPTIONS

The numerical integration parameter, α, has been introduced in Eqn. (4.18) to suppress the spurious high frequency deformation modes that may arise in a smeared fracture analysis under seismic loadings. The local instability caused by a zero value of α in a subsequent seismic fracture analysis is discussed in section 7.5.1. Artificial restraints on the cracking of finite elements, that may be caused by a linear viscous damping model (section 4.4.1), are investigated in section 7.5.2. Influences of the elasto-brittle damping model (section 4.4.1) on seismic fracture response of the dam are studied in section 7.5.3. Sensitivity of the seismic fracture response of dam to material parameters and mesh refinement, is also discussed in that section.

7.5.1 Local instability in finite element fracture analysis

An analysis has been performed assuming the numerical integration parameter $\alpha=0$ (Eqn. 4.18), to determine the influences of high frequency modes that may cause a local instability in the finite element fracture analysis of concrete structures. The cracking response of dam in this analysis has followed the same sequence, as described for the analysis with a non-zero α parameter (Fig. 7.3). The CMOD responses on the upstream and the downstream sides, and the deformed configurations at the instances of significant crack opening are identical to those in Figs. 7.4 and 7.5, until the solution with $\alpha=0$ collapses with a high energy balance error (about 12%) at 4.652 sec (Fig. 7.7(a)). No apparent discrepancies are obvious in the time-history of horizontal displacement at the

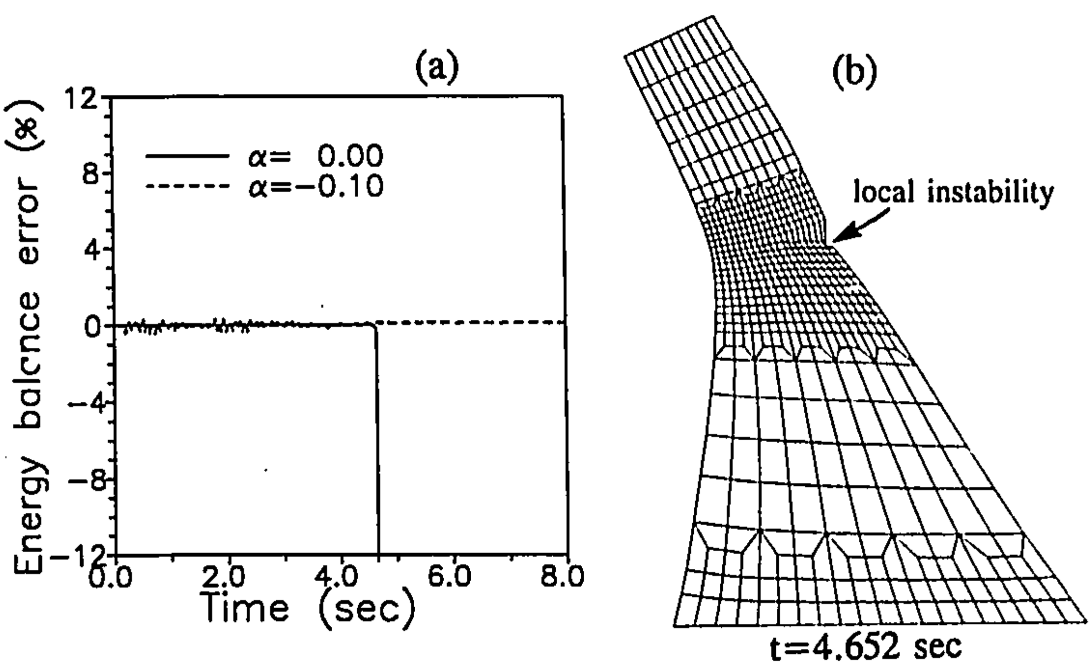

Figure 7.7 Effects of assuming $\alpha=0$: (a) energy balance error, and (b) local instability in the finite element model.

top of the dam (Fig. 7.3(a)). The deformed configuration at that instance (4.652 sec) reveals a local instability in the finite element model (Fig. 7.7(b)). The mode of global deformation also appears to be of high order. Parametric analyses with the constitutive model parameter, μ_c, in the range of 0.90-0.9999, have not eliminated the instability in this particular case. Application of the four point integration rule does not appear to ensure the local stability in strain softening quadrilateral elements, especially when the cracks begin to close under cyclic loading conditions. This observation is consistent with the prediction of de Borst and Rots [50], who anticipated such spurious mechanisms from the eigen-property analysis of strain softening elements. Suppression of the high frequency deformation modes by using a non-zero α parameter effectively eliminates the local instability in strain softening finite elements. Preliminary analyses have shown that the optimum value of α may be influenced by the value of μ_c, that determines the closing and reopening of cracks in finite elements (section 3.7). However, the value of α in the range of -0.20 to -0.05 has been found to be adequate with μ_c varying between 0.95 to 0.9999. Effects of the spurious local deformation modes may also be eliminated by considering only the contributions of few dominant modes in a nonlinear time history analysis (Léger and Dussault [100]).

7.5.2 Influences of the linear viscous damping model

A seismic fracture analysis of the finite element model in Fig. 7.2(a) has been performed using the LDM (Eqn. 4.16), where the viscous damping matrix is kept constant irrespective of the cracking condition in finite elements. This analysis has predicted a very diffused crack pattern (Fig. 7.8(a)), and no evident localization of the crack profile is observed in the deformed configuration of the dam (Fig. 7.8(b)). The solution has remained very stable even with $\alpha=0$, and the maximum energy balance error has been less than 0.003% after 6 seconds of analysis. Time histories of the major principal stress in elements i_1 and i_2 (Fig. 7.8(a)) are shown in Fig. 7.8(c)). Retention of the linear (constant) damping term in the cracked element, i_2, helps to transmit significant tensile stresses in the adjacent element i_1. These tensile stresses are negligible

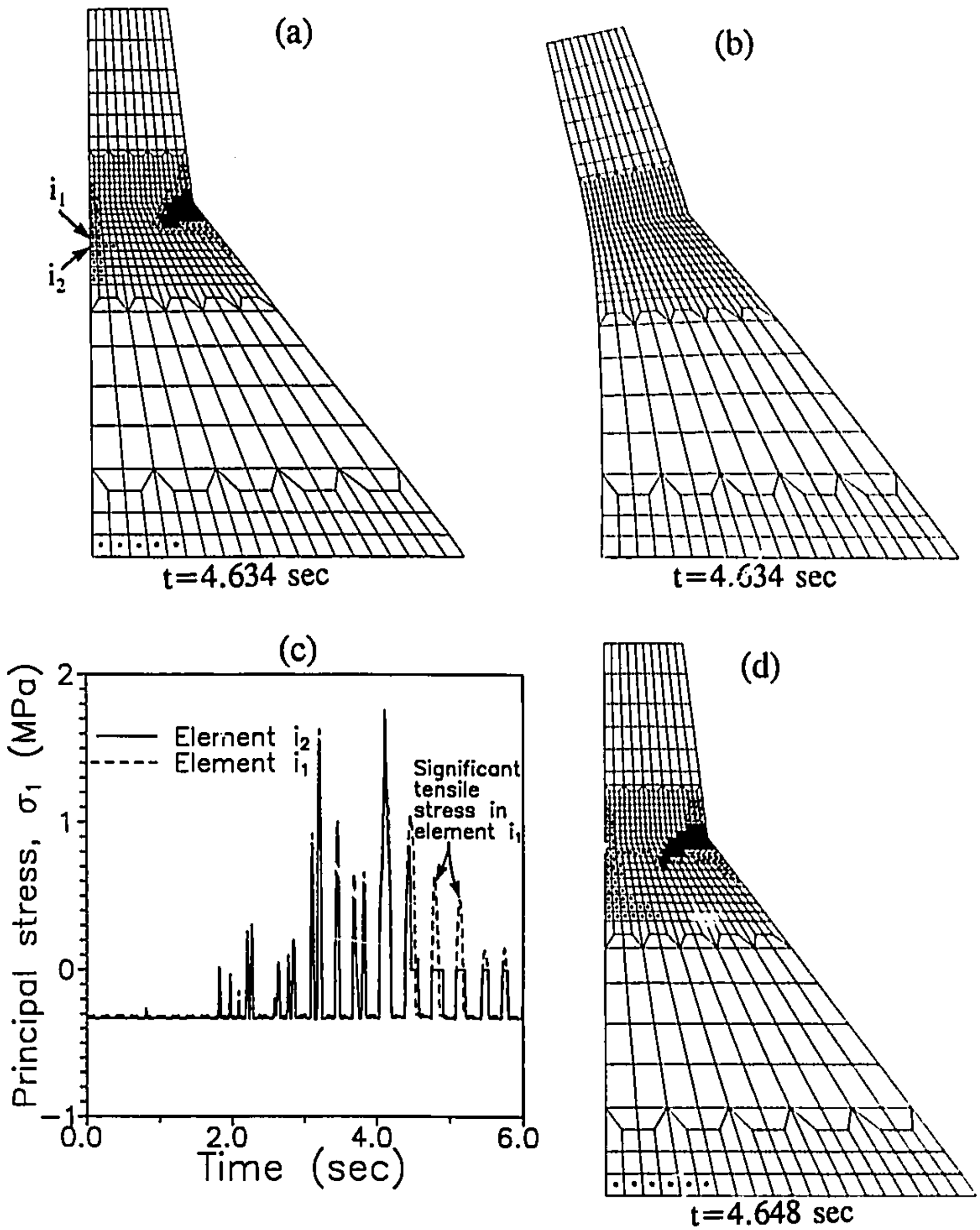

Figure 7.8 (a,b,c) Responses obtained with the LDM (5% damping in the fundamental mode), (d) cracking response obtained for 3% damping.

in Fig. 7.4(a), when the QDM is used. The fictitious tensile stresses sustained by the constant damping term in cracked elements has resulted in a higher diffusion and less penetration of the crack zone inside the dam. A reanalysis with reduced amount of linear damping, 3% damping in the initial fundamental mode, has predicted the coalescence of cracks in zones A and B (Fig. 7.8(d)). However, the spurious diffusion of micro-cracking along the height of the dam in zones A and B is still very significant. Apparently, the viscous damping model is more responsible than the smeared crack finite element models for predicting diffused crack patterns in the past investigations.

7.5.3 Influences of the elasto-brittle viscous damping model

Figure 7.9 illustrates the seismic fracture response of Koyna Dam, predicted using the EDM, where the viscous resistance of an element is completely eliminated after the softening initiation. The cracking response obtained by using this damping model is

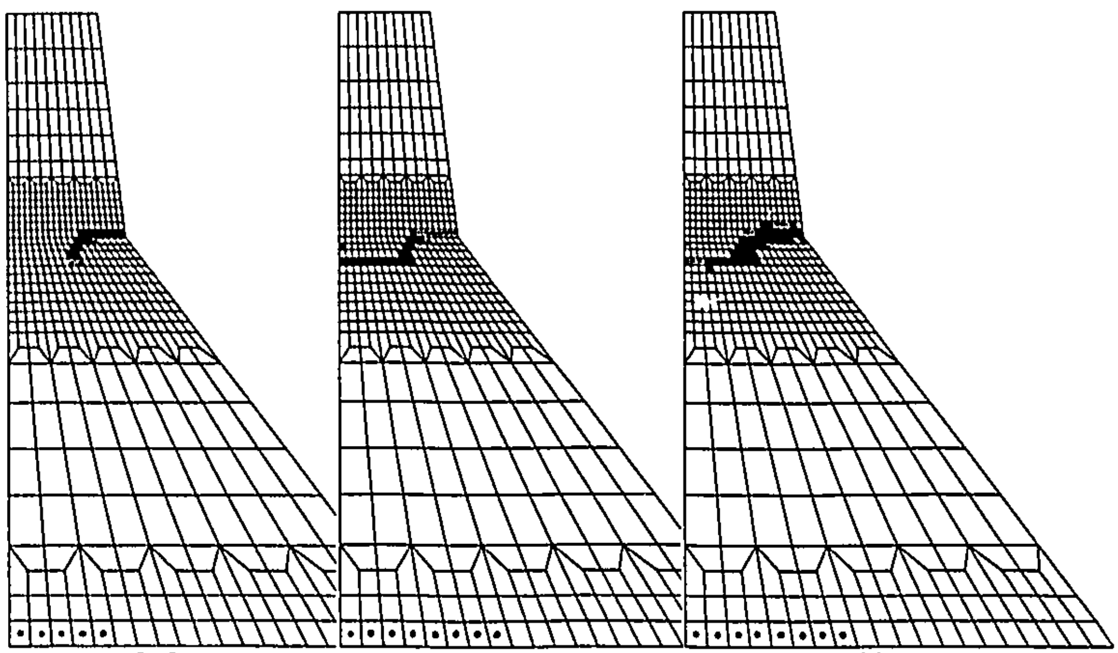

Figure 7.9 Fracture response predicted using the elasto-brittle damping model.

more severe than that predicted using the QDM (Fig. 7.3). Complete elimination of the viscous damping terms in the EDM analysis has resulted in a relatively deeper penetration of the downstream crack profile at the first instance (3.970 sec). The upstream crack profile has also localized earlier (4.190 sec), and subsequently merged with the downstream crack profile. The average crack propagation velocities have been computed to be 400 m/s and 550 m/s for downstream and upstream crack extensions respectively. A subsequent EDM analysis with a refined finite element mesh has predicted the following crack profiles in Fig. 7.10, that are almost identical to those in Fig. 7.9. The crack propagation velocities during the extensions of downstream and

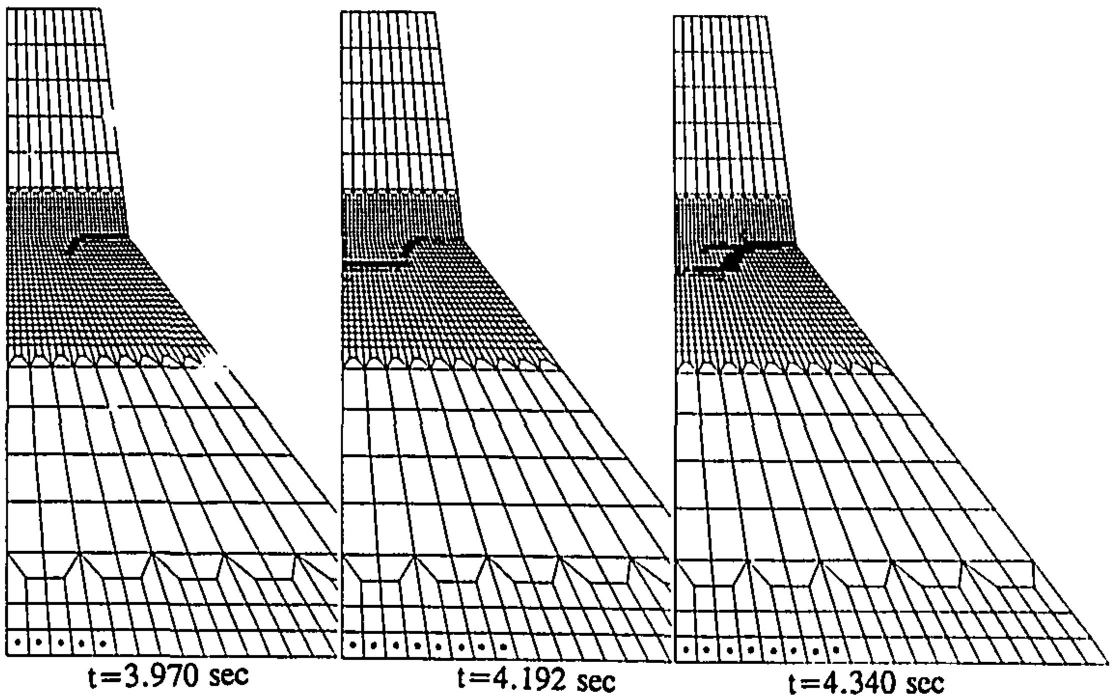

Figure 7.10 Influences of mesh refinement on the fracture response predicted using the elasto-brittle damping model.

upstream cracks in the refined mesh analysis are 320 m/s and 400 m/s respectively, which are slightly less than those of the coarse mesh analysis. Use of the EDM has significantly reduced the diffusion of micro-cracking along the height of dam in zones A and B of both finite element meshes (Figs. 7.9 and 7.10). However, the crack propagation velocity is relatively higher with this damping model, which is the consequence of a brittle elimination of the viscous damping resistance in strain softening elements. The diffusion of crack bands during severe deformations of the cracked elements is existent in both analyses (time=4.334 sec in Fig 7.9, and 4.340 sec in Fig.

7.10). The energy dissipations due to viscous damping and tensile fracture, obtained from the EDM analyses of two meshes, are compared in Fig. 7.11 with the results obtained from the QDM analysis of the coarse mesh. The total viscous energy

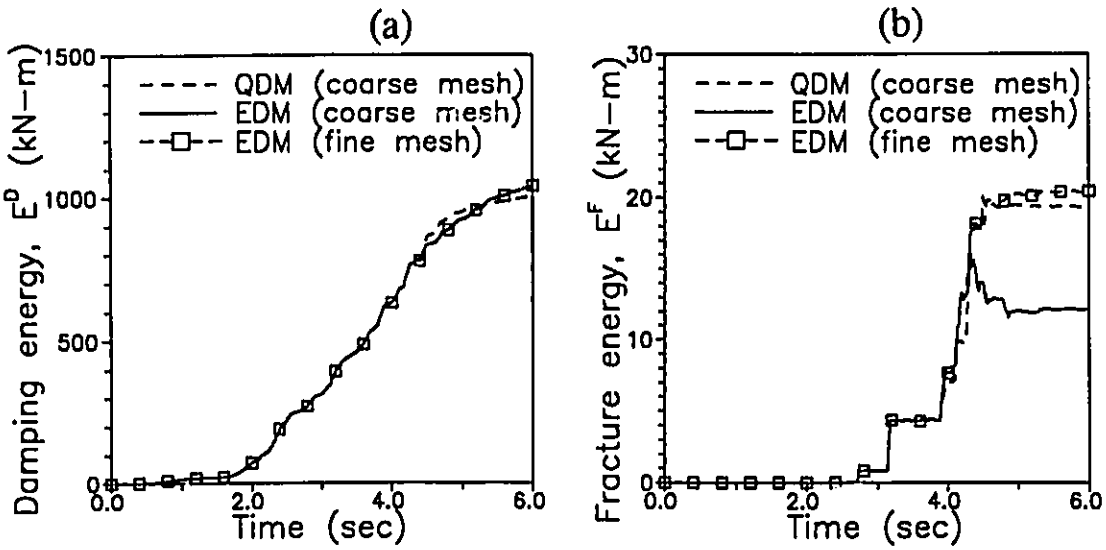

Figure 7.11 Influences of the damping model and the mesh refinement on energy dissipations due to (a) viscous damping and (b) tensile fracture (Eqn. 4.31).

dissipation has not been significantly influenced by either the damping model or the refinement of finite element mesh. The difference in fracture energy dissipation, as observed in the presentation, is difficult to qualify since the crack bands have been significantly diffused during severe deformations of the cracked elements.

The early localization as well as the propagation of cracks, observed in EDM analyses, is also dependent on the constitutive parameters assumed in a seismic fracture analysis. Figure 7.12 demonstrates the crack propagation sequence, predicted by a QDM analysis, when the fracture parameters have been reduced by a factor of 1.5 (σ_i=1.0 MPa, G_f=100 N/m) uniformly over the entire structure. The sequence of cracking in this particular QDM analysis is similar to that of EDM analyses (Figs. 7.9 and 7.10). Comparison with the previous QDM results (Fig. 7.3) reveals that the relatively milder degradation of element stiffness and damping terms during the softening phase has caused a higher diffusion of micro-cracking on both faces of the dam in the present analysis. However, the final crack trajectory is localized, and extends from one face to

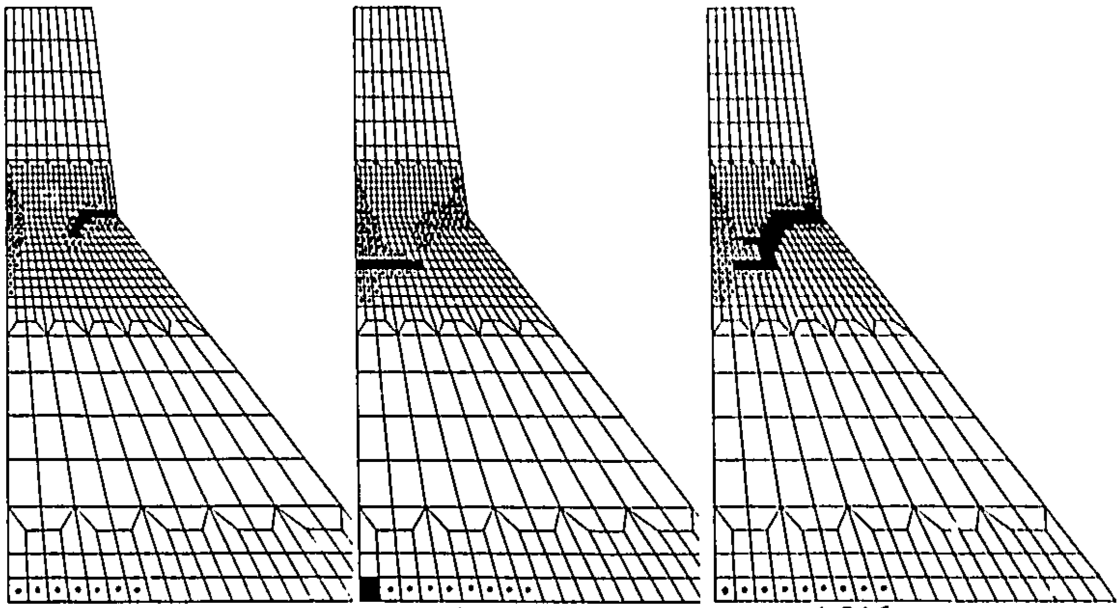

Figure 7.12 Influences of the reduced material resistance (σ_t=1.0 MPa, G_f=100 N/m) on the fracture response predicted using the quasi-linear damping model.

the other. A subsequent QDM analysis with an increased pre-softening resistance (σ_i=2 MPa, G_f=200 N/m) (not presented here) has shown a cracking response similar to that in Fig. 7.3, but with a reduced diffusion of micro-cracking in the vertical direction. The exact instance of a crack localization on the upstream face is, thus, influenced by the damping model as well as by the fracture parameters used in an analysis. Nevertheless, the final crack trajectory in Koyna Dam is not strongly dependent on either the viscous damping model or the fracture parameters when varied within a reasonable range.

7.6 INFLUENCES OF THE WESTERGAARD RESERVOIR INTERACTION MODEL ON THE FRACTURE RESPONSE

This particular seismic fracture analysis of the finite element model in Fig. 7.2(a) has been performed using the QDM, to investigate the influences of the reservoir interaction effects, that are represented by the Westergaard [159] added mass technique. The analysis has been performed with no reduction of the fracture parameters assumed in section 7.2. Cracks in zones A and B have localized exactly at the same elevations predicted from the analysis without reservoir added mass (shown in Fig. 7.3). The evolution of crack profiles and the CMOD responses obtained from this analysis are shown in Fig. 7.13. Following a significant penetration of the downstream crack (Fig.

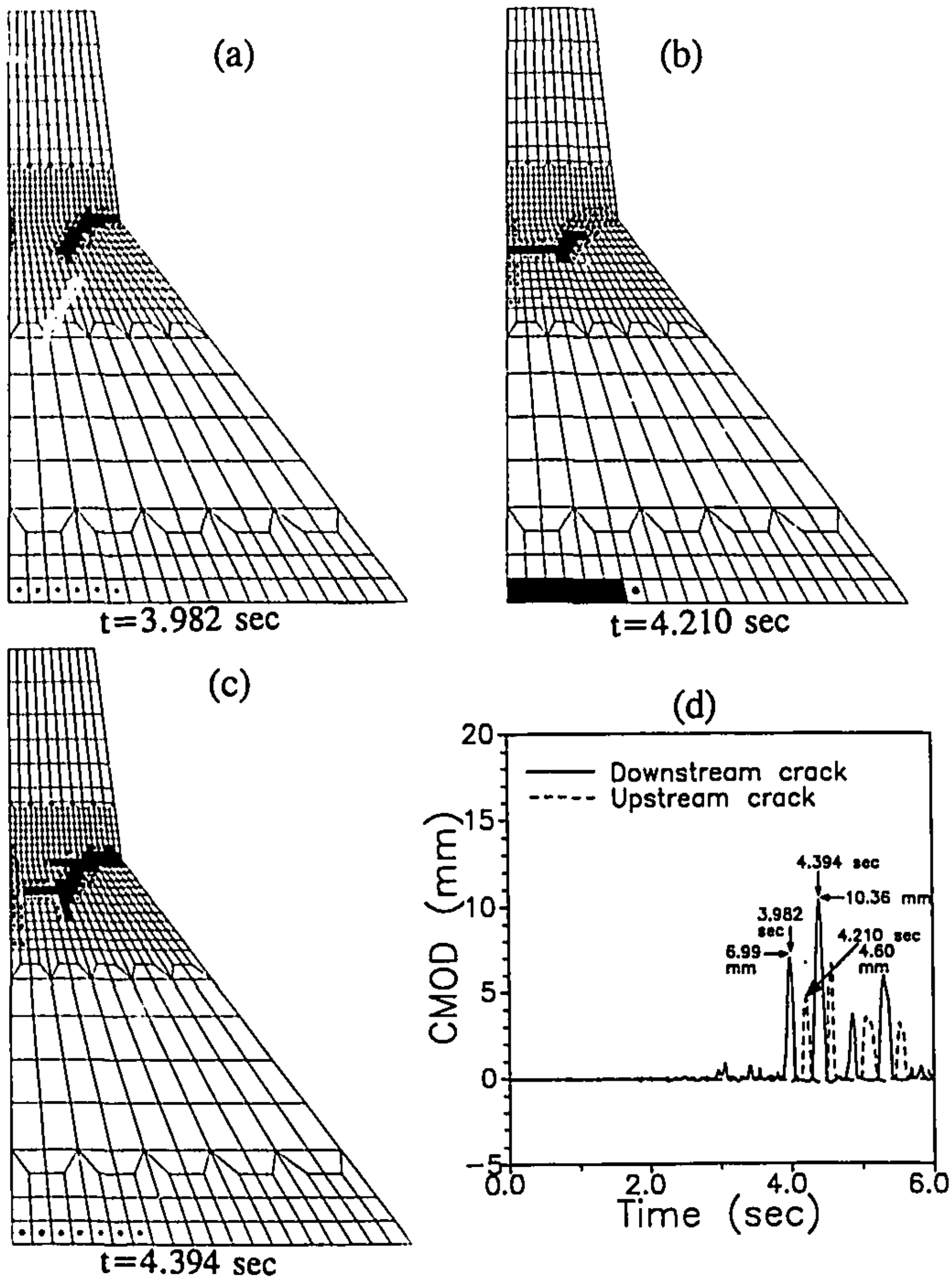

Figure 7.13 Influences of the Westergaard added mass on fracture response of the dam.

7.13(a)), the upstream crack propagates deep inside the dam, and merges with the downstream crack profile (Fig. 7.13(b)). During a subsequent reopening of the downstream crack (Fig. 7.13(c)), severe deformation demands on the structure, due to the added mass effects, cause a significant branching of the crack trajectory. Despite a relatively higher number of significant openings of the two crack mouths (Fig. 7.13(d)), the stability of the separated top profile is maintained with the added mass effects.

7.7 CONCLUSIONS

The seismic fracture response of Koyna Dam has been favourably reproduced by using the nonlinear smeared fracture model. A crack trajectory has been predicted propagating through the entire thickness at about the elevation of the downstream slope change. Nevertheless, the gravitational effect has been adequate to secure stability of the top profile of the dam. The predicted cracking response and the stability of the structure are consistent with those observed in the actual structure as well as in the subsequent model tests. The development of a significant separation at the base of the dam does not appear to decrease the seismic damage in the top part. The ultimate stability of the structure against sliding and overturning, however, should be decided from a separate analysis which is beyond the scope of continuum mechanics models.

The exact instance of a crack evolution on the upstream side may be dependent on the damping model and the material parameters applied in an analysis. The linear damping model provides artificially restraints on the evolution of cracking damage in finite elements, and therefore, this model is not recommended for seismic fracture analysis of concrete gravity dams. The final crack trajectories computed with two other damping models, QDM and EDM, are not significantly different. The refinement of finite element mesh and the variation of fracture parameters within a reasonable range have also predicted similar behaviour. The Westergaard added mass model, which is generally considered conservative, has not caused dynamic instability of the structure.

The total fracture energy dissipation is insignificant compared to the magnitude of other energy components. However, the fracture energy, G_f, is an important constitutive parameter to determine the seismic safety of concrete dams. The conservation of fracture energy and the evolution of cracking damage in finite elements are basically determined by this parameter. Nonlinear finite element analysis results should be rigorously scrutinized to make an effective prediction about the seismic safety of concrete dams. The convergence index of nonlinear solutions, for example the energy balance error, may indicate an instability in the computational model, and not necessarily failure of the actual structure. The dynamic magnification of constitutive parameters should be selected on a rational basis, since the viscous damping model significantly modifies the element behaviour. Application of a phenomenological model for the material damping effects is largely dependent on the availability of adequate experimental data, which is lacking particularly for the mass concrete.

The present study has shown that the continuum mechanics approach can effectively predict the localized cracking response of concrete gravity dams, provided the deformation demand on cracked elements is not very severe. Under high intensity deformations, a smeared crack analysis with quadrilateral elements appears to predict diffused crack patterns, causing an increased amount of fracture energy dissipation in the finite element model. Local adjustment of the softening constitutive model, even with a reduced value of the fracture energy parameter, does not appear to cause a significant reduction of the total dissipated energy. The averaging process of local response parameters should be carried over more than one element with a spatial distribution function to reduce the energy dissipation in individual elements on the crack band. Higher order finite elements may also be considered to obtain more localized deformations caused by the cracking damage. However, the material behaviour in a completely cracked condition may be better idealized with discrete mechanics models such as interface joint elements or discontinuous shape functions. The diffusion of cracked zones may still exist, as was predicted by Feltrin et al.[63] using an aggregate interlock model in the post-softening phase of the discrete crack analysis.

CHAPTER 8

SEASONAL TEMPERATURE EFFECTS ON SEISMIC FRACTURE RESPONSE OF CONCRETE GRAVITY DAMS

8.1 INTRODUCTION

The recent earthquake activities in Eastern Canada, particularly the 1988 Saguenay earthquake (M5.9), have raised considerable concerns regarding the seismic safety of existing concrete dams in that region. Moreover, the seasonal variation of ambient temperature has been observed to play a significant role in the degradation of strength and stiffness properties of the critically ageing dams (Tahmazian et al. [148], Veltrop et al.[156]). Figure 8.1 indicates the locations of main concrete dams (above 25m in height) in the province of Quebec, the yearly normal freezing index in degree days (°C), and the epicentral location of the 1988 Saguenay earthquake that contained high energy in the frequency range of concrete gravity dams.

A comprehensive seismic safety evaluation of concrete dams requires the modelling of ground motions at the site, analytical models to represent the dynamic interactions in a dam-reservoir-foundation system, and the determination of structural response under the combined action of self-weight, hydrostatic and hydrodynamic pressures, temperature changes, and seismic excitations. Long term volumetric deformations caused by alkali-aggregate reactions, shrinkage, and creep effects may also have significant effects on the initial conditions at which the earthquake strikes a dam. The progressive degradation of structural resistance over the service life of a dam requires several seismic safety evaluations, considering the initial conditions at different critical instances (NRC [114]). The definition of a proper load combination for the dam safety evaluation may make a difference between an adequate safety margin or costly repairs and structural modifications (Léger et al. [104]).

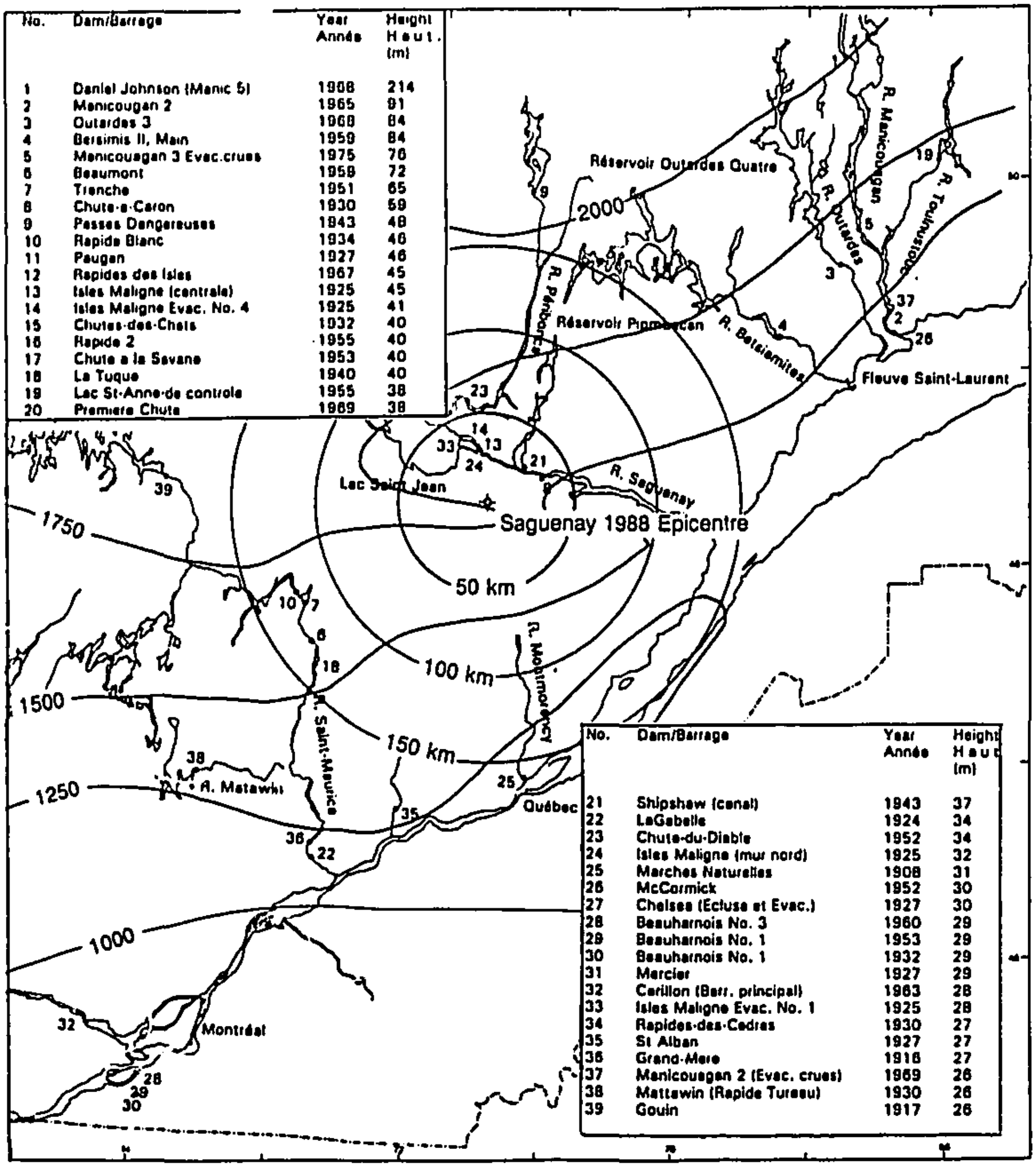

Figure 8.1 Seismic and thermal exposure of concrete dams in Quebec. (adopted from Léger et al. [102])

The main objective of this chapter is to investigate the influences of severe winter temperature conditions on the seismic fracture response of concrete gravity dams. The temperature gradient inside a relatively old concrete dam is predominantly determined by the seasonal temperature and climatic variations. A critical internal temperature distribution, obtained from rigorous heat transfer analyses (Venturelli and Léger [157]), is applied with self-weight and hydrostatic pressure loads to determine the pre-seismic stress-strain state inside a 90 m high concrete gravity dam. Seismic fracture response of the dam is investigated by considering progressive complexity in the analytical models to represent dynamic interactions in the dam-reservoir-foundation system. The 1988 Saguenay earthquake, modified to represent a possible maximum credible scenario in Eastern Canada (Léger et al. [101]), is considered in seismic fracture analyses.

8.2 SYSTEM ANALYSED

Two finite element models of a 90 m high concrete gravity dam, that approximately corresponds to the taller gravity dams in Quebec (Manic-2 91m, Outarde-3 84m) are shown in Fig. 8.2. The relatively coarser finite element mesh has been applied in heat transfer analyses to determine the critical temperature condition inside the dam. The temperature data, computed with the coarser mesh (Venturelli and Léger [157]), has been

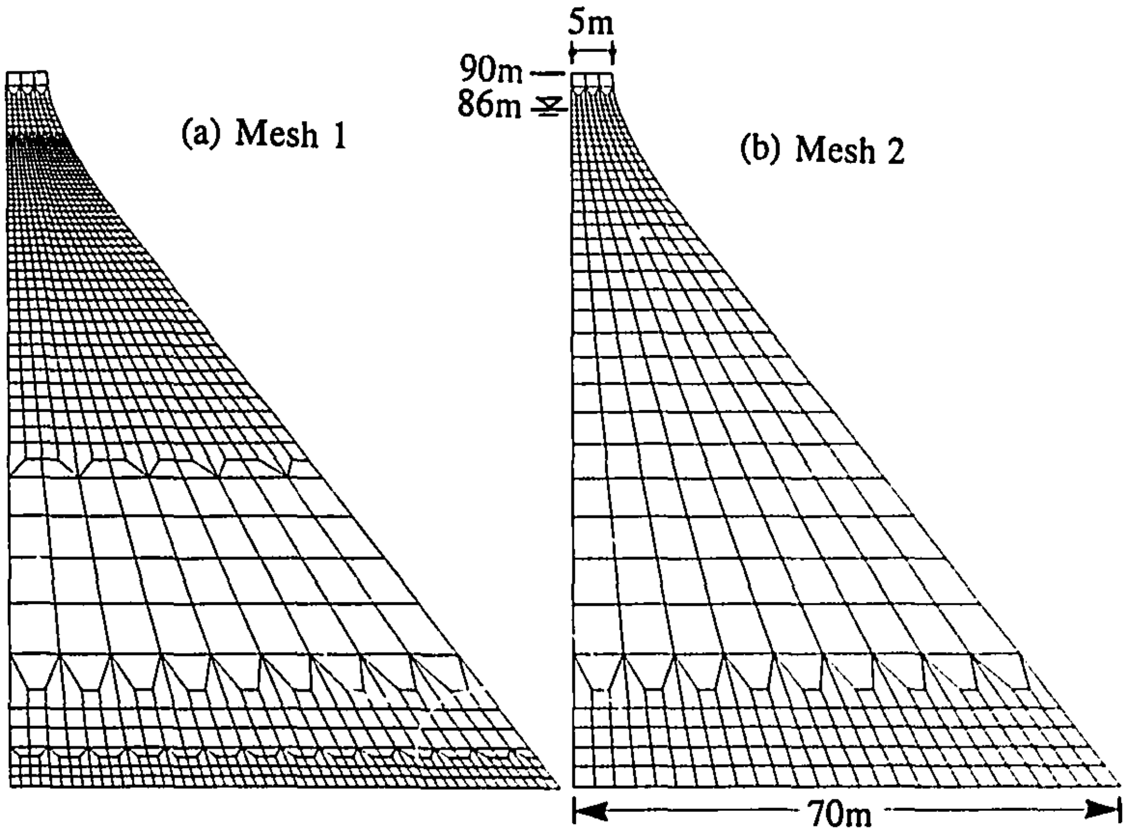

Figure 8.2 Finite element models of a tall concrete gravity dam.

interpolated to determine the temperature state in finer mesh, for application in the subsequent seismic fracture analyses.

The thermal response of individual monoliths, that are generally not keyed and lightly grouted in most cases, may be influenced by restraint effects in the longitudinal direction of a dam. However, during severe ground excitations, the monoliths are expected to vibrate independently with the pre-seismic temperature state remaining unaltered inside the structure. A two-dimensional plane-stress idealization is considered to compute the stress response of finite element models. The following material properties are assumed in smeared fracture analyses: E=27960 MPa, ν=0.2, mass density=2400 kg/m^3, σ_i=2 MPa, G_f=200 N/m, DMF_e=DMF_f=1.2, and the thermal expansion coefficient A=8.6x10^{-6} /^{0}C with a relaxation factor ψ=0.35 (Léger et al. [102]). The first five periods of vibration of the refined finite element model are computed to be T_1=0.206 sec, T_2=0.092 sec, T_3=0.075 sec, T_4=0.054 sec, and T_5=0.004 sec. The stiffness proportional damping coefficient, b, is calibrated to provide 5% critical damping in the initial fundamental mode of the dam. The dynamic equilibrium equations are integrated with a time step of 0.0025 sec, and the algorithmic damping parameter is assumed α=-0.2. Self-weight, hydrostatic pressure, and temperature (if applicable) loads are considered to determine the pre-seismic stress state inside the dam.

The temperature condition considered in seismic fracture analyses is presented in the following section. The seismic input motion, that characterizes a maximum credible scenario consistent with the tectonic characteristics of Eastern Canada, is discussed in section 8.4. Section 8.5 is devoted to investigate the influences of severe winter temperature condition on seismic fracture response of the dam, considering the Westergaard [159] reservoir interaction model. More rigorous models to represent the dynamic interactions with the reservoir and the foundation are progressively taken into consideration in section 8.6. Parametric investigations to determine the severe winter temperature effects on seismic safety of concrete gravity dams have also been presented in Bhattacharjee et al. [27] and Léger et al. [104].

8.3 SEASONAL TEMPERATURE DISTRIBUTIONS INSIDE THE DAM

The early age thermal behaviour of large concrete dams is mainly determined by internal heat of hydration and mass cooling systems. However, after many years of service, the heat of hydration is dissipated, and seasonal temperature changes dominate the dam's response. The reference temperature state, around which the seasonal variation of internal temperature oscillates, is often taken approximately equal to the long term mean air temperature at the site (Baylosis[9], Paul and Tarbox [126]). Temperature distributions inside a dam can be determined using either a simplified analysis procedure (Leliavsky[105], USBR[154]), or conducting a rigorous finite element analysis of the transient heat flow problem , or from in situ measurements. Figure 8.3 shows a finite element model and the thermal boundary conditions that can be considered in a thermal analysis.

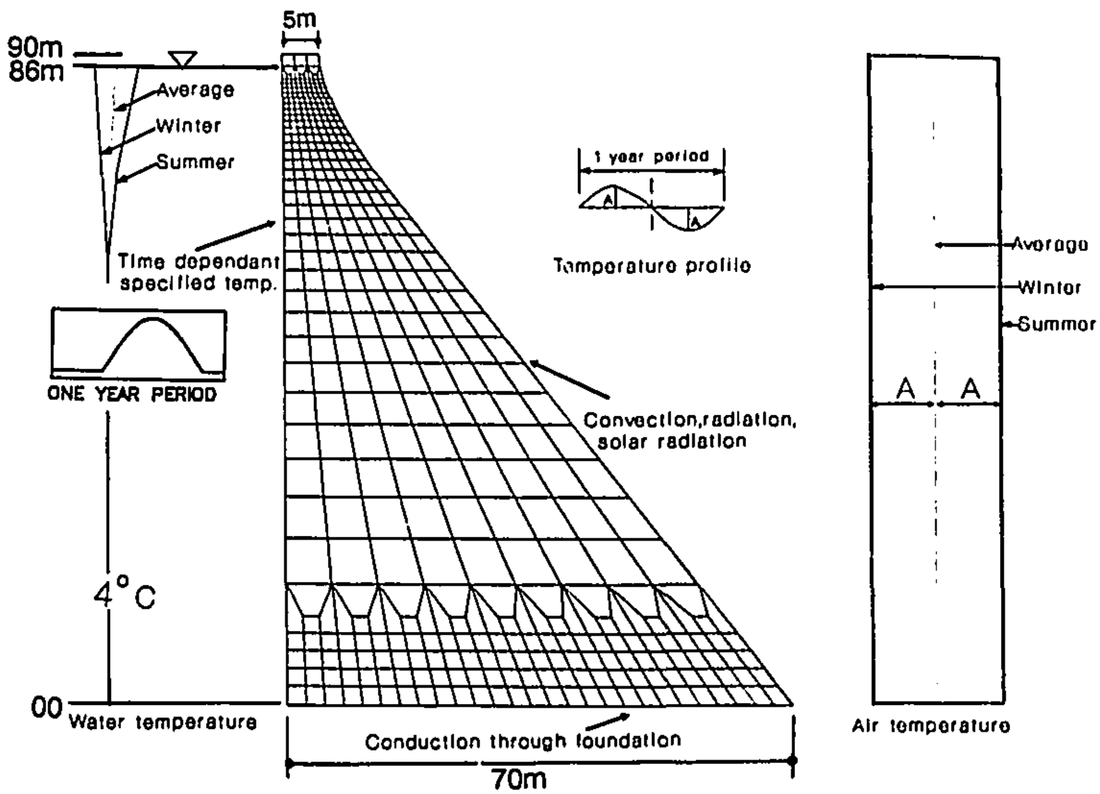

Figure 8.3 A finite element model of thermal analysis.

Venturelli and Léger [157] have performed rigorous transient heat flow analyses of the model, considering the solar radiation and the air, reservoir, and foundation temperature data that are characteristic of the lower St. Lawrence region in Quebec, Canada, where several dams are located.

Figure 8.4(a) shows the critical temperature distribution that induces a high stress gradient in the vicinity of the downstream face at the top region (Léger at al. [102]). The

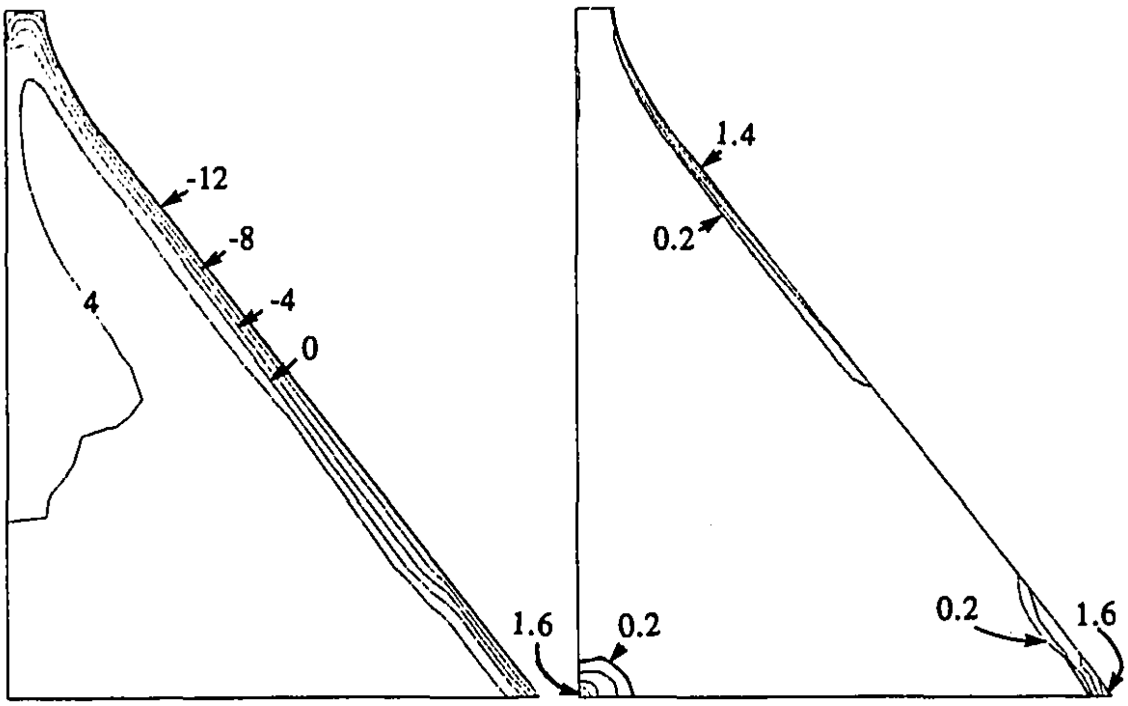

Figure 8.4 (a) Critical winter temperature distribution (°C), and (b) the corresponding principal tensile stresses including self-weight and hydrostatic pressure effects (MPa). (Temperature data adopted from Venturelli and Léger [157])

principal tensile stress contours in the dam, assuming a rigid base, and considering the critical temperature distribution as well as self-weight and hydrostatic pressure loads, are shown in Fig. 8.4(b). Significant tensile stresses occur on the downstream side near the neck region, that is vulnerable to seismic cracking. The maximum tensile stress of 1.6 MPa at the toe (Fig. 8.4(b)) mainly results from the constraint effects caused by a rigid foundation assumption. The stress response remains linear elastic in all regions of the dam under the combined actions of self-weight, hydrostatic pressure, and severe temperature condition. However, the computation of stresses directly in the downstream surface nodes may show significant tensile stresses (Léger et al. [102]), that are capable of inducing surface cracking in the top region.

8.4 INPUT GROUND MOTION

The expected seismic excitation at a site is generally defined in terms of a smooth design spectra. Ideally, a series of actual earthquake records, scaled to cover the range of important structural periods, should be used in seismic safety evaluation of critical facilities such as dams. However, the worldwide database is deficient in large magnitude near source records with tectonic environments consistent with the Eastern Canadian condition, which is very rich in high frequency motion. Strong motion accelerograms, corresponding to a maximum credible scenario likely to occur in Eastern Canada, have been developed by Léger et al. [101] using the Atkinson and Boore [4] attenuation functions to obtain a peak ground acceleration (PGA) value of 0.49g. The smooth design spectrum has been defined for an event of moment magnitude M7, with an epicentral distance of 20 km and a focal depth of 15 km. Spectrum-compatible accelerograms have been generated by modifying the 1988 Saguenay earthquake records (M5.9) that represent the best available strong motion accelerograms to characterize the Eastern Canadian seismic environment (Léger et al. [101]). The recorded acceleration time histories are converted to the frequency domain to adjust some of the Fourier amplitudes, while preserving the original phase angles. This procedure is used to correct the observed spectral deficiencies in matching the smooth spectra in the frequency range of interest. The inverse Fourier transform is then used to obtain the spectrum-compatible acceleration time histories. Figure 8.5(a) shows the smooth target spectra with 5% damping, and the elastic spectra obtained from the modified horizontal and vertical accelerograms. The time histories of horizontal and vertical components of the spectrum compatible modified Saguenay earthquake are shown in Figs. 8.5(b) and 8.5(c).

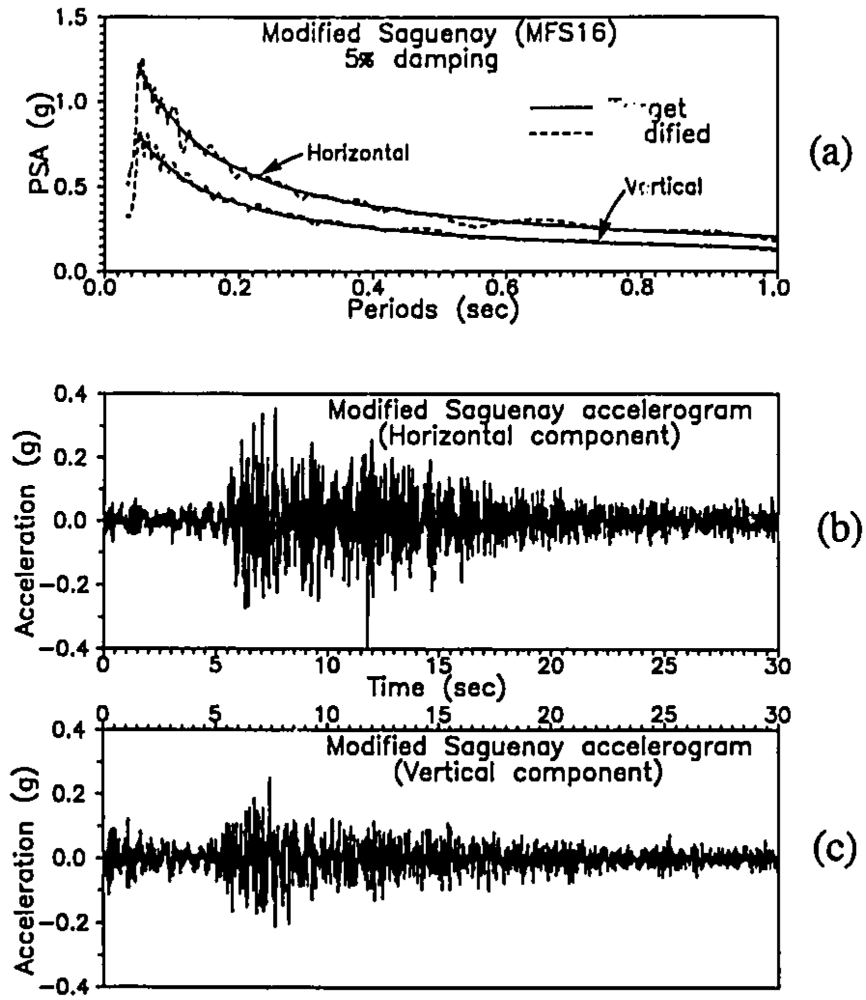

Figure 8.5 (a) Elastic response spectra of the accelerograms, and (b,c) time histories of the accelerograms (data adopted from Léger et al. [101]*).*

8.5 SEVERE WINTER TEMPERATURE EFFECTS ON SEISMIC FRACTURE RESPONSE OF THE DAM

Two analyses have been performed assuming a rigid base condition and considering the Westergaard reservoir added mass technique to take account of the reservoir interaction effects. The elasto-brittle damping model (EDM) has been applied in both analyses to determine the relative significance of considering severe winter temperature effects in seismic fracture analyses.

The first analysis has been performed without considering any temperature effects in the dam. This analysis predicts softening of few elements on the downstream side in the top region of the dam (Fig. 8.6(a)). However, no localized crack band appears in that region of the dam. Despite the occurrence of a long crack profile along the dam-foundation interface, the selected ground motion does not appear to be critical to the safety of the structure when no temperature effects are taken into consideration.

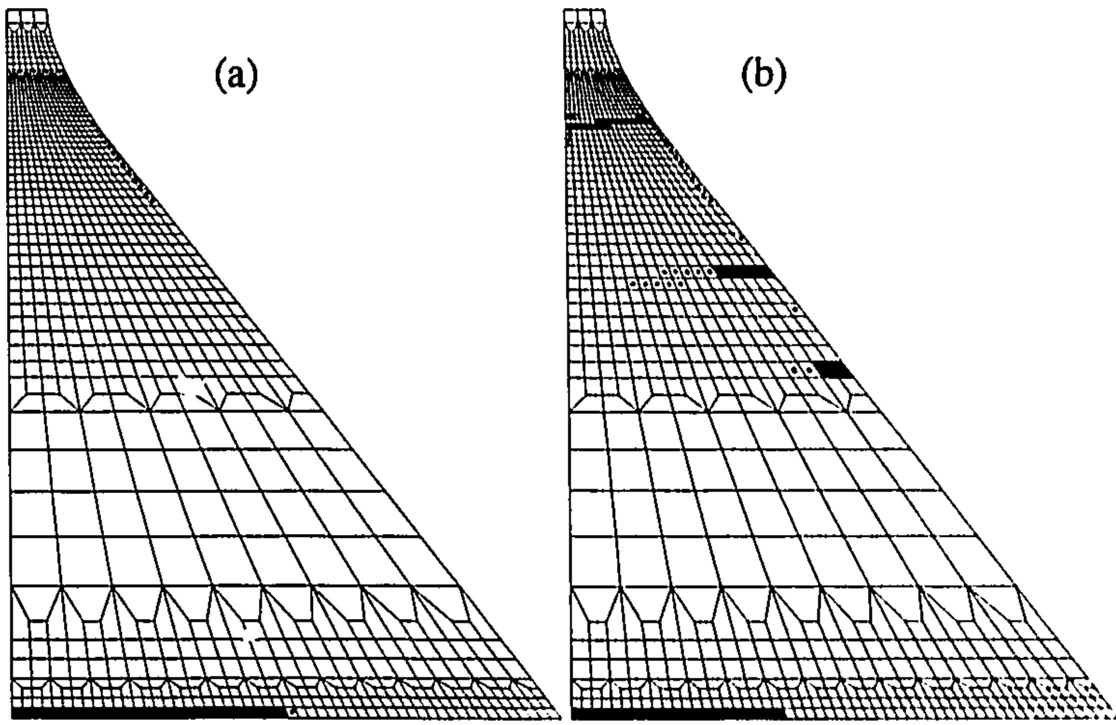

Figure 8.6 Crack profiles in the dam: (a) without temperature effects, and (b) with temperature loads (t=6.640 sec).

The second analysis, taking account of the severe winter temperature condition, has predicted severe cracking in the top part of the dam (Fig. 8.6(b)). Although three cracks have initiated on the downstream side, only the upper crack has propagated all the way up to the upstream side. It thus appears that, even if there are many damaged zones along the downstream face, a single dominant crack profile will emerge separating the top profile from the rest of the dam. The time histories of crack openings on the two faces of the dam show that the top part sustains a large number of significant crack openings after a complete separation of the top profile at 6.64 sec (Fig. 8.7). However, the self-weight appears to be adequate to maintain the stability of the upper potion that

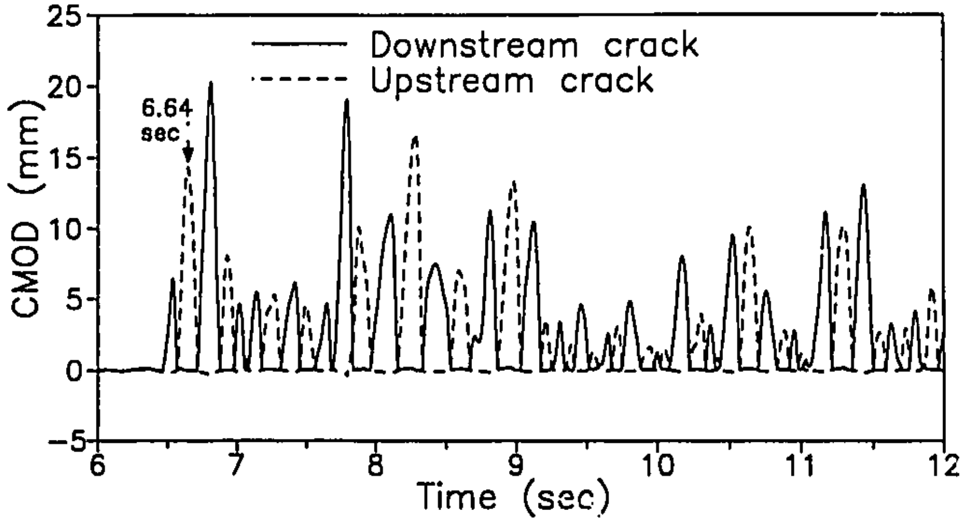

Figure 8.7 Crack openings on two faces of the dam.

responds primarily in a rocking mode. The severe winter temperature distribution appears to cause an early localization of the all through crack trajectory, and thereby subjects the dam to a long duration of strong motions at the completely fractured state. Preliminary analyses by progressively increasing the PGA value of a relatively weaker input ground motion have also indicated that the critical PGA value, required to initiate and propagate seismic cracks in the dam, is approximately 30% less when temperature stresses are included in the analysis (Bhattacharjee et al. [27]). However, with the presence of initial defects in the dam, the ground acceleration record of Fig. 8.5 induces an all through crack profile irrespective of the temperature state considered in seismic fracture analyses (Léger et al. [104]). Application of the quasi-linear damping model (QDM) does not prevent the occurrence of an all through cracking under that condition.

Limitations of the reservoir and the foundation interaction models should be taken into consideration during the interpretation of above observations. More rigorous models to take account of the dynamic interaction effects are considered in the following section.

8.6 RESERVOIR AND FOUNDATION INTERACTION EFFECTS ON SEISMIC FRACTURE RESPONSE OF THE DAM

Dynamic interaction effects of the reservoir and the foundation have been rigorously considered in the past, using frequency-domain analysis procedures (Chopra[41]) or using the boundary element method to model the reservoir and the foundation (Feltrin et al.[62], Humar and Chandrashaker[86], Medina et al.[111]). Rigorous finite element modelling of the reservoir interaction effects (El-Aidi and Hall[57], Fenves and Vargas-Loli[66]) is generally expensive to apply in a nonlinear time-domain seismic analysis. Reduced frequency-independent models to consider energy dissipations in the reservoir and the foundation have been presented in Léger and Bhattacharjee[103]. A time domain model of energy dissipation in the reservoir has been developed by providing boundary dampers on the upstream face of the dam, along with the added mass and/ or stiffness matrices. The foundation interaction effects have been modelled by added stiffness and damping coefficients. A general procedure to develop time-domain models, that are consistent with the frequency-domain models, is outlined in Fig. 8.8. The added property matrices in time-domain models are iteratively calibrated so that the low level elastic response, predicted from the time-domain solution, is similar to that obtained by using the frequency-dependent system properties.

The frequency dependence of foundation spring and dashpot coefficients is generally weak enough to assume constant values for these parameters (El-Aidi[56]). The principal energy dissipation mechanism in a reservoir involves the absorption of hydrodynamic pressure waves by the reservoir bottom sediments. This absorption effect has been considered using a wave reflection coefficient, α_r ($0 \leq \alpha_r \leq 1$), in the past frequency domain analysis models (Fenves and Chopra[65]). Preliminary frequency domain analyses using the computer program EAGD-84 (Fenves and Chopra[64]) have shown a minor variation of tensile stresses inside the dam-foundation system, when the reservoir bottom wave reflection coefficient, α_r, is varied between 0.5 and 1.0. A short duration of ground acceleration records, containing significant energy in the typical frequency range

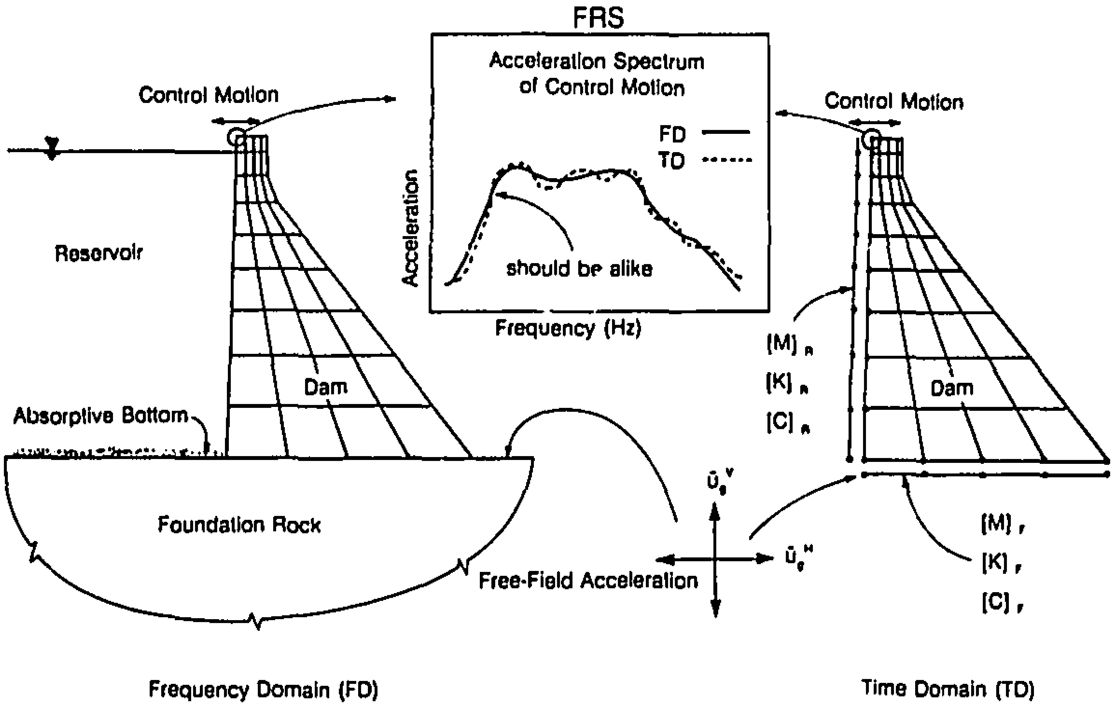

Figure 8.8 Consistent frequency-domain and time-domain models. (Léger and Bhattacharjee [103])

of interest for seismic analysis of dams, can be considered to calibrate the time-domain properties, representing an average behaviour over the frequency range of interest. An elaborate description of the calibration methodology, and extensive comparisons between frequency-domain and time-domain results have been presented in Léger and Bhattacharjee [103]. In the present investigation, the added system properties have been calibrated using the modified Saguenay accelerograms (Figs. 8.5(b) and (c)), that are also applied in the following nonlinear time-domain seismic analyses. The reservoir added damping terms (Fig. 4.8(a)) have been calibrated to approximately represent the energy dissipation corresponding to a reservoir bottom wave reflection coefficient $\alpha_r \approx 0.7$. The foundation added stiffness terms (Wolf[161]) have been calibrated, assuming the elastic modulus of foundation material to be same as that of dam concrete. The stiffness proportional foundation added damping terms have been determined using the proportionality factor, b, that has been defined to provide 5% damping in the fundamental mode of the dam alone.

The dynamic interaction effects are progressively taken into consideration in seismic fracture investigations of the dam shown in Fig. 8.2(a), using the input accelerograms discussed in section 8.4. The first analysis is performed considering the reservoir added damping and the Westergaard[59] added mass effects, but assuming a rigid foundation condition. The time-domain seismic analysis is preceded by a static analysis considering self-weight, hydrostatic pressure, and severe winter temperature loads. The seismic fracture analysis has predicted an all through crack profile in the top region of the dam (Fig. 8.9(a)). However, the severity of crack opening is significantly less than that

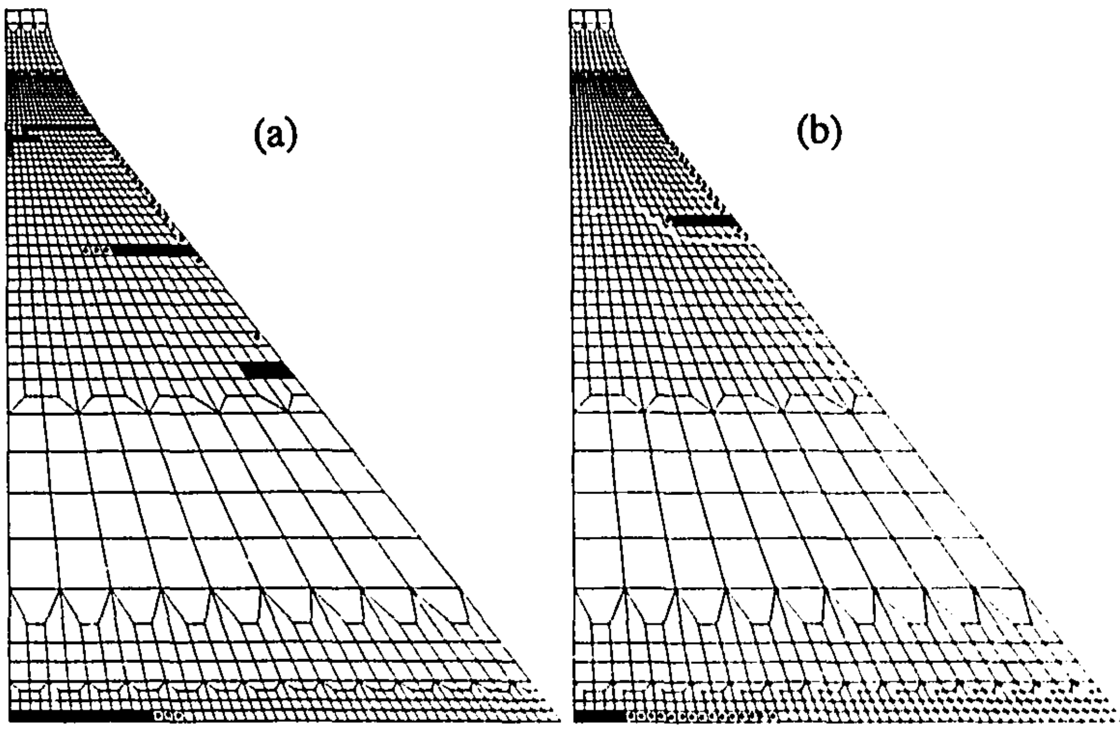

Figure 8.9 Fracture response of the dam considering (a) reservoir interaction effects only, and (b) both reservoir and foundation interaction effects.

observed in the previous analysis, where only reservoir added mass, with no added damping terms, has been considered (Fig. 8.7). Incorporation of the foundation added flexibility and damping in the second analysis has predicted significantly less severe crack profiles (Fig. 8.9(b)). The foundation flexibility and added damping appear to relieve the upstream face of high tensile stresses that can initiate cracking in top part of the dam.

8.7 CONCLUSIONS

When only the reservoir added mass is taken into consideration in seismic fracture analyses, and not the added damping and foundation flexibility effects, the seismic induced damage is increased significantly due to the severe winter temperature effects. Although many cracks can be initiated on the downstream side, a single crack in the upper part will emerge as the dominant failure mechanism. For the selected maximum credible earthquake (MCE), the severe winter temperature has resulted in early evolution of the all through crack profile, and thereby subjected the fractured dam to strong ground shaking for a considerable period of time. The simultaneous occurrence of MCE and winter temperature loading is the most severe loading combination applied to the dam. In a more rigorous safety evaluation procedure, several analyses should be performed considering the MCE to occur at different instances of a year.

The cracking hazard predicted with the most severe load combination is significantly reduced when dynamic interaction effects of the reservoir and the foundation are rigorously taken into consideration. However, extensive parametric investigations with different dam heights should be performed to conclusively decide on the seismic safety of concrete gravity dams built in Eastern Canada. Smaller dams possessing relatively heavier crest mass, and possibly with sharper changes in the downstream slope, may be prone to severe cracking under the circumstances considered in the present investigation. Pre-existing damage zones, caused by seasonal temperature changes and other environmental factors, may expedite significant cracking of concrete dams during seismic excitations.

CHAPTER 9

CONCLUSIONS

9.1 SUMMARY OF THE THESIS

Constitutive models:

Constitutive model of concrete cracking is the key issue in a numerical simulation of the nonlinear behaviour of mass concrete structures. Concrete fracture theories and the relevant computational models have been primarily developed in the literature to predict the fracture response of elementary structural components subjected to monotonic static loads. The behaviour of dam concrete is considerably different from structural concrete behaviour. Fracture analysis models developed on the basis of structural concrete behaviour require adequate validation prior to the application in full scale dam fracture analyses. The standard LEFM fracture analysis, that results in a pair of traction free surfaces instantly upon fulfilling the propagation criterion, appears to have limited resemblance with the fracture process behaviour of concrete. The considerably large material characteristic length of dam concrete may not be negligible in comparison to the dimension of concrete gravity dams, especially around the neck region which is the most vulnerable location for seismic cracking. Moreover, in the range from short term static loading to seismic induced strain rates, nonlinear fracture mechanics models, considering the strain softening of concrete in the fracture process zone (FPZ), appear to be more appropriate.

The discrete crack propagation model is expensive to apply in seismic analyses of mass concrete dams. Smeared crack models are very efficient to represent the tensile crack propagation in complex structural analyses, when crack profiles are not known *a priori*. Fixed smeared crack models generally cause a significant stress locking due to the zigzag propagation of crack bands in a finite element model. Shear softening formulations can be applied to reduce the stress locking in smeared crack analyses.

Concrete gravity dam monoliths, that are generally not keyed and often lightly grouted, are expected to vibrate independently during strong ground excitations. A similar behaviour was observed during the incidence at Koyna Dam. Numerical simulations of the seismic fracture behaviour of concrete gravity dams can be performed with plane stress finite element models. Review of the past investigations revealed that, during severe ground excitations, tall gravity dam monoliths would experience cracking in the heel, and in the top region at about the elevation of change in the downstream slope. However, considerable doubts exist about the reliability of computational models applied in previous investigations, due to the absence of an adequate validation scheme presented in the literature.

A general constitutive model, applicable to both static and seismic fracture analyses of plain concrete structures, has been developed. An energy based softening initiation criterion, the fracture energy conservation during the strain softening response of concrete, the dynamic magnification of concrete fracture parameters, the closing and reopening of cracks during seismic excitations, shear deformations in the FPZ and the subsequent rotation of crack planes, and the pre-seismic gravity and temperature load effects have been considered in the development of constitutive models. Local strain responses at Gauss integration points have been averaged over each element to determine the state of strain softening, and establish the average stress resistance in a finite element. Smearing of the cracking damage and the consequent energy dissipation over the entire element area, and the determination of constitutive parameters based on the average element response ensure the correct energy dissipation and an improved element behaviour during the curvilinear crack propagation in finite element models.

The strain softening of concrete has been simulated using two numerical techniques: (i) the secant stiffness model based on a total stress-strain relationship (SMS model), and (ii) the tangent softening model using an incremental stress-strain relationship (TMS model). Two options have been considered with respect to the orientation of crack bands in the strain softening elements: (i) the coaxial rotating crack model (CRCM) that uses an implicit definition of the shear resistance for fractured elements, and (ii) the fixed crack model with a variable shear resistance factor (FCM-VSRF). A novel criterion has been considered to determine the closing and reopening of cracks in seismic fracture analyses. The proposed one-parameter criterion is consistent with the continuum mechanics implementation of constitutive models, and is very efficient in two-dimensional seismic fracture analyses of concrete dams.

The proposed constitutive models have been implemented in a new computer program to predict the FRACture and DAMage (FRAC_DAM) response of plain concrete structures subjected to static and seismic loads. An indirect displacement control analysis procedure has been developed to predict the post-failure behaviour of concrete structures subjected to general static loads. Three viscous damping models have been considered to investigate their influences on seismic fracture response of concrete gravity dams. The dynamic interactions in a dam-reservoir-foundation system are considered by adding stiffness, mass, and damping terms to the system property matrices. A numerical dissipation parameter, α, has been introduced in the dynamic equilibrium equations to suppress localized spurious deformation modes, that may arise in a smeared fracture analysis of concrete dams. A seismic energy balance computation, and an eigenvalue analysis to determine the fundamental period of the structure, are performed at each time step to monitor the numerical stability of nonlinear finite element analyses, and assess the relative significance of seismic input, kinetic, damping, fracture, and elastic energy components in the system. An approximate finite element analysis procedure has been developed to take account of the long term relaxation of temperature induced stresses in the energy based constitutive modelling procedure.

Investigations of structural behaviour:

A wide variety of structures, experimentally or numerically investigated in the past, has been considered for validation of the computational models as well as for the behavioural investigation of plain concrete structures. Numerical models have been subjected to progressively complex applied loads and structural systems during the course of analyses. A simple tension specimen and a notched beam under three-point loading have been analysed using the displacement control analysis technique. Relative advantages and inconveniences of using the SMS and the TMS models, to simulate the strain softening behaviour of finite elements, have been investigated. Energy response and damage in the structure have also been studied.

The indirect displacement control analysis technique has been applied next to predict the failure behaviour of concrete structures subjected to relatively complex loading configurations. The snap-back response of a notched shear beam, that was investigated extensively in the literature, has been studied to validate the analysis procedure. The method has been subsequently applied to predict the fracture behaviour of a model concrete dam and a full scale gravity dam. The standard incremental load control analysis of the full scale dam has also been performed to determine the ultimate structural resistance. A comparative evaluation of the CRCM and the FCM-VSRF has been presented. Results obtained from smeared crack analyses have been compared with those reported in the literature from experimental and numerical investigations.

The seismic fracture response of Koyna Dam, a 'classic' example of earthquake induced damage in concrete dams, has been investigated to validate the nonlinear dynamic analysis models. Parametric analyses have been conducted to determine the sensitivity of numerically predicted responses to different analysis parameters and assumptions. Particularly, the interaction between viscous damping models and smeared crack analysis parameters has been examined. Seismic energy response of the dam has also been studied. Final analyses have been performed to investigate the severe winter temperature effects on seismic fracture response of a typical concrete gravity dam in Eastern Canada. The reservoir and foundation interaction effects on seismic fracture response of the dam have also been investigated using the frequency-independent dynamic interaction models.

9.2 CONCLUSIONS

The following conclusions can be made based on the numerical analyses and the observed structural behaviour presented in previous chapters:

- The degraded secant modulus approach to simulate the strain softening behaviour of concrete provides stable response predictions even with relatively coarse finite element meshes. The computational expense of this approach may not be significantly different from that of the tangent modulus approach, when applied in practical structural analyses with a shear softening constitutive formulation.

- The degradation of shear resistance with an increasing cracking damage in finite elements significantly reduces the stress locking of smeared crack analysis models. The fracture response of elementary structural members is sensitive to the constitutive formulations. Application of the smeared crack models has not produced perfect crack profiles in the shear beam problem. Horizontal mesh lines in the model dam apparently influence the crack trajectory predicted by the CRCM. The fixed crack model, applied with a degrading shear resistance formulation, predicts a crack profile that is in excellent agreement with the experimentally observed response of the model dam. However, the fixed crack model is less reliable to predict the post-failure structural resistance. The discrete crack analysis of model dam, as reported in the literature, does not appear to perform significantly better than the smeared crack models.

- The spurious influence of finite element meshes on the behaviour of CRCM is insignificant in the analysis of a full scale dam subjected to reservoir overflow. The material resistance to fracture propagation does not appear to strongly influence the ultimate structural resistance. The considerable redistribution of internal resistances causes a stable crack growth, and a generally increasing structural resistance against the reservoir overflow. The ultimate failure of the structure may be of global nature, caused by a sliding or overturning instability of the top part. The application of standard load control analysis may be more efficient to predict the failure behaviour of full scale dams. However, more rigorous analyses should be performed considering water penetration and uplift pressure inside cracks. Structural behaviour should also be investigated with multiple cracks competing to propagate simultaneously.

- The seismic fracture response of Koyna Dam has been favourably reproduced using the CRCM. A crack propagates through the entire thickness of the dam at the elevation of change in the downstream slope. The severity of cracking in the dam has been similar in two analyses, using the quasi-linear damping model (QDM) and the elasto-brittle damping model (EDM). The complete elimination of viscous damping in the strain softening elements causes a relatively faster crack propagation velocity in an EDM analysis. However, the response is also dependent on the rate of degradation of the secant modulus during the softening phase. The linear damping model (LDM) appears to impose artificial restraints on the evolution of cracks in finite elements, and therefore, not recommended for application in the seismic fracture analysis of concrete gravity dams.

- The severe winter temperature condition apparently reduces the seismic safety margin of a homogeneous dam with no pre-existing defects. However, physical factors such as a sharp change in the slope of downstream face or a pre-existing defective zone in the structure, principally determine the fracture response of concrete dams. Energy dissipations caused by dynamic interactions with the reservoir and the foundation appear to reduce the severity of cracking in the dam.

- In the presence of several cracks competing to propagate from the downstream face, only one of them propagates through the entire thickness, and separates the top profile that responds mainly in a rocking mode during subsequent ground shocks.

- The total fracture energy dissipation during seismic responses of concrete gravity dams is insignificant compared to the magnitudes of other energy components, and particularly in comparison to the viscous damping energy. The seismic fracture response of concrete gravity dams appears to be of brittle type. After the localization, cracks propagate with velocities typical of that observed during experimental investigations of the dynamic fracture behaviour of concrete. The self-weight of concrete gravity dams appears to be the only mechanism maintaining the stability during the rocking response of separated top profiles.

9.3 RECOMMENDATIONS FOR THE INDUSTRIAL APPLICATION OF NUMERICAL MODELS

Utility companies responsible for the operation and maintenance of existing concrete dams are actively seeking adequately validated computational models to apply in the periodic safety assessment of the installations. The following recommendations are presented for industrial application of the analysis procedures developed in this thesis:

- The elastic modulus and the tensile strength of concrete should be determined from experimental investigations with recovered dam concrete specimens. Any arbitrary dynamic magnification of the Young's modulus is unwarranted in a rigorous finite element analysis, with explicit considerations for the inertia and the viscous resistance of the material. The apparent tensile strength may be assumed 20-30% higher than the true static strength. A maximum 20% dynamic magnification of the apparent static strength is recommended for seismic analyses of concrete dams. The fracture energy value of concrete can be determined by experimentally measuring the ultimate resistance of notched concrete beams subjected to three-point loading. Parametric analyses, similar to those discussed in Chapter 5, can be performed to calibrate the fracture energy value that closely reproduces the experimentally determined ultimate load resistance of the specimens. The dynamic magnification of fracture energy value can be generally assumed equal to that of the tensile strength.

- Damping values estimated from the forced vibration test of existing concrete dams generally include energy dissipations through the reservoir and the foundation. Field tests with different reservoir levels in different seasons may be conducted for qualitative determination of the reservoir interaction effects. The interference of several mode shapes during the forced vibration tests may also lead to a high damping value. The conservative assumption of elasto-brittle damping model (EDM) should be applied in the absence of a reasonable material damping value.

- Finite element mesh in a zone of homogeneous material should be made uniform to the maximum possible extent. In the absence of a fairly uniform finite element discretization, the material parameters must be adjusted to approximately represent the uniform material softening behaviour over a homogeneous zone. In seismic fracture analyses of dams, the SMS constitutive model with a linear strain softening assumption may not be used with an extremely fine mesh, such as element sizes less than three or four times the maximum aggregate dimension.

- Physical defects in a structure, such as a sharp change in the downstream slope and weak joints or isolated material zones damaged by severe environmental distress, predominate the seismic fracture behaviour of concrete dams. Such factors must be explicitly considered in a seismic safety analysis. Severe winter temperature effects may also expedite cracking in a dam during strong ground motions.

- The Westergaard added mass technique, which is generally considered conservative, can be considered first to investigate the seismic fracture response of concrete gravity dams. Rigorous models to represent energy dissipations in the reservoir and the foundation can be considered only if the dam experiences severe cracking in the first analysis.

- Nonlinear finite element analysis results should be rigorously scrutinized to make effective predictions about the seismic safety of concrete dams. The convergence index of nonlinear solutions, for example the energy balance error, may indicate instability in the computation, and not necessarily failure of the actual structure.

- The coaxial rotating crack model, that predicted realistic crack profiles of full scale concrete dams, is recommended for general applications. A fixed crack analysis may be performed as a subsequent verification of the predicted response. Application of numerical dissipations through a non-zero α value is recommended to suppress localized spurious deformation modes that may arise in seismic fracture analyses of concrete dams.

Finally, the material fracture resistance does not appear to strongly dominate the ultimate resistance of concrete gravity dams subjected to reservoir overflow or seismic excitations. The structural safety of dams may not be ensured by concrete tensile strength alone. Possibly, the structural safety of critical dams will be better protected by structural modifications such as application of prestressing tendons, reduction of the crest mass, gradual curvature in the slope of downstream face etc. A pre-assigned weak point near the top region of a dam may relieve the rest of the dam of experiencing severe cracking. The suitable positioning of weak points may reduce the risk of a catastrophic reservoir release in the case of an overturning instability of the separated top profile.

9.4 FUTURE RESEARCH AND DEVELOPMENTS

The following features can be considered in the future research and development of computational models to predict the fracture behaviour of mass concrete structures:

- Horizontal construction joints, that are generally weaker than the virgin material, can be modelled explicitly in finite element analyses.

- Phenomenological modelling of the strain rate effects on concrete behaviour can be considered in the seismic fracture investigation of concrete dams. The present constitutive formulations may be extended to compute the stress response by solving the dynamic equilibrium equations of individual element. Quantitative information on the part of stresses sustained by viscous and inertia resistances of a finite element can be obtained using this technique. Application of an explicit numerical integration technique, instead of the implicit technique as used in this research, may be more efficient to solve the system equilibrium equations.

- Constitutive models can be implemented with higher order finite elements or with modified element formulations to reproduce the localized cracking damage. The use of quadrilateral elements in the present investigations could not contain the curvilinear crack profiles in narrow bands, particularly during the severe deformation of cracked elements. The averaging of local response quantities may be carried over more than one element to dissipate the correct amount of fracture energy in a finite element analysis. After complete cracking, finite element stiffness matrices may be determined using a discrete mechanics approach instead of maintaining the continuum mechanics formulation throughout the analysis. The use of triangular elements in the discretization of gravity dams may be considered to obtain a uniform element size over a particular homogeneous material zone. The degradation of Young's modulus during the strain softening phase may be defined with more rigorous analytical expressions to take account of the Poisson's ratio effects on the damage evolution. Nonlinear softening relations may also be considered for parametric investigations. The present constitutive model can be extended to consider a second orthogonal crack in the finite elements.

- Further parametric investigations can be conducted to determine the fracture behaviour of concrete dams with different heights, geometric configurations, and inhomogeneous distribution of material properties. Dynamic interactions with the impounded reservoir and the foundation can be considered rigorously in future developments. Water penetration and uplift pressure inside cracks should also be considered in fracture analyses of concrete dams.

- Apparently, the difference between plane stress and plain strain crack propagation has not been rigorously considered in the fracture mechanics of concrete structures.

- The earthquake effects in fracture analyses of concrete dams can be represented as imposed displacements of the base, instead of the traditional equivalent inertia force representation as adopted in the present study. The stability of nonlinear dynamic analyses may be better ensured in a dynamic displacement control analysis procedure.

- Experimental investigations may be conducted to correlate the strain rate sensitivity of concrete behaviour and the modal damping response of small scale laboratory specimens. The proposed new criteria for softening initiation and crack closing/ reopening may also be validated with relevant laboratory experiments.

- Rigorous analytical models can be developed to determine the dynamic stability of concrete dams at the fractured condition.

- Different uncertainties relating to applied loading, numerical analyses, and structural and material information, may be considered in a probabilistic modelling procedure.

REFERENCES

1. Amadei, B., Illangasekare, T., Morris, D.I., and Boggs, H. "Estimation of uplift in cracks in older concrete gravity dams: analytical solution and parametric study", *Journal of Energy Engineering*, ASCE, 115(1): 19-38, **1989**.

2. American Concrete Institute. "Fracture mechanics of concrete: concepts, models and determination of material properties", *ACI 446.1R*, Reported by ACI Committee 446 on Fracture Mechanics, **1991**.

3. Arrea, M., and Ingraffea, A.R. *Mixed-Mode Crack Propagation in Mortar and Concrete*, Department of Structural Engineering Report 81-13, Cornell University, **1981**.

4. Atkinson, G.M., and Boore, D.M. "Recent trends in ground motion and spectral response relations for North America", *Earthquake Spectra*, 6(1): 15-35, **1990**.

5. Ayari, M.L. *Static and Dynamic Fracture Mechanics of Concrete Gravity Dams*, Ph.D. Thesis, Department of Civil, Environmental and Architectural Engineering, University of Colorado, Boulder, USA, **1988**.

6. Ayari, M.L., and Saouma, V.E. "A fracture mechanics based seismic analysis of concrete gravity dams using discrete cracks", *Engineering Fracture Mechanics*, 35(1/2/3): 587-598, **1990**.

7. Ayari, M.L., and Saouma, V.E. "Static and dynamic contact/impact problems using fictitious forces", *International Journal for Numerical Methods in Engineering*, 32: 623-643, **1991**.

8. Bathe, K.J., and Ramaswamy, S. "On three-dimensional nonlinear analysis of concrete structures", *Nuclear Engineering and Design*, 52: 385-409, **1979**.

9. Baylosis, R.B. *Probabilistic Structural Reliability Study of Concrete Gravity Dam*, Ph.D. dissertation, The University of Tennessee, **1988**.

10. Bažant, Z.P. "Prediction of concrete creep effects using age-adjusted effective modulus method", *Journal of the American Concrete Institute*, 69(4): 212-217, **1972**.

11. Bažant, Z.P., and Cedolin, L. "Blunt crack band propagation in finite element analysis", *Journal of the Engineering Mechanics Division*, ASCE, 105(2): 297-315, **1979**.

12. Bažant, Z.P., and Gambarova, P. "Rough cracks in reinforced concrete", *Journal of the Structural Division*, ASCE, 106(4): 819-842, **1980**.

13. Bažant, Z.P. "Comment on orthotropic models for concrete and geo-materials", *Journal of Engineering Mechanics*, ASCE, 109(3): 849-865, **1983**.

14. Bažant, Z.P., and Cedolin, L. "Finite element modelling of crack band propagation", *Journal of Structural Engineering*, ASCE, 109(1): 69-92, **1983**.

15. Bažant, Z.P., and Oh, B.H. "Crack band theory for fracture of concrete", *Materials and Structures*, 16(93): 155-177, **1983**.

16. Bažant, Z.P. "Size effect in blunt fracture: concrete, rock, metal", *Journal of Engineering Mechanics*, ASCE, 110(4): 518-535, **1984**.

17. Bažant, Z.P., and Gambarova, P.G. "Crack shear in concrete: crack band microplane model", *Journal of Structural Engineering*, ASCE, 110(9): 2015-2035, **1984**.

18. Bažant, Z.P. "Fracture in concrete and reinforced concrete", in *Mechanics of Geomaterials: Rocks, Concrete, Soils*, Edited by Z.P. Bažant, John Wiley & Sons, 259-303, **1985**.

19. Bažant, Z.P., and Chern, J.C. "Strain softening with creep and exponential algorithm", *Journal of Engineering Mechanics*, ASCE, 111(3): 391-415, **1985**.

20. Bažant, Z.P., and Pfeiffer, P.A. "Determination of fracture energy from size effect and brittleness number", *Materials Journal*, ACI, 84: 463-480, **1987**.

21. Bažant, Z.P. ed. *Mathematical Modelling of Creep and Shrinkage of Concrete*, John Wiley and Sons, **1988**.

22. Bažant, Z.P., and Lin, F.B. "Nonlocal smeared cracking model for concrete fracture", *Journal of Structural Engineering*, ASCE, 114(11): 2493-2510, **1988**.

23. Bažant, Z.P., and Prat, P.C. "Effect of temperature and humidity on fracture energy of concrete", *Materials Journal*, ACI, 85: 262-271, **1988**.

24. Bažant, Z.P. "A critical appraisal of 'no-tension' dam design: a fracture mechanics viewpoint", *Dam Engineering*, 1(4): 237-247, **1990**.

25. Bažant, Z.P., He, S., Plesha, M.E., Gettu, R., and Rowlands, R.E. "Rate and size effects in concrete fracture: implications for dams", *Dam Fracture*, Proceedings from the International Conference, Boulder, Colorado, 413-425, **1991**.

26. Bhattacharjee, S.S. and Léger, P. "Concrete constitutive models for nonlinear seismic analysis of gravity dams - state-of-the-art", *Canadian Journal of Civil Engineering*, 19: 492-509, **1992**.

27. Bhattacharjee, S.S., Léger, P., and Venturelli, J. "Thermo-seismic analysis of concrete gravity dams", in *Fracture Mechanics of Concrete Structures*, Edited by Z.P. Bažant, Elsevier Applied Science, Proceedings of the First International Conference on Fracture Mechanics of Concrete Structures, Breckenridge, Colorado, 361-366, **1992**.

28. Bićanić, N., and Zienkiewicz, O.C. "Constitutive model for concrete under dynamic loading", *Earthquake Engineering & Structural Dynamics*, 11: 689-710, **1983**.

29. Bittencourt, T.N., Ingraffea, A.R., and Llorca, J. "Simulation of arbitrary, cohesive crack propagation", in *Fracture Mechanics of Concrete Structures*, edited by Z.P. Bažant, Elsevier Applied Science, Proceedings of the First International Conference on Fracture Mechanics of Concrete Structures, Breckenridge, Colorado, 339-350, **1992**.

30. Brooks, J.J. and Samaraie, N.H. "Influence of rate of stressing on tensile stress-strain behaviour of concrete", *Fracture of Concrete and Rock: Recent Developments*, Edited by S.P. Shah, S.E. Swartz, and B. Barr, Elsevier Applied Science, 397-408, **1989**.

31. Brühwiler, E. "Fracture of mass concrete under simulated seismic action", *Dam Engineering*, 1(3): 153-176, **1990**.

32. Brühwiler, E., and Wittmann, F.H. "Failure of concrete subjected to seismic loading conditions", *Engineering Fracture Mechanics*, 35(1/2/3): 565-571, **1990**.

33. Brühwiler, E., and Saouma, V.E. "Water fracture interaction in cracked concrete dams", *Dam Fracture*, Proceedings from the International Conference, Boulder, Colorado, 551-568, **1991**.

34. Canadian Electrical Association (CEA), Research & Development. *Safety Assessment of Existing Dams for Earthquake Conditions*, Background Volume C-4, Seismic Analysis of Concrete Dams, CEA No. 420 G 547, Montreal, **1990**.

35. Carpinteri, A., Valente, S.V., Ferrara, G., and Imperato, L. "Experimental and numerical fracture modelling of a gravity dam", in *Fracture Mechanics of Concrete Structures*, Edited by Z.P. Bažant, Elsevier Applied Science, Proceedings of the First International Conference on Fracture Mechanics of Concrete Structures, Breckenridge, Colorado, 351-360, **1992**.

36. Cervera, M., Oliver, J., Herrero, E., and Oñate, E. "A computational model for progressive cracking in large dams due to the swelling of concrete", *Engineering Fracture Mechanics*, 35(1/2/3): 572-585, **1990**.

37. Cervera, M., Oliver, J., and Galindo, M. "Numerical analysis of dams with extensive cracking resulting from concrete hydration: simulation of a real case", *Dam Engineering*, 3(1): 1-22, **1992**.

38. Chapuis, J., Rebora, B., and Zimmermann, T. "Numerical approach of crack propagation analysis in gravity dams during earthquakes", *Commission Internationale Des Grands Barrages*, Quinzième Congrès des Grands Barrages, Lausanne, 57(26): 451-473, **1985**.

39. Chen, E., and Schnobrich, W.C. "Models for the post-cracking behaviour of plain concrete under short term monotonic loading", *Computers & Structures*, 13: 213-221, **1981**.

40. Chopra, A.K., and Chakrabarti, P. "The earthquake experience at Koyna dam and stresses in concrete gravity dams", *Earthquake Engineering & Structural Dynamics*, 1: 151-164, **1972**.

41. Chopra, A.K. "Earthquake response analysis of concrete dams", in *Advanced Dam Engineering for Design, Construction, and Rehabilitation*, Edited by R.B. Jansen, Van Nostrand Reinhold, 416-465, **1988**.

42. Cook, R.D., Malkus, D.S., and Plesha, M.E. *Concepts and Applications of Finite Element Analysis*, Third Edition, John Wiley & Sons, 491-494, **1989**.

43. Cope, R.J., Rao, P.V., Clark, L.A., and Norris, P. "Modelling of reinforced concrete behaviour for finite element analysis of bridge slabs", *Numerical Methods for Nonlinear problems*, Edited by C. Taylor, E. Hinton, and D.R.J. Owen, Pineridge Press, Swansea, 1: 457-470, **1980**.

44. Crisfield, M.A. "A fast incremental/iterative procedure that handles snap-through", *Computers & Structures*, 13: 55-62, 1981.

45. Dahlblom, O., and Ottosen, N.S. "Smeared crack analysis using generalized fictitious crack model", *Journal of Engineering Mechanics*, ASCE, 116(1): 55-76, **1990**.

46. Dasgupta, G., and Chopra, A.K. "Dynamic stiffness matrices for viscoelastic half planes", *Journal of the Engineering Mechanics Division*, ASCE, 105(5), **1979**.

47. de Borst, R., and Nauta, P. "Non-orthogonal cracks in a smeared finite element model", *Engineering Computations*, 2: 35-46, **1985**.

48. de Borst, R. "Smeared cracking, plasticity, creep, and thermal loading - a unified approach", *Computer Methods in Applied Mechanics and Engineering*, North-Holland, 62: 89-110, **1987**.

49. de Borst, R. "Computation of post-bifurcation and post-failure behaviour of strain-softening solids", Computers & Structures, 25(2): 211-224, **1987**.

50. de Borst, R., and Rots, J.G. "Occurrence of spurious mechanisms in computations of strain-softening solids", *Engineering Computations*, 6: 272-280, **1989**.

51. Donlon , W.P. *Experimental Investigation of the Nonlinear Seismic Response of Concrete Gravity Dams*, Report No. EERL 89-01, Earthquake Engineering Research Laboratory, Caltech, Pasadena, California, **1989**.

52. Donlon, W.P., and Hall, J.F. "Shaking table study of concrete gravity dam monoliths", *Earthquake Engineering & Structural Dynamics*, 20: 769-786, **1991**.

53. Droz, P. *Modèle Numérique du Comportement Non-linéaire D'ouvrages Massifs en Béton non Armé*, Thesis No. 682, Département de Génie Civil, EPFL, Switzerland, **1987**.

54. Du, J., Yon, J.H., Hawkins, N.M., Arakawa, K., and Kobayashi, A.S. "Fracture process zone for concrete for dynamic loading", *Materials Journal*, ACI, 89: 252-258, **1992**.

55. Dungar, R., Saouma, V.E., and Wittmann, F.H. "Conference report: the application of fracture mechanics in dam engineering", *Dam Engineering*, 2(1): 3-20, **1991**.

56. El-Aidi, B.M. *Nonlinear Earthquake Response of Concrete Gravity Dam Systems*, Ph.D. Thesis, Caltech, Pasadena, USA, **1988**.

57. El-Aidi, B., and Hall, J.F. "Non-linear earthquake response of concrete gravity dams, part 1: modelling", *Earthquake Engineering & Structural Dynamics*, 18: 837-851, **1989**.

58. EL-Aidi, B., and Hall, J.F. "Non-linear earthquake response of concrete gravity dams, part 2: behaviour", *Earthquake Engineering & Structural Dynamics*, 18: 853-865, **1989**.

59. Fanelli, M. "General report on theme A: concrete dams - fracture problems", *International Symposium on Analytical Evaluation of Dam Related Safety Problems*, Copenhagen, II: 19-35, **1989**.

60. Feenstra, P.H., de Borst, R., and Rots, J.G. "Numerical study on crack dilatancy. I: models and stability analysis", *Journal of Engineering Mechanics*, ASCE, 117(4): 733-753, **1991**.

61. Feenstra, P.H., de Borst, R., and Rots, J.G. "Numerical study on crack dilatancy. II: applications", *Journal of Engineering Mechanics*, ASCE, 117(4): 754-769, **1991**.

62. Feltrin, G., Wepf, D., and Bachmann, H. "Seismic cracking of concrete gravity dams", *Dam Engineering*, 1(4): 279-289, **1990**.

63. Feltrin, G., Galli, M., and Bachmann, H. "Influence of cracking on the earthquake response of concrete gravity dams with reservoir". *Proceeding of the Tenth World Conference on Earthquake Engineering*, Madrid, Spain, 8: 4627-4632, **1992**.

64. Fenves, G., and Chopra, A.K. *EAGD-84: A Computer Program for Earthquake Analysis of Concrete Gravity Dams*, Report no. UCB/EERC 84/11, University of California, Berkeley, **1984**.

65. Fenves, G., and Chopra, A.K. "Reservoir bottom absorption effects in earthquake response of concrete gravity dams", *Journal of Structural Engineering*, ASCE, 111: 545-562, **1985**.

66. Fenves, G., and Vargas-Loli, L.M. "Non-linear dynamic analysis of fluid-structure systems", *Journal of Engineering Mechanics*, ASCE, 114: 219-239, **1988**.

67. Fok, K.L., Hall, J.F. and Chopra, A.K. *EACD-3D: A Computer Program for Three-Dimensional Analysis of Concrete Dams*, Report no. UCB/EERC 86/09, University of California, Berkeley, **1986**.

68. Freund, L.B. *Dynamic Fracture Mechanics*, Cambridge University Press, **1990**.

69. Gajer, G., and Dux, P.F. "Crack band based model for FEM analysis of concrete structures", *Journal of Structural Engineering*, ASCE, 116(6): 1696-1713, **1990**.

70. Gambarova, P.G., and Valente, G. "Smeared crack analysis for fracture and aggregate interlock in concrete", *Engineering Fracture Mechanics*, 35(4/5): 651-663, **1990**.

71. Gerstle, W.H., and Xie, M. "FEM modelling of fictitious crack propagation in concrete", *Journal of Engineering Mechanics*, ASCE, 118(2): 416-434, **1992**.

72. Ghali, A., and Favre, R. *Concrete Structures: Stresses and Deformations*, Chapman and Hall, New York, **1986**.

73. Gioia, G., Bažant, Z.P., and Pohl, B.P. "Is no-tension dam design always safe? - a numerical study", *Dam Engineering*, 3(1): 23-34, **1992**.

74. Goodman, R.E., Taylor, R.L., and Brekke, T.L. "A model for the mechanics of jointed rock", *Journal of the Soil Mechanics and Foundation Division*, ASCE, 94(3): 637-659, **1968**.

75. Graves, R.H., and Derucher, K.N. "Interface smeared crack model analysis of concrete dams in earthquakes", *Journal of Engineering Mechanics*, ASCE, 113(11): 1678-1693, **1987**.

76. Gupta, A.K., and Akbar, H. "Cracking in reinforced concrete analysis", *Journal of Structural Engineering*, ASCE, 110(8): 1735-1746, **1984**.

77. Guthrie, L.G. "Earthquake analysis and design of concrete gravity dams", *Proceedings of the third U.S. National Conference on Earthquake Engineering*, Charleston, South Carolina, 717-727, **1986**.

78. Hall, J.F., and Dowling, M.J. "Response of jointed arches to earthquake excitation", *Earthquake Engineering & Structural Dynamics*, 13: 779-798, **1985**.

79. Hall, J.F. "The dynamic and earthquake behaviour of concrete dams: review of experimental behaviour and observational evidence", *Soil Dynamics and Earthquake Engineering*, 7(2): 58-121, **1988**.

80. Hall, J.F., Dowling, M.J., and El-Aidi, B. "Defensive earthquake design of concrete gravity dam", *Dam Engineering*, 3(4): 244-263, **1992**.

81. Hilber, H.M., Hughes, T.J.R., and Taylor, R.L. "Improved numerical dissipation for time integration algorithms in structural dynamics", *Earthquake Engineering & Structural Dynamics*, 5: 283-292, **1977**.

82. Hillerborg, A., Modéer, M., and Petersson, P.E. "Analysis of crack formation and crack growth in concrete by means of fracture mechanics and finite elements", *Cement and Concrete Research*, 6: 773-782, **1976**.

83. Hilsdorf, H.K., and Brameshuber, W. "Code-type formulation of fracture mechanics concepts for concrete", *International Journal of Fracture*, 51: 61-92, **1991**.

84. Hinton, E., and Campbell, J.S. "Local and global smoothing of discontinuous finite element functions using a least squares method", *International Journal for Numerical Methods in Engineering*, 8: 461-480, **1974**.

85. Hohberg, J.M. *A Joint Element for the Nonlinear Dynamic Analysis of Arch Dams*, Ph.D. Dissertation No. 9651, ETH Zürich, Switzerland, **1992**.

86. Humar, J.L., and Chandrashaker, R. "Treatment of interaction effects in the seismic response of gravity dams", *Proceeding of the Tenth World Conference on Earthquake Engineering*, Madrid, Spain, 8: 4657-4662, **1992**.

87. Ingraffea, A.R. "Case studies of fracture in concrete dams", *Engineering Fracture Mechanics*, 35(1/2/3): 553-564, **1990**.

88. International Commission on Large Dams (ICOLD). *Finite Element Method in Analysis and Design of Dams*, Bulletin No. 30, Edited by R.W. Clough and O.C. Zienkiewicz, **1978**.

89. International Commission on Large Dams (ICOLD). *Méthodes de Calcul Sismique pour Barrages, État de la Question*, Bulletin No. 52, **1986**.

90. Irwin, G.R. "Analysis of stresses and strains near the end of a crack traversing a plate", *Journal of Applied Mechanics*, 24(September): 361-364, **1957**.

91. Jansen, R.B. "Conventional concrete for dams", in *Advanced Dam Engineering for Design, Construction, and Rehabilitation*, Edited by R.B. Jansen, Van Nostrand Reinhold, 193-201, **1988**.

92. Jansen, R.B. ed. *Advanced Dam Engineering for Design, Construction, and Rehabilitation*, Van Nostrand Reinhold, **1988**.

93. Jenq, Y.S., and Shah, S.P. "A two parameter fracture model for concrete", *Journal of Engineering Mechanics*, ASCE, 111(10): 1227-1241, 1985.

94. Karihaloo, B.L., and Nallathambi, P. "Notched beam test: Mode I fracture toughness", in *Fracture Mechanics Test Methods for Concrete*, RILEM Report 89-FMT, Edited by S.P. Shah and A. Carpinteri, Chapman and Hall, 1-86, **1991**.

95. Kreuzer, H., Wilk, W., and Tschegg, E.K. "Fracture energy of concrete under biaxial loading", *Dam Fracture*, Proceedings from the International Conference, Boulder, Colorado, 445-457, **1991**.

96. Kuo, J.S. *Fluid-Structure Interactions: Added Mass Computations for Incompressible Fluid*, Report no. UCB/EERC 82/09, University of California, Berkeley, **1992**.

97. Léger, P., and Katsouli, M. "Seismic stability of concrete gravity dams", *Earthquake Engineering & Structural Dynamics*, 18(6): 889-902, **1989**.

98. Léger, P., Bhattacharjee, S.S., and Sauvé, G. "Reservoir models for time-domain seismic analysis of gravity dams", Proceedings of the *CSCE Annual Conference*, Vancouver, May, II: 52-61, **1991**.

99. Léger, P., Sauvé, G., and Bhattacharjee, S.S. "Dynamic substructure analysis of locally nonlinear dam-foundation-reservoir systems", *Dam Engineering*, 2(4): 323-336, **1991**.

100. Léger, P., and Dussault, S. "Nonlinear seismic response analysis using vector superposition methods", *Earthquake Engineering & Structural Dynamics*, 21: 163-176, **1992**.

101. Léger, P., Tayebi, A.K., and Paultre, P. "Spectrum-compatible accelerograms for inelastic seismic analysis of short-period structures located in Eastern Canada", to be published in *Canadian Journal of Civil Engineering*, **1993**.

102. Léger, P., Venturelli, J., and Bhattacharjee, S.S. "Seasonal temperature and stress distributions in concrete gravity dams, part 1: modelling, and part 2: behaviour", to be published in *Canadian Journal of Civil Engineering*, **1993**.

103. Léger, P., and Bhattacharjee, S.S. "Reduced frequency-independent models for seismic analysis of concrete gravity dams", *Computers & Structures*, 44(6): 1381-1387, **1992**.

104. Léger, P., Bhattacharjee, S.S., and Venturelli, J. "Seismic analysis of gravity dams considering severe seasonal temperature variations", Proceedings of the *International Workshop on Dam Safety Evaluation*, Grindelwald, Switzerland, 2: 217-228, **1993**.

105. Leliavsky, S. *Design Text Books in Civil Engineering: Volume 4, Dams*, Chapman and Hall, London and New York, **1981**.

106. Lin, C.S., and Scordelis, A.C. "Nonlinear analysis of RC shells of General forms", *Journal of the Structural Division*, ASCE, 101: 523-538, **1975**.

107. Linsbauer, H.N., Ingraffea, A.R., Rossmanith, H.P., and Wawrzynek, P.A. "Simulation of cracking in large arch dam: part I", *Journal of Structural Engineering*, ASCE, 115(7): 1599-1615, **1989**.

108. Linsbauer, H.N., Ingraffea, A.R., Rossmanith, H.P., and Wawrzynek, P.A. "Simulation of cracking in large arch dam: part II", *Journal of Structural Engineering*, ASCE, 115(7): 1616-1630, **1989**.

109. Linsbauer, H.N. "Application of the methods of fracture mechanics for the analysis of cracking in concrete dams", *Engineering Fracture Mechanics*, 35(1/2/3): 541-551, **1990**.

109a. Lombardi, G. "Opening remarks", *International Symposium on Analytical Evaluation of Dam Related Safety Problems*, Copenhagen, II: 12-18, **1989**.

110. Mamet, J.C., Pigeon, Y., Bonazzi, D., and Aubin, L. "Non-linear analysis of the Daniel Johnson Dam", *International Symposium on Analytical Evaluation of Dam Related Safety Problems*, Copenhagen, I: 205-213, **1989**.

111. Medina, F., Domingez, J., and Tassoula, J.L. "Response of dams to earthquakes including effects of sediments", *Journal of Structural Engineering*, ASCE, 116: 3108-3121, **1990**.

112. Mlakar, P.F. "Nonlinear response of concrete gravity dams to strong earthquake-induced ground motion", *Computers and Structures*, 26(1/2): 165-173, **1987**.

113. Molenkamp, F., Kidger, D.J., and Smith, I.M. "Accuracy of four-node standard finite element", *International Journal for Numerical and analytical Methods in Geomechanics*, 16: 323-333, **1992**.

114. National Research Council (NRC). *Earthquake Engineering for Concrete Dams: Design, Performance, and Research Needs*. National Academy Press, Washington D.C., USA, **1990**.

115. Newmark, N.M. "A method of computation for structural dynamics", *Journal of the Engineering Mechanics Division*, ASCE, 85(3): 67-94, **1959**.

116. Ngo, D., and Scordelis, A.C. "Finite element analysis of reinforced concrete beams", *Journal of the American Concrete Institute*, 64(3): 152-163, **1967**.

117. Niwa, A., and Clough, R.W. "Nonlinear seismic response of arch dams", *Earthquake Engineering & Structural Dynamics*, 10: 267-281, **1982**.

118. Nomura, N., Mihashi, H., and Izumi, M. "Correlation of fracture process zone and tension softening behaviour in concrete", *Cement and Concrete Research*, 21: 545-550, **1991**.

119. O'Connor, J.P.F. "The modelling of cracks, potential crack surfaces, and construction joints in arch dams by curved surface interface elements", *Commission Internationale des Grands Barrages*, Quinzième Congrès des Grands Barrages, Lausanne, 57(22): 389-406, **1985**.

120. Oh, B.H., and Kim, J.S. "Advanced fracture analysis of concrete dams", *International Symposium on Analytical Evaluation of Dam Related Safety Problems*, Copenhagen, 1: 70-79, **1989**.

121 Oliver, J. "A consistent characteristic length for smeared cracking models", *International Journal for Numerical Methods in Engineering*, 28: 461-474, **1989**.

122. Ortiz, M., Leroy, Y., and Needleman, A. "A finite element method for localized failure analysis", *Computer Methods in Applied Mechanics and Engineering*, North-Holland, 61: 189-214, **1986**.

123. Oughourlian, C.V., and Powell, G.H. *ANSR-III: General Purpose Computer Program for Nonlinear Structural Analysis*, Report No. UCB/EERC-82/21, University of California, Berkeley, California, **1982**.

124. Pal, N. *Nonlinear Earthquake Response of Concrete Gravity Dams*, Report No. EERC 74-14, Earthquake Engineering Research Center, University of California, Berkeley, **1974**.

125. Pal, N. "Seismic cracking of concrete gravity dams", *Journal of the Structural Division*, ASCE, 102(9): 1827-1844, **1976**.

126. Paul, J.W., and Tarbox, G.S. "Definition of critical thermal states in arch dams, a prerequisite for cracking analysis", *Dam Fracture*, Proceedings from the International Conference, Boulder, Colorado, 643-657, **1991**.

127. Pekau, O.A., Chuhan, Z., and Lingmin, F. "Seismic fracture analysis of concrete gravity dams", *Earthquake Engineering & Structural Dynamics*, 20: 335-354, **1991**.

128. Pekau, O.A., and Batta, V. "Seismic crack propagation analysis of concrete structures using boundary elements", *International Journal for Numerical Methods in Engineering*, 35: 1547-1564, **1992**.

129. Priscu, R., Popovici, A., Stematiu. D., and Stere, C. *Earthquake Engineering for Large Dams*, Editura Academiei and John Wiley & Sons, **1985**.

130. Raphael, J.M. "Tensile strength of concrete", *Journal of the American Concrete Institute*, Title No. 81-17, 81(2): 158-165, **1984**.

131. Rashid, Y.R. "Analysis of prestressed concrete pressure vessels", *Nuclear Engineering and Design*, 7(4): 334-344, **1968**.

132. Reinhardt, H.W., and Walraven, J.C. "Cracks in concrete subject to shear", *Journal of the Structural Division*, ASCE, 108(1): 207-224, **1982**.

133. Reinhardt, H.W. "Loading rate, temperature, and Humidity effects", in *Fracture Mechanics Test Methods for Concrete*, RILEM Report 89-FMT, Edited by S.P. Shah and A. Carpinteri, Chapman and Hall, 199-230, **1991**.

134. Reinhardt, H.W., and Weerheijm, J. "Tensile fracture of concrete at high loading rates taking account of inertia and crack velocity effects", *Internal Journal of Fracture*, 51: 31-42, **1991**.

135. Rescher, O.J. "Importance of cracking in concrete dams", *Engineering Fracture Mechanics*, 35(1/2/3): 503-524, **1990**.

136. Riggs, H.R., and Powell, G.H. "Rough crack model for analysis of concrete", *Journal of Engineering Mechanics*, ASCE, 112(50: 448-464, **1986**.

137. Rossi, P. "Influence of cracking in the presence of free water on the mechanical behaviour of concrete", *Magazine of Concrete Research*, 43: 53-57, **1991**.

138. Rots, J.G., and de Borst, R. "Analysis of mixed-mode fracture in concrete". *Journal of Engineering Mechanics*, ASCE, 113(11): 1739-1758, **1987**.

139. Rots, J.G. "Smeared and discrete representations of localized fracture". *International Journal of Fracture*, 51: 45-59, **1991**.

140. Saini, S.S., and Krishna, J. "Overturning of top profile of the Koyna Dam during severe ground motion", *Earthquake Engineering & Structural Dynamics*, 2: 207-217, 1974.

141. Saouma, V.E., Broz, J.J., Boggs, H.L., and Brühwiler, E. "A comprehensive investigation of fracture mechanics of concrete dams", *International Symposium on Analytical Evaluation of Dam Related Safety Problems*, Copenhagen, I: 118-127, **1989**.

142. Saouma, V.E., Brühwiler, E., and Boggs, H.L. "A review of fracture mechanics applied to concrete dams", *Dam Engineering*, 1(1): 41-57, **1990**.

143. Saouma, V.E., Broz, J.J., Brühwiler, E, and Boggs, H.L. "Effect of aggregate and specimen size on fracture properties of dam concrete", *Journal of Materials in Civil Engineering*, ASCE, 3(3): 204-218, **1991**.

144. Saouma, V.E., Broz, J.J., and Boggs, H.L. "In situ field testing for fracture properties of dam concrete", *Journal of Materials in Civil Engineering*, ASCE, 3(3): 219-234, **1991**.

145. Shah, S.P., and Carpinteri, A. ed. *Fracture Mechanics Test Methods for Concrete*, Report of Technical Committee 89-FMT, RILEM, Chapman and Hall, 1991.

146. Skrikerud, P.E., and Bachmann, H. "Discrete crack modelling for dynamically loaded, unreinforced concrete structures", *Earthquake Engineering & Structural Dynamics*, 14: 297-315, **1986**.

147. Suidan, M., and Schnobrich, W.C. "Finite element analysis of reinforced concrete", *Journal of the Structural Division*, ASCE, 99(10): 2109-2122, **1973**.

148. Tahmazian, B., Yeh, C., and Paul, W.J. "Thermal cracking and arch action in Daniel Johnson Dam", *International Symposium on Analytical Evaluation of Dam Related Safety Problems*, Copenhagen, I: 235-244, **1989**.

149. Tang, T., Shah, S.P., and Ouyang, C. "Fracture mechanics and size effect of concrete in tension", *Journal of Structural Engineering*, ASCE, 118(11): 3169-3185, 1992.

150. Tinawi, R., and Guizani, L. "Seismic hydrodynamic pressures inside cracks in concrete gravity dams", Proceedings of the *International Workshop on Dam Safety Evaluation*, Grindelwald, Switzerland, 2, **1993**.

151. Uang, C.M., and Bertero, V.V. "Evaluation of seismic energy in structures", *Earthquake Engineering & Structural Dynamics*, 19: 77-90, **1990**.

152. Underwood, P. "Dynamic Relaxation", *Computational Methods for Transient Analysis*, Edited by T. Belytschko and T.J.R. Hughes, Elsevier Applied Science, 245-65, **1983**.

153. Unites States Committee on Large Dams (USCOLD), Committee on Earthquakes. *Bibliography on Performance of Dams During Earthquakes*, **1984**.

154. United States Department of the Interior Bureau of Reclamation (USBR). *Design of Gravity Dams*, A Water Resources Technical Publication, Denver, Colorado, **1977**.

155. Vargas-Loli, L., and Fenves, G. "Effects of concrete cracking on the earthquake response of gravity dams", *Earthquake Engineering and Structural Dynamics*, 18: 575-592, **1989**.

156. Veltrop, J.A., Yeh, C.H., and Paul, W.J. "Evaluation of cracks in a multiple arch dam", *Dam Engineering*, 1(1): 5-12, 1990.

157. Venturelli, J., and Léger, P. *Seasonal Temperature and Stress Distributions in Concrete Gravity Dams*, Report No. EPM/GCS-1992-08, Department of Civil Engineering, Structural Division, Ecole Polytechnique, Montreal, 1992.

158. Walraven, J.C. "Fundamental analysis of aggregate interlock", *Journal of the Structural Division*, ASCE, 10(11): 2245-2270, **1981**.

159. Westergaard, H.M. "Water pressures on dams during earthquakes", *Transactions*, ASCE, 98: 413-433, **1933**.

160. Wilson, E.L., and Khalvati, M. "Finite elements for the dynamic analysis of fluid-solid systems", *International Journal for Numerical Methods in Engineering*, 19: 1657-1668, **1983**.

161. Wolf, J.P. *Soil-Structure-Interaction Analysis in Time Domain*, Prentice Hall, New Jersey, 1988.

162. Yon, J.H., Hawkins, N.M., and Kobayashi,A.S. "Numerical simulation of mode - 1 dynamic fracture of concrete", *Journal of Engineering Mechanics*, ASCE, 117(7): 1595-1610, **1991**.

163. Zienkiewicz, O.C., and Taylor, R.L. *The Finite Element Method*, Fourth Edition, Volume 1, McGraw-Hill Book Company, 474-475, **1989**.